# Development of a 3D Printed Intranasal Stent for Improving Post-Operative Recovery

*Lari K Dkhar*

*School of Science*

*August 2019*

***A thesis submitted in complete fulfilment of the requirements for the degree of Doctor of Philosophy, Auckland University of Technology, 2019.***

## Abstract

Chronic rhinosinusitis (CRS) is a clinical condition associated with inflammation of the nasal mucosa and paranasal sinuses, which persists for more than 12 weeks. Primary symptoms for chronic sinus inflammation include nasal obstruction, thick nasal discharge, reduction or loss of olfaction and facial pressure or pain, which are confirmed by endoscopic examination and/ or sinus computed tomography (CT) scans. Treatments available for CRS include the prescription of antibiotics, topical nasal steroids and/or oral steroids, antihistamines, nasal decongestant and saline irrigants. But some patients do not respond to medical treatment alone; in such cases, functional endoscopic sinus surgery (FESS) is an alternative treatment that is widely considered. Current commercially available non-dissolvable and dissolvable nasal packings and dressings are frequently used after surgery, but they fail to provide consistent wound healing and breathability when they are packed into the nasal cavity. There is an increasing interest in the development of drug-eluting stents that can provide structural support while reducing post-operative tissue adhesions.

The purpose of this thesis is to develop a 3D printed intranasal stent that facilitates post-operative recovery. This intranasal device will have the following features: 1) an expandable structure fitting a patient's intrasinus morphology, 2) the capability for sustained release of anti-inflammatory drugs from the polymer matrix within the sinus cavity and 3) immediate release of an anti-fibrinolytic drug to control bleeding after surgery and aid in wound healing.

Using engineering and design methodology, the final stent design that was conceived presented a 3-part mechanism assembly featuring a cage like shape with six limbs evenly spaced, attached to two tapered conical revolves that allow the nasal stent to be easily deployed into the nasal passage (**Chapter 3**). This prototype intranasal stent can shape

itself to the individual's anatomy after being deployed. The successful development of a 3D printed functional intranasal prototype showed that 3D printing could bring about the conception of a new era of complex geometrical stents incorporated with drug components. To explore this possibility, the anti-inflammatory drug, dexamethasone was loaded into a composite thermoplastic blend that could be used for 3D printing drug eluting implants/stents in the future (**Chapter 4**). In this chapter, the anti-inflammatory drug was loaded into poly vinyl alcohol (PVA) and polylactic acid (PLA) matrices by melt blending and a sustained release of dexamethasone for more than 40 days was observed. This shows that melt processing of composite polymers with the drug is a viable method of producing novel drug loaded polymeric filaments for potential future drug delivery applications. However, the major drawbacks of using the melt blending method is the inability to process these drugs loaded polymeric sample in the form of filaments that are suitable for FDM 3D printers. Additionally, this could be a serious drawback for thermosenstive drugs.

For this reason, in **Chapter 5,** an alternative approach was used where multi-layer crosslinked films were created by using a simple layer-by-layer technique with natural polymers such as chitosan and gelatine. Results from the *in vitro* anti-inflammatory drug release assessment carried out showed that the addition of multi-layers slowed down the drug release profile to 30 days in comparison to single layer films which lasted for 3-6 days, respectively.

Bleeding usually occurs after surgery and adequate haemostasis is desirable. Therefore, in **Chapter 6** a coating was developed to provide a rapid release for an anti-fibrinolytic agent, tranexamic acid. In the medical and pharmaceutical fields, gelatine has been widely used as a matrix that can be easily applied as thin coating for drug-eluting stents due to their superior swelling ratio and biocompatibility while being incorporated with drugs.

Hence, in this study the printed cylindrical scaffold was dip-coated with drug loaded gelatine with varying cycles. From the result, it was observed that release of tranexamic acid lasted for 6 hours, with the release rate increasing as the coating-cycle increased. Additionally, gelatine as a coating component is favourable for this application, due to its capability to transition into a gel like component when it absorbs high amount of water, which provides a soft contact area between the stent and the surrounding biological tissue. Hence, from this study it can be observed that gelatine coating can be an effective drug delivery vehicle for intranasal applications post-surgery.

In conclusion, to stipulate the proof of concept for the development of this novel drug eluting intranasal stent with the possibility of improving existing technological knowledge gaps and post-sinus surgical outcomes, the data presented in these experimental studies was first carried out independently **(Chapter 3-6)**. But, for future research, combining these independent studies together to understand the requirements for further advancement of the design and tweaking of the drug loaded intranasal 3D printable prototype that are biocompatible and comply with 3D printing requirements are the next step. On the other hand, oxidative degradation of the drug loaded 3D printable composite polymer can be caused by cellular components and cyclic mechanical load. These occurrences would affect the degradation speed of the 3D printed intranasal stent, as such for this reason an improved evaluation and optimisation of the physics of the stent in *in vivo* studies should be incorporated for the experimental setup as a future prespective.

# Table of contents

## List of tables

## List of figures

## Attestation of Authorship

**“**I hereby declare that this submission is my own work and that, to the best of my knowledge and belief, it contains no material previously published or written by another person (except where explicitly define in acknowledgements), nor material which to a substantial extent has been submitted for the award of any other degree or diploma of a university or other institution of higher learning.”

Signed:

Date: 13/08/2019

## Publications arising from this thesis

### Papers published or submitted

1. Dkhar, L. K., Bartley, J., White, D., & Seyfoddin, A. (2018). Intranasal drug delivery devices and interventions associated with post-operative endoscopic sinus surgery. *Pharmaceutical development and technology*, *23*(3), 282-294.

2. Dkhar, L. K., Roy, S., & Seyfoddin, A. Development of multi-layer hydrogel films for sustained delivery of dexamethasone. To be submitted.

3. Dkhar, L. K., Roy, S., & Seyfoddin, A. Development of composite thermoplastic blends for 3D printing dexamethasone-releasing implant. To be submitted.

4. Dkhar, L. K., Etxabide. A., & Seyfoddin, A. Development of gelatine coating as an anti-fibrinolytic drug carrier. To be submitted.

### Oral presentations

1. Dkhar, L. K., Bartley, J., White, D., & Seyfoddin, A. Development of a 3D Printed Intranasal Drug Delivery Device. Proceedings of the Auckland University of Technology Postgraduate Symposium, 2016; Auckland, New Zealand.
2. Dkhar, L. K., Bartley, J., White, D., & Seyfoddin, A. Intranasal drug delivery devices. Proceedings of the NZ control release society, New Zealand chapter, 2017; Auckland, New Zealand.
3. Dkhar, L. K., & Seyfoddin, A. 3D printed shells for drug delivery. Proceedings of the Queenstown Research week, 2018; Queenstown, New Zealand.
4. Dkhar, L. K., & Seyfoddin, A. Development of multi-layer hydrogel films for sustained delivery of dexamethasone. Proceedings of the School of science graduate research showcase, 2018; Auckland, New Zealand.
5. Dkhar, L. K., Roy, S., Bartley, J., White, D., & Seyfoddin, A. Investment pitch for a biodegradable intranasal drug delivery stent. Proceedings of the KiwiNet Emerging innovator fund, 2019; Hamilton, New Zealand.

**Awards**

Winner of the best PhD talk award at School of science graduate research showcase (2018), Auckland University of Technology, Auckland, New Zealand.

Awardee of KiwiNet Emerging innovator fund (2019), KiwiNet, Auckland, New Zealand.

## Acknowledgments

Life as a PhD student for me was filled with many life-changing experiences, and at the end of the journey I have grown not only as a researcher but as an individual as well. Getting to the end was not an easy task, I know it would have not been possible to get this far without the support and guidance from so many people. They have all played an important role in their own way, showing me that life as a PhD student is not always about work. These people have made my journey an exciting, fun-filled and knowledgeable experience.

First, I would like to express my sincere gratitude to my main supervisor, Dr Ali Seyfoddin. His guidance, encouragement and support throughout my doctoral study have taught me the importance of being a critical thinker and to always look at the bigger picture, as a researcher and an individual. I will always be grateful to Dr Ali for believing in me and for his patience to guide me when I would get lost in my own research. From the beginning, Dr Ali would always challenge me to do more than what I think I am capable off and because of that I had the opportunity to work with various people from outside the academia field. Dr Ali, thank you for inspiring me to be more and for showing me that anything is possible, if we are willing to step up and try.

I sincerely appreciate the time and effort contributed by all the members of my supervisory committee, Dr. Jim Bartley, Dr. David White and Dr Sudip Roy in helping me get this far.

I enjoyed working with Dr Jim for his innovative mind-set. The numerous engaging discussion and support provided by Dr Jim helped me a lot, early on in my research. Dr Jim is always prompt in providing feedbacks with any reports and presentations. Thank

you, Dr Jim, your dedication, persistence and passion about research made me realise that these qualities go a long way, in turning an idea into reality.

I want to thank Dr David for his technical expertise required in this thesis. The designing work for the prototype stent presented was largely the result of the guidance provided by Dr David. Being new to the bio-designing field, designing and developing a prototype intrasinus stent was a challenging aspect for me and it was quiet daunting. I did not know where to start but Dr David was always very supportive and patient. Dr David helped me understand the importance of being able to look from a different perspective and what are the possibilities that can come about by linking two different field together (biological sciences and bioengineering). Due to his entrepreneurial mind-set, Dr David has inspired me to always be on the lookout for ways on how I can connect or bridge the gap for any situation. Thank you for being an inspiration to many students like me.

I would also like to acknowledge Dr Sudip from University of Auckland, with whom I have had the privilege to work with during my PhD. Dr Sudip had helped me overcome many technical issues regarding instrument availability throughout my PhD. He has always been very accommodating, his support, guidance and critical comments helped me a lot with my thesis. Also, I want to thank him for his friendly and numerous engaging discussions further refining my understanding in polymer science, required for the work carried out in this thesis.

Though I did not work with them on the work presented here, I would like to recognise; Dr. Rothman Kam and Rahul Permal for always helping me in the lab, making it fun and especially in teaching me how to use new instruments that I have never worked with before; Dr Brent Seale for his vast knowledge on microbiology and on teaching me how to work with different microbes (even with microbes not included in my research) and finally Dr Marcel Schaefer for giving me a one on one lesson on learning Raman

spectroscopy and SEM, even with his busy schedule. I would also like to thank the lab technicians: Saeedeh, Meie, Minaxi, Yan and Adrian for the cakes, chocolates, coffees and biscuits that they would get for me when working late in the lab. They have always been so patient and helped me with whatever I needed in the lab. Thank you for making me laugh all the time, I always had fun working in the lab because of you all.

I want to also extend my gratitude to my friends and colleagues in the Drug delivery group, AUT; Abbey, Sara, Soniya, Ghada, Hamideh and other fellow lab mates. Over the years, you all have been so supportive being there with me through the good and bad times. I really enjoyed the valuable intriguing discussions about your projects that we would have in the meeting every week, giving me a broader perspective on the areas you all are working in. To my amazing friends Riya, Paul, Niby, Abbey, Erika and Tom, who has always been so understanding, thank you for always being there for me through thick and thin. A special thanks to my sister Riya who has always been there for me when I needed someone to rely on, you are irreplaceable.

Finally, I owe my deepest gratitude to my parents. This would have not been possible without their loving support and guidance. I want to thank my sibling, Copper for being an incredible role model throughout my life, and always inspiring me to be a modern version of onna- bugeisha. I also want to thank my fiancé, Nikky for his positive vibes, always cheering me on and encouraging me to move ahead, one step at a time.

## List of abbreviations

| | |
|---|---|
| °C | Degree Celsius |
| 3D | Three dimensional |
| 4D | 4-dimensional |
| AM | Additive manufacturing |
| AFRS | Allergic fungal rhinosinusitis |
| AUT | Auckland University of Technology |
| AUTEC | Auckland University of Technology Ethics Committee |
| ABS | Acrylonitrile butadiene styrene |
| ATR | Attenuated total reflectance |
| BL | Bilayer film |
| CRS | Chronic rhinosinusitis |
| CAD | Computer aided design |
| CT | Computerised tomography |
| CRSwNP | Chronic rhinosinusitis with nasal polyps |
| CRSsNP | Chronic rhinosinusitis without nasal polyps |
| CNS | Central nervous system |
| CH | Chitosan |
| CG | Chitosan: gelatine |
| CFU | Colony-forming units |
| CMC | Carboxymethyl cellulose |
| DESs | Drug eluting stents |
| DDS | Drug delivery systems |
| DEX | Dexamethasone |
| EDX | Energy Dispersive X-Ray |

| | |
|---|---|
| ECM | Extracellular matrix |
| EWC | Equilibrium water content |
| FESS | Functional endoscopic sinus surgery |
| FDM | Fused deposition modelling |
| FDA | Food and Drug Administration |
| FE | Finite element analysis |
| FTIR | Fourier transform infrared spectroscopy |
| GA | Glutaraldehyde |
| GP | Genipin |
| GC | Gelatine coating |
| LMW | Low molecular weight |
| LOD | Limit of Detection |
| LOQ | Limit of Quantification |
| MRI | Magnetic resonance imaging |
| MCC | Mucociliary clearance |
| MMW | Medium molecular weight |
| NZD | New Zealand dollar |
| OTC | Over the counter |
| PLA | Poly lactic |
| PVA | Poly-vinyl alcohol |
| PBS | Phosphate-buffered saline |
| PLGA | Poly(lactic-co-glycolic acid) |
| PEG | Poly (ethylene glycol) |
| PGLA | Polyglycolic acid |
| PCL | Polycaprolactone |
| PC | Polycarbonate |

| | |
|---|---|
| PPSF | Polyphenylsulfone |
| RP | Rapid prototyping |
| RGD | Arginine-glycine-aspartic |
| SFF | Solid free-form technology |
| STL | Stereolithography |
| SL | Single layer |
| SEM | Scanning electron microscope |
| SD | Standard deviation |
| TXA | Trans-4-(aminomethy1) cyclohexanecarboxylic acid |
| TSS | Toxic shock syndrome |
| Tg | Glass transition temperature |
| Tc | Crystallisation temperature |
| Tm | Melting temperature |
| TL | Trilayer film |

# Chapter 1. Introduction

## 1.1. Research background

Chronic rhinosinusitis (CRS) is an inflammatory condition that persists in the paranasal sinuses for more than 12 weeks. Symptoms include nasal obstruction, thick nasal discharge and loss of olfaction. Currently, CRS treatments options include the prescription of antibiotics, topical nasal steroids and/or oral steroids, oral antihistamines, and saline irrigation. When patients do not respond to medical treatment, functional endoscopic sinus surgery (FESS) is an advanced treatment option [1]. The success of FESS is mainly dependent on clearing diseased mucosa and removing infection. The main goal of surgery is to restore sinus ventilation and restoring normal drainage pathways in order to restore mucociliary clearance [2]. However, surgery may only provide temporary relief and post-surgery recovery may be further complicated by haemorrhage, adhesions, middle turbinate lateralisation, persisting infection and recurrent disease [3]. At present, in order to reduce immediate and delayed surgical complications, a variety of temporary postoperative nasal packings and dressings can be used [4]. Devices such as silastic splints, absorbable and non-absorbable spacers and biodegradable stents [5] have been utilized after endoscopic sinus surgery to keep the sinuses open and to promote post-surgical healing [6].

Presently, a range of sinus stents and packings, have been evaluated post FESS in clinical and animal studies, but these stents may dislocate, as well as cause the formation of granulations tissue, scar tissue and late stenoses [7, 8]. Additionally, these stents and packings can hinder the application of post-surgery saline nasal irrigation and nasally inhaled drugs [9]. Therefore, the current methods used for FESS post-operative care can be improved. As such, developing drug eluting stents (DESs) or scaffolds could enhance tissue recovery by releasing loaded therapeutic drugs locally while providing post-surgery

structural support preventing tissue adhesions [10] and eliminating or reducing the need for recurrent surgeries leading to improved patient outcomes [4].

## 1.2. Motivation

Various studies have carried out to assess the efficacy of silastic splints, absorbable and non-absorbable spacers and biodegradable stents in resolving postoperative complications after nasal surgery. Reports from these studies have shown that nasal packings have potential drawbacks associated with obligatory mouth breathing, headache, dysphagia and risk of aspiration, airway obstruction, eustachian tube blockage and pain during removal [11]. Nasal packing may also cause osteogenic [12], allergic or neurotoxic reactions [13] and the use of collagen constituted packings may increase synechiae and granulation tissue formation [14]. Additionally, the use of animal derivative products has the risk of antibody formation and disease transmission [15]. Nasal packing also adheres to the mucosa causing additional bleeding and discomfort during removal which may cause mucosal injury and ciliary dysfunction [16]. Soaking of these packing with drugs has also shown unreliable results [17], due to the uncontrolled and inconsistent release of the medication. This may in part explain the unpredictable outcome of this treatment. Studies on intranasal splints have shown that they may worsen postoperative discomfort [18] and removal of these splints are painful causing discomfort to the patient that may lead to toxic shock syndrome in certain cases [19]. Propel™ is a sinus drug-eluting implant that is currently considered to be a cutting-edge invention with many advantages [10] but this implant has certain drawbacks. It cannot be used in patients who are sensitive to mometasone furoate which limits their options [20]. In addition, the dosage for mometasone in Propel™ is 370 µg, which is insufficient for patients suffering from CRS with advanced inflammation [21]. Hence, studies of various nasal postoperative nasal packings and dressings demonstrate unpredictability in post-surgical outcomes [22]. There is a need to come up with a solution for an improved post-operative

FESS recovery. The development of a structurally expandable and biodegradable intranasal drug delivery device fitting a patient's intranasal morphology while providing programmed release of anti-fibrinolytic and anti-inflammatory drugs with dosage flexibility could provide an innovative treatment option for positive post-operative outcomes after FESS surgery.

## 1.3. Research problems and objectives

Currently, several drug-delivery nasal devices are used to treat CRS however, these devices have several limitations that need to be addressed. A recently developed biodegradable nasal stent is similar to a spring, made with lattice pattern structures, but a lack of optimal design method, often leads to weaker mechanical properties and stent dislocation resulting in early recoil and potential dislodgement post implantation [23]. Additionally, the traditional method of fabricating stents made of biodegradable polymer have been to braid monofilaments of the polymers into a tubular structure. This process is both time-consuming and expensive, while also lacking accurate detail control over the stent microstructure. Therefore, the traditional methods of fabricating stents lead to poor repeatability and limits the design improvements. An emerging fabrication technique called fused deposition modelling (FDM) three-dimensional (3D) printing allows for more flexible fabrication capability for manufacturing custom-designed stents while being able to deposit precise quantities of therapeutic substances within the designed spatial patterns. This is done by creating complex geometrical structures using different proportions of drugs and biodegradable polymers which increases precision eliminating room for error and reduces production wastes, minimising costs which are otherwise difficult to control using conventional manufacturing techniques. 3D printing technology is becoming a promising emerging technology for the fabrication of complex drug delivery devices, particularly after the Food and drug administration (FDA) has published guidelines for manufacturing drug delivery devices using 3D printers. These guidelines

are promoting the development of 3D printing in medical applications and drug delivery systems for future applications [24]

This research is aimed at developing a novel 3D printed intranasal drug eluting stent for post-operative care after sinus surgery. The diagrammatical representation of the functionality of the intranasal drug eluting stent is shown in Figure 1.1. This drug eluting intranasal stent would be compressed within a deployment mechanism and once deployed the expanded stent would then pass through and sit in the required nasal passageway or sinuses to improve post-operative recovery.

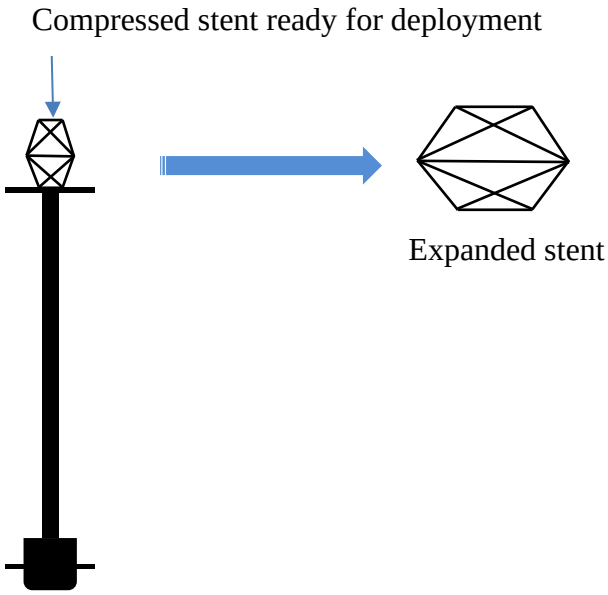


Figure 1.1: Diagrammatical representation of the intranasal device with the deployment mechanism.

The central hypothesis of the research question in this thesis is developing a prototype intranasal stent with independent formulations to stipulate the proof of concept for the delivery of anti-inflammatory and anti-fibrinolytic drugs, which can be assembled in the future for its specific applications (Figure 1.2).

The objectives of this thesis are to:

1. Develop an expandable intranasal stent, designed to fit a patient's intransinus morphology.

2. Develop a composite polymer loaded with an anti-inflammatory agent within its matrix to provide sustained drug release profile (Technique 1).

3. Develop a cross linked natural film loaded with an anti-inflammatory agent within its matrix to provide a better sustained drug release profile (Technique 2).

4. Develop a gelatine coating loaded with an anti-fibrinolytic agent able to provide an immediate drug release profile within 4 hours for haemostatic effect.

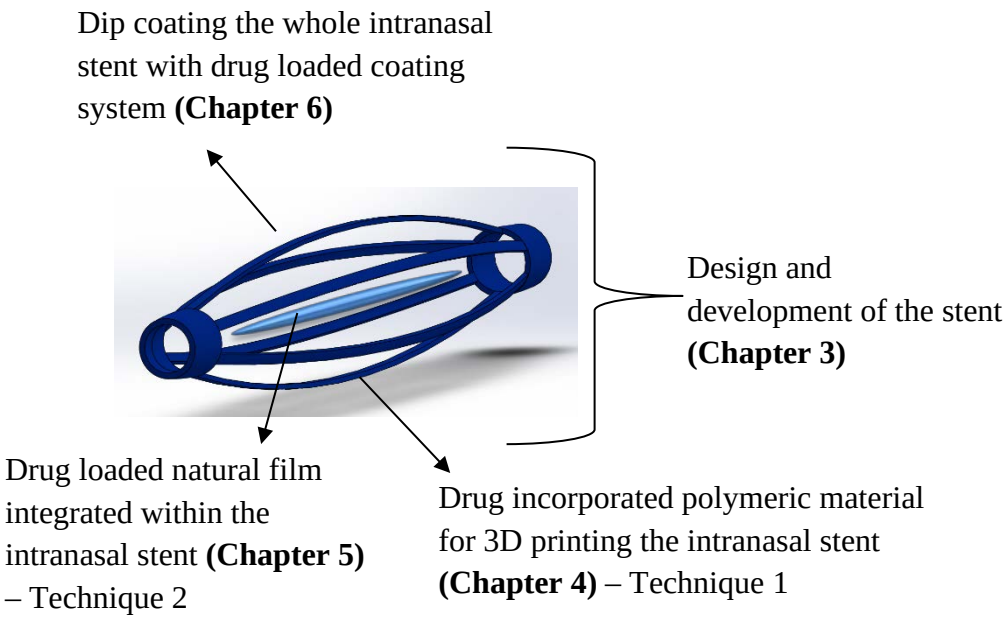


Figure 1.2: Diagrammatical representation of the independent studies of the intranasal stent that will be carried out in this research.

## 1.4. Outline of the thesis

The brief outline of each chapters of this thesis is laid out in six chapters as follows:

**Chapter 2:** presents a literature review on drug delivery devices and interventions associated with post-operative endoscopic sinus surgery.

**Outline :** What is CRS, what are the various treatments accessible to patients, how the currently available nasal drug delivery systems could be advantageous and dis-advantageous for intranasal post-operative care and the future objectives for improvements of post-operative care are discussed. Therefore, the primary aim of this

literature review is to evaluate the need of a novel post-surgery treatment that acts as a bio-degradable intranasal drug-eluting stent. This drug eluting stent can release the drug(s) locally to the affected site for a prolonged period of time improving surgical outcomes, and reducing the need for further revision surgery while being more patient friendly [10].

**Chapter 3:** present the designing and development of a prototype for a 3D printed intranasal stent. This chapter presents the work in Objective 1.

**Outline:** The key requirements in this chapter was to develop an expanding prototype intranasal stent that can be printed with an FDM 3D printer. The other objective was to design a prototype that will provide structural support to the nasal passageway/ sinuses to prevent adhesions while delivering drugs locally. The development of this prototype was formulated by using engineering and design methodology to build the most functional intranasal stent to date.

**Chapter 4:** documents a study developing a drug loaded composite thermoplastic blend that can be used for 3D printing drug eluting implants, which aims to complete Objective 2.

**Outline:** The main aim of this chapter was to develop a drug loaded (anti-inflammatory agent) composite thermoplastic blend (Poly lactic acid (PLA)/ poly-vinyl alcohol (PVA)) of different ratios, to determine their morphological, thermal and mechanical properties while assessing whether composite blend can provide a targeted sustained release for the anti-inflammatory agent.

**Chapter 5** documents the development of multi-layer natural films as an alternative approach using hydrogel films that can be integrated into the stent, allowing the anti-

inflammatory drug-eluting component to be independent of the stent's structure. This study aims to complete the work towards Objective 3.

**Outline:** The main aim of this chapter was to develop and optimise multi-layer chitosan and chitosan-gelatine composite films (1:1 ratio) crosslinked with glutaraldehyde for the sustained delivery of an anti-inflammatory drug, dexamethasone.

In **Chapter 4 and 5,** the objective of these studies respectively is to develop the sustained release of an anti-inflammatory drug. Hence, these two chapters are classified as two different techniques or formulations with the same purpose, but they can be used independently for precise applications in the future assembled 3D printed intranasal stent.

**Chapter 6:** presents the study on dip coating of a 3D printed model into gelatine loaded anti-fibrinolytic drug solution for an immediate release system. This chapter is carried out to achieve the final Objective 4.

**Outline:** The main aim of this chapter was to dip-coat the entire 3D printed structure and study the immediate release profile of an anti-fibrinolytic therapeutic agent entrapped within the coating. To further improve the coating properties of gelatine, lactose was used as a cross-linker in this study to link the gelatine matrices that acted as a reservoir for the drug, to allow the gradual elution of the drug within 24 hours.

**Chapter 7:** presents the conclusions drawn from this research, followed by study limitations and possible future work.

# Chapter 2. Intranasal drug delivery devices and interventions associated with post-operative endoscopic sinus surgery

## 2.1. Rationale

Chronic rhinosinusitis (CRS) is a common, chronic, inflammatory condition of the paranasal sinuses that persists for more than 12 weeks. CRS is classified into two types – with polyps (CRSwNP) and without polyps (CRSsNP) [25]. Symptoms associated with CRS include nasal obstruction, thick nasal discharge, reduction or loss of olfaction and facial pressure or pain [26]. If untreated, sinus blockage can hinder the drainage of mucus, interfere with breathing and increase the risk of nasal and sinus infections [27]. Treatment options for CRS include oral antibiotics, topical nasal steroids and/or oral steroids, oral antihistamines and nasal saline irrigation. Functional endoscopic sinus surgery (FESS) is an option for patients who do not respond to medical treatment [28]. Surgery clears diseased mucosa, removes infection, and restores normal drainage pathways [2]. Post-surgical recovery may be complicated by haemorrhage, adhesions, middle turbinate lateralisation, persisting infection and recurrent disease [29]. Temporary postoperative nasal dressings may be used to reduce immediate and delayed post-surgical complications [30]. Silastic splints, absorbable and non-absorbable spacers have been used after ESS to keep the sinuses open to promote post-surgical healing, and enhance drug delivery and nasal saline irrigation [5].

Devices currently available to assist post FESS recovery are associated with inconsistent outcomes [31]. Commercially available non-absorbable spacers and silastic splints reduce adhesions after FESS, but increase early nasal obstruction [5] and cause bleeding and discomfort to patients during removal in the clinic [2]. Dissolvable nasal packings are another popular option that are placed inside the nasal cavity to support the

newly opened sinus passages. These are used to prevent haemorrhage and aid in post-surgical recovery [32] but can hinder the application of post-surgery saline nasal irrigation and nasally inhaled drugs [9]. After FESS, patients often require ongoing systemic and topical medication to minimise post-operative complications, reduce the need for further surgery and improve patient outcomes [10]. An intranasal drug delivery device or implant through local release of loaded therapeutic drugs, could enhance tissue recovery while providing post-surgical structural support to prevent tissue adhesions [10]. The primary aim of this literature review is to evaluate currently available post-operative interventions and drug delivery devices.

## 2.2. Nasal physiology

The nose is a complex multifunctional organ that plays a critical role in airway homeostasis and olfaction. The nose transports, warms and humidifies air travelling into the lungs, filtering out incoming particles from the air providing a first-line defence [33]. In the nose, the mucosa helps to avert allergens, pathogens or foreign particles from reaching the lungs. Other significant functions of the nose include, mucociliary activity which removes mucus to the nasopharynx, immunological activities comprising of numerous immunocompetent cells and absorption of endogenous substances [34]. The nasal cavity is also connected to other cavities such as the frontal and maxillary, ethmoid and sphenoid sinuses.

## 2.3. Functional zones

The nasal cavity has three diverse functional zones; vestibular, respiratory and olfactory which are differentiated according to their anatomic and histologic characteristics (Figure 2.1 and Table 2.1).

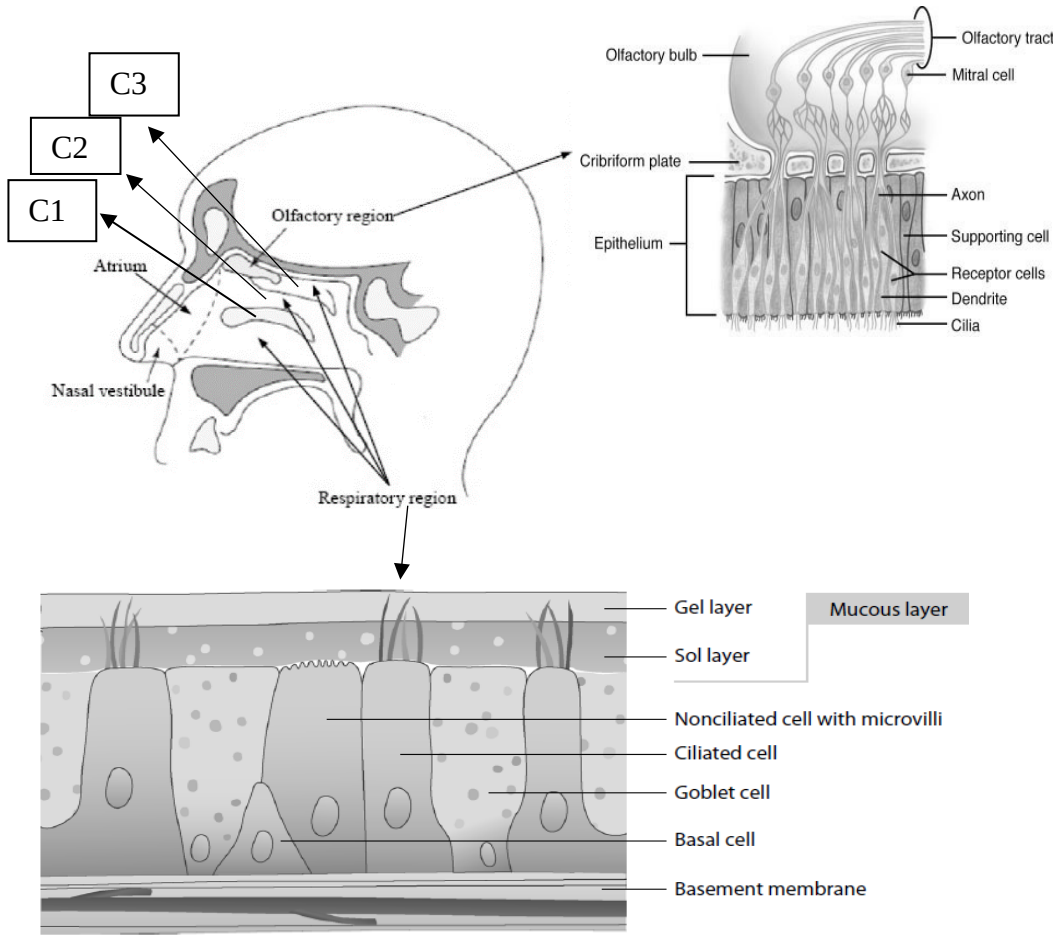


Figure 2.1: Anatomy and histology of human nasal cavity where C1: inferior turbinate, C2: middle turbinate, C3: superior turbinate (adapted from [35]).

### 2.3.1. Vestibule

The vestibular area, the front-part of the nasal cavity within the nostrils, is approximately 0.6 cm² [36] and is covered by stratified squamous keratinised epithelial cells [37]. The nasal hairs, also called vibrissae, filter the inhaled air acting as a barrier system. The atrium is the segment between the nasal vestibule and the respiratory region. The anterior segment of the atrium consists of stratified squamous epithelium and the posterior segment consists of a pseudostratified columnar cell adorned with microvilli.

### 2.3.2. Respiratory region

The nasal valve, the primary flow-limiting segment, extends to the anterior head of the inferior turbinates, which is 2–3 cm from the nostril opening. The nasal cavity is characterised by conchae/turbinates which project from the lateral nasal walls. There are three turbinates projecting from the lateral nasal wall the superior, middle and inferior

turbinates. The respiratory area-including the conchae is approximately 130 cm² [38]. The turbinates are responsible for humidification and temperature regulation of the inhaled and expired air. The lower area consists of a pseudostratified, ciliated columnar epithelium covered by a dense mucus layer [39]. The cilia form an important physiological part of the mucosal immune system as it transports foreign particles in the mucus layer towards the posterior region of the nasal cavity. The spaces between the conchae are called meati [37]. These passageways are responsible for the airflow created within the respiratory area. The inferior and middle meati drain the nasolacrimal ducts and ostiomeatal complexes respectively. The sinuses are air-filled pockets located within the skeleton of the face and around the nasal cavity. The nasal respiratory mucosa (important region for drug absorption) comprises pseudostratified ciliated columnar epithelial cells, goblet cells, basal cells, and mucous and serous glands [38]. The apical surfaces of many epithelial cells are enclosed with microvilli, while the other epithelial cells have fine projected cilia [37]. In the respiratory region, microvilli aid in enhancing the surface area. The epithelium in this region is lined with a mucus layer created by secretory glands and goblet cells. These glands and cells secrete a glycoprotein called mucin which is filled with granules. Mucin is also responsible for defining the viscosity of the mucus [40, 41]. The mucus comprises 95% water, 2.5-3% mucin and 2% electrolytes, proteins, lipids, enzymes, antibodies, sloughed epithelial cells and bacterial products [41]. Additionally, the mucus also provides enzymatic and physical defence to the nasal epithelium. Mucin is also able to trap large molecular weight therapeutic agents such as peptides and proteins [42].

### 2.3.3. Olfactory region

The olfactory area is approximately 15 cm² and is found in the roof of the nasal cavity which lies in-between the nasal septum and the lateral nasal wall [38]. This area is mainly responsible for olfactory sensitivity. The neuroepithelium in the olfactory region is the

only part of central nervous system (CNS) that is exposed to the external environment [43]. The nasal mucosal area is divided into two types: olfactory and non-olfactory epithelia. The non-olfactory epithelial region is highly vascularised and is covered by pseudostratified columnar and ciliated epithelium. The olfactory epithelium is comprised of specialised ciliated olfactory nerves projected into the nasal cavity. They are essential for awareness of smell [44]. This olfactory area is also comprised of supporting cells, mucus glands and small serous glands (glands of Bowman). These small serous glands produce secretions that act as a solvent for odorous substances [38] (Table 2.1).

Table 2.1: Characteristics of the human nose [36, 38, 44, 45].

| **Nasal Zones** | **Permeability** | **Characteristics** |
|---|---|---|
| Vestibule | Least permeable | -Nasal hairs called vibrissae<br>Stratified squamous<br>-Keratinised epithelial cells |
| Atrium | Less permeable | -Anterior segment of the atrium consists of stratified squamous epithelium<br>-Posterior segment consists<br>of a pseudostratified columnar<br>cells adorned with microvilli |
| Respiratory region | Most permeable | -Pseudostratified ciliated columnar epithelium<br>-Goblet cells, basal cells and mucous and serous glands<br>-Apical surfaces of many epithelial cells are enclosed with microvilli<br>-Other epithelial cells have fine projected cilia |
| Olfactory region | Direct access to cerebrospinal fluid | -Olfactory sensitivity<br>-Specialised ciliated olfactory nerve cells for smell perception |

## 2.4. Nasal pathology

### 2.4.1. Rhinosinusitis

Rhinosinusitis is a group of disorders characterised by inflammation of the nasal and paranasal sinus mucosa [46]. Causes are viral, bacterial, fungal and allergic [47]. Rhinosinusitis symptoms includes nasal obstruction, nasal congestion, nasal discharge, nasal purulence, postnasal drip, facial pressure and pain, alteration in the sense of smell, cough, fever, halitosis, fatigue, dental pain, pharyngitis, otologic symptoms (e.g., ear fullness,clicking and headache) [48]. Based on the duration of symptoms, rhinosinusitis is subdivided into acute, subacute, recurrent acute and chronic [47].

#### 2.4.1.1. Acute rhinosinusitis

Adjunctive treatments for symptomatic relief of acute rhinosinusitis include analgesics, decongestants, antihistamines, saline nasal irrigation, mucolytics and intranasal corticosteroids [49]. Antibiotics like amoxicillin, trimethoprim/sulfamethoxazole and macrolides can be used in cases where symptoms are severe and persistent for more than five days, those with moderate illness (moderate to severe pain or temperature ≥ 101°F 38.3°C); or those who are immunocompromised [50].

#### 2.4.1.2. Chronic rhinosinusitis

CRS management includes medical and surgical therapies. Medical treatment often requires combining multiple medications including antibiotics, nasal decongestants and saline irrigation [49]. Recommended treatment for CRS is first nasal saline irrigation, intranasal and oral corticosteroids and oral antibiotics and secondly sinus surgery [51]. For CRS, topical corticosteroid nasal sprays are commonly used and oral antihistamines are beneficial in patients with underlying allergic rhinitis [52]. In most cases, when patients do not respond to a three-month period of full medical treatment, endoscopic sinus surgery is recommended [52]. In CRS with nasal polyps a brief dose of oral

corticosteroids for 10-15 days will help to shrink nasal polyps [50]. In cases of severe polyposis, sinus surgery with debulking of nasal polyps is necessary and topical corticosteroid nasal sprays are recommended post-surgery to prevent nasal polyp recurrence [53].

#### 2.4.1.3. Allergic fungal rhinosinusitis (AFRS)

In AFRS, sinus surgery is always required to establish the diagnosis, remove inspissated mucus and restore sinus patency [49]. Oral corticosteroids are recommended after surgery with a gradual tapering of the dose to maintain and control sinus symptoms. AFRS is associated with nasal polyps and topical corticosteroid nasal sprays are recommended to control inflammation and prevent recurrence of nasal polyps after surgery [49].

## 2.5. Drug delivery applications

### 2.5.1. Localised drug delivery

Locally administered drugs are effective in low doses and the risk of systemic toxic effects is low in comparison to systemic drug delivery therapy [54]. As a result, intranasal therapeutic drug delivery is a relevant option for the local treatment of nasal symptoms. The most commonly used locally administered therapeutic drugs for nasal conditions are antihistamines and corticosteroids for allergic rhinitis [55]. There are an increasing number of drugs being investigated for intranasal administration, some examples are included in Table 2.2.

### 2.5.2. Systemic drug delivery

Intranasal administration offers rapid drug delivery with a high absorption rate for certain drug candidates as the nasal mucosa provides an entrance for systemically acting molecules. Systemic delivery of therapeutics through intranasal administration provides a rapid onset by avoiding the first-pass effect or gastrointestinal degradation of

therapeutic drugs [54]. The intranasal route of administering therapeutics is non-invasive and is easily administered by patients or physicians in emergency settings. The intranasal administration provides an alternative route for systemic drugs presently delivered more conventionally by oral or parenteral routes [54]. An increasing number of drugs are being developed for intranasal administration; some examples are included in Table 2.2.

Table 2.2: Example of nasal formulations commercially available.

| Compound | Class | Indication | Product development | Reference |
|---|---|---|---|---|
| **Local delivery** | | | | |
| Azelastine | Antihistamine | Management/treatment of symptoms of seasonal and perennial rhinosinusitis | Astelin | [56] |
| Beclometasone | Steroid | Management/treatment of symptoms of seasonal and perennial rhinosinusitis | Beconase | [57] |
| Mometasone | Steroid | Management/treatment of symptoms of seasonal and perennial rhinosinusitis | Nasonex | [58] |
| Mupirocin | Antibiotic | Eradication of nasal staphylococci | Bactroban | [59] |
| **Systemic delivery** | | | | |
| Estradiol | Steroid | Hormone replacement Therapy | Aerodiol | [60] |
| Oxytocin | Hormone | Lactation Stimulation | Syntocinon | [61] |
| Sumatriptan | Triptan | Migraines, cluster headaches | Imigran | [62] |
| Zolmitriptan | Triptan | Migraines | Zomig | [63] |

## 2.6. Intranasal drug delivery barriers

When evaluating the therapeutic feasibility for intranasal drug delivery, the pathologic condition (acute or chronic) and the intended use (local, systemic or CNS) should be considered at the pre-formulation state. Physiological barriers to intranasal drug delivery include the following:

### 2.6.1. Nasal mucociliary activity

Nasal mucociliary activity (Figure 2.2) plays a significant role in protecting the respiratory tract, as it prevents the invasion of foreign substances, pathogens and particles inhaled into the lungs. The cilia provide the driving force whereas mucus acts as a sticky fluid that collects and disposes foreign particles towards the nasopharynx and the gastrointestinal tract for elimination [64]. The efficiency of mucociliary clearance (MCC) depends on the length, density and the beating frequency of cilia and the viscoelastic properties of mucous. Factors that increase mucus production, decrease mucus viscosity or increase ciliary beating frequency may increase the MCC [38]. The mucus layer filters the air by capturing fine particulate materials that enter the nose. These agents adhere to the mucus layer, are transported to the nasopharynx and eventually to the gastrointestinal tract [44, 65]. In normal conditions, nasal mucus clearance functions at a rate of 5 mm/min and the mucous blanket in the human nasal cavity is replaced every 15-20 min [36]. The mucins and mucopolysaccharides released from the mucosa attaches to the cilia to form a brush like structure, or remains un-grafted and moves into the mucus layer based on the gel-on-brush model [66]. Pathological conditions can hamper mucociliary function. The nasal mucous membrane stops ciliary activity when dehydrated where humidifying the region will re-establish the normal activity. A reduction of mucociliary clearance activity increases residing time for drugs on the nasal mucosa improving bioavailability. However, when ciliary clearance activity increases the effect is reversed, leading to drugs being transferred from the nasal cavity toward the nasopharynx

decreasing drug absorption. The site of deposition also influences removal from the nasal cavity. The ciliary activity is slower in the anterior part of the nose compared to the ciliated posterior part. Hence, the posterior region of the nose is cleared more rapidly in comparison to the anterior region [38, 65].

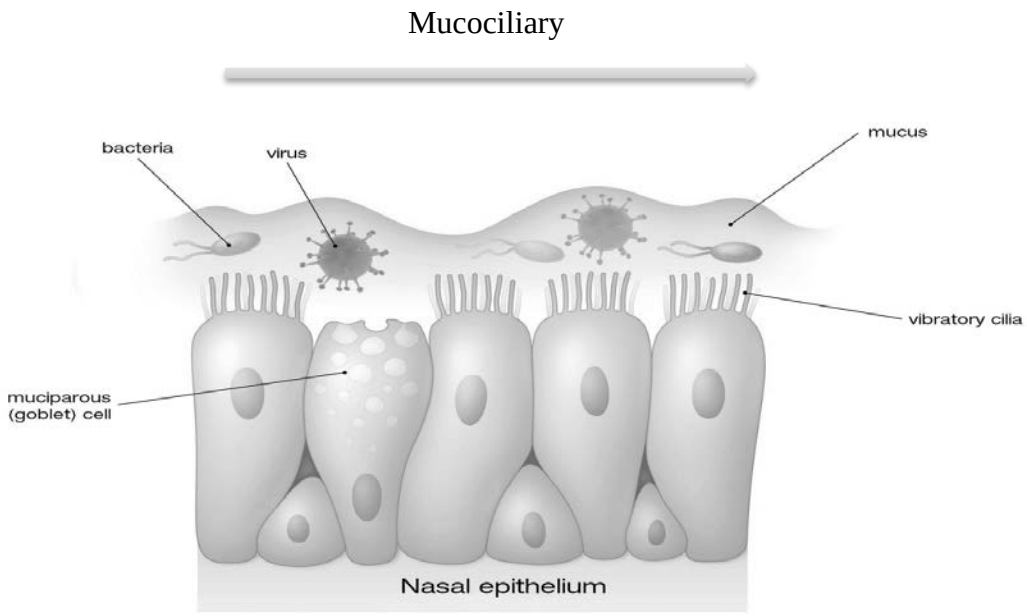


Figure 2.2: Nasal mucociliary activity (adapted from [67]).

### 2.6.2. Nasal blood flow

The nasal mucosa has a large surface area with an abundant blood flow, making it an ideal localised area for drug absorption. However, the rate of blood flow effects the systemic absorption of drugs in the nose. The absorption of drugs is dependent on diffusion through mucosa [68]. Vasodilative and vasoconstrictive agents can be used to regulate the blood flow and the amount of drug absorbed. When nasal blood flow increases, the amount of administered drugs in the nasal mucosal membrane remains low. This phenomenon enhances drug absorption by increasing the drug infiltration through the mucosal membrane by passive diffusion [69]. Various agents that can increase nasal blood flow include histamine, leukotriene D4, prostaglandin El, isoprenaline and terbutaline [70].

### 2.6.3. Enzymatic degradation

When drugs are administered through the nasal pathway, gastrointestinal and hepatic first-pass metabolism are avoided. When drugs pass through the nasal epithelial barrier, the existence of a wide range of metabolic enzymes in nasal tissues can also lead to their degradation. These metabolic enzymes are secreted from goblet cells, nasal glands and transudate from plasma. They cause drug degradation especially peptides and proteins. The metabolic enzymes found in nasal epithelial cells which degrade drugs in nasal mucosa are: cytochrome P-450-dependent monooxygenase, lactate dehydrogenase, oxidoreductase, leucine aminopeptidase and phosphoglucomutase carboxyl esterases, epoxide hydrolases and gluthatione S-transferases [38, 71, 72]. Certain drugs such as cocaine, nicotine, alcohols, progesterone and decongestants are metabolised by cytochrome P450 isozymes [73]. Likewise, other metabolic enzymes such as proteolytic enzymes, aminopeptidases and proteases, are also known to limit the bioavailability of peptide drugs such as calcitonin, insulin and desmopressin [38, 41]. The extent of drug degradation in the nasal cavity is weaker in comparison to hepatic and intestinal degradation, but it cannot be disregarded [74].

### 2.6.4. Correlated concerns

In intranasal administration, the nasal anatomy and physiology play a significant role in the rate of absorption of therapeutic drugs. Various components such as temperature, humidity, airflow and the nasal breathing cycle can influence the absorption rate in the nasal mucosa. However, certain pathological and structural issues such as inflammation, anatomical obstruction, septal deviations, acute sinusitis and chronic sinusitis can also influence intranasal absorption. The magnitude of these influences is still unknown [45].

### 2.6.5. Physiochemical properties of drugs

The physicochemical properties of drugs (molecular weight, lipophilicity, pKa, stability and solubility) can influence nasal absorption [38]. The molecular size of the drug influences the rate and degree of absorption of the drug through the nasal route. Lipophilic drugs with molecular weights lower than 1 kDa are quickly and efficiently absorbed across the nasal membrane in comparison to lipophilic drugs bigger than 1 kDa [75]. In the case of polar drugs, the rate of absorption is low and highly dependent on the molecular weight [75, 76]. The drug's hydrophilic, lipophilic and uncharged nature also affects the process of absorption. Increasing the lipophilicity of the drug and depending on its pKa and the pH of the absorption site (5.0-6.5 in human nasal mucosa) [77], the permeation of the compound increases through nasal mucosa. However, if the drug's lipophilicity is too high, the drug will not dissolve easily in the nasal membrane resulting in a reduced permeation through the wall [78]. Thus, for polar drugs, pH plays a major factor in influencing its permeability through nasal mucosa. In rats, compounds such as benzoic acid, salicylic acid and alkaloid acid (water soluble) show greater nasal absorption at pH values where these compounds are in the non-ionised form. The nasal cavity has the ability to metabolize drugs by defensive enzymatic mechanisms, reducing the stability of nasally administered drugs [79]. Thus, biological, chemical and physical drug stability studies are important, to overcome degradation through the use of prodrugs [80] and enzymatic inhibitors.

## 2.7. Approaches to increasing intranasal drug bioavailability and absorption

The intranasal route is efficient for topical, systemic and CNS delivery of a wide range of drugs and the use of prodrugs, enzymatic inhibitors, absorption enhancers, development of mucoadhesive delivery systems and new pharmaceutical forms can help increase drug bioavailability and absorption.

### 2.7.1. Prodrugs

Prodrugs have been used to overcome a drug's poor solubility, insufficient stability and inadequate absorption across barriers. Lipophilic drugs can pass through bio membranes, and are poorly soluble in water, but when administered with a prodrug with a higher hydrophilic character they produce an aqueous nasal formulation with a suitable concentration [38]. L-Dopa is poorly soluble in water and developing an intranasal aqueous formulation with an effective dose has been reported challenging [81]. When different prodrugs of L-Dopa were produced, it was observed that their solubility was enhanced leading to the development of rapid and completely absorbed nasal formulations. Additionally, very hydrophilic polar drugs cannot cross bio membranes and substitution with lipophilic prodrugs increases the penetration through the membrane [82]. The prodrug approach has also been used for improving enzymatic stability of drugs as well [83]. Prodrugs can protect peptide drugs from nasal enzymatic degradation and increase their bioavailability when administered intranasally [42, 80]. The nasal mucus layer and nasal mucosa have a wide variety of enzymes that acts as enzymatic barriers during nasal drug delivery [38]. Proteases and peptidases inhibitors have been used to avoid enzymatic degradation. For example, bacitracin, amastatin, boroleucin and puromycin [84, 85] have been used to prevent enzymatic degradation of drugs such as leucine enkephalin [86] and human growth hormone [87].

### 2.7.2. Promoters enhancing intranasal drug bioavailability

Promoters enhancing drug bioavailability such as chitosan and cyclodextrins have an absorption enhancing effect that cancel out any modification caused in the mucosa and act by opening the tight junctions [38]. Absorption enhancers in combination with hydrophilic drugs improves their absorption and induce reversible modifications on the structure of the epithelial barrier [38]. Most absorption enhancers used in intranasal drug delivery are surfactants (laureth-9), bile salts, fatty acids (taurodihydrofusidate) and

polymeric enhancers (chitosan, cyclodextrins, poly-L-arginine and aminated gelatine) [43, 88-93]. Absorption promoters enhance drug bioavailability and there can be a direct relation between the promoter's effect and the damage caused in the membrane [94, 95]. Surfactants, bile salts, fatty acids, phospholipids and lyso-phospholipids modif cell structures and leach-out proteins or can even strip off the outer layer of the mucosa [36, 74]. Polymeric enhancers with high molecular weight are not absorbed, minimising systemic toxicity in comparison with enhancers of low molecular weight [96].

#### 2.7.2.1. Chitosan

Chitosan is extensively used in intranasal formulations as it interacts with the protein kinase C system and opens the tight junctions between epithelial cells, increasing paracellular transport of polar drugs [97]. Additionally, chitosan enhances the contact time for the transport of the drug across the membrane as it interacts with the nasal mucus layer [36, 98-100]. Chitosan also improves the dissolution rate of low water soluble drugs [77, 101].

#### 2.7.2.2. Cyclodextrins

Cyclodextrins can improve nasal drug absorption by increasing drug solubility and stability [42]. As absorption enhancers, they interact with the lipophilic components of biological membranes changing their permeability [102-104]. However, cyclodextrins demonstrate local and systemic toxicity and also cause alterations to nasal morphology, ciliary beat frequency and erythrocyte haemolysis [105].

#### 2.7.2.3. Mucoadhesive drug delivery systems

Mucoadhesive drug delivery systems that prolong the contact time between the drug and nasal mucosa can improve nasal drug absorption [96]. It involves attaching the delivery system to the mucus, where a synthetic or natural polymer called mucoadhesive agent

then interacts with mucin [106-110]. Initially, the mucoadhesive systems swell as they absorb water from the mucus layer. The polymer then penetrates into the mucus and localises the formulation within the nasal cavity, enhancing the drug concentration gradient across the epithelium [44].

#### 2.7.2.4. Nano-formulations

New nasal formulations containing liposomes, microspheres and nanoparticles are also used for intranasal drug delivery. These formulations increase drug absorption, enhance nasal retention time and stability of the drug. Liposomes are phospholipids vesicles consisting of lipid bilayers of one or more aqueous compartments where drugs and other substances are enclosed. Liposomal drug delivery is effective in encapsulating small and large molecules, with a wide range of hydrophilicity and pKa values [111]. Liposomes enhance nasal absorption of peptides such as insulin and calcitonin by increasing their membrane penetration [112, 113]. Liposomes can increase the nasal retention of peptides [113] and can protect the entrapped peptides from enzymatic degradation [114] and mucosal membrane disruption [115]. Liposomal drug delivery is also useful for the influenza vaccine [106] and non-peptide drugs such as nifedipine [116].

## 2.8. Intranasal post-surgical interventions

Pharmaceutical treatments in the form of tablets, drops or sprays, and dissolvable and non-dissolvable adjunctive devices are often used after FESS and nasal surgery to aid in reducing scarring and opening the middle meati, controlling bleeding, preventing haematoma formation and supporting septal flap apposition [117]. The advantages of non-absorbable versus dissolvable nasal packing are widely debated, but both interventions are commonly used after FESS. Post-operative success can be limited by postoperative tissue adhesion formation, middle turbinate lateralisation, chronic inflammation, polyp recurrence and ostial stenosis [118]. Overcoming these

postoperative issues can improve long-term patient outcomes after surgery [4]. Currently, to reduce postoperative FESS complications, pharmaceutical treatments, which include oral or topical steroids in the form of tablets, drops or sprays, are used [119]. Oral steroids decrease mucosal oedema, granulation tissue formation and fibrin deposition which helps reduce postoperative complications [120, 121]. However, risks are associated with administering long-term systemic steroids [122, 123]. Additionally, the ability of intranasal steroid sprays to reduce post-operative complications is hindered by inadequate drug delivery, postoperative oedema, un-dissolved packing, crusting and secretions and reduced patient compliance [124].

### 2.8.1. Nasal drops

Nasal drops were originally administered by sucking liquid into a glass dropper and inserting the dropper into the nostril with an extended neck before squeezing the rubber top to emit the drops. Drops have been replaced by metered-dose spray pumps which are inexpensive single-dose spray pumps produced by “blow-fill-seal” technique. Due to inadequate clinical efficacy of spray pumps in patients with nasal polyps, a nasal drop formulation of fluticasone in single-dose pipettes was introduced in Europe for the treatment of nasal polyps. However, their popularity is limited by the need for head-down body positions and/or the extreme neck extension required for the desired gravity-driven deposition of drops. Compliance is often poor as patients with CRS often experience increased headache and discomfort in head-down positions [125, 126].

### 2.8.2. Spray pumps

Several types of spray pumps are available; squeeze bottles being mainly used to deliver over the counter (OTC) products such as topical decongestants. By squeezing a partly air-filled plastic bottle, the drug is atomised when delivered from a jet outlet. The dose and particle size vary with the force applied and when the pressure is released, nasal secretions

and microorganisms may be sucked into the bottle; they are not recommended for children [127]. Metered spray pumps have dominated the nasal drug delivery market. The pumps typically deliver 100 µl (25–200 µl) per spray offering high reproducibility of the emitted dose and plume geometry in *in vitro* tests [127]. Traditional spray pumps replace emitted liquids with air and preservatives are required to prevent contamination, but due to negative effects of preservatives, manufacturers have developed preservative-free spray systems. These systems use a collapsible bag, a movable piston or a compressed gas to compensate the volume for emitted liquids [127, 128]. These offer the additional advantage that they can be emitted upside down, without the risk of sucking air into the dip tube which compromises the subsequent spray. Another method used for avoiding preservatives is that the air that replaces the emitted liquid is filtered through an aseptic air filter, whereas some systems have a ball valve at the tip to prevent contamination of the liquid inside the applicator tip [129]. Recently, pumps have been designed with side-actuation and introduced for the delivery of fluticasone furoate (Figure 2.3) for the management of seasonal and perennial allergic rhinitis [130]. These new pumps were designed with a shorter tip to avoid touching sensitive mucosal surfaces. To reduce the need for priming and re-priming pumps were incorporated with pressure point to improve dose counter and reproducibility with lock-out mechanisms for enhanced dose control and safety [129]. Metered-dose spray pumps are well suited for daily drug administration over a prolonged duration, but due to the priming procedure and limited control of dosing, they are less suited for drugs with a narrow therapeutic window [131]. For expensive drugs and vaccines intended for single administration or sporadic use and where tight control of the dose and formulation is of particular importance, single-dose or duo-dose spray devices are preferred [129].

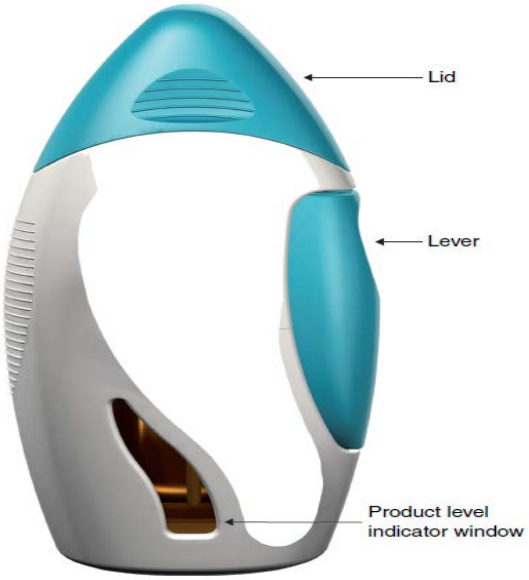


Figure 2.3: The fluticasone furoate nasal drug delivery system (adopted from [131]).

### 2.8.3. Powdered inhalers

Powdered formulations offer advantages such as greater stability in comparison to liquid formulations and the potential that preservatives may not be required. Powders tend to stick to the moist surface of the nasal mucosa, before being dissolved and cleared and along with the use of bio-adhesive agents there is a possibility of slowing ciliary action decreasing clearance rates and improving absorption [132, 133]. A number of factors such as moisture sensitivity, solubility, particle size, particle shape and flow characteristics will impact on deposition and absorption [127]. Powder actuators with a compressible compartment provide a pressure that upon releasing will create a plume of powder particles like that of a liquid spray. With breath-actuated inhalers, the subject can use his/her own breath to inhale the powder into the nostril from a blister or capsule. Nasal insufflators are devices consisting of a mouthpiece and a nosepiece that are fluidly connected and delivery occurs when the subject exhales into the mouthpiece to close the velum, and the airflow carries the powder particles into the nose through the device nosepiece [130].

### 2.8.4. Dissolvable packings

A variety of adjunctive devices have been applied to the sinuses after FESS to keep the middle meati open with varying success. Following endonasal surgery, various nasal packing materials are used to control bleeding, prevent hematoma formation and support septal flap apposition [134, 135].These include packing materials, injectable space-filling gels or structured stents [136]. Soaking these packing materials with drugs during surgery has shown inconsistent results in terms of wound healing, maintenance of ostium patency and prevention of polyposis recurrence [17]. Moreover, drug release from nasal packing materials is uncontrolled and inconsistent, which may explain the erratic outcome of this treatment strategy [137]. Nasal packing is primarily, used to control bleeding in epistaxis and after surgical procedures to the nose such as septoplasty, conchotomy and paranasal sinus surgery [138]. It is also used for internal stabilisation after operations involving the cartilaginous-bony skeleton of the nose [137]. In addition to haemostasis, packing is used to prevent synechiae or restenosis, particularly after surgery [138].

#### 2.8.4.1. Sinu knit ™

Sinu knit (Figure 2.4) is a dissolvable post-operative nasal dressing with a mesh-like material made of carboxymethyl cellulose (CMC), which converts to gel after hydration and dissolves within 5-7 days. This dressing can be optimised as required before insertion to fit into the nasal cavity. Sinu-knit gel acts as a moist barricade minimising post-operative bleeding and adhesions [139].

Figure 2.4: SINU-KNIT [139].

**2.8.4.2. Stammberger SINU-FOAM ™**

Stammberger post-operative dissolvable nasal dressing (Figure 2.5) is a dry carboxy-methylated cellulose (CMC) plug fitted within a syringe and when mixed with sterile water converts to a gelatinous foam. The foam conforms to the nasal and sinus cavities providing a moist barricade that dissolves within 7-10 days. This intervention helps reduce bleeding and oedema while preventing adhesions within the nasal cavity [139].

Figure 2.5: Stammberger SINU-FOAM [139].

**2.8.4.3. Merogel**

Merogel (Figure 2.6) post-operative bioresorbable, nasal packing and sinus stent uses hyaluronic acid. This packing can be applied in a dry or hydrated state, after FESS. Hyaluronic acid aids in decreasing adhesions and reducing healing time. In its dry state this post-operative intervention also helps reduce bleeding. When hydrated, it transforms into a mucoadhesive gel in about 24-48 hours, separating mucosal surfaces before dissolving after 2 weeks [140].

Figure 2.6: MeroGel ® nasal packing [140].

**2.8.4.4. MEROGEL nasal packing**

Merogel (Figure 2.7) post-operative bioresorbable gel stent is made of cross-linked polymers of hyaluronic acid and is directed with a flexible catheter into the nasal cavity after FESS. When hydrated, this biopolymer transforms into a muco-adhesive gel in approximately 24-48 hours, which separates mucosal surfaces before dissolving in 2 weeks. This nasal packing prevent adhesions, reduces bleeding and enhances wound healing while eliminating the need for removing nasal packing [140].

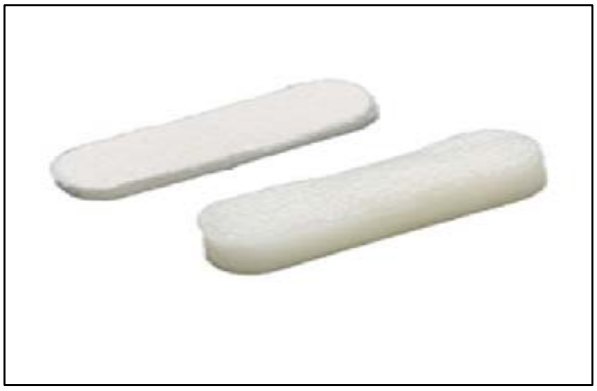

Figure 2.7: MeroGel ® Injectable nasal packing [140].

**2.8.4.5. Meropack**

Meropack (Figure 2.8) is the first blend of dressing designed for postoperative haemostasis and wound healing. Consisting of 80% of esterified hyaluronic acid and 20% collagen, it minimises bleeding after nasal trauma or surgery. This packing is biocompatible, possessing mucoadhesive properties and can absorb fluid, providing exceptional stenting abilities and dissolving within 2 weeks [140].

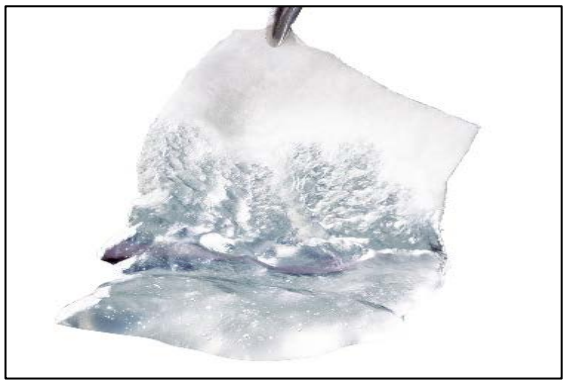

Figure 2.8: MeroPack ® Bioresorbable nasal packing [140].

#### 2.8.4.6. Nasopore®

Nasopore (Figure 2.9) consists of synthetic biodegradable and disintegrating foam that absorbs water and enables it to support the surrounding tissue and provide pressure against bleeding vessels. Nasopore is one of the most commonly used absorbable agents with advantages such as biodegradability, ease of manipulation and no need for post-operative removal. However, during the early stages of post-operative wound healing Nasopore was found to induce excessive granulation tissue formation [141].

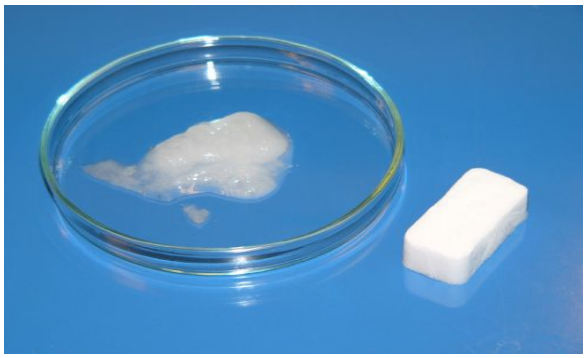

Figure 2.9: Nasopore [142].

## 2.9. Non-absorbable packings

### 2.9.1. Merocel® nasal packing

This non-absorbable nasal packing (Figure 2.10) is a compact, dry sponge composed of hydroxylated polyvinyl acetate (PVA). It swells up through rehydration with normal saline, which facilitates the constriction of bleeding vessels. Merocel is one of the most popular nasal dressings because of its low price, easy manipulation and elasticity. On hydration it provides sufficient post-surgery support to the nasal walls but it’s major

drawback is pain and occasional bleeding upon removal [140].


Figure 2.10: Merocel packing [143].

### 2.9.2. Intranasal splints

Intranasal splints (Figure 2.11) support the nasal septum and minimise the adhesion risk between septum and lateral nasal wall following FESS. They are made of soft, flexible medical grade silicone. The use of intranasal splints has increased due to their ability to keep the operated septum in the midline, preventing epistaxis and nasal synechiae [144]. They also improve haemostasis after surgery [138]. Nasal splinting can be an alternative to other non-absorbable packing but trans-septal suturing of the splints is challenging and time consuming [145].The existing evidence concerning the value of for these devices in the literature is contradictory. Some previous studies preferred biodegradable packings, while others stated an equal outcome with non-absorbable packing compared to no packing [141]. In addition, the cost-effectiveness of the biodegradable material currently used in this splint remains controversial [141].

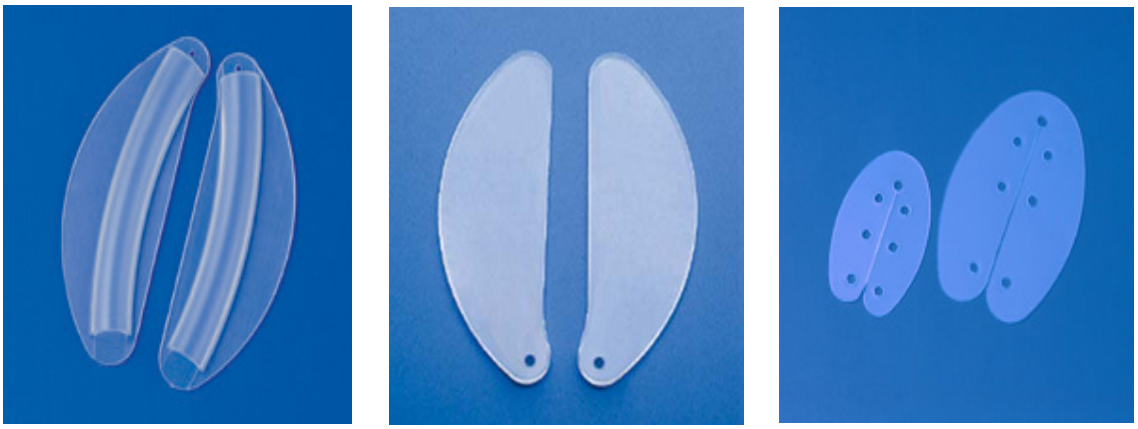

Figure 2.11: Nasal splints [146].

## 2.10. Post-operative drug delivery devices

Post-operative intranasal drug delivery devices are also referred to as stents or implants. According to the US Food and Drug Administration (FDA), a stent is a device placed temporarily into a cavity to keep it open, promote wound healing and/or relieve obstruction. An implant is a device placed into a naturally or surgically formed cavity of the human body for a period of 30 days or more [147]. However, to safeguard public health and dependent on the application of the device, the FDA may also define devices placed for shorter periods as implants [10, 148]. Such drug delivery devices can release entrapped medications in a controlled manner from polymer matrices to the affected target sites within the sinuses or nasal cavities for the required period. Intranasal drug delivery devices can be used as adjunctive treatment after FESS; with their main aim to reduce haemorrhage, prevent adhesions and promote drainage of the sinus mucosa further aiding in wound healing by sustained local drug release [144, 149]. Incorporation of therapeutic drugs such as steroids, antibiotics or anti-neoplastic agents is the primary focus of developing drug-eluting nasal implants [150].

### 2.10.1. PROPEL™ steroid-releasing implant

The PROPEL steroid-releasing implant (Figure 2.12 A and Figure 2.12 B) [10] is used in chronic sinusitis patients undergoing sinus surgery. The implant is advantageous as it offers controlled drug delivery directly to the affected sinus tissue. The lodging mechanism of the implant is like a spring, which is inserted by a physician to maintain the surgical opening. The implant then inflates within the ethmoid sinus, slowly delivering a corticosteroid (mometasone furoate) with anti-inflammatory properties to the sinus lining while the implant gradually dissolves. This implant also has a mini option; PROPEL mini offering local drug delivery to patients with smaller anatomy and frontal sinus disease. Both PROPEL and PROPEL mini are FDA approved [10].

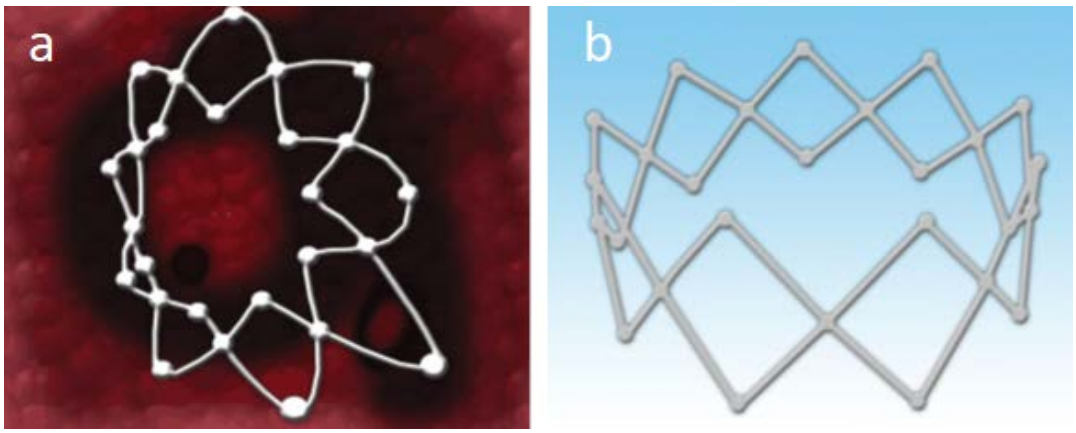


Figure 2.12: A and B) Mometasone loaded spring like Propel ™ sinus implant (adopted from [21]).

The Intersect ENT (Menlo Park, CA) is a steroid-eluting device (Figure 2.13) comprising of poly (lactic-*co*-glycolic acid) (PLGA) bio-absorbable polymer that self-expands into the postoperative ethmoid sinus cavity [151]. This model is similar to the Propel™ sinus implant, but is enhanced for treating CRS patients with polyps [152]. This new design further widens the congested sinus cavity due to its radial strength supporting the polypoid tissue [152]. Mometasone furoate is incorporated in the polymer matrix, comprising of poly (lactic-co-glycolic acid)-PLGA and a poly (ethylene glycol)-PEG [153], to provide slow release of the drug over a 3 month period [151]. A non-randomised *in-vivo* drug release study of this device was conducted in the United States which demonstrated technical accomplishment, patient acceptability and improved clinical outcomes [151, 152].

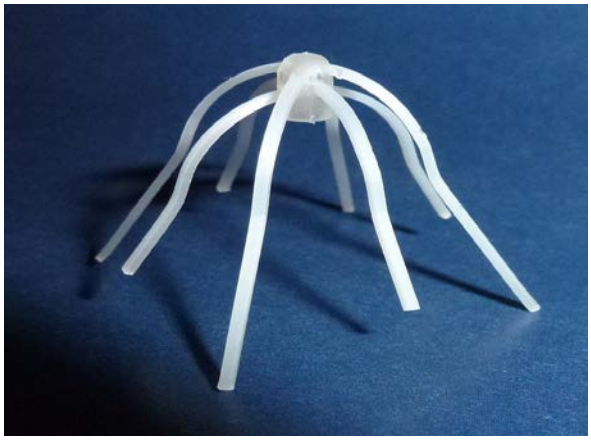

Figure 2.13: The Intersect ENT [Menlo Park, CA] steroid eluting sinus implant with 1350 μg of Mometasone furoate (adopted from[151]).

### 2.10.2. Relieva Stratus™ microflow spacer

Relieva Stratus™ (Figure 2.14) is a drug delivery device for treating chronic ethmoid sinus mucosal disease [154]. This device is composed of a deployment guide and a Microflow spacer. This spacer has a reservoir membrane containing several microspores for continuous release of the therapeutic drugs via a catheter tube [155]. The drug is released in a controlled manner for the required time. A study has shown that this device is capable of releasing the steroid triamcinolone acetate for 2–4 weeks before being removed in an office setting [154]. However, certain disadvantages associated with this device were found - the balloon shape affected drug release and reduced patient acceptability to manual removal after 30 days [22, 155]. This device has also caused orbital violation [154] and is no longer used with an active drug substance due to welfare and efficacy issues as it may lead to serious adverse situations [10]. This device is currently approved by the FDA for use with saline only [10, 154].

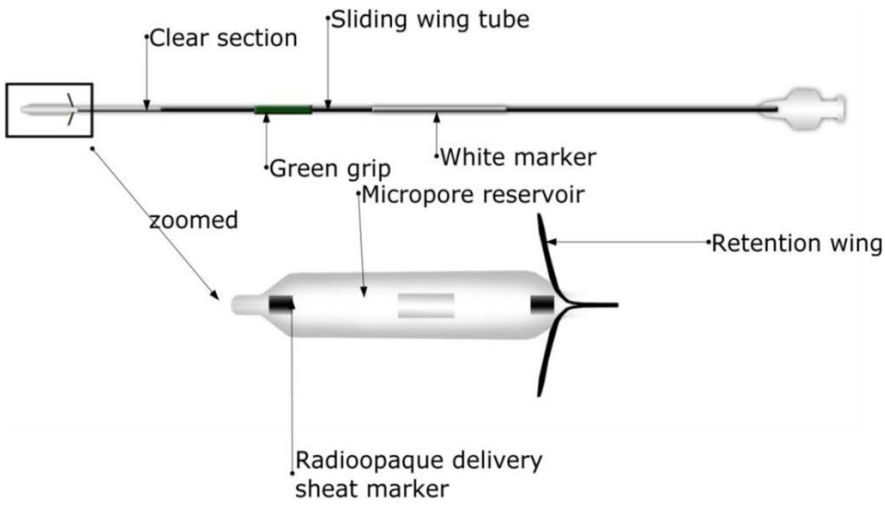


Figure 2.14: Relieva stratus ™ Microflow spacer [adopted from [10]].

## 2.11. Discussion

The efficacy of biodegradable nasal packings in resolving postoperative complications after nasal surgery was compared to non-absorbable packings. Nasal packings have potential drawbacks associated with obligatory mouth breathing, headache, dysphagia, risk of aspiration, airway obstruction, eustachian tube blockage and pain during removal

[11]. MeroGel nasal packing may have tendencies to cause osteogenic [12], allergic or neurotoxic reactions [13]. Collagen constituted packings may increase synechiae and granulation tissue formation [14], whereas animal product derivatives can have risks such as antibody formation with disease transmission [156]. Merocel packing has been reported to adhere to the mucosa causing additional bleeding and discomfort during removal, which may cause mucosal injury and ciliary dysfunction [157]. Soaking these packing with drugs has also shown unreliable results [158], due to the uncontrolled and inconsistent release of the medication, [10]. Some studies of intranasal splints have shown that they may worsen postoperative discomfort [159]. Intranasal splints removal is also painful and causes discomfort to the patient, and may lead to toxic shock syndrome in certain cases [19]. With regards to intranasal drug delivery and in comparison to other devices, the Propel™ sinus drug-eluting implant is considered a cutting-edge invention with many advantages [10]. However, the dosage for mometasone in Propel™ is 370 µg, which can be insufficient for patients suffering from CRS with advanced inflammation [21, 160]. In addition, the drawback of using the Relieva Stratus™ Microflow spacer is its short duration of use which is insufficient for treating chronic rhinosinusitis. In the end, the negative impact of using these archaic post-operatve care is the frequent requirement for additional surgery after removal [155]. Hence, studies of various drug delivery devices (e.g.; Propel™ sinus implant and Microflow spacer) have demonstrated unpredictability in post-surgical outcomes and further research is required to validate the efficacy of these drug delivery devices [22].

## 2.12. Conclusion

Many advantages are associated with the use of drug-delivery nasal devices used to treat CRS; however many challenges still persist. As these drugs and delivery devices are foreign materials, the risk of developing toxic shock syndrome (TSS) is a possibility. This

risk is particularly acute when using non-biodegradable materials [144, 150, 161]. Clinical studies have shown that frontal sinus stents can also lead to complications with implant blockage and granulation build-up [22]. Drug delivery nasal devices with the capability of biodegradation are new inventions. As such, further research is required to demonstrate their superior clinical efficiency and improved post-surgery outcomes in FESS patients. The development of nasal drug delivery devices could overcome the limitations of current strategies but requires further research to evaluate drug delivery profile. This requires formulation with the most appropriate polymer while considering the dosage flexibility. Hence, producing such a delivery device could provide an innovative treatment option for post-operative complications in FESS patients.

## 2.13. Rationale for selected components

### 2.13.1. Anti-inflammatory drug

Dexamethasone (DEX) (Figure 2.15), known as maxidex or prednisolone F, is a corticosteroid used as an anti-inflammatory agent to interfere with substances released in the body that may cause acute and chronic inflammation. Dexamethasone can inhibit the production of essential factors generating an inflammatory response, such as vasoactive and chemo attractive factors, lipolytic and proteolytic enzymes, and the extravasation of leukocytes to the wound [162]. Current evidence from the literature suggests that oral corticosteroids such as dexamethasone can be used as an adjunctive therapy to oral antibiotics, as they are found to be an effective treatment for short-term relief of symptoms in patients suffering from acute/chronic rhinosinusitis [163].

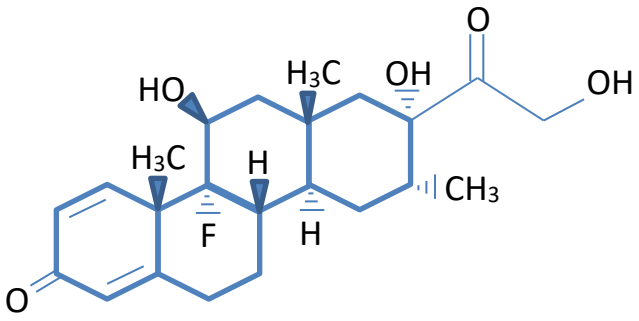


Figure 2.15: Dexamethasone structure.

### 2.13.2. Antifibrinolytic drug

Tranexamic acid (TXA) (Figure 2.16) is a synthetic derivative of the amino acid lysine that exerts its antifibrinolytic effect through the reversible blockade of lysine binding sites on plasminogen molecules [164]. Tranexamic acid is useful in a wide range of haemorrhagic conditions [165]. The drug reduces postoperative blood losses and transfusion requirements in a number of types of surgery, with significant cost and tolerability advantages, and appears to reduce rates of mortality and urgent surgery in patients with upper gastrointestinal haemorrhage [165]. Tranexamic acid has been found to be well tolerated in patients and as such incorporating this therapeuting agent in the intranasal stent can aid in reducing nasal blood loss after sinus surgery [164].

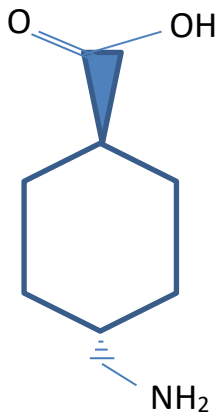


Figure 2.16: Tranexamic acid structure.

### 2.13.3. Chitosan

Chitosan (Figure 2.17) aids in rapid blood clotting and has recently gained approval in the United State and Europe for use in bandages and other hemostatic agents as it reduce

blood loss in comparison to gauze dressings increasing patients' survival [166]. Chitosan's hemostatic properties reduce pain as it blocks nerve endings, is hypoallergenic and has natural antibacterial properties [167, 168]. Recently developed hydrogel-based chitosan bandages are also used to treat burn wounds [168]. Additionally, chitosan's properties enable it to be used in transdermal drug delivery as it is mucoadhesive in nature, reactive and has a positive charge under acidic conditions. This molecule will maintain its structure in a neutral environment but will solubilise and degrade in an acidic environment enabling it to be used to transport a drug to an acidic environment, where the chitosan packaging will then degrade, releasing the drug to the desired environment. Additionally, chitosan salts are biocompatible and biodegradable making them useful as absorbable haemostats [169].

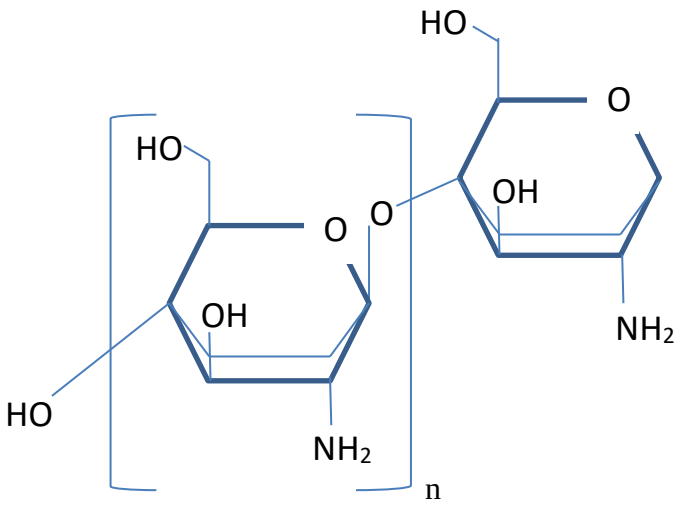


Figure 2.17: Chitosan structure.

**2.13.4. Gelatine**

Gelatine (Figure 2.18) is a denatured collagen, water-soluble functional protein having the ability of forming transparent gels under specific conditions [170]. Gelatin is well known for its unique gel-forming ability making it a valuable material for investigating the fundamental functional properties in colloid studies [170]. Natural biomaterials such as collagen and gelatine have been widely used for drug delivery [171]. For this research, after sinus surgery gelatine can also provides hemostatic effectiveness and when used in

combination with thrombin will provide a rapid coagulation effect. Additionally, gelatin has been used before in internal bleeding cases owing to its safe use in terms of superior biocompatibility and biodegradability [172].

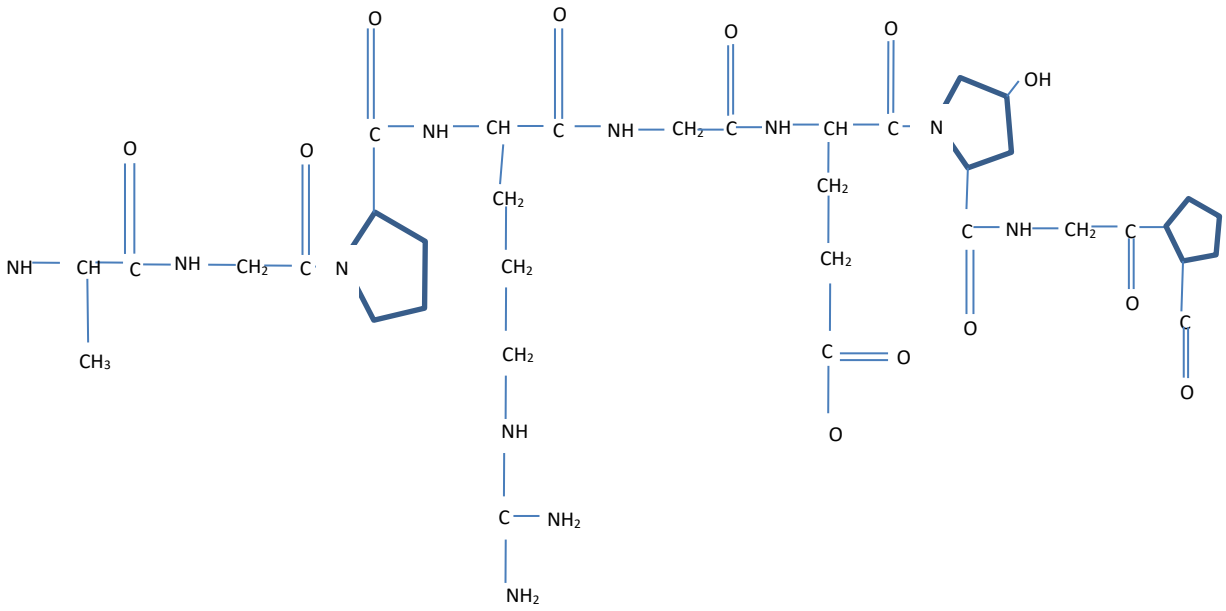

Figure 2.18: Gelatine structure.

### 2.13.5. PLA (Poly lactic acid)

PLA (Polylactic acid) or polylactide (Figure 2.19) is a hydrophobic aliphatic polyester with a renewable source, making it affordable and easily accessible for biomedical applications [173]. PLA is biodegradable by hydrolysis and enzymatic activity, while having a large range of mechanical and physical properties that can be engineered appropriately to suit multiple applications [174]. In innovative drug delivery carriers, PLA is mainly used due to its biocompatibility, low levels of immunogenicity and toxicity. For this research, PLA was chosen as one of the polymer as it has already been approved by the US Food and Drug Administration (FDA) [175] for human use in sutures, bone implants, and screws, and even in formulations for sustained drug delivery. Additionally, three-dimensional (3D) printing has also further expanded the potentials of PLA in biomedical applications, making PLA a suitable polymer to work with for developing the intranasal stent [173].

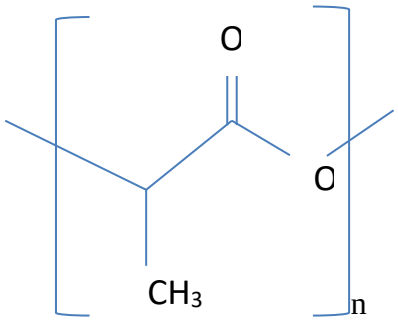


Figure 2.19: Polylactic acid (PLA) structure.

**2.13.6. PVA (Polyvinyl alcohol)**

Poly (vinyl alcohol) is a synthetic polymer (Figure 2.20) with good flexibility, transparency, toughness, biocompatibility, barrier properties, nontoxicity and biodegradability, and has been widely used in various fields such as biomedicine, the packaging industry, pharmacy and biosensors. PVA is one of the most frequent and oldest synthetic polymers that has been used in wound dressings and wound management as well as drug delivery systems [176].

PLA can be biodegraded under compost conditions; but it takes up to a year to degrade in real and simulated soil burial conditions because PLA must be hydrolysed before microorganisms can use it as a source of nutrients [177]. However, adding small quantities of compatible hydrophilic polymers such as PVA, which is biodegradable, hydrophilic and flexible is an alternative way to enhance the biodegradability of PLA. In previous studies, it has been reported that polyvinyl alcohol (PVA) can accelerate the degradation of PLA, by increasing the hydrophilicity of the blend and breaking the crystallinity of PLA. Furthermore, the hydroxyl groups in PVA readily form hydrogen bonds with the ester groups of PLAs, furthermore, favouring the compatibility of their blends [176].

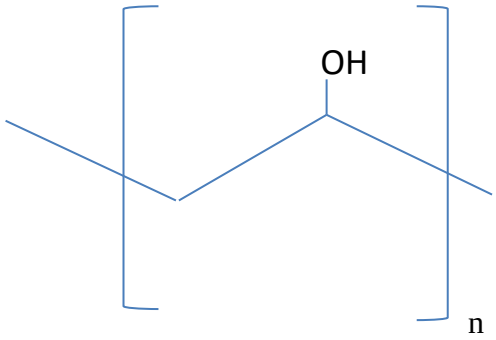


Figure 2.20: Poly (vinyl alcohol) PVA structure.

In general, the processing of polymer blends is an interesting goal for both research groups and industrial companies because it is an easy, low-cost, scalable way to enhance the properties of the pristine homopolymers. Hence in this thesis, a combination of these components was necessary due to the specificity that was required to fabricate the intra-nasal drug delivery device. The polymers used in this study are biocompatible and biodegradable and exhibit a wide range of erosion profiles with tuneable mechanical properties required for intranasal support.

# Chapter 3. Designing and development of a prototype intranasal stent

As discussed in **Chapter 1**, this thesis aims to develop a novel three dimensional [3D] printed intranasal drug eluting stent for improving post-operative care after sinus surgery for patients suffering from chronic rhinosinusitis (CRS). In this **Chapter**, the design, development and expandability feature of the prototype intranasal stent will be investigated (Figure 3.1).

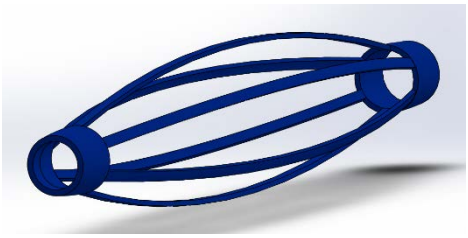


Figure 3.1: Diagrammatical representation of the the prototype intranasal stent.

## 3.1. Introduction

### 3.1.1. Need for a drug eluting intranasal stent

A clear gap exists in available technologies currently to treat CRS patient's post-surgery to improve their outcomes. The development of a new intranasal drug delivery device could provide structural support to the nasal passageway to prevent adhesions while locally administering drugs for an improved post-operative recovery after sinus surgery.

With the assistance from Auckland University of Technology (AUT) Bio Design Lab, the aim of this chapter is to develop a prototype intranasal stent that is biodegradable, provides local release of loaded therapeutic drugs, and enhances tissue recovery while providing post-surgical structural support to prevent tissue adhesions. This developed prototype stent will be more functional than what is currently available for post-surgical support and recovery. According to the US Food and Drug Administration (FDA), a stent is a device placed temporarily into a cavity to keep it open, promote wound healing and/or

relieve obstruction. Depending on the anatomy, physiology, disease, and surgery varying form or structures of stents have been developed that would possess several physical characteristics such as; good flexibility, low recoil (the ability of a stent to maintain its initial expansion diameter) is clinically desirable, necessary radial strength and high scaffolding ability [178]. Therefore, a rational starting point in nasal stent designing would be the selection of polymers with desirable mechanical, thermal and biodegradability properties while taking into consideration the varying design of the stent required for the anatomy and physiology of the nose. The selection criteria are imperative as primarily the structure or form developed for the stent will be able to account for properties and constraints resulting within the intranasal cavity. For this thesis, the prototype intranasal stent will be sized for fitting in a 3D printed nasal model, where, both the prototype stent and 3D printed nasal model will be developed via a Fused Deposition Modelling (FDM) 3D printer. Nevertheless, the prototype design and the paradigm developed behind this design are also scalable to smaller version for future *in vivo* work.

## 3.2. Design selection criteria

### 3.2.1. Prototype intranasal stent and 3D printing

Currently, the utilisation of 3D printing in personalised medicine is an emerging manufacturing technology for biomedical and pharmaceutical applications because of its flexibility and fabrication capability for manufacturing complex and multi-compartmental custom-designed scaffolds and drug delivery systems [179]. 3D printed systems also allows the incorporation of high doses of therapeutic ingredients within the designed spatial patterns of the polymer matrix, which provide sufficient drug delivery to the target sites leading to enhanced therapeutic efficacy, safety and patient compliance [180]. Recently, the US Food and Drug Administration (FDA) has published guidelines for the manufacture of drug delivery devices using 3D printers, promoting the

development of this innovative technology in medical applications and drug delivery systems for future applications [24]. 3D printing systems use computer-aided designs (CAD) to facilitate the creation, modification, optimisation and analysis of 3D designs in the form of a digital file to create free form geometries. Using additive processes, successive layers of materials are assembled on top of one another to build the desired object [181]. In this process, items can be assembled directly from a digital model, not relying on removal (by cutting, drilling, chopping, etc.) as in the case of conventional machining techniques, which increases precision, eliminates errors, reduces production wastes and minimises costs [182]. 3D printing also accomplishes the fabrication process by using only one machine to make a range of different structural designs, making the whole operation easy and cost efficient. One of the future objectives in this thesis is to study the functionality of the fully assembly stent with active drug components being incorporated or loaded into its polymer matrix. FDM 3D printer technology offers accurate control of the drug delivery dosage by rapid prototyping, precision of quantity and versatility in incorporation of concentration gradients within the polymer matrix in comparison to conventional techniques. Accordingly, this process was selected for developing the stent. Thus, 3D printing remains a novel practice with room for developing increasingly sophisticated applications that could play a major role in the future on how to treat, manage, and prevent diseases [183].

### 3.2.2. Biodegradable synthetic polymers

In recent times, research in drug-eluting biodegradable stents have been getting extensive attention as they are only needed temporarily in the body. Drug eluting stents (DESs) or scaffolds can enhance tissue recovery by releasing loaded therapeutic drugs locally while providing post-surgery structural support and preventing tissue adhesion [10]. As such, these biodegradable polymeric candidates must be considered as each polymer have varying properties that can be used for developing an ideal drug eluting stent. Similarly,

for this thesis, when selecting a polymer for 3D printing the intranasal stent, several properties has to be considered such as: strength of the polymer, toxicity, biocompatibility (property of a material being compatible with living tissue) and mechanisms of polymer degradation including mechanical, thermal and chemical processes. For a synthetic polymer, degradation occur by an autocatalytic process via chemical hydrolysis in which the weak parts in the polymeric chain react with water molecules and crack into oligomers and monomer fragments. This chemical hydrolysis causes backbone chains to break down into carboxyl end groups, creating an acid environment accelerating hydrolysis rate [184]. This degradation of synthetic polymer such as PLA, occurs through active metabolism reaction causes the monomer fragments to be converted into non-toxic products (i.e., lactic acids) that can be easily expelled from the body through normal cellular activities [185]. Accordingly, information gathered from previous studies reported in a literature review in chapter 2, showed that the most commonly used biocompatible polymeric materials for constructing varying medical stents comprise of polylactic acid (PLA), polyglycolic acid (PGLA), polyvinyl alcohol (PVA), polycaprolactone (PCL), and blends of polyethylene glycol [153]. Polylactic acid (PLA) is a biodegradable thermoplastic that is derived from renewable resources, such as corn starch, tapioca roots, or sugarcane and is widely employed in various biomedical devices [186]. Therefore, in this work PLA is selected as the biodegradable thermoplastics to be used for developing a 3D printed prototype intranasal stent.

### 3.2.3. Design selection

There are various key requirements that were established to develop a design selection criterion to evaluate potential concepts. These concepts were devoped after evaluating various literatures for drawbacks in the present post-operative care options currently available in the market. Furthermore, these key requirements were established after meeting with Dr. Jim Bartley, the surgical advisor. This meeting was necessary to

establish early boundaries for the project and design recommendations that could be developed into a design criterion to assist in creating the most functional possible solution for surgeons to apply as treatment to their patient. The characteristics are as follows;

1. Structural support for the nasal passageway.
2. Easy deployment of compressed intranasal stent into the nose.
3. Ease of breathability for the patient when the stent is in its expanded form within the nose.
4. Easy manufacturing capability.
5. Biodegradable polymer to be used.
6. 3D printable structure.

### 3.2.4. Nasal physiology - Intranasal device location

The design process or the intranasal stent focuses on its functionality. This is defined by its expansion upon displacement from the deployment mechanism into the required location within the nose. It was determined, after discussing with Dr. Jim Bartley an ENT surgeon, that the intranasal device would be inserted through the vestibule and up into the nasal cavity where it would then pass through and sit in the passageway connecting the middle meatus to the maxillary sinus (Figure 3.2 and 3.3). It is well known from literature that a patient suffering from recurring CRS will need to undergo FESS if conventional treatments fail. The aim of the surgery is to remove the infectious material by draining it through the middle meatus by passing through the semilunar hiatus and out through the nasal cavity [187].

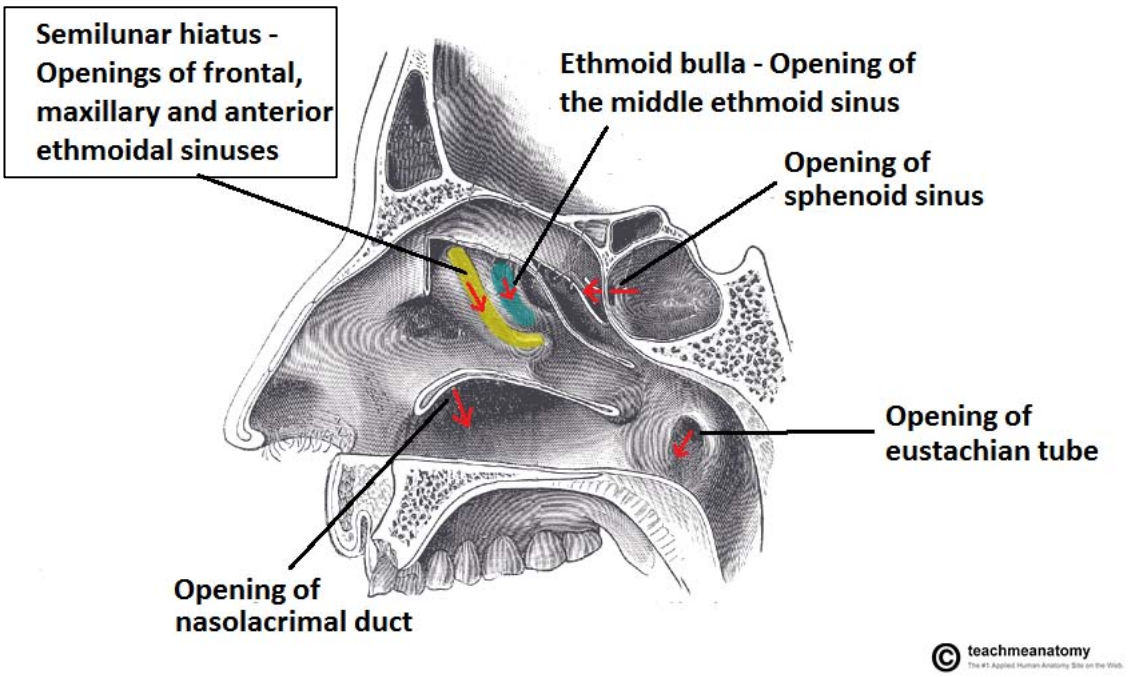


Figure 3.2: The conchae have been removed, showing the semilunar hiatus and various openings on the lateral wall of the nasal cavity (Adapted from [188]).

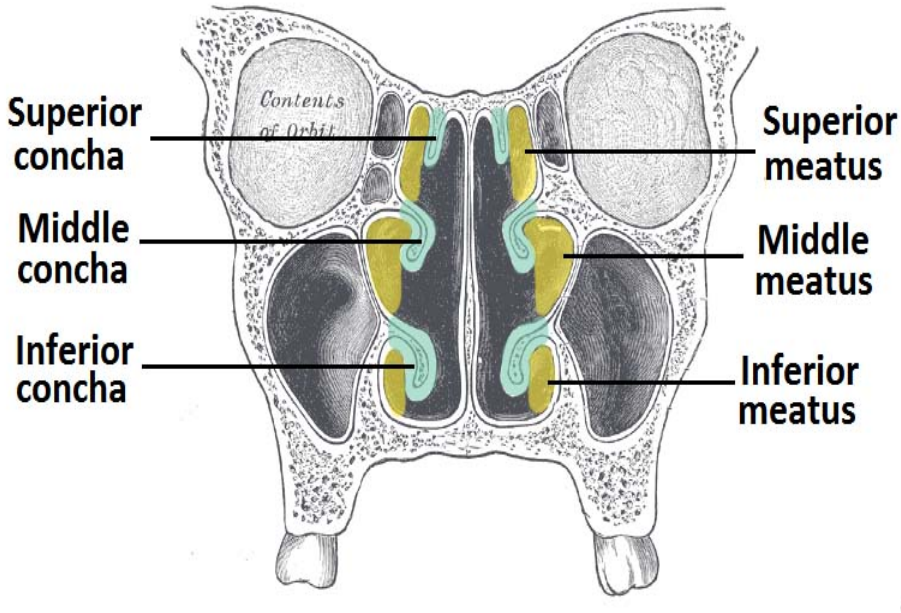


Figure 3.3: Coronal section of middle meatus (adapted from [188]).

## 3.3. Design concepts research

The following sections review potential stent configuration based on different concepts to evaluate which one would ideally provide the functionality required to create the prototype intranasal stent.

### 3.3.1. Folding structure-origami

Recently, the ancient art of paper folding known as origami has been studied on a mathematical level covering basic principles of origami design, kinematics, and structural properties [189, 190]. Diverse folding methods can be achieved by using six Huzita Axioms (HAs) and one Hatori Axiom [190, 191]. The axiom outlines a folding method by merging pre-existing points and lines together. Hence, with the development of advanced computational simulation technology, the testing of an origami design can be improved with reduced development cost [192]. Currently, parametric graphical software such as Tree Maker [193], Origamizer [194], Rigid Origami Simulator [195] and E-origami system [196] can transform an origami design into reality within hours when combined with modern 2D and 3D rapid prototyping techniques. Origami design can be transformed either into a flat or expanded forms just with folds in the paper. In such a case, origami folds can be used in transforming a functional form to a compact form for storage. Using this concept space abiding packages and furniture have already been created [197]. Hence, design concepts created from origami could be used to create collapsible medical devices that can be designed in a way to reduce manufacturing costs by requiring fewer materials and simpler construction technique. Additionally, an origami-based structure created for a minimally invasive surgical device could be inserted into the body in its compact form through a small incision, be placed in an inaccessible area of the body and then upon reaching its destination, it can expand into its functional form [197, 198].

### 3.3.2. Miura-Ori tessellation

The Miura-Ori or the Miura fold named after Koryo Miura is a flat-foldable origami tessellation [199]. In Miura-Ori fold, the shape of the structure can be transformed when the initial parameters of the structure were determined by futher modification of the dihedral angles between the foldable panels [200]. The Miura-Ori method has been

used in folding of deployable structures for various applications because of its simple design and efficient performance [201]. The Miura-Ori tessellation in Figure 3.4 and Figure 3.5 is a captivating structure, where a folding ball is created out of this unique pattern. This folded ball displays an expanding force and in its compressed form this design could be potentially applied to develop an intranasal stent.

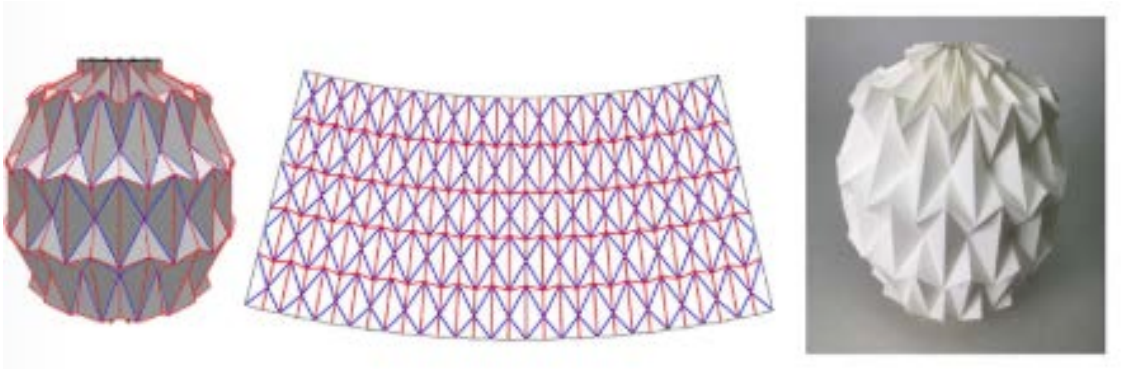

Figure 3.4: Fabricated Miura-Ori Tessellation sphere (adapted from [202]).

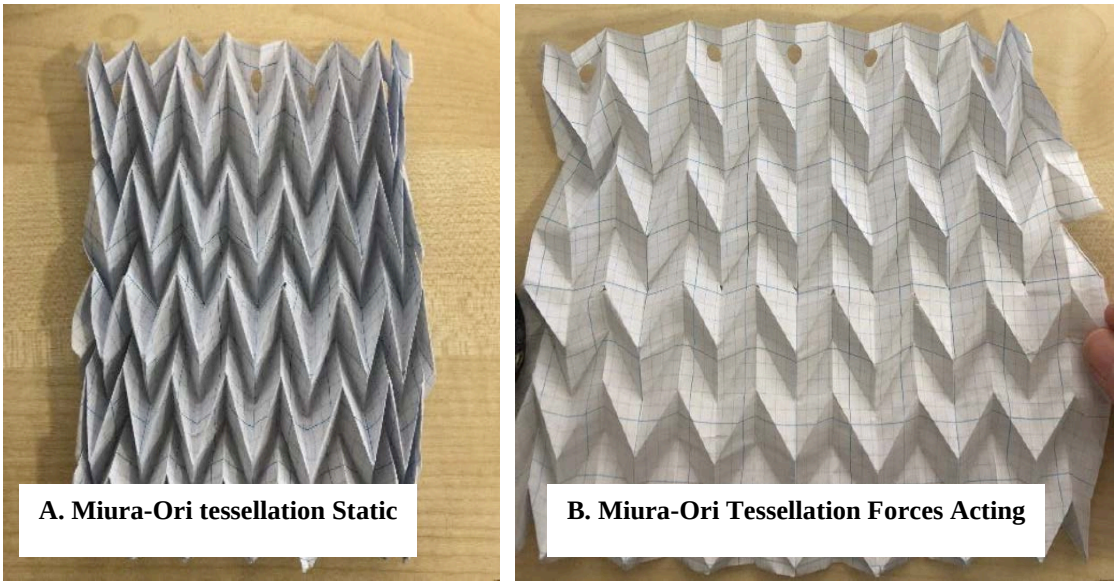


Figure 3.5: Above in Figure A) we see the Miura-Ori tessellation pattern in resting form with no external forces applied, and in Figure B) we see the tessellation pattern when an external pull force is applied lengthwise along the X-axis which also causes the folds to expand outwards along its Y-Axis.

### 3.3.3. Miura unit cell geometry

A Miura unit cell can be defined mathematically in several ways. Here we define the unit cell by the dimensions of the pattern's smallest component, a parallelogram. The parallelogram is made up of sides a, b, acute angle $\gamma$ and dihedral fold angle $\theta \in [0, \pi/2]$

between one side and the *xy* plane (Figure 3.6). For materials such as the Miura-Ori tessellation pattern the mechanical properties are usually characterized in a partially folded state [203]. The outside dimensions for a Miura-Ori unit cell in a partially folded state can be represented with the following mathematical equations.

1. $\boldsymbol{H = a.\sin\theta \sin\gamma}$
2. $\boldsymbol{S = b.\frac{\cos\theta \tan\gamma}{\sqrt{1+cos^2\theta\ tan^2\gamma}}}$
3. $\boldsymbol{L = a.\sqrt{1 - sin^2\theta\ sin^2\gamma}}$
4. $\boldsymbol{V = b.\frac{1}{\sqrt{1+ cos^2\theta\ tan^2\gamma}}}$

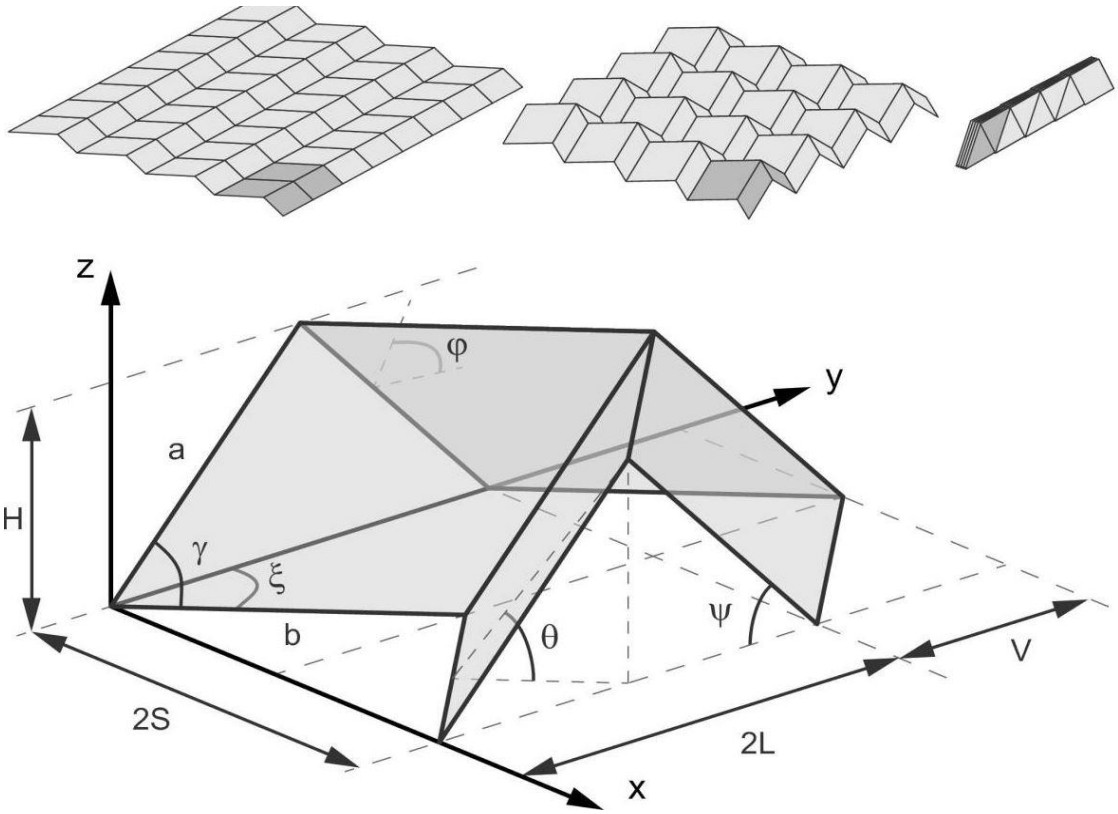


Figure 3.6: All three figures are representation of the geometric parameters of a Miura Unit Cell (adapted from [204]).

### 3.3.4. Orimetric rubberised origami

This soft moulded plastic structure motivated by traditional Japanese paper folding origami make use of intelligent patterns to save material and create an extremely elastic computational structure (Figure 3.7). The Orimetric rubberized origami features a moulded auxetic memory material that allows the folds of the structure to collapse easily when compressed in lengthwise directions yet offers high deformations when

compression is perpendicular to the sheet. This structure can retain its originally designed profile no matter the forces acting on the material [205].

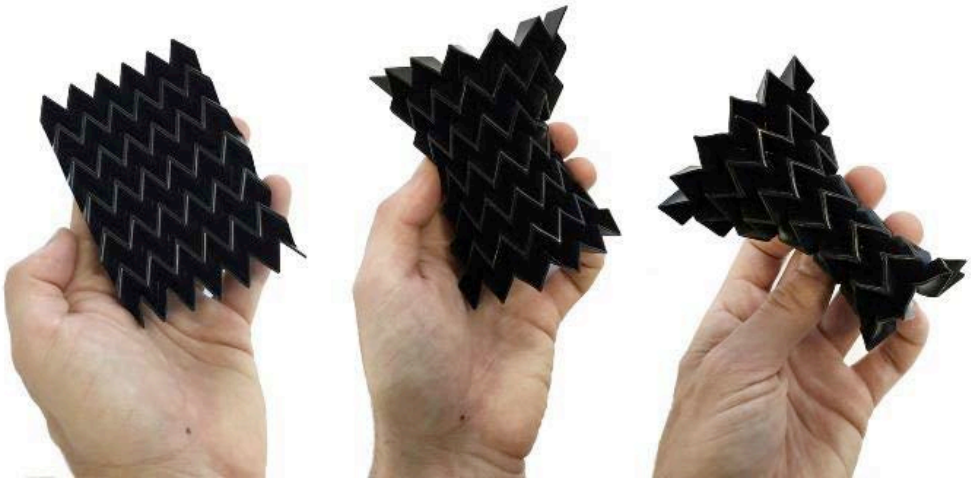

Figure 3.7: Orimetric rubberized origami (Adapted from [206]).

### 3.3.5. Auxetic structures

Normal structural materials contract laterally when they are stretched in the longitudinal direction, but auxetic materials are contradictory as they expand laterally when stretched longitudinally and becomes thinner when compressed [207]. Materials exhibiting auxetic properties have a negative Poisson's ratio and even when an external force is applied, this materials has the ability to recover elastically. A very wide range of materials can be used to fabricate auxetic structural form including metallic foams, fibre reinforced composite laminates and polymers [208]. In relation to biomedical application, auxetic materials (microporous and cellular) are used in a dilator for opening the cavity of an arterial vessel to be used use in coronary angioplasty and related procedures. From Figure 3.8, the lateral expansion of a flexible auxetic polytetrafluoroethylene (PTFE) hollow rod or sheath under tension is used in opening the artery [209].

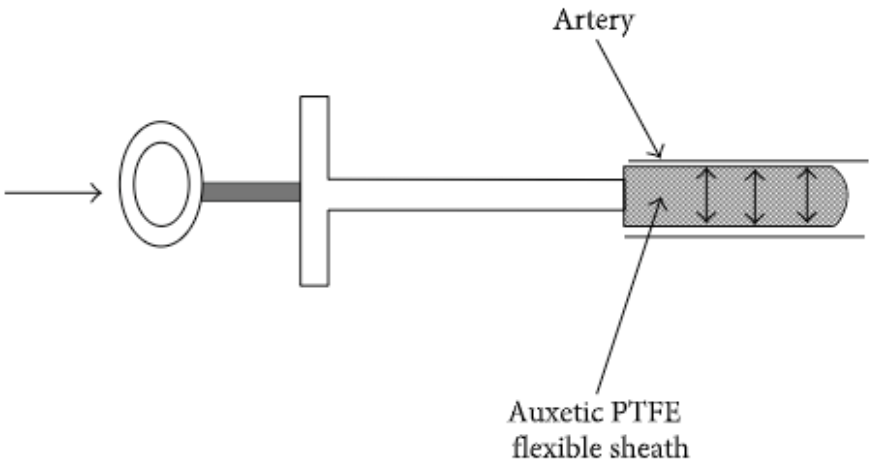


Figure 3.8: Dilator employing an auxetic end sheath (adapted from [209, 210]).

For this project, therefore auxetic pattern structures still needs more research for it to be developed for use in a suitable 3D intranasal stent. Hence, auxetic pattern could be an exciting research topic for future projects, but since this pattern can cause hindrance in the breathability for the patient it was not considered in this project.

### 3.3.6. 3D printed structures

Fused Deposition Modelling (FDM) is an additive manufacturing process that is widely implemented for 3D printing of solid objects. FDM technology based on fused fibre material deposition has recently become one of the widely used rapid prototyping methods for various applications as it is cost effective for companies and individuals to invest in. This technology offers the prospect to design and introduce new materials, including composites that can be generated from commonly used FDM materials such as acrylonitrile butadiene styrene [211], polycarbonate (PC), polylactic acid (PLA), polyphenylsulfone (PPSF), polycaprolactone (PCL) and poly-vinyl alcohol (PVA) [212]. The capability of this technology to introduce new materials for rapid prototyping in this way are vast.

### 3.3.6.1. Living hinges

Living hinges are thin section of hinge made from an extension that acts as a connection between two parent structures and are usually made from polymers or plastics. Typically, the parent plastic pieces and the living hinge "bridge" will form one continuous piece of plastic. The flexibility and thinness of the living hinge enables the hinge to rotate about one axis 180 degrees or more without breaking. Usually, traditional hinges involves assembly of multiple parts, but living hinges present a purposeful fault line at a predetermined point in the material which is carefully designed such that it doesn't fail after repeated bending [213].

When a hinge closes it is exposed to bending forces with the outer surface of the hinge being placed under tension which causes it to stretch and the inner surface to compression forces. To account for these forces, the living hinge should have a long-curved length on the outer surface and a short inner surface as shown in Figure 3.9 [214].

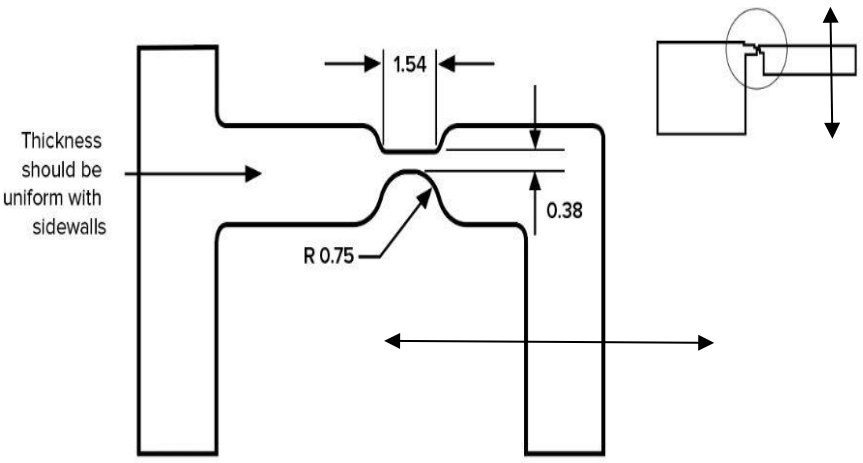


Figure 3.9: Example of injection moulded living hinge demonstrating this principle (adapted from [214]).

### 3.3.7. 4-Dimensional (4D) printing

4D printing, is a new field with various potential applications. 4D printing ability relies on an applicable combination of smart materials in the three-dimensional space with mathematical modelling for the design of the distribution of multiple materials in the

structure (Figure 3.10). 4D printing describes the process of achieving's self-assembly, multi-functionality and self-repair as it is time-dependent and printer-independent [215].

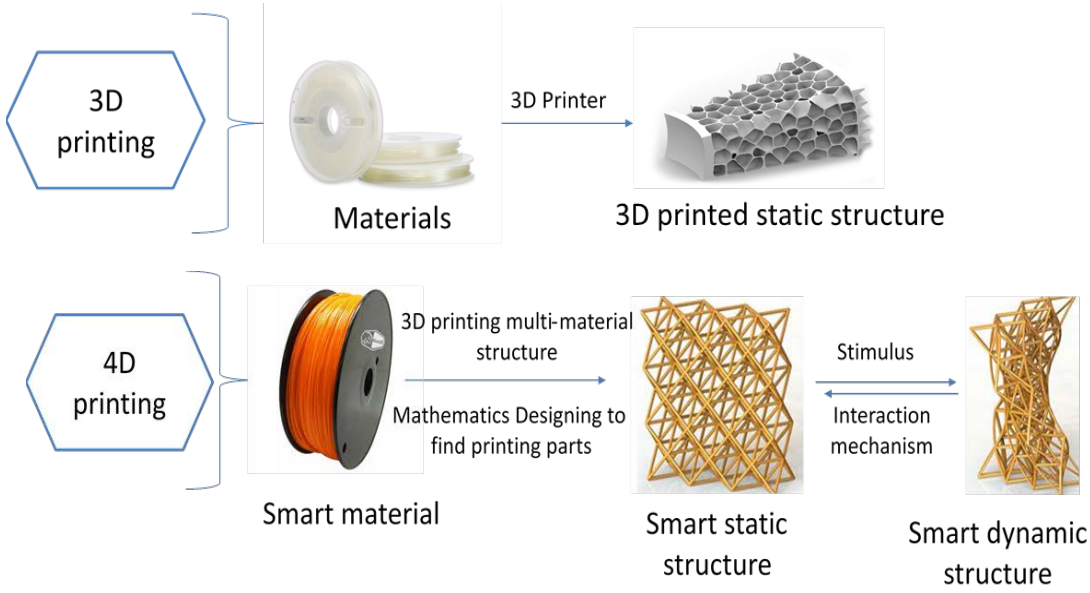


Figure 3.10: The general outline of 3D printing and 4D printing considering both materials and processes (adopted from [215]).

#### 3.3.7.1. Water sensitive 4D structures

Water sensitive 4D structures, are printed with two different materials, with water-absorbing material being printed on one side and a rigid waterproof material on the other side. When the printed structure was immersed in water, the water-absorbing material takes up about 150% volume of water; however, the waterproof material remained unchanged causing the structure to bend toward the rigid side. Finally, after reaching the final-state configuration when rigid elements contacted each other the 4D folding halts [216]. Hence, a 4D printing design could be beneficial for the development of biomedical stent.

## 3.4. Initial concept's evaluation

### 3.4.1. Expanding stent with solution

In this design, the stent features an external film coating that will expand when filled with saline solution while allowing airflow through the stent (Figure 3.11). A small extension tube is used to ensure the needle of the syringe doesn't directly reach into the patient's nasal cavity. A one-way valve will allow the syringe to deliver saline solution to the stent for expansion purposes. Afterwards, the syringe is then withdrawn from the stent and the valve prevents solution from leaking out. With this design, the main limitation would be the swelling and degradation of the film coating when it takes up water which can compromise the structure leading to the failure of the stent to properly support the nasal passageway. This limitation, however, could potentially be offset by using a bio-compatible cross linker to reduce film degradation or by increasing the compound ratio of hydrophobic and hydrophilic natural biomaterials along with a bio-compatible cross-linker to extend the film coating life span.

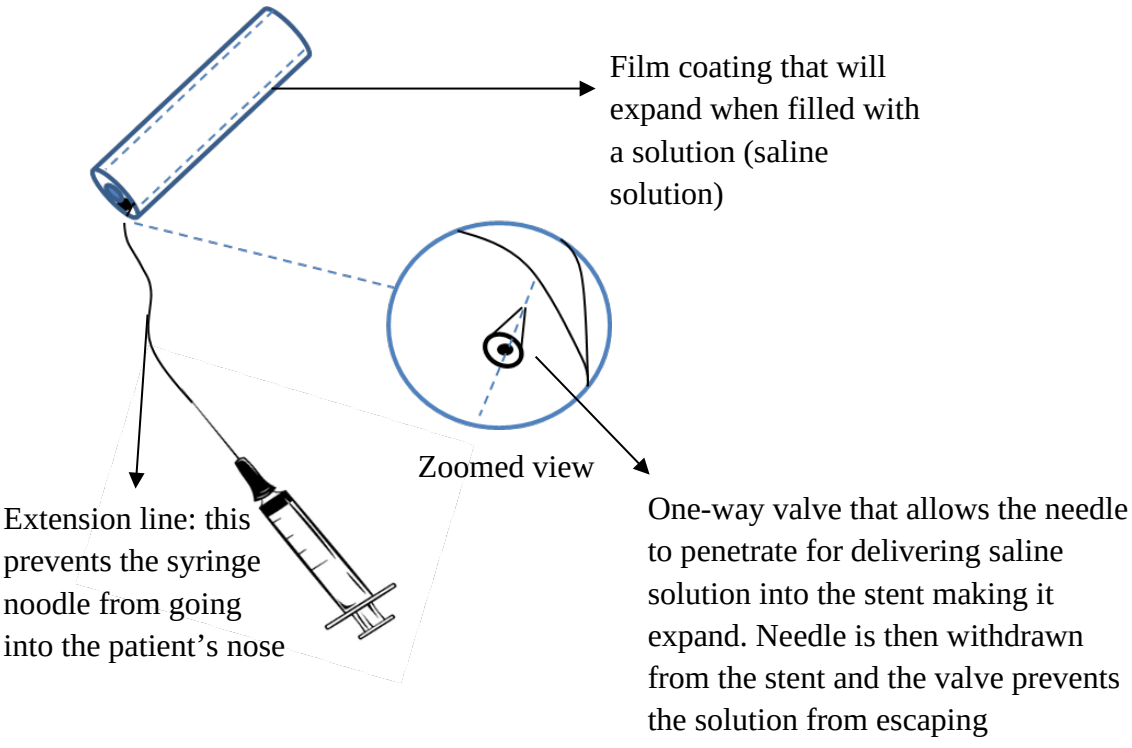

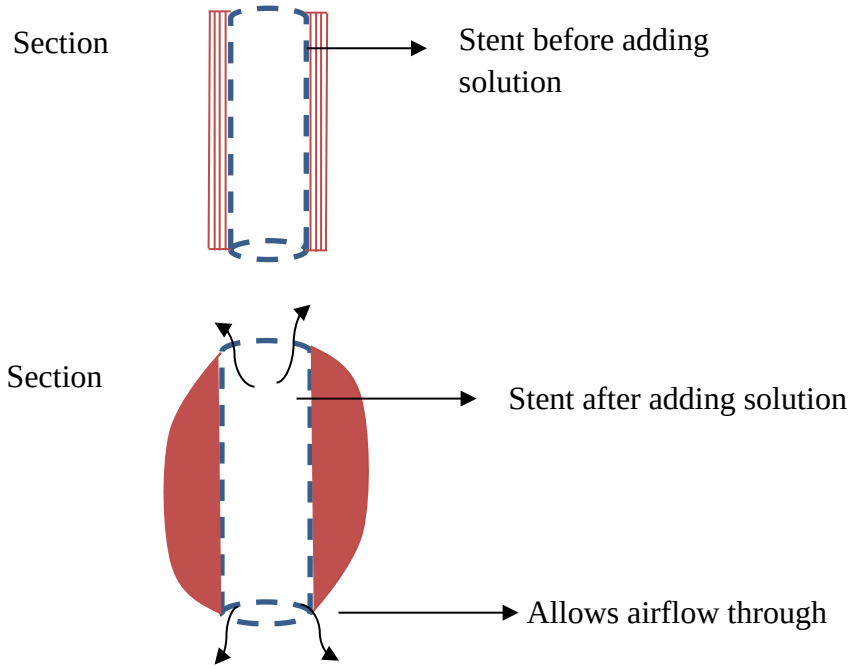


Figure 3.11: Expanding stent with solution.

### 3.4.2. Flexible weave stent

This design was inspired by an existing nasal stent developed by Alaxo Gmbh featuring a nitinol braid weave that provides the required force to keep the nasal passageway open while the patient sleeps to treat obstructive sleep apnea (Düring, 2018).

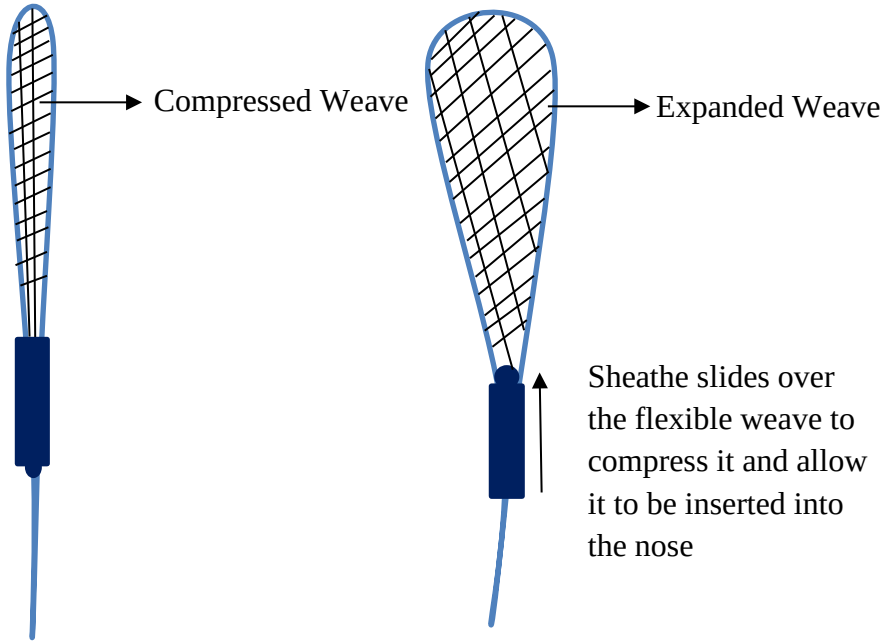


Figure 3.12: Flexible weave stent.

For this study, the stent (Figure 3.12) features a plastic sheathe that slides over the flexible weave that is compressed before insertion into the nasal passage. In this design, the flexible weave expansion mechanism can be adjusted by removing sheathe while allowing airflow through the stent. Also, the cable attachment clipped to the end of the stent can be easily removed once the stent has expanded. This flexible weave can be made from compound biomaterials (materials combined either between different natural or synthetic polymers).

### 3.4.3. Rod and ball stent

This design (Figure 3.13) features a stent that expands when a round node attached to a rod is forced through the stent. When the stent reaches an appropriate level of expansion against the nasal passageway the rod is twisted, releasing the rod and locking the stent in place. This further solidifies the expansion of the stent while allowing the rod to be easily removed for the nasal cavity creating an open passageway for tidal breath.

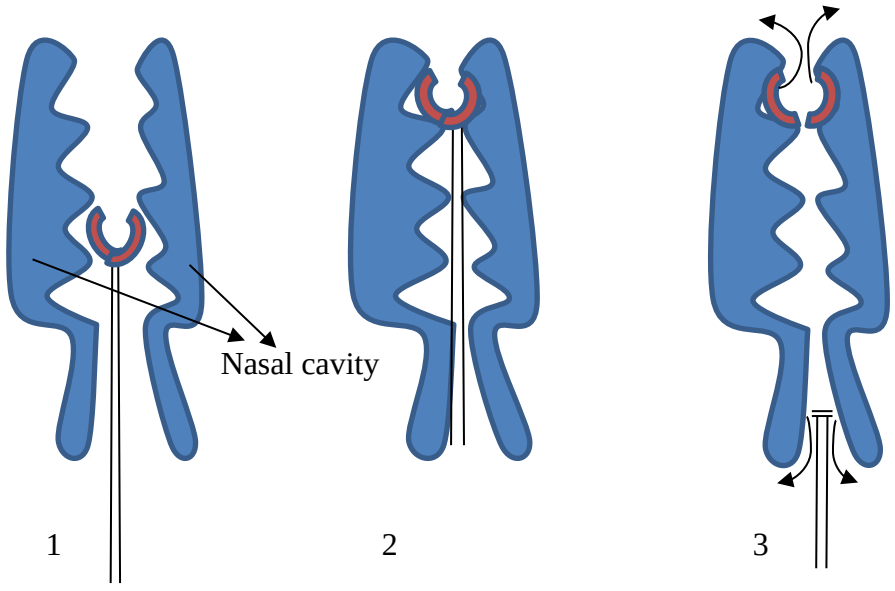


Rod is pushed through the stent making it expand pushing up against the nasal cavity

Rod is pushed until the stent reaches an appropriate level of expansion, where the rod will be twisted and dislodged releasing the stent

Airflow can take place once the rod has been removed

Figure 3.13: Rod and ball stent.

However, a limitation with this strategy is the lack of porosity in the design which would hinder breathability for the patients. This problem can be overcome by designing a stent with many holes to allow for maximum air flow without restriction.

### 3.4.4. Miura-Ori concept 1

This design features a unique Auxetic origami structure adapted into a stent design concept. From Figure 3.14, a lot of ridges on the design can be observed which is mainly due to the folds of the Miura-Ori pattern. These folds will provide a certain level of friction in the nasal passageway to assist in keeping the stent static. The Auxetic nature of the stent will enable it to withstand the nasal passageway compression due to the defects added in evenly spaced locations around the stent's circumference. These defects in the Miura-Ori pattern works in such a way by preventing the stent from closing completely thus keeping the nasal passageway open for breathability.

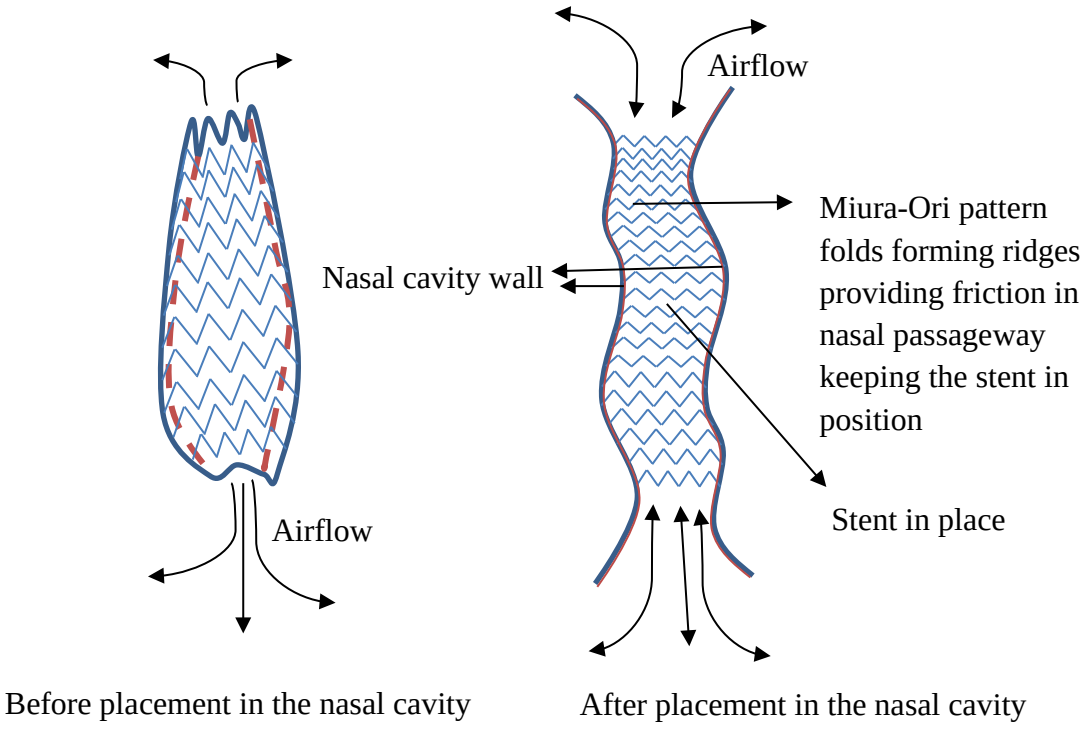


Figure 3.14: Miura-Ori concept 1.

The advantage of this design would be that any minor contraction that can occur in the patient's nasal passageway should have no negative impact on the stent structure due to its auxetic nature. Both this and its flexibility should improve patient comfort and breathability.

### 3.4.5. Miura-Ori concept 2

The main drawback with the Miura-Ori concept 1 is the lack of porosity that could make it difficult for a patient to nasally breathe. As such, there was a need to improve on this previous concept. In this design (Figure 3.15), porosity in the structure is achieved by adding extruded cuts through the pattern panels while leaving enough material for the design and folds to still be functional.

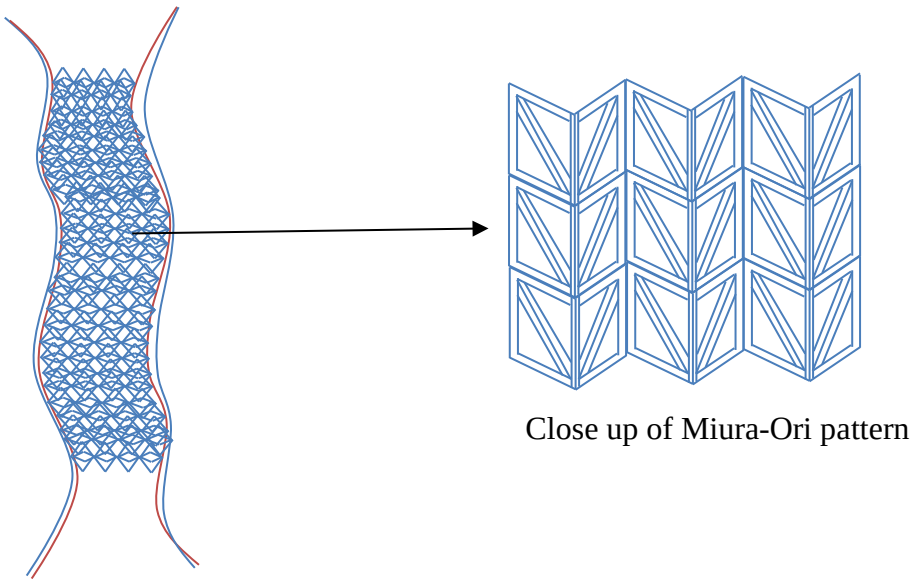


Figure 3.15: Miura-Ori concept 2.

## 3.5. Evaluation of concepts

From the first meeting with the surgeon we were able to establish several key requirements for a potential nasal stent design. The final design needed to accomplish the following criteria for the project to be deemed successful;

1. Provide enough structural supportability to the nasal cavity

2. Expand easily in the nasal passageway with the use of tool and/or mechanism
3. Provide a way to locally release drugs to the patient
4. Allow the patient to have maximum breathability with stent in place
5. Be comfortable for the patient

After the meeting with the surgeon and the assistance of David from the Bio design lab, a Design Selection Criteria was developed to weight potential concepts against the key attributes. Throughout the project continued guidance from the surgical advisor and David was essential in developing a solution in accordance to the medical requirements. Finally, to evaluate the different concepts a table (Table 3.1) was created to determine the best possible design functions and components that can be developed further for the final design.

Table 3.1: Selection criteria for designing concepts.

| **Selection criteria** | **Weight (%)** |
|---|---|
| Ease of breathing | 20 |
| Ease of installation | 15 |
| Ease to manufacture | 15 |
| Structural supportability | 20 |
| Comfort level | 15 |
| Bio-degradability | 15 |
| Total | 100 |

Table 3.2: Evaluation of various design concepts based on the requirements of an ENT surgeon for developing an expandable intranasal stent (Rating: 1 = poor and 10 = Excellent).

| Selection criteria | Expanding stent with solution | | Flexible weave stent | | Rod and ball stent | |
|---|---|---|---|---|---|---|
| | Rating | Weighted score | Rating | Weighted score | Rating | Weighted score |
| Ease of breathing | 4 | 0.8 | 10 | 2 | 4 | 0.8 |
| Ease of installation | 8 | 1.2 | 8 | 1.2 | 8 | 1.2 |
| Ease to manufacture | 3 | 0.45 | 7 | 1.05 | 8 | 1.2 |
| Structural supportability | 7 | 1.4 | 7 | 1.4 | 7 | 1.4 |
| Comfort level | 6 | 0.9 | 7 | 1.05 | 3 | 0.45 |
| Bio-restorability | 7 | 1.05 | 8 | 1.2 | 4 | 0.6 |
| Total score | | 5.8 | | 7.9 | | 5.65 |
| Rating | | 5 | | 2 | | 6 |
| **Continue development?** | | **No** | | **Yes** | | **No** |

| Selection criteria | Compress and clip stent | | Miura-ori stent 1 | | Miura-ori stent 2 | |
|---|---|---|---|---|---|---|
| | Rating | Weighted score | Rating | Weighted score | Rating | Weighted score |
| Ease of breathing | 8 | 1.6 | 6 | 1.2 | 10 | 2 |
| Ease of installation | 8 | 1.2 | 6 | 0.9 | 6 | 0.9 |
| Ease to manufacture | 5 | 0.75 | 8 | 1.2 | 8 | 1.2 |
| Structural supportability | 8 | 1.6 | 9 | 1.8 | 9 | 1.8 |
| Comfort level | 6 | 0.9 | 8 | 1.2 | 9 | 1.35 |
| Bio-restorability | 7 | 1.05 | 8 | 1.2 | 8 | 1.2 |
| Total score | | 7.1 | | 7.5 | | 8.45 |
| Rating | | 4 | | 3 | | 1 |
| **Continue development?** | | **No** | | **No** | | **Yes** |

## 3.6. Prototype intranasal stent design

After evaluating various concepts options of compressed and expanded forms of the intranasal stent, the flexible weave stent and Miura-Ori design seemed to be the two most promising concepts. But due to the size limitation of the Miura-Ori pattern and unavailability of the required manufacturing machinery for the flexible weave stent, it was difficult to manufacture these two-stent design using conventional method available at the university. This led to the development of a design with a simple expansion mechanism that would be easily manufacturable with the 3D printers available.

For this project, based on the key design selection criteria mentioned in Tables 3.1 and 3.2, the stent design was finally conceived featuring a 3-part mechanism assembly that allows the nasal stent to exist in two forms; ‘relaxed’ and ‘expanded’ state indicating that the stent can be forced to a smaller size that can be easily deployed into the nasal passage. The main nasal stent design features a cage like shape with six limbs evenly spaced attached to two tapered conical revolves allowing the stent to be flexible. This flexibility and expansion characteristic of the intranasal stent after being deployed with in the nasal passageway enables the stent to conform to an individual’s unique nasal geometry thus improving patient’s comfort and breathability. Figures 3.16 and 3.17 show images of the intranasal stent in its relaxed and expanded form respectively.

Figure 3.16: Extended form of the final intranasal stent design.

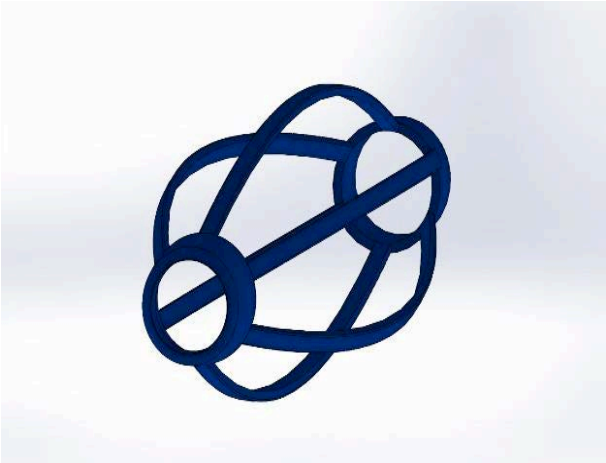

Figure 3.17: Relaxed from of the final intranasal stent design.

Figure 3.18 shows a close-up image of the spring stent component of a 3-Part mechanism. In Figure 3.18, we can observe the nasal stent (blue stent) slides onto the installation device (red tube) until it engages into a groove. At this point, the nasal stent can be grasped and stretched by sliding it up the installation device reducing the size of the stent. Lastly, the deployment tool (green tube) is then inserted into the installation device which forces the hinges to attach the nodes outwards locking the nasal stent in place. The intranasal stent can then be inserted into the nasal passageway in the correct location as determined by the ENT surgeon. When the stent is deployed to spring open, the installation device and deployment tool is then removed by releasing the lock mechanism allowing the nasal stent to expand and support the nasal cavity as required.

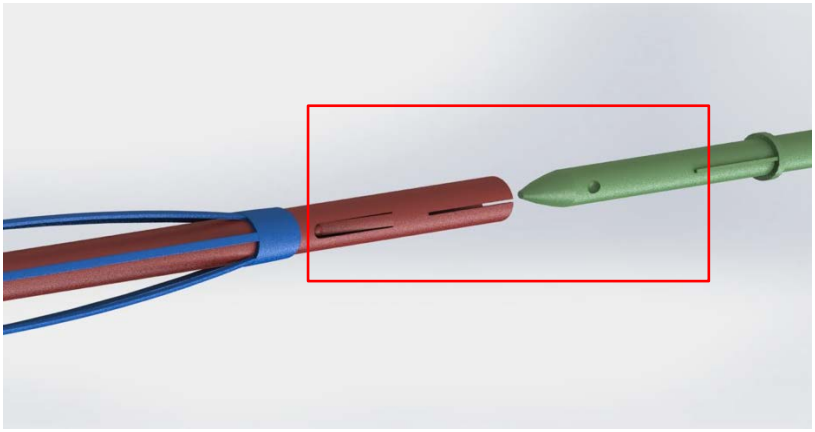

Figure 3.18: Close up image of the 3-part mechanism.

Finally, in Figure 3.19 we can observe the image of the intranasal stent in a compressed locked position frame as the mechanism is being released but just before the stent has had a chance to expand. This image clearly shows the node on the installation device will lock the nasal stent in a contracted position.

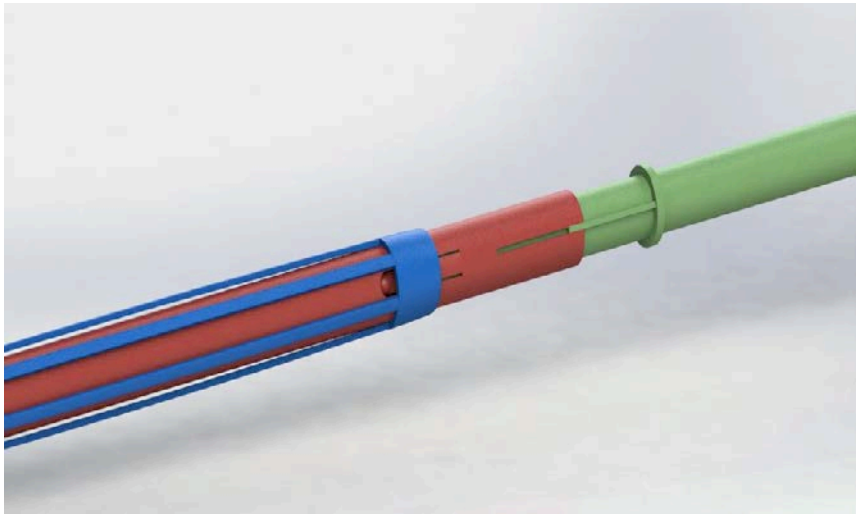

Figure 3.19: Intranasal stent in a compressed locked position.

## 3.7. Detailed drawing of the prototype intranasal stent

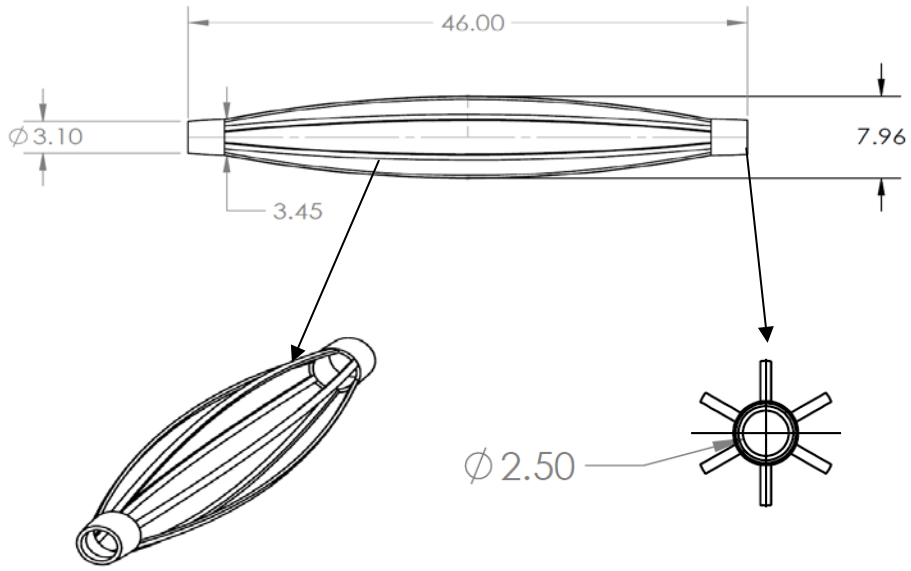


Figure 3.20: Detailed drawing of the prototype intranasal stent (Unit = mm).

## 3.8. Pictorial representation of the stent in a 3D printed nasal model

A 1½ x scale of the nasal model was designed using a high-resolution magnetic resonance imaging (MRI) scan data obtained under Ethics approval AUTEC. The selected scan data exhibited healthy paranasal sinuses with no indication of inflammatory changes. The selection criteria did not consider scans from individuals with deviated septum, inflammation or swelling of the lining of the nasal passages and sinuses as it would create narrowing of the nasal corridor and thus inhibit the ability to insert the intranasal stent into the phantom. Using the MRI scan data, the digital processing of the nasal model is processed by using scan IP software. The rapid prototyping machine used for fabricating the nasal model template was based on a fused-deposition modelling (FDM) technology. The material selected for fabricating the nasal model template is, acrylonitrile butadiene styrene [ABS] for durability and reusability. The design time including MRI scan data import, segmentation and stereolithography (STL) file export takes 2 to 4 hours. The 3D printing time for a whole structure typically take about ~8 hours along with dissolving time of the supporting materials depending on the complexity of the structure. The cost of in-house fabrication in the AUT 3D printing lab is about $600 (NZD). The 3D printed physical model of the nasal model and prototype intranasal stent is shown in Figure 3.21.

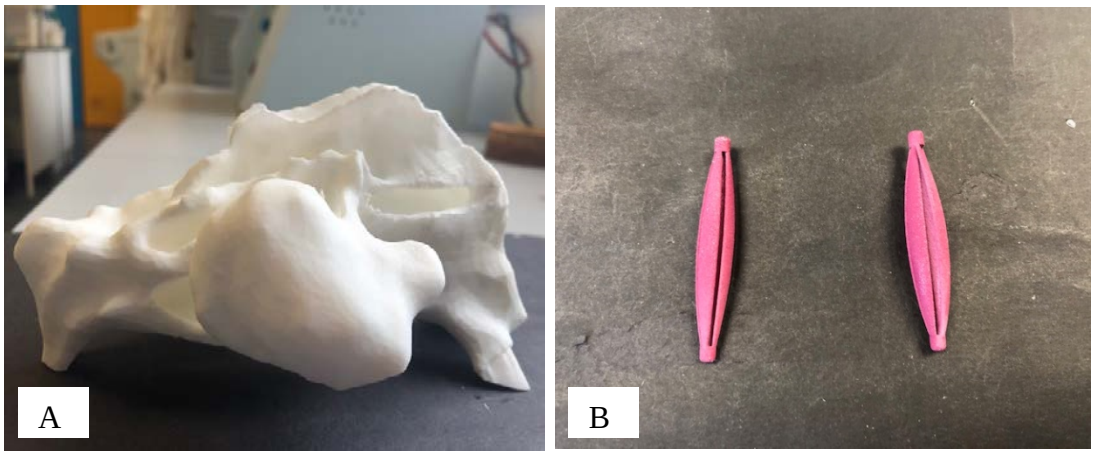


Figure 3.21: 3D printed model of the A) complete nasal and paranasal maxillary sinus and B) shows reduced diameter of the extended intranasal stent sample.

Figure 3.22 shows the intranasal stent (3D printed with Polylactic acid (PLA)) inserted into the 3D printed nasal cavity model to show a pictorial representation of the placement of the stent within the nasal cavity.

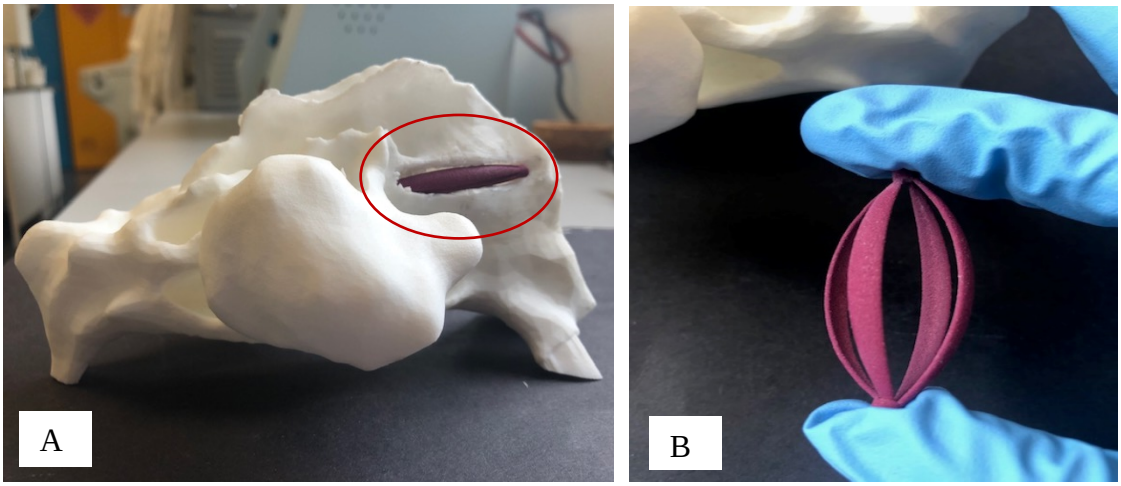


Figure 3.22: A) pictorial representation of the intranasal stent in a 3D printed nose and B) expanded form of the prototype intranasal stent.

## 3.9. Limitations

During the project, limitations were identified in the prototype design. Most of the designing objectives were achieved, however the initial prototype intranasal stent requires further development due to time and budget restraints and limitations of 3D printer available. For the full-size nose, the key struggle will be developing the stent deployment tool into a miniature size that would fit in the nasal passageway.

## 3.10. Conclusion

Based on literature research, gaps were identified in the post-operative care current treatments for patients after FESS surgery for CRS and through alternate expanded research, the required components were identified that could be combined to form a successful design. Applying design methodology while combining these various required components, a 3-part assembly mechanism for an intranasal stent was developed that addresses all the key requirements established in the design selection conditions. In this chapter, the design and development of the 3D printed intranasal stent that will provide a

structural support to the nasal cavity to prevent adhesions, enhances breathability for the patient over current treatment methods was successfully completed. This project displays the design and development of a complete functional prototype.

## 3.11. Future directions

Future work for the prototype intranasal stent with expansion mechanism is to focus on design optimisation and in validating the model through finite element (FE) analysis and experiments. FE is a tool used for computational analysis of various designed stents/medical devices by providing stress distributions within the stent. The analysis can also carry out simulation contact between the stent with other structures such as the intranasal stent and nasal passageway and the simulation can account for elastic, plastic, and other properties of the stent. For this project, a preliminary assumption on the analysis of the stent was carried out based on an elliptical leaf spring as each of the limbs in the stent design is similar in shape and function to the elliptical leaf spring. However, these preliminary assumptions are subject to change in all dimensions hence the data was not shown in this chapter. For the purpose of this study, designing a functional prototype was the main focus rather than perfecting the complex physics of stenting. Hence in the future, when a physical model with the right bio-resorbable and bio-material has been chosen and developed, further design optimisation along with appropriate FE and experimental testing will be carried out.Therefore the design and development of a complete functional prototype intranasal stent was carried out in this chapter while addressing all the key requirements established in the design selection conditions. From the next chapter onwards, specific independent experimental objectives of the intranasal stent will be carried out. **Chapter 4** presents the first technique of the independent experiment examining the development of drug loaded composite thermoplastic blend that can be used for 3D printing drug eluting implants.

# Chapter 4. Development of thermoplastic polymer blends for 3D printing dexamethasone-releasing implant.

Results from **Chapter 3** demonstrate the development of a complete functional prototype intranasal stent. In **Chapter 4**, the first independent objectives of the experimental technique for the development of drug loaded composite thermoplastic blend was investigated so that this formulation can then be used in future studies for 3D printing the intranasal stent (Figure 4.1).

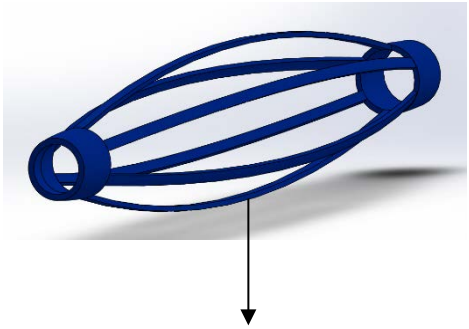


Figure 4.1: Diagrammatical representation of the DEX loaded composite thermoplastic for 3D printing intranasal stent.

## 4.1. Introduction

### 4.1.1. PLA and PVA polymers in biomedical applications

Polymers are the most widely used materials in biomedical applications due to their biocompatibility and varying mechanical properties with the capability to be able to control these properties by composition and fabrication of varying polymer materials making it an added benefit. Over the past decade, the use of biodegradable composite polymers for the administration of pharmaceuticals and biomedical devices have played an important role in the treatment of diseases [217]. The good processability, biocompatibility, biodegradability and mechanical properties makes polylactic acid

(PLA) a polymer with positive attributes for developing sutures, stents, drug delivery systems and tissue engineering scaffolds in biomedical applications [218]. Since PLA polymers are derived from the fermentation of renewable resources such as corn starch or sugarcanes, this makes PLA a versatile material with applications in various industries such as medical, textile, and packaging fields [219, 220]. PLA has high modulus and tensile strength but its low deformation at break and slow degradation process limits PLA in its applications. Recently from various literature in polymer studies, substantial research on changing the basic structure of PLA has been carried out by blending it with different polymers[221-227]. Lately, blending PLA with some hydrophilic polymers, such as starch, cellulose, pluronic [triblock copolymers of poly(ethylene oxide) (PEO) and poly (propylene oxide) (PPO)], polyvinyl alcohol (PVA), poly ethylene glycol [153] and hyaluronic acid have been carried out to study the blended polymer miscibility, morphology, physical properties, biodegradability and drug release properties [222, 228, 229]. For this study PLA is blended with PVA, since PVA is a favoured polymer due to its flexibility, biocompatibility, nontoxicity, biodegradability and has been widely used in research for various fields such as biomedicine, pharmacy and biosensors [137, 230-232]. Also, the hydroxyl groups in PVA can form hydrogen bonds with the ester groups of PLAs, favouring the miscibility or partial miscibility of their blend. Hence, in this study adding hydrophilic polymers such as PVA to accelerate the degradation of PLA while increasing the flexibility and hydrophilicity of the blend is of interest. From prvius literature, it was observed that the addition of a PVA can change the physical and/or mechanical properties of PLA material enhancing their elasticity while reducing their brittleness and shrinking for handling and storage, making it easier for manufacturing [233].

Melt blending of polymers with drugs is an alternative technique that can be used to improve the dissolution of insoluble drugs, develop controlled release formulations and

homogeneous mixtures. Some advantages of this process includes ease of use, lack of residual solvents, decreased environmental hazards, costs and the possibility of continuous processing [234-236]. Currently, several implantable medical devices made of various polymers/polymeric blends are widely used in the pharmaceutical field for local and controlled drug delivery. Hence, these PLA/PVA blends in this study can be prospective materials that can be used as future implantable drug carriers and functional materials of medical devices [237].

The purpose of this study is to prepare the PLA/PVA blends by a simple melt blending method. Melt blending or composite moulding of composite fillers and polymers has been used for various biomedical applications [238-240]. Melt blending method minimises the risk of toxicity as it is a solvent free process, where the molten polymer can function as a thermal binder during processing, reducing processing steps and time-consuming drying steps resulting in a more uniform dispersion of materials. Furthermore, materials composed of either PLA or PVA polymer respectively tend to be too flexible or too brittle. Therefore, the combined outcome of composites polymer may result in improved flexibility, thermal and mechanical properties as opposed to the neat polymer. In a study, Yeh et al., (2008) found that a compatible blend for PLA: PVA prepared by melt blending method is around the ratio of 80: 20, wt. %: wt. % [229]. In this context, Zhang et al., (2012) reported that increasing the PVA content from 10 to 80 wt. % in PLA/PVA blends produced a less smooth surface. This was attributed to an excessive PVA content that led to strong and extensive intermolecular hydrogen bonding, which in turn resulted in PLA aggregation [241]. Other reports showed higher development of pores for 50/50 PLA/PVA blends, suggesting the formation of two separate phases; a PLA-rich phase forming domains leading to porosity and a continuous PVA-rich phase. PLA/PVA blends with 20 wt.% of PVA tend to reduce mechanical properties of PLA. However, the addition of low quantities of PVA (10 wt. %) do not reduce the tensile strength in PLA/PVA

blends, because of better compatibility between PLA and PVA [223]. Hence, the objective of this study is to explore the feasibility of melt blending drug loaded composite polymer with PLA/PVA ratios: 100/0, 95/5 and 90/10 for preparing a bioresorbable, mechanically strong, thermally stable matrix while providing targeted sustained release of DEX.

## 4.2. Materials and methods

### 4.2.1. Materials

PLA (2003D grade) pellets were kindly supplied from Clariant Limited (Auckland, New Zealand), PVA powder (hydrolysis: 78.5–81.5 mole %, Mw: 120,000–132,000) was purchased from Chemiplas (Auckland, New Zealand), Dexamethasone (DEX, melting point – 262 °C) used as an anti-inflammatory drug was purchased from Zhejiang Xianju Pharmaceutical Ltd and Phosphate buffered saline (PBS) tablets were purchased from Sigma-Aldrich (Auckland, New Zealand). All other chemicals were analytical grade.

### 4.2.2. Sample preparation

The PLA/PVA blends were prepared by the melt blending method using a Brabender (Plasti-Corder Lab-station). Prior to the experiment, PLA, PVA and the drug were dried in vacuum at 80 °C for 6 h. For the preparation of blends, the mass ratios of PLA to PVA were chosen as 100/0, 90/5 and 90/10 ratios (w/w %). A determined amount of PLA and PVA mixture was put into the Brabender instrument with rotor speed and blending temperature at 100 rpm and 170 °C, respectively. To ensure PLA and PVA were blended completely, the operation lasted for 5 mins and using compression moulding films were formed with 15 MPa pressure for 2 mins. The films were then put into a dryer for cooling and standard specimens (2 x 2 cm) were cut from the films for characterisations. For drug loaded PLA/PVA samples, the films were prepared following the same processing conditions with 1 % (w/w) drug/polymer ratio was added into the mix during melt mixing (Table 4.1).

Table 4.1: PLA/PVA thermoplastic blended film formulation with different ratios.

| Formulation | Designation (w/w %) | DEX (w/w %) |
|---|---|---|
| PLA C | PLA 100 control | - |
| PLA WD | PLA 100 with drug | 1 |
| PLA/PVA C1 | PLA/PVA (95:5) control | - |
| PLA/PVA WD1 | PLA/PVA (95:5) with drug | 1 |
| PLA/PVA C2 | PLA/PVA (90:10) control | - |
| PLA/PVA WD2 | PLA/PVA (90:10) with drug | 1 |

#### 4.2.3. Metrological data

Samples were characterised in terms of thickness uniformity. Each, five specimens of size 2 cm × 2 cm of all PLA/PVA films were measured by using a digital calliper (0–150 mm, TD2082, Jaycar Electronics) at five different positions of the film with 0.001 mm of accuracy. Cross-section images of the samples were obtained by breaking the samples in liquid nitrogen into small squares, fixed on aluminium stubs using carbon tapes and sputter-coated with platinum for 20 s using a sputter coater (Hitachi E-1045, UK). SEM (Hitachi SU-70, UK) was used to observe the cross-sectioned morphology at an accelerating voltage of 5 kV and three specimens for each composition were used. After that, the samples qualitative elemental analysis of nitrogen (N), carbon (C), oxygen (O), and Fluorine (F) was performed using an Energy Dispersive X-Ray Analyzer (EDX) at 15 kV with Noran System 7 (NSS) microanalysis system software (Thermo Scientific).

#### 4.2.4. Thermal analysis

Thermal properties of the samples were determined using differential scanning calorimetry (DSC) (DSC Q1000, TA Instruments, NZ). An accurate amount of samples were weighed (5 mg) and subsequently sealed in aluminium pans. The tests were performed under nitrogen atmosphere at a heating rate of 10 °C/min between the temperature ranges of 30–220 °C. Additionally, thermal stability of pure PLA, PVA's and

their blends was evaluated using a Thermogravimetric analyser Netzsch TGA 209 F3 (Tarsus, Selb, Germany). TGA scans were carried out at 10 °C/min under nitrogen atmosphere (20 ml/min), from 35 to 600 °C.

#### 4.2.5. Tensile test

The tensile strength, Young's modulus and elongation at break of the samples were measured using a TA.XT plus texture analyser (Stable Micro Systems, Godalming, Surrey, UK) (HDP/90) with an initial distance between the grips of 30 mm and a crosshead speed of 0.5 mm $s^{-1}$. Three samples from each blend were cut (50 mm in length and 20 mm in width) and conditioned in a desiccator for 72 hours before analysis.

#### 4.2.6. Fourier transform infrared (FTIR) spectroscopy

FTIR spectra were obtained using a Spectrum Two PE instrument equipped with a horizontal attenuated total reflectance (ATR) crystal (ZnSe) (Nicolet iS10, Thermo Scientific, USA). The samples were placed directly onto the ATR crystal and spectra were collected in transmittance mode. Each spectrum was the result of the average of 32 scans at 4 $cm^{-1}$resolution. Measurements were recorded in the wavelength range of 4000–800 $cm^{-1}$ at 23 °C.

#### 4.2.7. *In vitro* degradation

The in vitro degradation tests under hydrolytic conditions were obtained by immersing the samples at 37 °C using a phosphate buffer solution (PBS), with a pH of 7.4 for 4, 10, 18, 32, and 42 days. Each sample was immersed in a 10 ml solution. The PBS was refreshed timely to maintain an approximate constant pH value. At predetermined time, the degradation media were removed, and the samples were blotted with wipes to dry off excess water, and then weighed on electronic balance (AUW220D, Shimadzu, Japan) and the mean weight was calculated.

### 4.2.8. Drug loading determination

For the determination of the drug loading for DEX, 2 x 2 cm cut film pieces weighting 274 mg were dissolved in 20 ml of a mixture of dichloromethane and methanol (5:3). Cut pieces were chosen from different area of the film, to ensure uniform distribution of DEX in the entire film. The amount of DEX was determined with UV spectrophotometer (Ultrospec 7000, Massachusetts, USA) using a calibration curve at an absorption wavelength of 242.3 nm (calibration equation was $y = 0.0243x - 0.0011$, $R^2 = 1$). The drug loading (DL) were calculated as typically reported.

$$\text{DL}\ (\%) = \frac{\text{Amount of drug}}{\text{Amount of polymer} + \text{drug}} \times 100$$

### 4.2.9. *In vitro* drug release

An *in-vitro* release study of different formulations of films with DEX was carried out in 40 ml of phosphate buffer solution (PBS). UV–Vis spectroscopy was used to determine the concentration and *in vitro* release of DEX under physiological conditions. First, the wavelength of maximum absorbance for DEX in PBS was measured ($\lambda max = 242.3$ nm) and then, standard solutions of DEX were prepared over a concentration range (0.5–30 µg/mL) to establish a calibration curve ($y = 0.0243x - 0.0011$, $R2 = 1$). The Limit of Detection (LOD) and Quantification (LOQ) [242] were calculated in order to describe the smallest concentration that can be reliably measured by UV–vis spectroscopy [243]. The values for LOD and LOQ were 0.312671 µg/mL and 1.042237 µg/mL, respectively.

*In vitro* drug release was carried out in physiological-simulated media (0.01 M PBS solution, pH = 7.4) under sink condition. The film was placed in a shaker containing buffer of pH 7.4 and speed was fixed to 100 rpm ± 5 at 37°C ± 0.5. Samples were withdrawn using 1 ml pipette at regular time interval. The volumes of withdrawn samples were replaced with buffer (pH 7.4) to maintain sink condition. The absorbance of the

samples was measured with a UV–Vis spectroscopy (Ultrospec 7000, Massachusetts, USA) at 242.3 nm. The release of DEX was quantified from a previously built analytical curve, designed from the plot of absorbance versus standard DEX solutions with known concentrations. From the value of absorbance, the percentage of drug release was calculated and graph of the cumulative percentage of drug release against time was plotted. Furthermore, drug release data were then fitted with different mathematical models.

#### 4.2.10. Statistical analysis

Data were subjected to one-way analysis [244, 245] of variant by means of a SPSS computer program (SPSS Statistic 20.0). Post-hoc multiple comparisons were determined by Tukey's test with a significance level set at $p < 0.05$. Error bars in the figures represent the standard deviation (SD).

## 4.3. Results and discussion

#### 4.3.1. Evaluation of drug loading

All composite blended films of PLA/PVA with different ratios (control and with drug) prepared by melt blending method had a smooth and almost opaque appearance while samples with higher PVA content has a cloudy appearance (Figure 4.2). For further testing's square pieces (2 x 2 cm) were cut from the films.

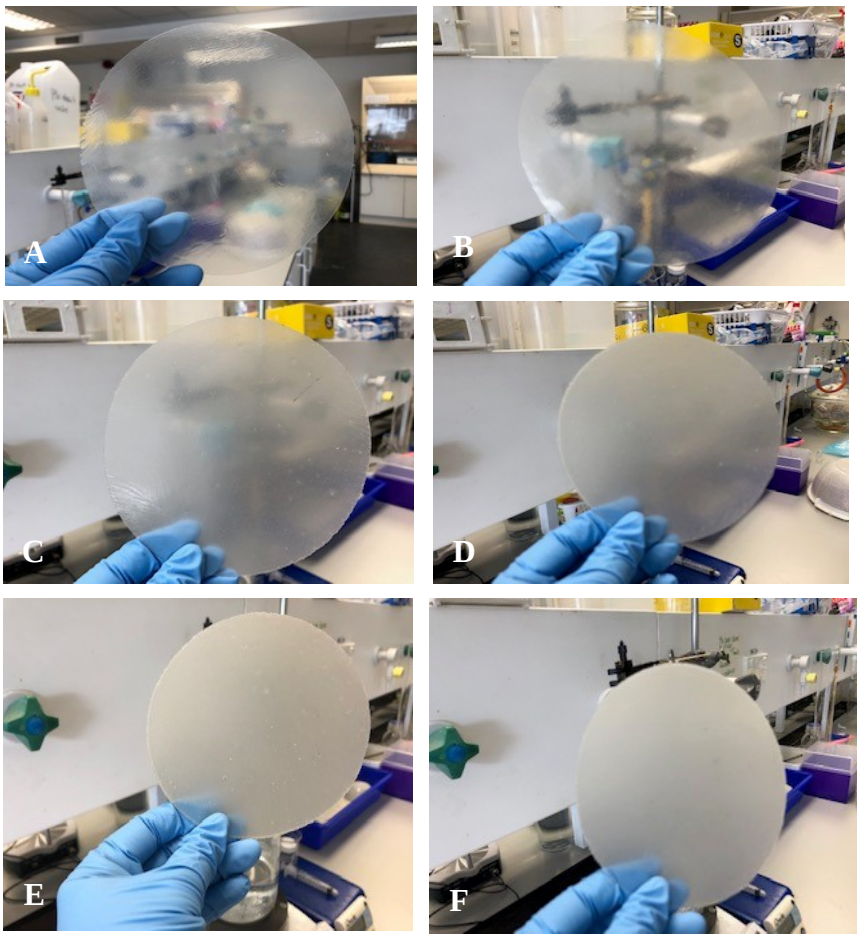


Figure 4.2: Photograph of different ratios of blended PLA/PVA films; A) PLA C (blank), B) PLA WD (with drug), C) PLA/PVA C1(blank), D) PLA/PVA WD1 (with drugs), E) PLA/PVA C2 (blank) and F) PLA/PVA WD2 (with drug).

It was observed in various literature [246-248] that drug loading efficiency of polymeric filaments prepared by passive diffusion of the drug into the ready-made filaments from a solvent was lower than the theoretical value, whereas melt blending of polymeric filaments at high temperature can also lead to unsatisfactory loading efficiency due to the thermal degradation of the drug. For this study, a temperature of 170 °C was used and the loading efficiency of DEX is shown in Table 4.2. The drug loading of all the cut films (2 x 2 cm) weighting 274 mg showed similar drug loading suggesting that composite polymeric mixtures can be processed by using melt blending method at a suitable temperature to produce solid dispersions (films)with sufficient loading efficiency.

Table 4.2: Drug Loading (DL) of 2 x 2 cm cut blended PLA/PVA films with theoretical DEX loadings of 1% w/w respectively ($n = 3$, mean ± SD).

| Polymers ratio | Theoretical drug loading of the whole film (%) | DL of 2x2 cm film (%) |
|---|---|---|
| PLA C | - | - |
| PLAWD | 1% | 0.026 ± 0.01 |
| PLA/PVA C1 | - | - |
| PLA/PVA WD 1 | 1% | 0.025 ± 0.01 |
| PLA/PVA C2 | - | - |
| PLA/PVA WD2 | 1% | 0.020 ± 0.03 |

### 4.3.2. Morphological studies of blended polymeric films

The morphological properties of composite polymeric films were observed using SEM. Figure 4.3 shows the cross-section of SEM images of pure PLA and PLA/PVA blends. In comparison to pure PLA, the blend of PLA/PVA showed porous morphology which is related to the partial miscibility nature of the polymeric blends. The content of PVA plays a significant influence on blends morphology, as blends with higher content of PVA have higher density of pores, indicating a greater phase separation, unlike blends containing less PVA. Increasing the PVA content in PLA/PVA blends can produce a rougher surface due to an extensive intermolecular hydrogen bonding, resulting in PLA aggregation [249]. Figure 4.4 shows SEM images of drug loaded samples. It can be observed that no drug particle was visible in PLA/PVA matrix after melt processing and re-aggregation of DEX within the polymer matrix did not occur after cooling down indicating that the drug was miscible and well dispersed within the host polymer matrix by thermal processing [176]. Furthermore, a qualitative analysis with EDX was also carried out to identify DEX in drug loaded PLA and PLA/PVA blend, and the results are shown in Table 4. 3. These results showed that dexamethasone fluorine anion (F) was present within the polymeric structures signifying the potential of melt blending method to fabricate drug loaded composite polymer for formulating individual dependent therapeutic doses [250].

Table 4.3: Atomic composition of PLA and PLA/PVA blend determined by Energy-dispersive X-ray (EDX spectroscopy).

| Atom (%) | C | O | F |
|---|---|---|---|
| PLA C | 55.59 | 44.41 | - |
| PLA WD | 55.52 | 43.77 | 0.61 |
| PLA/PVA C1 | 55.51 | 44.49 | - |
| PLA/PVA WD1 | 56.03 | 42.96 | 0.88 |
| PLA/PVA C2 | 56.13 | 43.87 | - |
| PLA/PVA WD2 | 55.49 | 43.63 | 0.73 |

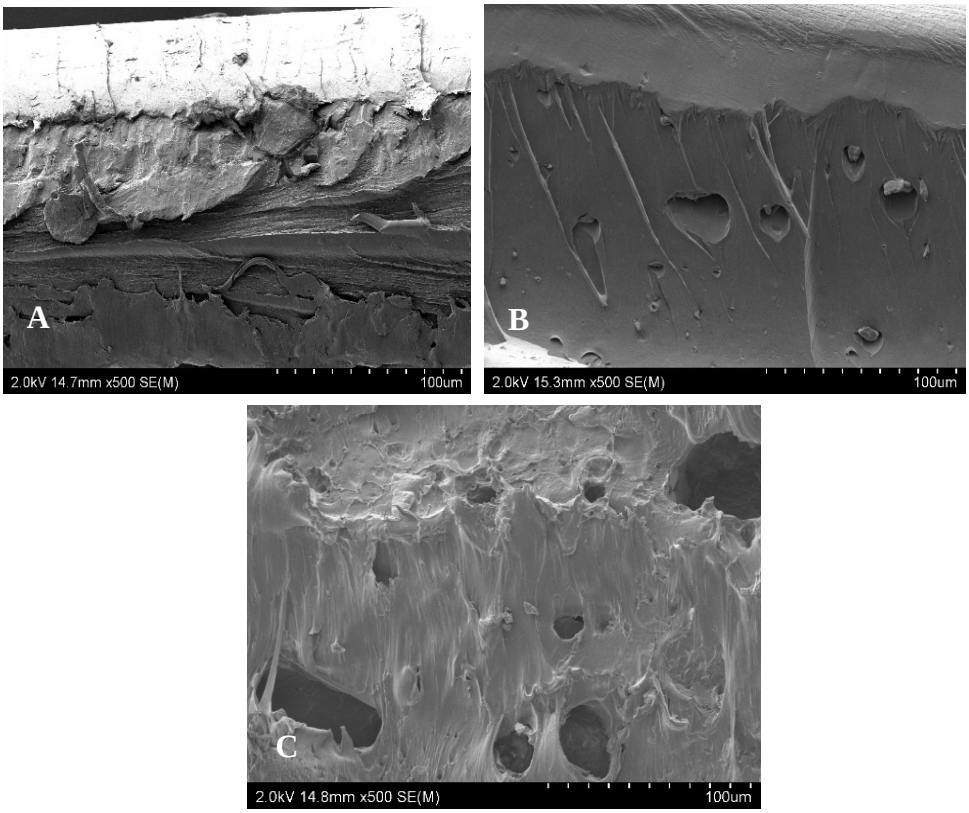


Figure 4.3: SEM images of A) PLA C, B) PLA/PVA C1 and C) PLA/PCA C2.

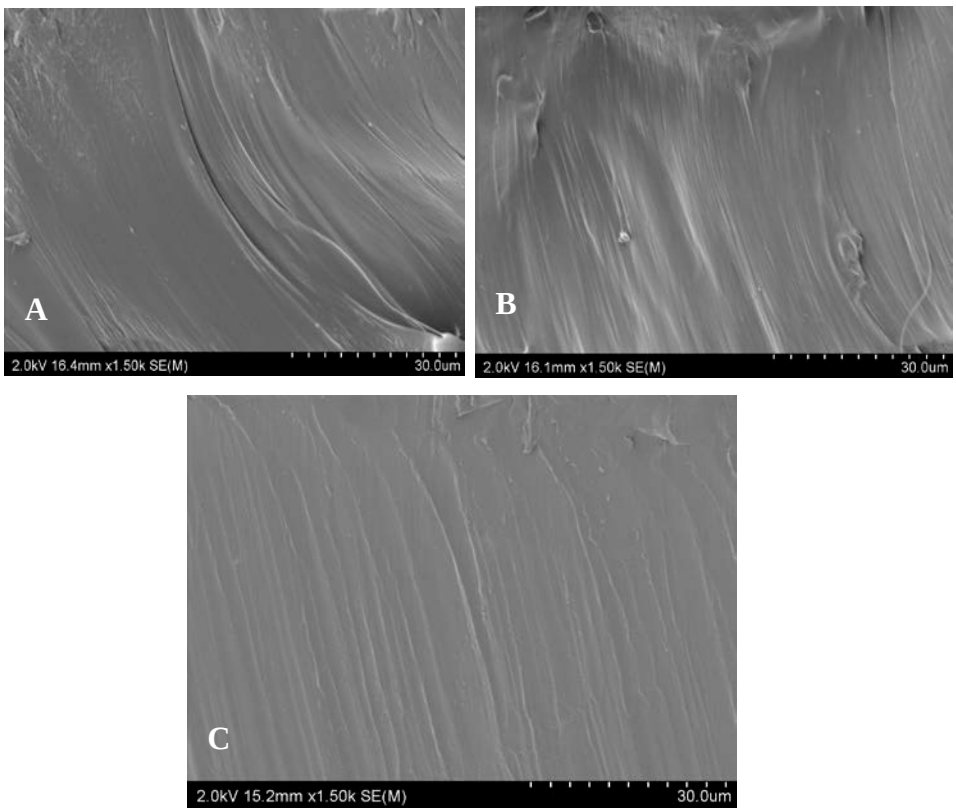


Figure 4.4: SEM images of A) PLA WD, B) PLA/PVA WD1 and C) PLA/PVA WD2.

### 4.3.3. The influence of melt blending process and drug addition on thermal transition of polymer

Melt blending of polymers involving heating and cooling can affect the properties of polymers, as polymers can undergo changes in their thermal transitions during the process. Integration or blending of two different polymers could influence their thermal transitions, as such, DSC studies were performed on drug loaded PLA/PVA films as shown in Figure 4.5. The results of these studies were compared with the DSC thermograms of pure PLA, PVA and DEX to determine the influence of the composite blend and the addition of drug on thermal changes of the polymers as a measure of glass transition (Tg), crystallisation (Tc) and melting (Tm) temperature (Table 4.4 and Figure 4.5). The pure PLA and PLA/PVA blend displayed two endothermic peaks of melting temperature due to the formation of two PLA crystal structures during its cold crystallization, known as melting temperatures Tm2 (α form) and Tm1 (β form) with the α-form having a higher melting temperature because of the higher size of its crystals [251]. Additionally, the melting temperatures of the blends are also shifted toward lower

temperatures, with increasing PVA content. The sharp endothermic peak of DEX is at 267.82 °C [252] which corresponds to its melting temperature and the pure PLA film, showed a Tg at 55.94 °C, endothermic crystalline melting peak Tm1 at 127.37 °C and Tm2 at 143.36°C with a broad exothermic peak at 58 °C due to the cold-crystallisation. This exothermic peak at 58°C signifies that the amorphous structure had undergone molecular and structured assembling to from crystals during the heating process. But the exothermic crystalline peak is lesser than the endothermic melting peak demonstrating the presence of original crystal in addition to this cold-crystalline structure [176]. Additionally, the pure PVA film showed an endothermic crystalline melting peak (Tm) at 117.85 °C (Table 4.4).

Table 4.4: DSC analysis of pure PLA, PVA and blended PLA/PVA with DEX 1% w/w.

| **Sample** | **Tg ($^0$c)** | **Tc ($^0$C)** | **Tm1 ($^0$C)** | **Tm2 ($^0$C)** | **ΔHf (J/g)** |
|---|---|---|---|---|---|
| Pure PLA | 55 | 58 | 127 | 143 | 40.47 |
| Pure PVA | - | - | - | 117 | 135.5 |
| PLA WD | 54 | 104 | 96 | 136 | 32.74 |
| PLA/PVA WD1 | 53 | 102 | 93 | 135 | 29.92 |
| PLA/PVA WD2 | 52 | 103 | 93 | 135 | 25.64 |
| DEX | - | - | - | 267 | 105.5 |

As shown in Table 4.4, for the different ratios of PLA/PVA blends, only one Tg value was observed and the Tg value decreases with an increasing PVA content showing that PLA and PVA have a partial miscible system. The variations in values of Tc and Tm, shows there is interactions between the two blended polymers at different ratios. Hence, interactions between blended PLA/PVA can cause shifts in the Tm values of PLA and PVA toward each other depending on the content of PVA, while increased PVA content in the blend can also lead to an increase in the Tc value of PLA/PVA sample indicating

that the crystallisation of PLA may be affected by the addition of PVA [223]. For drug loaded PLA and bended PLA/PVA samples, the absence of the endothermal peak of the drug was observed which is likely due to the thermal dissolution effect of the drug in the polymer mixtures leading to its dispersion at the polymer matrix during processing. It was observed that incorporation of DEX in PLA, PLA/PVA WD1 and PLA/PVA WD2 blend shifted the cold-crystallisation peak towards higher temperature from 58°C to 104 °C, 102°C and 103°C respectively, showing the decrease of molecular chain mobility and structure formation of PLA and PLA/PVA blend during heating, obstructing the process of crystallisation, leading to higher values of Tc. On the other hand, the effect of the addition of the drug on Tg of the PLA sample, showed a mild plasticisation effect as the Tg was reduced to 54.87 °C from 55 °C and for the enthalpy of fusion ($\Delta H_f$) the measure of energy required for polymer melting transition was reduced from 40 J/g to 32 J/g (Table 4.4). This signifies that even just 1% of DEX along with the addition of PVA into the PLA polymer blend induced crystallisation equilibrium. Since melt processing of PLA at higher temperature can lead to polymer degradation, incorporating this drug additive or another polymer would depress the melting point of PLA making it an advantage for material processing [253].

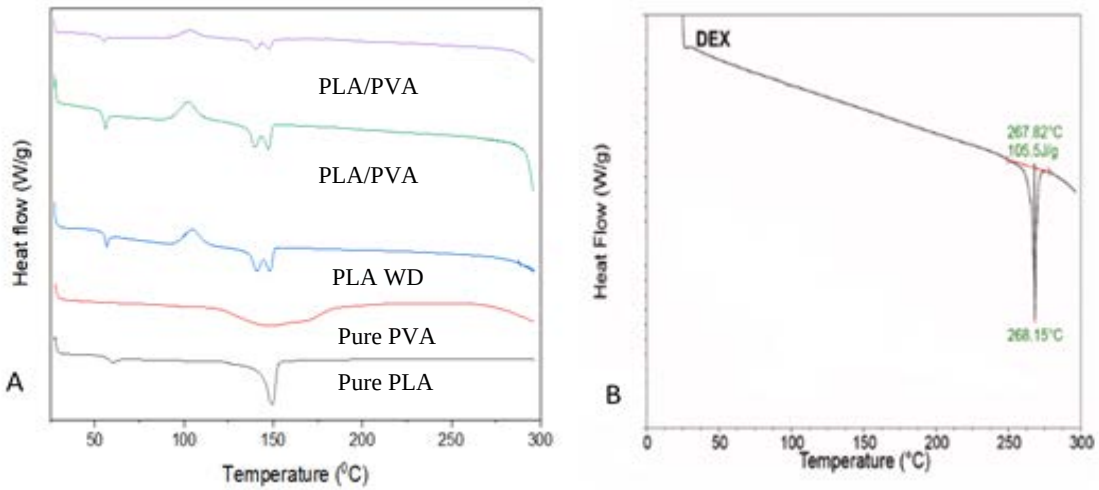


Figure 4.5: DSC curves of A: Pure PLA, Pure PVA, PLA WD, PLA/PVA WD1 and PLA/PVA WD2; B: DSC of DEX.

On the other hand, TGA curves shown in Figure 4.6 also indicates that the pure PLA, PVA, DEX and blended PLA/PVA drug loaded components are stable at 170 °C. The thermal stability of PLA, PVA, DEX and PLA/PVA blends (control and drug loaded) was studied by measuring the initial degradation temperature and maximum degradation temperature from TG and DTG curves as shown in Figure 4.6 and 4.7. The initial degradation temperature of PVA is the lowest and the order of thermal stability of these samples are PLA>PLA/PVA C1>PLA/PVA C2>PVA. This is mainly due to the thermal instability of PVA as compared to pure PLA. For PVA sample, there are two separated weight-loss turns (280–400 °C and 400–500 °C) in the TG and DTG curve. According to the result, PLA thermally degrades in one step (320 °C- 380 °C) but PVA has a two-step-degradation mainly because the first degradation step involves the elimination reactions, and the second step involves chain-scission and cyclisation reactions. For PLA/PVA blends in this study, a combined one step thermal degradation process is detected and with increasing PVA content in the blends, the degradation step is shifted significantly to lower temperatures as PVA absorbs higher amount of water in comparison to PLA, favouring hydrolytic degradation of PLA/PVA blends (Figure 4.6). Hence, from the above result obtained on thermal stability of the composite polymers, we can conclude that intramolecular entanglement between PVA and PLA, by esterification of PVA hydroxylic groups and PLA carboxylic groups, improved the thermal stability of PVA in the blend. Furthermore Figure 4.6 and 4.7 further demonstrates that drug loaded PLA/PVA blends also showed similar decomposition profile when compared with control samples which can be attributed to the relatively small amount of DEX used in developing these composite polymers. In conclusion, the TGA and DTG data shows that DEX loaded PLA/PVA blended materials possess good thermal stability at temperatures below 200 °C and is an efficient method for drug loading and drug diffusion into the PLA/PVA blend system [254-257].

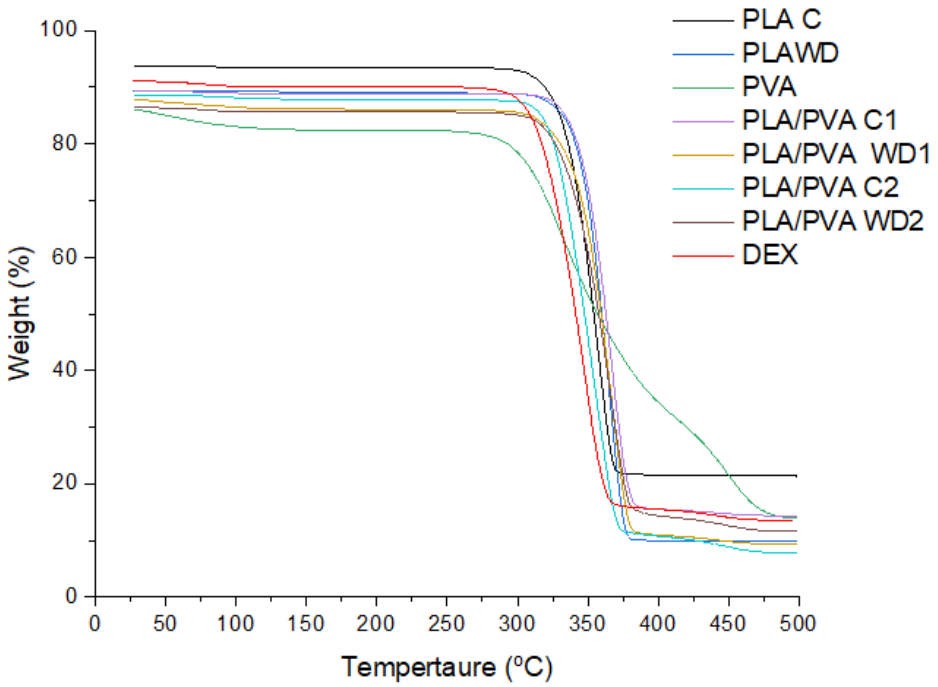


Figure 4.6: TG thermograms of pure PLA, PLA WD, PVA, PLA/PVA C1,PLA/PVA WD1, PLA/PVAC2, PLA/PVA WD2 and DEX.

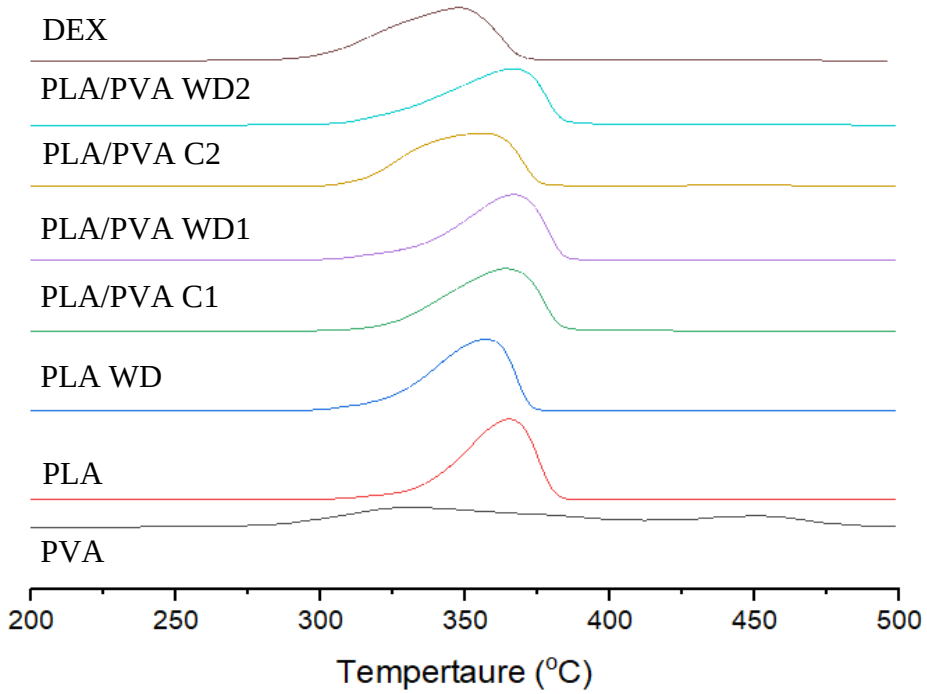


Figure 4.7: DTG thermograms of PVA, PLA, PLA/PVA C1, PLA/PVA WD1, PLA/PVA C2, PLA/PVA WD2 and DEX.

**4.3.4. Chemical interactions between the drug and polymer**

FTIR spectra were obtained for pure PLA, pure PVA, pure DEX and drug loaded blended PLA/PVA samples as shown in Figure 4.8. The spectra of the pure PVA and PLA are shown in Table 4.5. In pure PLA, the absorbance of the carbonyl group occurs at 1758 $cm^{-1}$ and for pure PVA the absorbance of the hydroxyl group at 3333 $cm^{-1}$ respectively. In comparison, the FTIR spectra of different ratio of blended PLA/PVA showed that the absorbance of carbonyl group and hydroxyl group moved towards lower wavelength due to the formation of hydrogen bonding between the hydroxyl groups of PVA and carbonyl group of PLA and the higher the extent of the shift between the carbonyl group and the hydroxyl group can lead to the formation of stronger hydrogen bonding for a miscible PLA/PVA system. Additionally, for pure PLA and pure PVA the C–H group stretching absorbance peaks was observed at 2943, 2943 and 2904 $cm^{-1}$ respectively. However, the intensity of the C–H stretching absorbance peak varied for blended PLA/PVA, when the intensity of the absorbance at 2943 $cm^{-1}$ and 2904 $cm^{-1}$ increased when the PVA content increases [229, 241]. The characteristic absorption bands for the spectra of pure DEX are shown in table 4.5 exhibiting characteristic C-H stretching at 2990 $cm^{-1}$ and C-F stretching at 1270 $cm^{-1}$ respectively. The characteristic peaks of DEX were also observed for methyl group at 2990 $cm^{-1}$ and 1270 $cm^{-1}$ in DEX loaded PLA and PLA/PVA samples. Additional shoulders were, observed in DEX loaded PLA and PLA/PVA samples at 860 $cm^{-1}$ and is also a contribution from DEX (Figure 4.8). The notable change however, was the shift for DEX at around 1660 $cm^{-1}$ to 1745$cm^{-1}$ which can be assigned to the carbonyl group of the drugs where the increase in the intensity of the band at 1745$cm^{-1}$ in drug loaded samples further confirms the incorporation of the drug in these blended polymers [252, 258]. From the result, it was observed that the spectra of DEX loaded samples were very similar to that of pure PLA and PVA samples, indicating no significant chemical changes occurred in the polymer backbone upon melt blending while

incorporating the drug. Hence, the incorporation of the drug within PLA and PLA/PVA samples suggested some interaction of the drug with the polymer matrix, a phenomenon also supported by DSC results.

Table 4.5: FTIR absorption assignment of pure PVA, PLA and DEX.

| **Sample** | **Wavenumber ($cm^{-1}$)** | **Assignment** |
|---|---|---|
| PVA | 3367 | OH stretching |
| | 3333 | Hydroxyl group |
| | 2943 | C-H stretching |
| | 2935 | $CH_2$ asymmetric/symmetric stretching |
| | 2904 | C-H stretching |
| | 1427 | $CH_2$ bending |
| | 1089 | C-O stretching |
| | 833 | CH bending |
| PLA | 2995 | $CH_3$ asymmetric/symmetric stretching |
| | 2943 | C-H stretching |
| | 1758 | Carbonyl group |
| | 1749 | C═O stretching |
| | 1452 | $CH_3$ bending |
| | 1183 | C-O-C stretching |
| | 1080 | C-O-C stretching |
| | 1043 | C-CH3stretching |
| | 865 | C-COO stretching |
| | 755 | C═O in-plane bending |
| DEX | 3390 | OH stretching |

| | |
|---|---|
| 3468 | OH stretching |
| 2990 | C-H stretching |
| 2878 | C-H stretching |
| 1706 | C═O stretching |
| 1660 | C═O stretching |
| 1616 | C═O stretching |
| 1270 | C–F stretching |

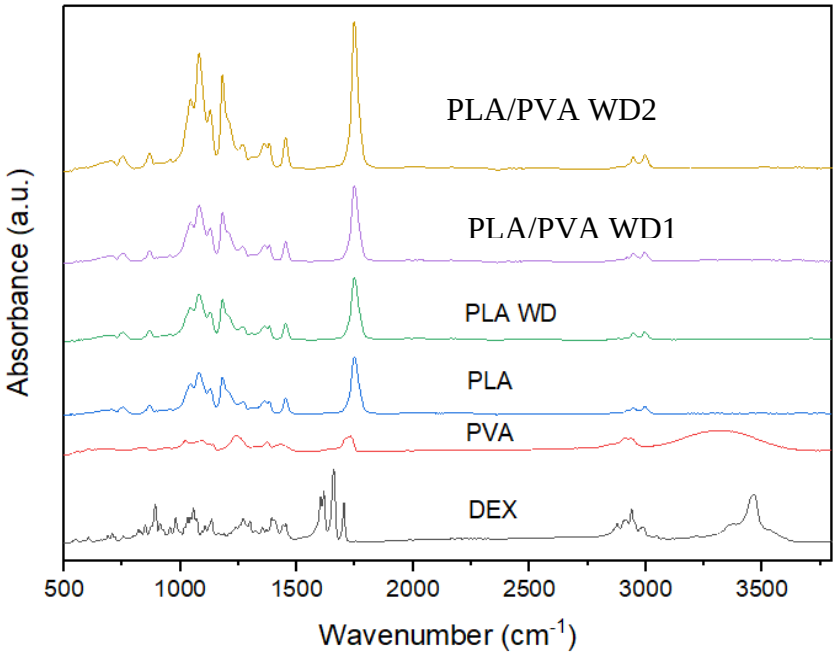


Figure 4.8: FTIR spectra of pure DEX, PVA, PLA, PLA WD, PLA/PVA WD1 and PLA/PVA WD2.

### 4.3.5. *In vitro* degradation

Figure 4.9 show the *in vitro* mass loss of pure PLA and PLA/PVA blend along with drug loaded samples. Samples were incubated in PBS with pH = 7.4 at 37 °C and it was observed that with the increase in PVA content, there was an increase in degradation rate. From figure 4.9, we can observe that PLA samples (drug loaded and drug free) did not lose weight even after 5 weeks of incubation, whereas blended PLA/PVA sample showed a weight loss of 1-2% depending on the content of the PVA. It can also be noted that the

sample containing more PVA content degraded faster than the samples containing less PVA content, as the degradation was caused by PVA absorbing higher amount of water in comparison to PLA, favouring hydrolytic degradation of PLA/PVA blends. Furthermore, drug loaded PLA/PVA sample showed a higher degradation in comparison to the control samples which can be attributed to higher pore formation from the surface to bulk in the polymeric matrix facilitated by the solvent treatment, promoting solvent uptake and drug dissolution, ultimately favouring higher hydrolytic degradation of drug loaded PLA/PVA blends [259, 260].

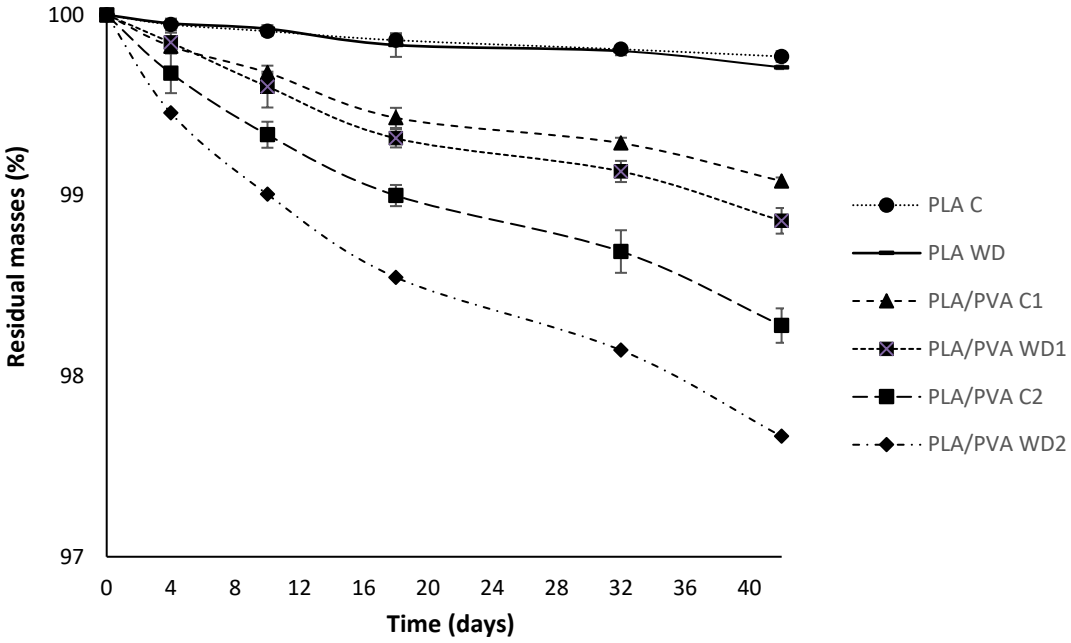


Figure 4.9: The degradation behaviour of PLA (control and drug loaded), PLA95:PVA5 (control and drug loaded) and PLA90:PVA10 (control and drug loaded) ($n$ = 3, mean ± SD).

### 4.3.6. Mechanical analysis

The tensile strength for PLA and PLA/PVA blends is shown in Figure 4.10. Compared to pure PLA, the tensile strength of the blend containing 5wt. % PVA (PLA/PVA C1) is very similar. However, as the PVA content increases the value of the tensile strength is reduced as seen in the PLA/PVA C2 blend. Additionally, influence of PVA was also observed when the PVA content increases, there is a decrease in the PLA/PVA elastic

modulus in comparison to pure PLA demonstrating that the presence of PVA affect the rigidity of PLA (Table 4.6). PVA capability to decrease the rigidity in PLA/PVA blends is due to its flexible characteristic, where the acetate groups present in PVA can influence the mobility of polymeric chains in the PLA/PVA blends. As such, addition of PVA can lower the crystallinity of PLA leading to a decrease in mechanical properties of PLA/PVA blends.

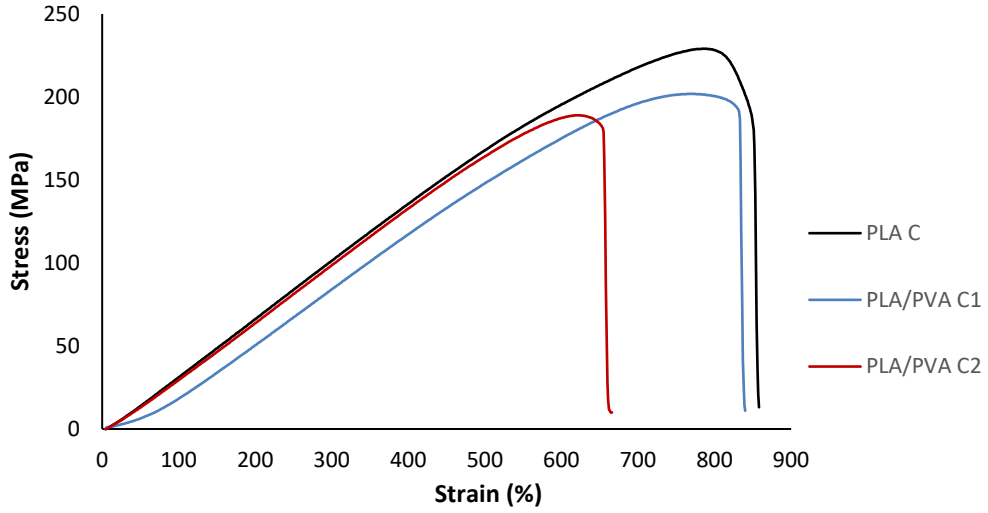


Figure 4.10: Stress-Strain curves of the PLA C, PLA/PVA C1 and PLA/PVA C2 ($n$ = 3, mean ± SD).

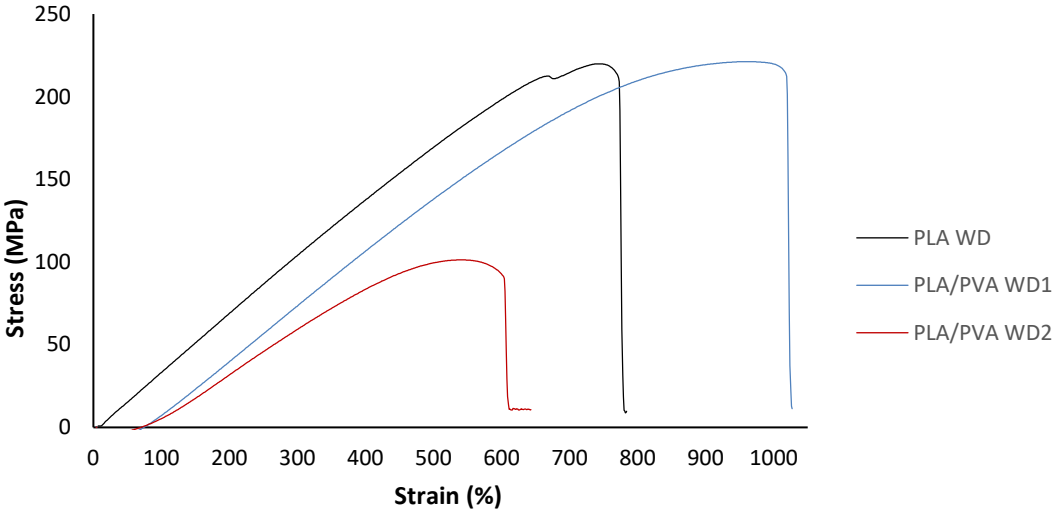


Figure 4.11: Stress-Strain curves of the drug loaded samples PLA WD, PLA/PVA WD1 and PLA/PVA WD2($n$ = 3, mean ± SD).

In addition, tensile strength for drug loaded PLA and PLA/PVA blends are shown in Figure 4.11. Just as in the control samples, the tensile strength of the drug loaded samples shows that the influence of PVA can also be observed. For drug loaded samples as the PVA content increases, there is a decrease in the PLA/PVA elastic modulus in comparison to pure PLA demonstrating that the presence of PVA affect the rigidity of PLA as seen in Table 4.6. In addition, drug loaded PLA and PLA/PVA sample showed an increased elastic modulus in comparison to the control samples which can be attributed to decreased rigidity in drug loaded PLA and PLA/PVA blends due to the decrease of molecular chain mobility. The addition of DEX into the PLA polymer blend induced crystallisation equilibrium increasing the flexible characteristic for drug loaded samples. As such, addition of PVA and DEX can lower the crystallinity of PLA leading to a decrease in mechanical properties of PLA/PVA blends as shown in DSC results.

Table 4.6: Mechanical properties of PLA and blended PLA/PVA ($n$ = 3, mean ± SD).

| **Sample** | **Elastic modulus [MPa]** | **Max stress [MPa]** | **Elongation at break [%]** |
|---|---|---|---|
| PLA C | 13.4 ± 2 | 230 ± 4 | 860 ± 18 |
| PLA WD | 15.58 ± 6 | 220 ± 7 | 780 ± 51 |
| PLA/PVA C1 | 12.8 ± 14 | 205 ± 1 | 940 ± 57 |
| PLA/PVA WD1 | 13.1 ± 6 | 220 ± 3 | 1020 ± 60 |
| PLA/PVA C2 | 8.87 ± 7 | 123 ± 3 | 885 ± 19 |
| PLA/PVA WD2 | 11.6 ± 9 | 126 ± 2 | 610 ± 75 |

Furthermore, the mechanical properties of drug loaded PLA and blended PLA/PVA samples after 32 days of *in vitro* degradation was also carried out (Figure 4.12, 4.13 and 4.14) and from the results in Table 4.7, it can be seen that as the PVA content increases there is a decrease in the PLA/PVA elastic modulus when compared to pure PLA. It is also observed that drug loaded PLA/PVA samples showed a decrease in elastic modulus as the *in vitro* incubation days increased with PLA/PVA WD2 sample at the 32$^{nd}$ day

showing the lowest elastic modulus value at 9.8 ± 10 among all the others. The information revealed that the softness of the blend was gradually increased as the incubation days was increased since PVA consist of a hydrophilic functional group and the sample with higher PVA content possessed higher water uptake than those of the samples with lower PVA contents. Furthermore, for drug loaded PLA/PVA sample the softness of the blend was gradually increased as the incubation days was increased which can be attributed to the solvent treatment increasing pore formation in the polymeric matrix by facilitating solvent uptake during drug dissolution [176, 261]. Hence, the of presence of PVA and DEX in the samples improved the flexibility and softness of the composite blend when treated with solvent showing that the development of such materials would be beneficial in printing or developing bio-degradable flexible implants to be used as drug delivery mechanism within the human body.

Table 4.7: Mechanical properties of PLA and blended PLA/PVA after *in-vitro* degradation (*n* = 3, mean ± SD).

| Sample | Elastic modulus [MPa] | Max stress [MPa] | Elongation at break [%] |
|---|---|---|---|
| PLA WD-0 | 15.5 ± 6 | 220 ± 7 | 780 ± 51 |
| PLA WD-10 | 13.5 ± 13 | 226 ± 4 | 840 ± 16 |
| PLA WD-18 | 12.7 ± 8 | 140 ± 3 | 520 ± 17 |
| PLA WD-32 | 11.8 ± 8 | 225 ± 3 | 1050 ± 50 |
| PLA/PVA WD1 D-0 | 13.1 ± 6 | 220 ± 3 | 1020 ± 60 |
| PLA/PVA WD1 D-10 | 12.2 ± 5 | 170 ± 1 | 720 ± 16 |
| PLA/PVA WD1 D-18 | 11.9 ± 8 | 170 ± 2 | 730 ± 89 |
| PLA/PVA WD1 D-32 | 11 ± 0.5 | 145 ± 1 | 660 ± 53 |
| PLA/PVA WD2 D-0 | 11.6 ± 9 | 100 ± 2 | 610 ± 75 |
| PLA/PVA WD2 D-10 | 11.5 ± 21 | 195 ± 1 | 800 ± 9 |
| PLA/PVA WD2 D-18 | 11.1 ± 12 | 160 ± 5 | 750 ± 63 |
| PLA/PVA WD2 D-32 | 9.8 ± 10 | 150 ± 1 | 750 ± 12 |

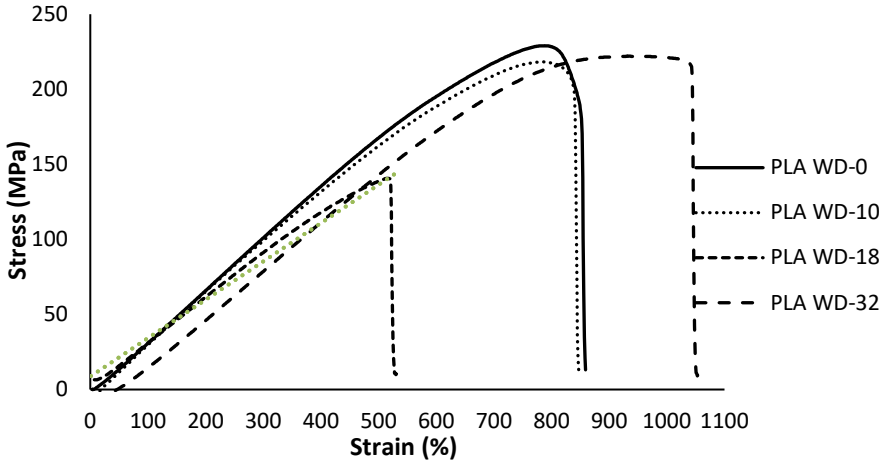


Figure 4.12: Stress-Strain curves of PLA WD after *in vitro* degradation for different days (Day 0 - Day 32) ($n$ = 3, mean ± SD).

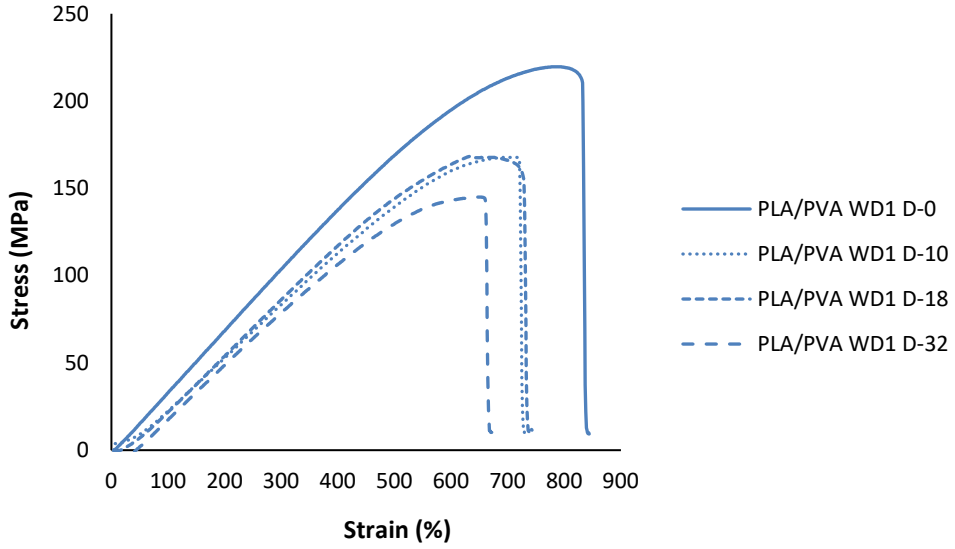


Figure 4.13: Stress-Strain curves of PLA/PVA WD1 blend after *in vitro* degradation (Day 0 – day 32) ($n$ = 3, mean ± SD).

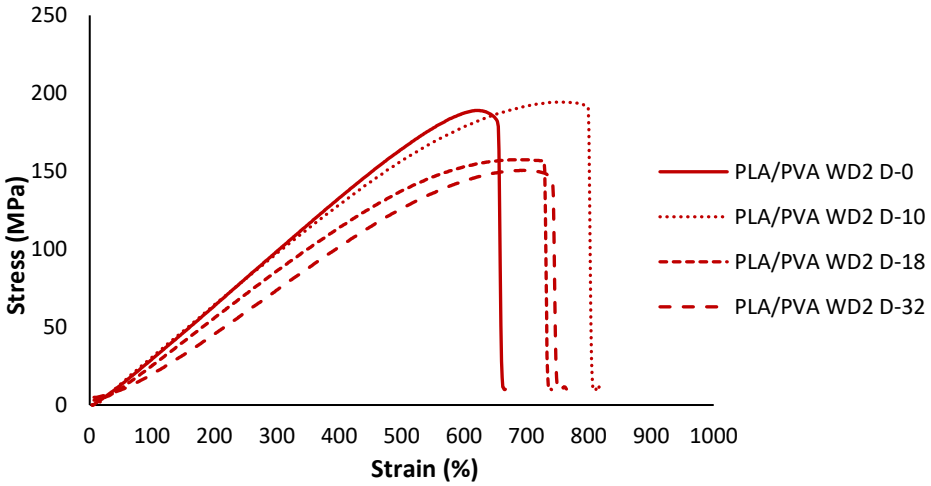


Figure 4.14: Stress-Strain curves of PLA/PVA WD2 blend after *in vitro* degradation (Day 0 – Day 32) ($n$ = 3, mean ± SD).

### 4.3.7. *In vitro* drug release study

In vitro release of DEX from PLA and different ratio of PLA/PVA blend was performed in a release assessment media containing PBS solutions (pH values of 7.4 at 35 ±2). The drug release data shown in Figure 4.15, indicates that all the formulations showed sustained release of DEX for 31 days as the target delivery timing [262].

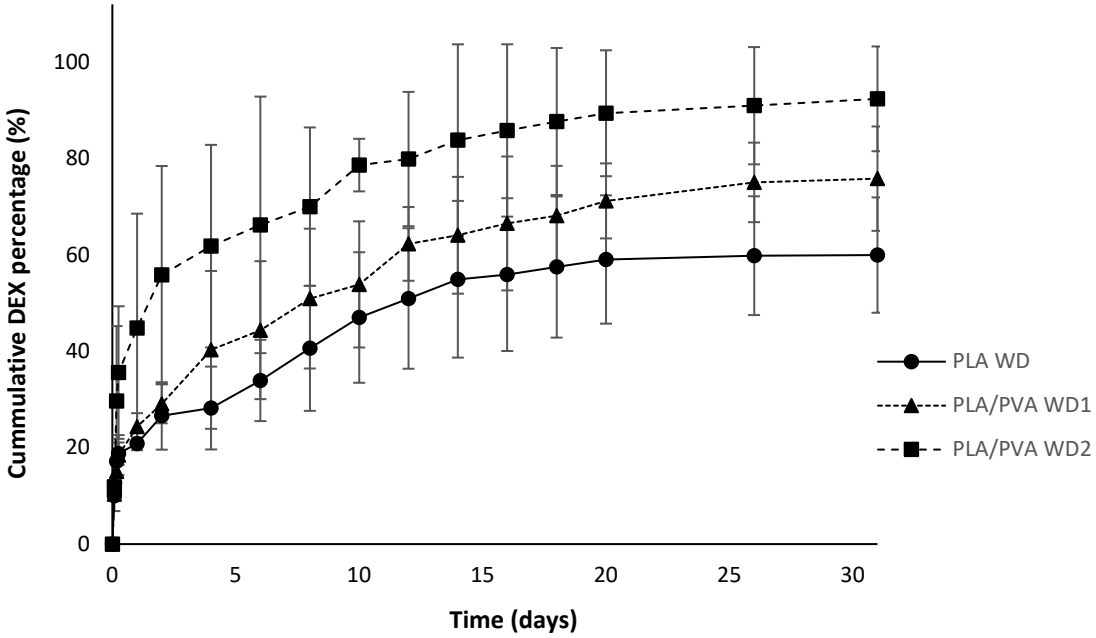


Figure 4.15: *In vitro* release profile of DEX from PLA and different ratios of PLA/PVA blend ($n$ = 3, mean ± SD).

The patterns of drug release were diverse with respect to the amount of PVA added to the composite blend. Figure 4.15 shows that faster and greater drug release was observed with PLA/PVA WD2 which has the highest percentage of PVA from the blend. PLA/PVA WD2 had a faster release (up to 11.8 %) in first 2 hours followed by a sustained release in the subsequent 18 days and it finally reached a plateau in the last remaining 11 days. Similarly, PLA/PVA WD1 and PLA WD samples exhibited slower release behaviours (9.9 % and 10.3 % released within 2 hours, respectively), followed by a continuous release DEX percentage of 9.9 % and 75.8 % respectively. In the end, the total drug released was 60 % and 75.8 % for PLA WD and PLA/PVA WD1 respectively, whereas 92.3 % was release for PLA/PVA WD2 sample. Hence from Figure 4.15 and SEM images

obtained below (Figure 4.16), we can conclude that when the drug incorporated within the polymeric matrix was undergoing solvent treatment, it facilitated pore formation from the surface to bulk promoting solvent uptake and drug dissolution.

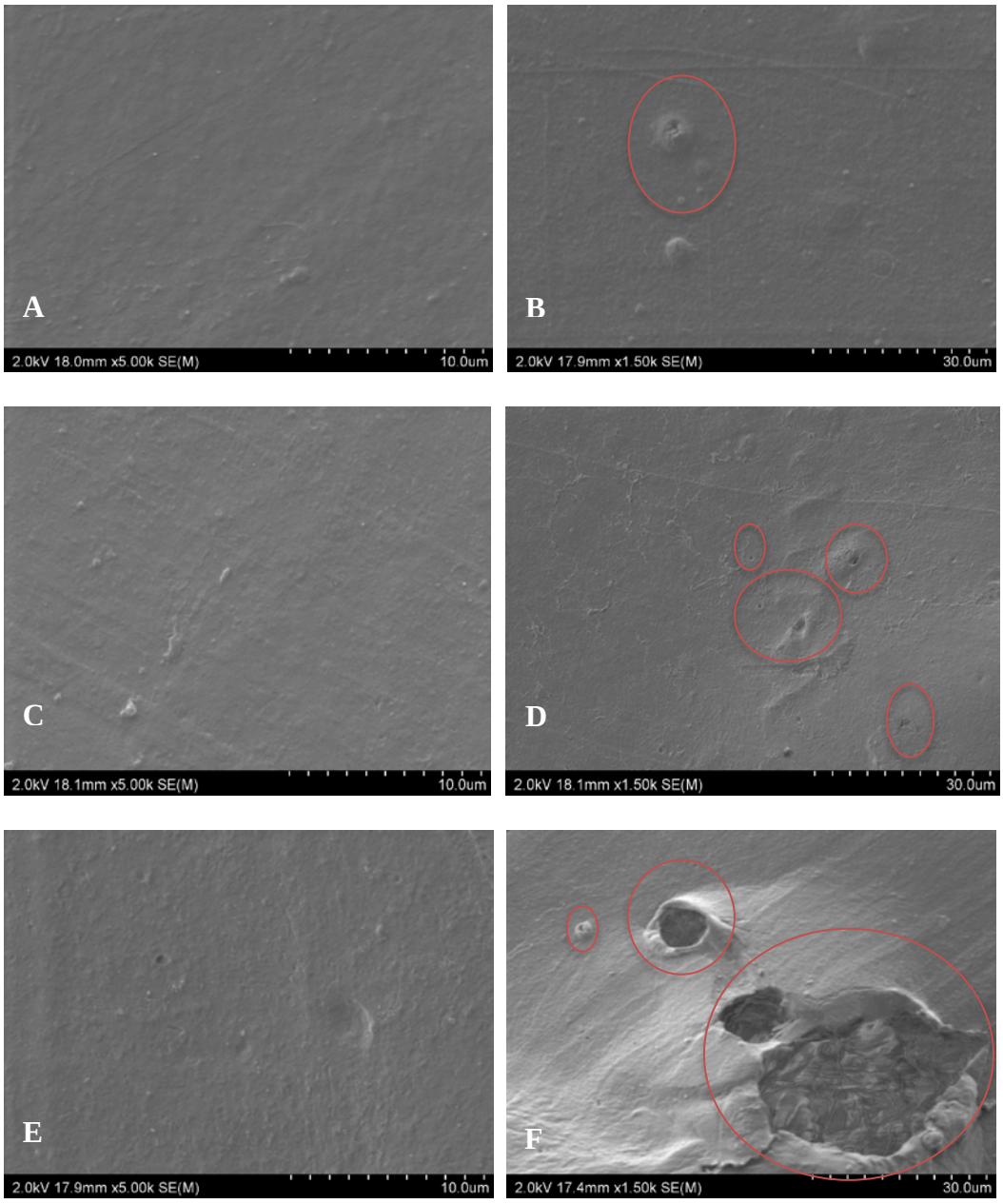


Figure 4.16: SEM surface image of A) PLA WD Day 0, B) PLA WD Day 32, C) PLA/PVA WD1 Day 0, D) PLA/PVA WD1 Day 32, E) PLA/PVA WD2 Day 0 and F) PLA/PVA WD2 Day 32. (Day 0 – before and Day 32 – after the dissolution study).

Additionally, mathematical models of the drug release behaviour from composite polymer blend is important to support the interpretation of the mechanisms involved in the control of the drug release process. The *in vitro* drug release data for DEX-composite

polymers best fitted these two mathematical models, Weibull and Korsmeyer-Peppas and their respective coefficients were estimated in Table 4.8.

Table 4.8: Release coefficients for DEX fitted with different mathematical models.

| **Samples** | **Weibull model** | | **Korsmeyer-Peppas** | |
|---|---|---|---|---|
| | **($R^2$)** | **(b)** | **($R^2$)** | **(n)** |
| PLA WD | 0.9849 | 0.390 | 0.9807 | 0.301 |
| PLA/PVA WD1 | 0.9905 | 0.474 | 0.9851 | 0.332 |
| PLA/PVA WD2 | 0.9897 | 0.362 | 0.9803 | 0.200 |

According to $R^2$ values, PLA WD, PLA/PVA WD1 and PLA/PVA WD2 fitted better with the Weibull model in which the release rate of incorporated drug is driven by Fickian diffusion mechanism (as shown in Eq. (4.1)).

$$F = 1 - \exp(-at^b)$$

In Weibull model the release mechanism of drug throughout the polymer matrix are interconnected with *b* coefficients values, and *b* values lower than 0.75 are related to Fickian diffusion. In this study, the composite blended film samples presented *b* coefficient values lesser than 0.75, further validating the concept that the drug release followed a fickian diffusion mechanism. Hence in this study, the drug was enclosed within the composite polymer, which was then released by passive diffusion from the polymer matrix. In the end, the quantitative release of DEX from the polymer matrix is evidence of an interaction between the drug loaded composite polymer and the surrounding medium [263].

## 4.4. Conclusion

Melt processing of composite polymers with DEX is a viable method of producing novel composites for potential future drug delivery applications. Based on the DSC result,

the absence of the endothermic peak of the drug can be attributed to the thermal dissolution effect of the drug in the polymer mixtures leading to its dispersion at the polymer matrix during processing. It was also observed that the incorporation of PVA and the drug additive into the PLA polymer reduced the melting point of PLA making it an advantage for material processing. In addition, the thermal stability of the composite blend was also improved due to the intramolecular entanglement between PVA and PLA, by esterification of PVA hydroxylic groups and PLA carboxylic groups. Similarly, DEX loaded PLA/PVA blended materials presented good thermal stability at 170 °C suggesting that melt blending is an efficient method for introducing drug into the PLA/PVA blend system. Furthermore, the partially compatible nature of PLA/PVA blends were evidenced from mechanical and morphological results. In this context, the presence of higher amount of PVA in the composite blend; lowered the crystallinity of PLA while increasing the density of pores leading to a greater phase separation in the PLA/PVA blend. This decrease in mechanical properties of the blends was due to the hydroxyl groups present in PVA influencing the mobility of polymeric chains in the PLA/PVA blends. From the result blends containing more PVA content degraded faster than the samples containing less PVA content, as the degradation was caused by PVA absorbing higher amount of water favouring hydrolytic degradation of PLA/PVA blends. But this hydrolytic degradation of the blends leads to improvement in the flexibility and softness of the composite blend obtained during the mechanical testing of these blended samples after different incubation time period in PBS solution. Moreover, *in vitro* release profile showed that faster and greater drug release was observed with composite blend with the highest percentage of PVA. Thus, result obtained from the *in vitro* study and SEM analysis showed a porous morphology indicating that the drug incorporated within the polymeric matrix facilitated pore formation from the surface to bulk promoting solvent uptake and drug dissolution. Hence, the results obtained from this study indicate that drug

loaded PLA/PVA blended samples would be beneficial novel materials that can be used in printing or developing bio-degradable flexible implants in the future to be used for drug delivery in the medical field.

## 4.5. Future directions

From this study, the blended samples prepared by melt blending have provided good drug loading capability and incorporation efficiency, showing drug release profile can be modified depending on the time frame required. For future studies, it would be interesting to explore the efficacy of the drug loaded composite blend extruded in the form of filaments to enable 3D printing of an implant. Such studies can provide critical data for translating the formulation from a theory to certainty. In addition, further studies on understanding the mechanical relation between the composite polymers and intranasal stent design will be a fascinating aspect. Although the drug release of DEX from polymeric blend has been reported *in-vitro*, further studies investigating the drug release mechanism from the drug loaded 3D printed intranasal stent by placing the stent intranasally in animal models for *in-vivo* studies are required to evolve this drug delivery platform. Therefore, the development of drug loaded composite thermoplastic blend by melt blending that can be used in future studies for 3D printing the intranasal stent to provide localised drug delivery was established. **Chapter 5** of this thesis presents the second technique of the independent experiment examining the formulation of a drug loaded crosslinked multi-layer biodegradable film aimed at sustained delivery of an anti-inflammatory drug for local drug delivery in the intranasal cavity for patient's post-surgery.

# Chapter 5. Development of multi-layer hydrogel films for sustained delivery of dexamethasone

Results from **Chapter 4** demonstrated the development of dexamethasone loaded polymer composite that can form the structure of the stent. **Chapter 5** will investigate an alternative approach using hydrogel films for sustained delivery of anti-inflammatory agent. This will allow the anti-inflammatory drug-eluting hydrogel film to be incorporated independently into the stent's structure (Figure 5.1).

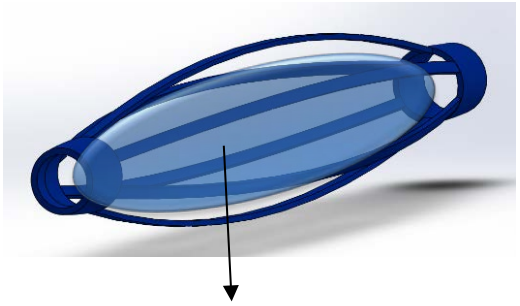


Figure 5.1: Diagrammatical representation of DEX loaded multi-layer hydrogel film integrated into a 3D printed intranasal stent.

## 5.1. Introduction

### 5.1.1 Biodegradable films as drug delivery carriers

Over the years, biodegradable films derived from natural products have received considerable interest as an alternate approach to conventional dosage forms [264]. Currently, these films have found applications in local and systemic drug delivery via oral, buccal, sublingual, ocular and transdermal routes [265]. These film are flexible and their biocompatibility makes them potential candidates for delivering drugs to sensitive and difficult to access pharmacological sites [266]. Biodegradable films can be developed from a wide selection of suitable synthetic and natural hydrophilic polymers with adjustable drug release rate, mechanical strength, water absorption and

degradation properties [267]. Natural polymers that have been investigated for wound healing applications include polysaccharides such as chitosan and chitin, cellulose, dextran and heparin; and proteins such as collagen, gelatine, fibrin and keratin [268]. In terms of drug delivery applications, biodegradable films are hydrophilic in nature but can incorporate drugs within their matrices. However, rapid drug diffusion is observed through the matrix when they are immersed in an aqueous environments [269]. On the otherhand, crosslinked biodegradable films form three-dimensional networks with the ability to swell in aqueous environments in a controlled manner. It is possible to adjust drug release rates by optimising cross-linking degree therefore slowing down the swelling rate [270].

Chronic rhinosinusitis (CRS) is a common, chronic, inflammatory condition of the paranasal sinuses that persists for more than 12 weeks [271]. Treatment options for CRS include the use of antibiotics, topical nasal steroids and/or oral steroids, oral antihistamines and nasal saline irrigation, with functional endoscopic sinus surgery (FESS) as the last option for patients who do not respond to therapeuticand adjunctive treatment [28]. The objective of this study is to design a DEX loaded natural polymeric film for local delivery of the drug into the intranasal cavity for post-surgical recovery. Chitosan has gained popularity due to its biocompatibility, absence of toxicity, high mucoadhesive features, and ability of producing solid or semisolid matrices for controlled drug release.Both chitosan and gelatine is renowned as a “generally recognised as safe” (GRAS material) by the FDA, possessing lower antigenic properties in comparison to others [272, 273]. Chitosan and gelatine unique gel and film forming properties, biocompatibility and biodegradability make them suitable carriers for drug delivery systems [274]. But gelatine’s weak mechanical strength is a drawback for drug release behaviour in this study due to its rapid dispersion in aqueous environments. Hence, blending gelatine with another natural polymer while adding a cross linker is proposed to

increase the films chemical stability and improve the mechanical properties [275]. Polymer blending is mainly dependent on the compatibility of polymer blends, affected by the intermolecular interactions between the components of the blends. Gelatine contains carboxyl groups that can form hydrogen bonding with chitosan. Gelatine has the capability to absorb excess water more than 5–10 times its weight and is well known as a non-antigenic as well as a wound healing agent. Additionally, chitosan can also provide a broad range of antimicrobial activity against gram-positive, gram-negative bacteria and fungi, controlled drug release properties and capability to aid in wound healing. In the present work, chitosan and chitosan-gelatine composite films (1:1 ratio) were developed and optimised for sustained delivery of DEX that can be integrated into the intranasal stent.

## 5.2. Materials and methods

### 5.2.1. Materials

Chitosan (LMW-low molecular weight, mol wt. 50,000-190,000 Da, 75-85 % deacetylated), chitosan (MMW-medium molecular weight, mol wt. 190,000-310,000 Da, 75-85 % deacetylated), gelatine (porcine type A with 300 Bloom value), phosphate buffered saline (PBS) tablets and glutaraldehyde (GA, 25 % in $H_20$) were purchased from Sigma-Aldrich, New Zealand. Dexamethasone (DEX) was purchased from Zhejiang Xianju Pharmaceutical Ltd, China. All other chemicals were analytical grade.

### 5.2.2. Preparation of chitosan and gelatine solution

Chitosan (CH) solution (LMW and MMW) of 2 % (w/v) was prepared in distilled water containing 1 % (v/v) acetic acid solution at room temperature and left overnight in the shaker with rotation rate of 250 rpm [276]. A viscous, pale yellow chitosan solution of 2% (W/V) was obtained. Gelatine 1.5 % (w/v) was dissolved in distilled water at 50 °C.

#### 5.2.2.1. Preparation of chitosan films

Single layer (SL) CH films (LMW and MMW) were prepared by a solvent casting method. They were prepared by adding GA (25% in $H_20$) directly to the chitosan solution, under vigorous stirring for 30 min at room temperature until it became increasingly viscous to ensure complete mixing. The percentages of crosslinking agent used were 0.2, 0.4 and 0.6 % (v/v) [277]. The homogenised solution was then poured into a Petri dish (polystyrene round plate with diameter of 100 mm and height of 10 mm). Finally, all mixtures formed films after drying at 37 °C for 24 hours and were labelled as shown in Table 5.1. For DEX loaded CH films, DEX powder of 1 % (w/v) was added to the CH mixture while stirring overnight at room temperature for homogenisation. Films were then dried in an oven at 37 °C for 24 hours. As mentioned above, DEX-loaded CH films were also produced and labelled as shown in table 5.1. All the prepared films were then wrapped with paraflim and kept in a desiccator before testing.

#### 5.2.2.2. Preparation of chitosan and gelatine films

SL Chitosan/gelatine (CG) composite film used in this study were also prepared by solvent casting method. Composite films of 1:1 chitosan/gelatine volume ratios (v/v %) were fabricated and stirred overnight to get a homogeneous blend solution. The cross-linked films were prepared by adding glutaraldehyde (25 % in $H_20$) directly to the chitosan gelatine solution, under vigorous stirring for 15 min to ensure complete mixing. The percentages of crosslinking agent used were 0.2 %, 0.4 % and 0.6 % (w/v). The homogenised solution was then poured into a Petri dish (polystyrene round plate with diameter of 100 mm and height of 10 mm). Finally, all mixtures formed films after drying at 37 °C for 24 hours were labelled as shown in Table 5.1. The same procedure as mentioned above was used to form DEX-loaded CG films and were labelled as shown in Table 5.1. About 1 % (w/v) DEX powder was added to the mixture while stirring

overnight at room temperature for homogenisation. All the prepared films were then wrapped with paraflim and kept in a desiccator before testing.

#### 5.2.2.3. Preparation of multi-layered films

Bilayer films (BL CG and BL CH) were prepared by a two-step layer-by-layer coating technique. This method involves forming one film where after drying, the second layer is poured directly on top of the previously dried layer. In this study, the CG/CH solution was used as the base component of the bilayer film, and another layer of CG/CH solution was poured on top of it. For drug loaded bilayer films, a two-step coating technique was used, where the CG/CH solution was used as the base component of the bilayer film, and another DEX loaded layer of CG/CH solution was poured on top of it. Similarly, trilayer films (TL CG and TL CH) were prepared by a three-step coating technique as mentioned above and for drug loaded trilayer films a three-step coating technique was used, where the DEX loaded polymer solution was sandwich in between two layer of either CG/CH solution. Finally, all mixtures formed films after drying at 37 °C for 24 hours were labelled as shown in Table 5.1. All the prepared films were wrapped with paraflim and kept in a desiccator before testing.

Table 5.1: Different formulations of CG and CH films.

| Formulation | Chitosan/gelatine Ratio (v/v) | Designation | Glutaraldehyde (V/V %) | DEX (W/V %) |
|---|---|---|---|---|
| CG1 | 50/50 | - | 0.2 | - |
| DCG1 | 50/50 | - | 0.2 | 1 |
| CG2 | 50/50 | - | 0.4 | - |
| DCG2 | 50/50 | - | 0.4 | 1 |
| CG3 | 50/50 | - | 0.6 | - |
| DCG3 | 50/50 | - | 0.6 | 1 |
| BLCG4 | 50/50 | - | 0.6 | - |
| DBLCG4 | 50/50 | - | 0.6 | 1 |

| | | | | |
|---|---|---|---|---|
| TLCG5 | 50/50 | - | 0.6 | - |
| DTLCG5 | 50/50 | - | 0.6 | 1 |
| CH6 | - | LMW-CH2 % | 0.2 | - |
| DCH6 | - | LMW-CH2 % | 0.2 | 1 |
| CH7 | - | LMW-CH 2 % | 0.4 | - |
| DCH7 | - | LMW-CH 2 % | 0.4 | 1 |
| CH8 | - | LMW-CH 2 % | 0.6 | - |
| DCH8 | - | LMW-CH 2 % | 0.6 | 1 |
| CH9 | - | MMW-CH2 % | 0.2 | - |
| DCH9 | - | MMW-CH2 % | 0.2 | 1 |
| CH10 | - | MMW-CH 2 % | 0.4 | - |
| DCH10 | - | MMW-CH 2 % | 0.4 | 1 |
| CH11 | - | MMW-CH2 % | 0.6 | - |
| DCH11 | - | MMW-CH2 % | 0.6 | 1 |
| BLCH12 | - | BLCH-LMW 2 % | 0.6 | - |
| DBLCH12 | - | BLCH-LMW 2 % | 0.6 | 1 |
| TLCH13 | - | TLCH-LMW 2 % | 0.6 | - |
| DTLCH13 | - | TLCH-LMW 2 % | 0.6 | 1 |
| BLCH14 | - | BLCH-MMW 2 % | 0.6 | - |
| DBLCH14 | - | BLCH-MMW 2 % | 0.6 | 1 |
| TLCH15 | - | TLCH-MMW 2 % | 0.6 | - |
| DTLCH15 | - | TLCH-MMW 2 % | 0.6 | 1 |

### 5.2.3. Thickness uniformity

For determination of CG and CH films thickness uniformity, (size 2 × 2 cm) of each film were randomly selected and triplicate samples of all types of films were measured by using a digital calliper (0–150 mm, TD2082, Jaycar Electronics) at five different positions of the film with 0.001 mm accuracy.

### 5.2.1. Water absorption

The equilibrium swelling behaviour of CG and CH films in deionised water was studied to investigate their equilibrium water content or moisture content in room temperature. CG and CH films were dipped into deionised water for 24 hours and the wet weights were determined after first blotting with filter paper to remove the surface water before weighing the films [278]. Triplicate measurements were obtained for each sample and expressed as mean ± SD. The EWC was calculated from the following equation:

$$\boldsymbol{EWC}\ (\%) = \frac{\boldsymbol{w_e - w_d}}{\boldsymbol{w_e}} \boldsymbol{x}\ \boldsymbol{100}$$

Where, $w_e$ and $w_d$ are the weight of the swollen hydrogel and the dried hydrogel films, respectively.

### 5.2.2. Fourier transform infrared (FTIR) spectroscopy

FTIR was used to characterise the presence of specific chemical groups in the films. CG and CH films cross-linked with GA were analysed by FTIR spectra using a Spectrum Two PE instrument equipped with a horizontal attenuated total reflectance (ATR) crystal (ZnSe) (Nicolet iS10, Thermo Scientific, USA) was used here. Samples were placed directly onto the ATR crystal and spectra were collected in transmittance mode. FTIR spectra were collected with wavenumber ranging from 3800 to 600 $cm^{-1}$ during 64 scans, with 2 $cm^{-1}$ resolution. The FTIR spectra were normalised and major vibration bands were identified and associated with the main chemical groups.

### 5.2.3. Film morphology

The morphology of the CG and CH films obtained was assessed by scanning electron microscopy (SEM, Hitachi SU-70, UK). Cross-section images of the samples were obtained by breaking the samples in liquid nitrogen into small squares, fixed on aluminium stubs using carbon tapes and sputter-coated with platinum for 20 s (Hitachi E-

1045, UK). The surface morphology of the films was observed at an accelerating voltage of 5 kV.

### 5.2.4. Swelling degree and weight Loss

The CG and CH film samples were immersed in PBS of pH 7.4. After swelling for 2, 4, 8, 12, and 24 hours the samples were removed, wiped off to remove excess surface liquid and immediately weighed. Triplicate measurements were obtained for each sample and expressed as mean ± SD. The swelling degree and weight loss of the films were determined according to the following equations:

$$\text{Swelling degree (\%)} = \frac{M_i - M_0}{M_0} x^{100}$$

$$\text{Weight loss (\%)} = \frac{M_i - M_0}{M_i} x^{100}$$

Where, $M_i$ and $M_0$ are the weights of the film before and after infiltration, respectively.

### 5.2.5. Antibacterial activity

The antimicrobial activity was evaluated against Gram-positive bacteria (*Bacillus subtilis* ATCC 6633 and *Staphylococcus aureus* ATCC 25923), Gram-negative bacteria (*Escherichia coli* ATCC 25922 and *Pseudomonas aeruginosa* ATCC 27853). *B. subtilis*, *S. Aureus*, *E. Coli* and *P. Aeruginosa* were grown aerobically in LB medium (Richard fort) at 37 °C for 24 h. The disc-agar diffusion method was used to test the antimicrobial activities for CG and CH solutions. Suspensions of the test microorganisms ($10^8$ colony-forming units [CFU]/mL) were spread on the agar plates containing the appropriate culture media. Sterile paper discs of 6 mm diameter (Schleicher and Schuell, Dassel, Germany) were impregnated with 200 µL of each solution. These paper discs were placed on the surface of the agar plates. Plates were incubated at the appropriate conditions and

the diameter of the inhibition zone around the paper discs were measured. The experiments were performed in triplicate.

### 5.2.6. Drug loading

For the determination of the drug loading of DEX, drug loaded CG and CH films were dissolved in a 10 ml PBS of pH 6.8 and stirred under magnetic stirrer for 24 hours at room temperature, followed by ultra-sonication for 10 min. The amount of DEX was determined with UV spectrophotometer (Ultrospec 7000, Massachusetts, USA) using a calibration curve at an absorption wavelength of 242.3 nm (calibration equation was $y = 0.0268x - 0.0045$, $R^2 = 0.999$). The drug loading (DL) and incorporation efficiency (IE) were calculated as typically reported.

$$DL\ (\%) = \frac{Amount\ of\ drug}{Amount\ of\ polymer+drug} \times 100$$

$$IE\ (\%) = \frac{Measured\ drug\ loading}{Theoretical\ drug\ loading} \times 100$$

### 5.2.7. *In vitro* drug release

An *in vitro* release study of different formulations was carried out in 40 ml of phosphate buffer solution (PBS). UV–Vis spectroscopy was used to determine the concentration and in *vitro* release of DEX under physiological conditions. First, the wavelength of maximum absorbance for DEX in PBS was measured ($\lambda_{max} = 242.3$ nm) and then, standard solutions of DEX were prepared over a concentration range (0.5–40 µg/mL) to establish a calibration curve ($y = 0.0356x + 0.01$, $R^2 = 0.999$). The Limit of Detection [LOD] and Quantification [LOQ] [242] were calculated in order to describe the smallest concentration that can be reliably measured by UV–vis spectroscopy [243]. The values for LOD and LOQ were 0.32554 µg/mL and 0.986484 µg/mL, respectively.

*In vitro* drug release was carried out in physiological-simulated media (0.01 M PBS solution, pH = 7.4) under sink condition. The film was placed in a shaker containing buffer of pH 7.4 and speed was fixed to 100 rpm ± 5 at 37 °C ± 0.5. Samples were withdrawn using 1 ml pipette at regular time interval. The volumes of withdrawn samples were replaced with buffer (pH 7.4) to maintain sink condition. The absorbance of the samples was measured with a UV–Vis spectroscopy (Ultrospec 7000, Massachusetts, USA) at 242.3 nm. The release of DEX was quantified from a previously built analytical curve, designed from the plot of absorbance versus standard DEX solutions with known concentrations. From the value of absorbance, the percentage of drug release was calculated and graph of the percentage of drug release against time was plotted. Release studies were performed in triplicate and expressed as mean ± SD.

### 5.2.8. Kinetics of drug release

Drug release data were fitted with different mathematical models in order to explain the mechanism of drug release (Table 5.2).

Table 5.2: Kinetic release mathematical models.

| Model | Equation[a] |
|---|---|
| Weibull | $F = 1 - \exp(-at^b)$ |
| Korsmeyer-Peppas | $F = k_p t^n$ |
| Hixson and Crowell | $F = [1 - (1 - k_{HC}t)]^3$ |
| Zero order | $F = k_p t$ |

[a] $F$ = amount of drug release at time $t$; kHC and $k_p$ = release rate constants for different equations; $n$ and $b$ = release exponents.

### 5.2.9. Statistical analysis

Data were subjected to one-way analysis of variant [244, 245] by means of a SPSS computer program (SPSS Statistic 20.0). Post-hoc multiple comparisons were determined by Tukey's test with a significance level set at $p < 0.05$. Error bars in the figures represent the standard deviation (SD).

## 5.3. Results and discussion

### 5.3.1. Thickness uniformity of CG and CH films

From table 5.3, it was also observed that the thickness of CG and CH films with different concentrations of GA showed no statistical differences [279], whereas multilayer films showed varying thickness in comparison to single layer films which can be mainly attributed to the development of layer-by-layer films ($p < 0.05$, ($F (2, 3 = 56.4$, $p = 0.004$, showing single layer < bilayer < trilayer in thickness)).

### 5.3.2. Water absorption capacity of CG and CH films

In non-cross-linked chitosan and gelatine films, samples were solubilised within 24 hours of immersion in water (data not shown in the table) showing the need of modifying chitosan and gelatine films for sustained drug delivery applications. In this study, significant variations were observed in the ability of the CG and CH (LMW and MMW) films to absorb water depending on the amount of GA (cross linker) used in developing the respective films. Table 5. 3, shows that CG and CH films cross linked with the lowest percentage of GA (0.2 %) such as DCG1, DCH6 and DCH9 showed the highest percentage of water absorption, whereas films with higher GA percentage (0.6 %) such as DCG3, DCH8 and DCH11 showed lower value of water absorption. This result shows that increasing GA concentration, decreased the water absorption of all the films significantly due to a more compact nature of the polymeric matrix leading to a further decrease in the polymer chain mobility (p value < 0.05, ($F (2, 9) = 5.426$, $p = 0.028$)) [280]. Additionally, it was observed that LMW CH films absorb more water than MMW CH films due to higher chain-relaxation ability in LMW CH compared to MMW CH. Subsequently, from the table 5.3 it can also be seen that CG films (DCG1, DCG2 and DCG3) shows the highest water absorption capacity even with the highest cross linker (0.6 % GA) in comparison to CH films which can be attributed to higher pores network

formed in the CG films due to the blending of two different polymers leading to increased presence of free charges in the films favouring the entry of water. Furthermore, it can be observed that multilayer films showed higher water absorption capability in comparison to single layer films which can be mainly attributed to the development of layer-by-layer films ($p < 0.05$, ($F(2,3 = 56.4$, $p = 0.004$)) [281, 282]. Physical characteristics of control CG and CH films (without drug) were not significantly different in comparison to drug loaded CG and CH films, as such the data was not shown in the table.

Table 5.3: Physical characteristic and water absorption capacity of the various films ($n = 3$, mean ± SD).

| Film name | Thickness ± SD (mm) | % EWC | Drug loading (%) | Incorporation Efficiency (%) |
|---|---|---|---|---|
| DCG1 (0.2 % GA) | 0.13 ± 0.03 | 11.2 ± 0.57 | 34.4 ± 3.2 | 90 ± 28 |
| DCG2 (0.4 % GA) | 0.16 ± 0.03 | 8.9± 0.15 | 34.7 ± 1.8 | 88.4 ± 14 |
| DCG3 (0.6 % GA) | 0.20 ± 0.02 | 6 ± 0.02 | 34.6 ± 1.4 | 88.7 ± 11 |
| DBLCG4 (0.6 % GA) | 1.16 ± 0.06 | 18.1 ± 0.4 | 34.4 ± 2 | 91 ± 16 |
| DTLCG5 (0.6 % GA) | 2.08 ± 0.16 | 22 ± 4.5 | 34.2 ± 3 | 92.7 ± 16 |
| DCH6 (0.2 % GA) | 0.152 ± 0.09 | 9.93 ± 0.14 | 35.76 ± 2.3 | 80.3 ± 17 |
| DCH7 (0.4 % GA) | 0.180 ± 0.10 | 7.63 ± 0.52 | 35.57 ± 2.1 | 81.7 ± 16 |
| DCH8 (0.6 % GA) | 0.208 ± 0.03 | 4.81 ± 0.01 | 35.52 ± 0.9 | 81.6 ±8 |
| DCH9 (0.2 % GA) | 0.220 ± 0.01 | 7.06 ± 0.80 | 35.58 ± 0.7 | 81.1 ± 6 |
| DCH10 (0.4 % GA) | 0.258 ± 0.04 | 4.57 ± 0.15 | 35.45 ± 2 | 82.6 ± 16 |
| DCH11 (0.6 % GA) | 0.274 ± 0.06 | 3.39 ± 1.10 | 35.63 ± 2 | 81.2 ± 15 |
| DBLCH12 (0.6 % GA) | 1.12 ± 0.06 | 13.9 ± 11 | 35.57 ± 1.5 | 81.4 ± 12 |
| DTLCH13 (0.6 % GA) | 1.142 ± 0.03 | 20.6 ± 17 | 35.46 ± 2.3 | 82.7 ± 18 |
| DBLCH14 (0.6 % GA) | 1.112 ± 0.06 | 12.3 ± 4 | 35.14 ± 0.9 | 84.7 ± 8 |
| DTLCH15 (0.6 % GA) | 1.136 ± 0.01 | 16.9 ± 13 | 35.44 ± 1.4 | 82.4 ± 12 |

### 5.3.3. Chemical interaction of the cross linker and drug with CH and CG films

The assignment of characteristic absorption bands of chitosan and gelatine are given in Table 5.4, whereas the FTIR spectra of chitosan, gelatine, CG and CH films crosslinked with GA are presented in Figure 5.2. The observed peaks for pristine chitosan and gelatine sample were consistent with those reported in earlier studies [283, 284].

Table 5.4: FTIR absorption assignment of pure chitosan and gelatine.

| Sample | Wavenumber ($cm^{-1}$) | Assignment |
|---|---|---|
| Chitosan (LMW & MMW) | 3369 | Overlapped O-H and N-H stretching vibrations |
| | 2885 | Symmetric C-H stretching vibrations |
| | 1667 | Stretching vibration of C=O |
| | 1434 | C–N stretching vibration |
| | 1560 | N-H bending vibrations |
| | 1322 | Stretching vibrations of $–CH_3$ |
| | 1275 | CH3 bending vibration |
| | 1154 | C–O–C bending vibration |
| Gelatin | 3280 | Amide-A, N-H and O-H stretching vibrations |
| | 1630 | Amide-I, C=O and N-H stretching vibrations |
| | 1530 | Amide-II, C-N stretching and N-H bending vibrations |
| | 1225 | Amide-III, N-H stretching and C-N bending vibrations |

In previous studies, it was observed that chitosan and gelatine could interact via electrostatic interactions and hydrogen bonding. In acidic conditions, the charged carboxyl groups of gelatine may have interacted ionically with the charged amine groups of chitosan. Also, the polar carboxylic, amine and hydroxyl groups of gelatine could form hydrogen bonds with the hydroxyl and amine groups of chitosan [285]. In the current study, a single band at 1630 $cm^{-1}$ was observed when chitosan was mixed with gelatine (Figure 5.2), a red shift of the –C=O band of chitosan. Furthermore, a blue shift of the amide II band and red shift of the N-H band of chitosan resulted in a band at 1555 $cm^{-1}$. These observations indicated possibility of electrostatic interactions between N-H and C=O groups of the polymers. The crosslinking reaction between chitosan, gelatine and GA may involve Schiff-base formation and acetalisation reaction [286]. The 3300 $cm^{-1}$ broad O-H and N-H absorption band of GA free chitosan/ gelatine mixture blue shifted to 3360 $cm^{-1}$ upon the addition of GA under acid conditions. This could be attributed to the Schiff-base formation amino groups of gelatine and aldehyde groups of GA. Additionally, the $A_{1630}/A_{1555}$ ratio was higher in the GA cross-linked sample compared to the GA free chitosan/ gelatine mixture which could be due to acetal formation of GA cross-linked chitosan chains [287]. FTIR spectroscopy, therefore, confirmed formation of a cross-linked chitosan–gelatine polymeric network via reactions with GA under acidic conditions (Figure 5.3). On the other hand, changes were observed in the spectrum of GA-chitosan films compared to pure chitosan films. In the cross-linked chitosan films spectrum, the O-H stretching vibration was broader and shifted to a lower wavenumber (3275 $cm^{-1}$) which can be attributed to the effect of the addition of GA. The C-H stretching peak split into two peaks due to the presence of methylene group in GA, and the interaction between –CHO groups of GA and $–NH_2$ groups of chitosan formed an imine structure (C=N bond) due to the cross linking of the chitosan films. Two strong peaks were observed at 1560 $cm^{-1}$ and 1637 $cm^{-1}$ due to the crosslinking reaction of

chitosan and GA. Also an increase in the intensity of the peak at 1562 $cm^{-1}$ and 1637 $cm^{-1}$ represents a stretching vibrations of C=N in Schiff's base reaction further confirming the cross link formation between chitosan and GA [288]. FTIR spectroscopy, therefore, confirmed formation of a crosslinked chitosan–gelatine and crosslinked chitosan polymeric network via reactions with GA under acidic conditions. In Figure 5.4, DEX exhibited characteristic C-F absorption band at 1244 $cm^{-1}$ and bands at 1716 $cm^{-1}$, 1666 $cm^{-1}$ and 1622 $cm^{-1}$ attributed to -C=O stretching vibration linked to -$COO^{-}$ asymmetric stretching and C=C stretching bonds. The typical characteristics peaks from DEX were all observed in DEX loaded cross-linked CG and CH films at 1716 $cm^{-1}$, 1661 $cm^{-1}$ and 1623 $cm^{-1}$ respectively. Additionally, the characteristic absorption bands at 3390 $cm^{-1}$ and 1268 $cm^{-1}$ were due to the stretching vibration of O-H and C-F bonds [289]. It can also be observed, that the characteristic absorption band at 3340 $cm^{-1}$ of CH and 3432 $cm^{-1}$ of DEX shifted to 3314 $cm^{-1}$ and 3376 $cm^{-1}$ respectively, suggesting a small shift in the –OH group indicating that GA-CG and GA-CH may have interacted with DEX through hydrogen bonding. But this shifting also indicates that those hydrogen bonds presented by DEX were at a weak level as only small amount of DEX was dissolved to interact with GA-CG and GA-CH films [258]. But, the major peaks of DEX were not visible in the spectra of the cross-linked polymer carrier loaded with the drug, possibly due to masking of the DEX absorptions by those of the cross-linked polymer carriers. The spectrum of DEX-loaded CG and CH films was very similar to that of CG and CH films suggesting that no significant chemical changes occurred in the polymer backbone. Hence, these observations suggest DEX existed in the crosslinked polymer matrix with a possible interaction between the drug, cross linker and the polymer matrix.

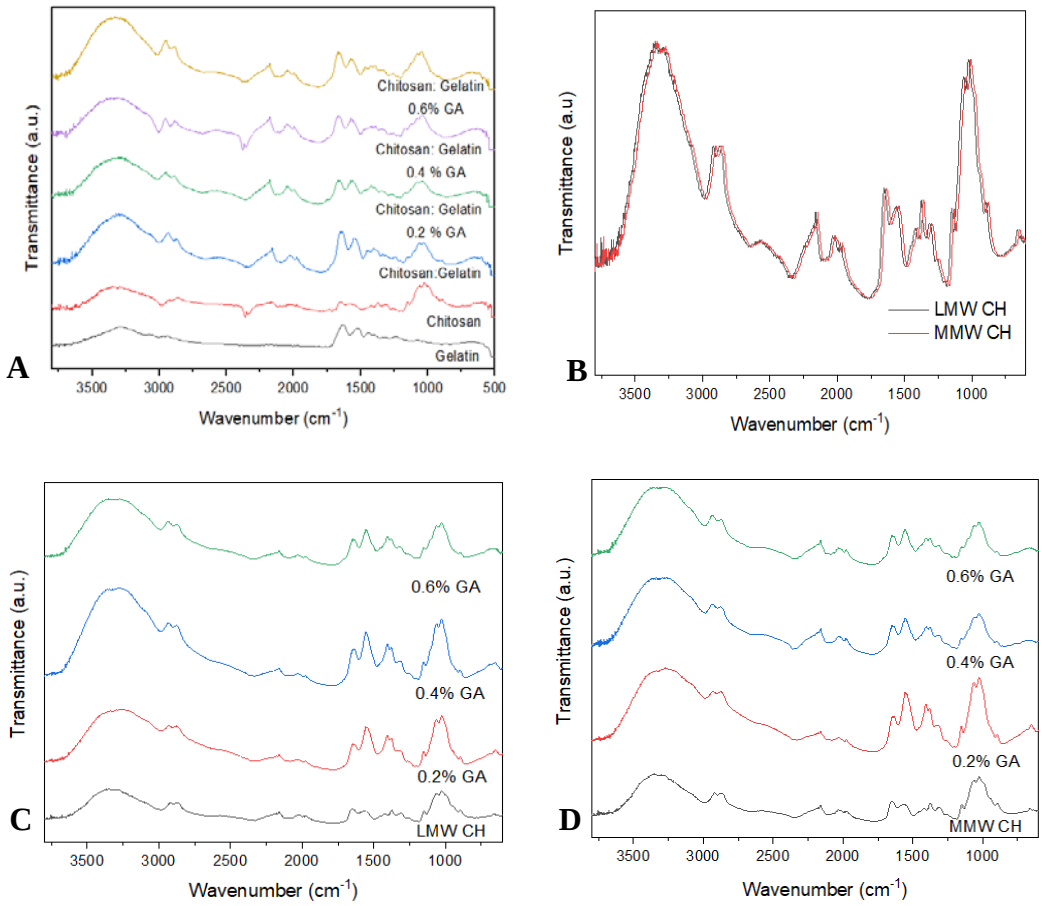


Figure 5.2: A) FTIR spectra of gelatine, chitosan, 1:1 chitosan/ gelatine blend and 1:1 chitosan/ gelatine blend cross-linked with different concentrations of GA; B) FTIR spectra of Pristine low molecular weight and high molecular weight chitosan; C) FTIR spectra of pristine LMW CH with cross-linked CH with different percentages of GA and D) FTIR spectra of pristine MMW CH with cross-linked CH with different percentages of GA.

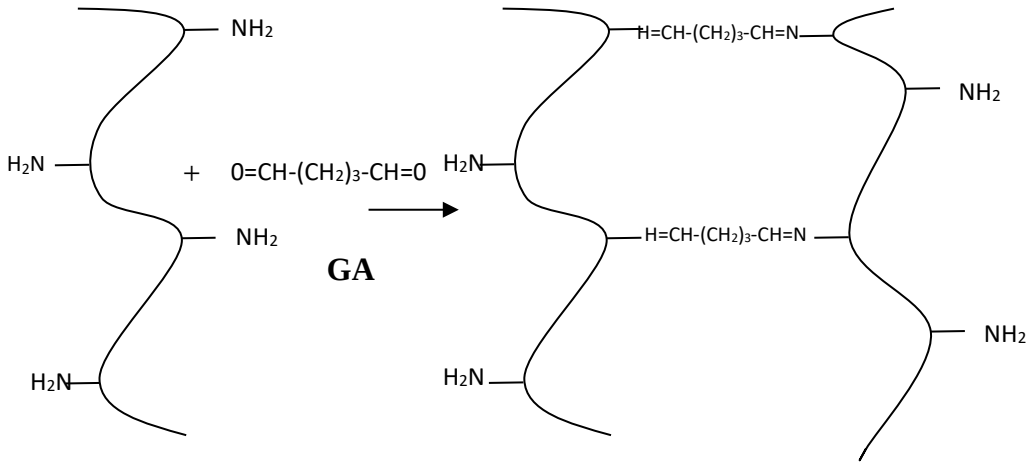


**Chitosan** **GA cross-linked with Chitosan**

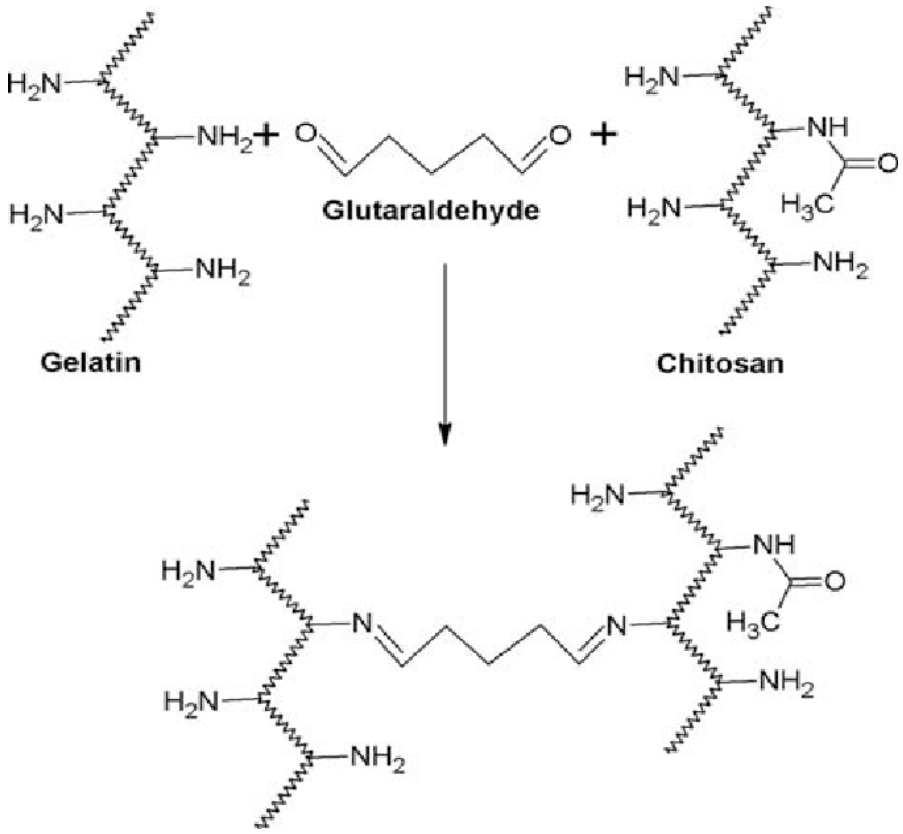


Figure 5.3: Structure of GA crosslinked with chitosan and gelatin to form Schiff base linkages (–C=N) because of its two active aldehyde groups [290].

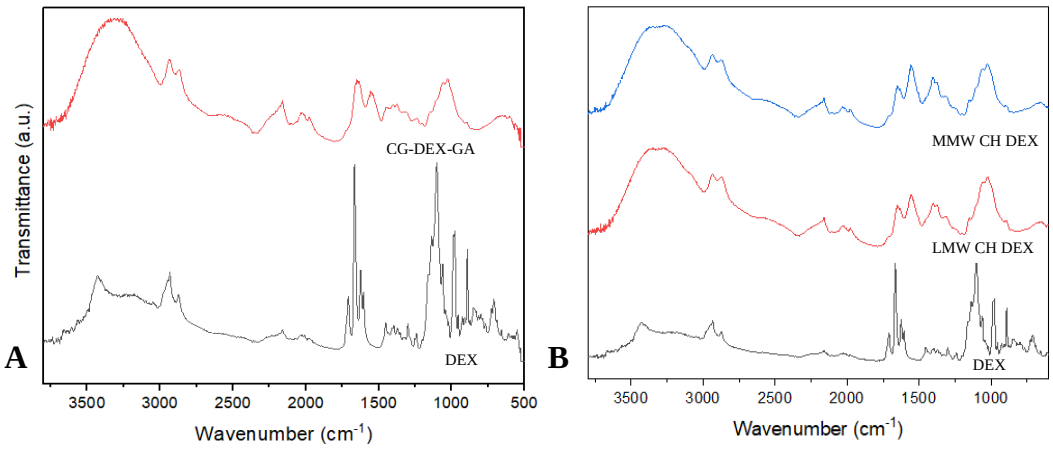


Figure 5.4: A) FTIR spectra of DEX loaded CG film cross-linked with GA (0.6%) and B) FTIR spectra of DEX loaded CH (LMW and MMW) cross linked with GA (0.6%).

### 5.3.4. Morphological analysis of CG and CH films

SEM observations was used to examine the microstructure of the developed multi-layer films of various formulations. Figure 5.5 shows the differences in the cross-section morphology of the drug loaded CG film crosslinked with GA. SEM images of the cross-section of different CG formulation showed a compact and homogenous structures

without any large pores as shown below. Additionally, no interfaces were observed in BL and TL samples, indicating a high compatibility between components demonstrating that chitosan and gelatine were completely miscible in this study. The SEM images also showed that no drug particle was visible in CG matrix indicating that the drug was miscible and well dispersed within the host polymer matrix [291].

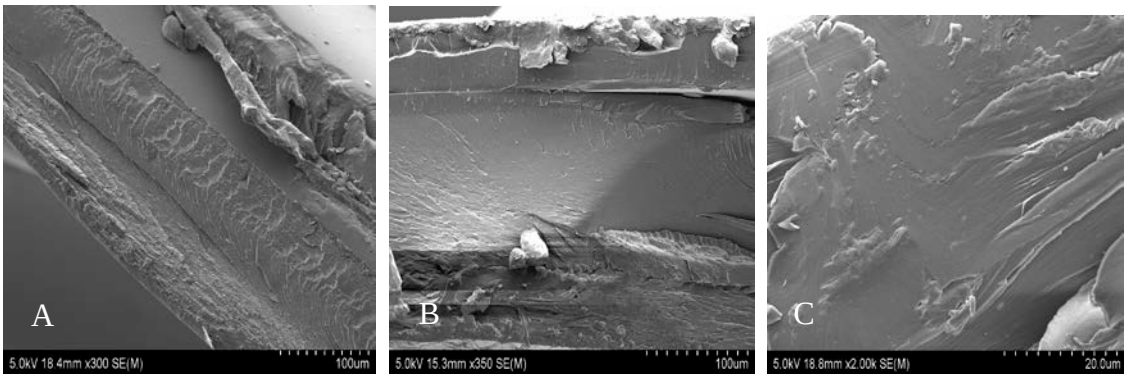


Figure 5.5: Cross section image of crosslinked DEX loaded CG film (0.6 % GA) for A) SL film B) BL film and C) TL film.

Similarly, Figure 5.6 and 5.7 shows the cross-section morphology of the drug loaded CH films (LMW and MMW) crosslinked with GA respectively. From the figure below, the cross-section images of the various CH films revealed a clean structure uniformly distributed along the film showing a compact morphology. Additionally, no interfaces were observed in the cross-section image of the BL and TL CH films showing a homogeneous structure, without pores and with excellent structural integrity. Furthermore, SEM images also showed that no drug particle was visible in the polymer matrix for various CH formulations indicating that the drug was miscible and well dispersed within the host polymer matrix [258].

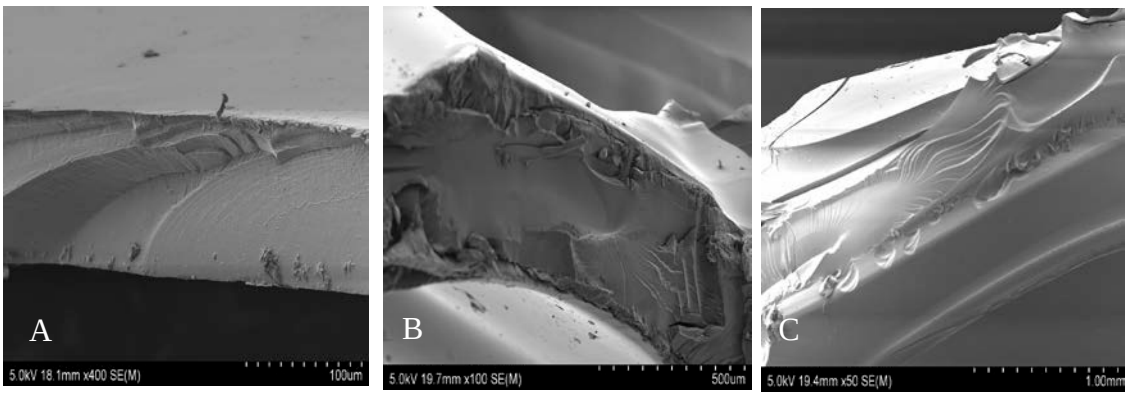


Figure 5.6: Cross section image of crosslinked DEX loaded LMW chitosan film (0.6 % GA) for A) SL film B) BL film and C) TL film.

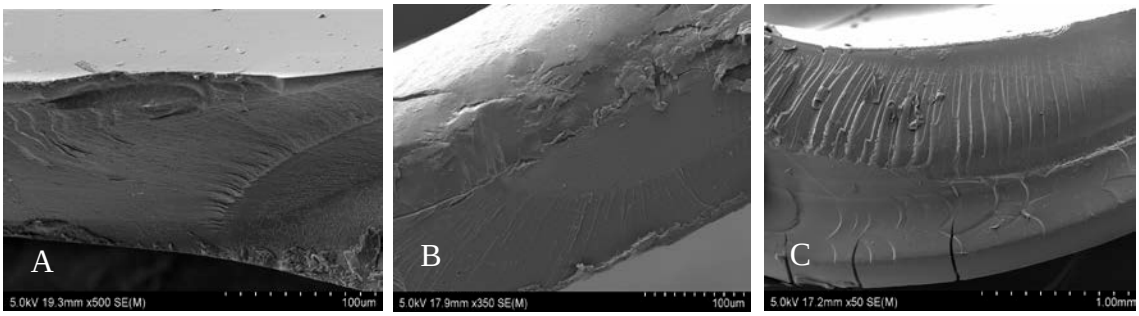


Figure 5.7: Cross section image of crosslinked DEX loaded MMW chitosan film (0.6 % GA) for A) SL film B) BL film and C) TL film.

It is also worth noting that the dense cross-sections of the BL and TL CH/CG films can be noticed because of the film thickness based on the formulation (Table 5.3).

### 5.3.5. Effect of cross linking on swellability and weight loss of CG and CH films

The degree of swelling obtained from different cross-linked drug loaded multi-layer formulations in PBS (pH 7.4) at 37 °C is shown in Figure 5.8 and 5.9. All cross-linked multi-layer films swelled rapidly and reached an equilibrium state within 24 hours [258, 292]. From both the figures, it can be observed that maximum hydration was obtained with TL formulations in comparison to SL films. The result in Figure 5.8, showed that drug loaded TL CG films (DTLCG5) has the highest swelling capability (285 wt. %) at 0.6 % concentration of GA with the fastest swelling in 1 hour, whereas drug loaded SL CG films (DCG3) showed the lowest swellability (101 wt. %) at the highest concentration of GA (0.6 %) showing that the swellability of the films was affected by the layer-by-layer assembly ($p < 0.05$). Similarly the result in Figure 5.9, showed that drug loaded TL

CH films (DTLCH13) has the highest swelling capability (154 wt. %) at 0.6 % concentration of GA with the fastest swelling in 1 hour, whereas drug loaded SL CH films (DCH11) showed the lowest swellability (81 wt. %) at the highest concentration of GA (0.6 %) in 1 hours ($p < 0.05$). Result from this study regarding swelling degree showed that maximum hydration was obtained with formulations containing TL films in comparison to BL and SL films, with SL< BL< TL. This high swelling capability in TL films can be attributed to the reasoning that the swelling extent was found to increase only with increasing number of layers, even though the cross linker would have restricted the movement of the polymer chains.

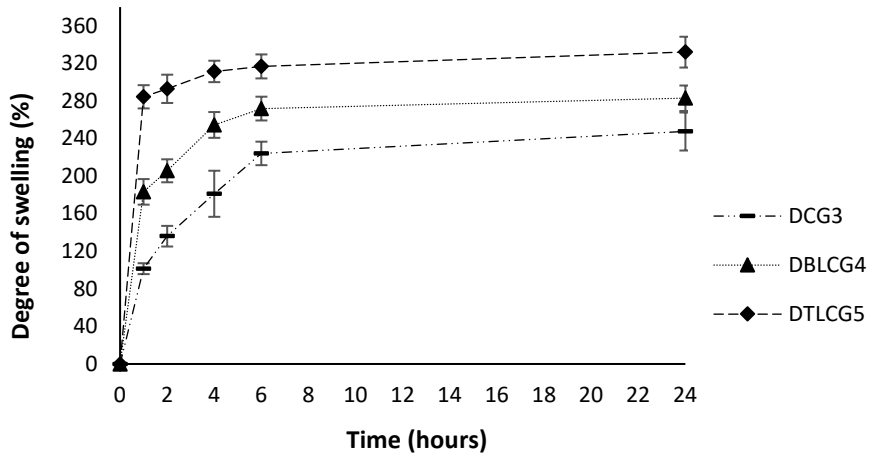


Figure 5.8: Swelling behaviour of crosslinked DEX loaded SL, BL, TL of CG films at different time points ($n$ = 3, mean ± SD).

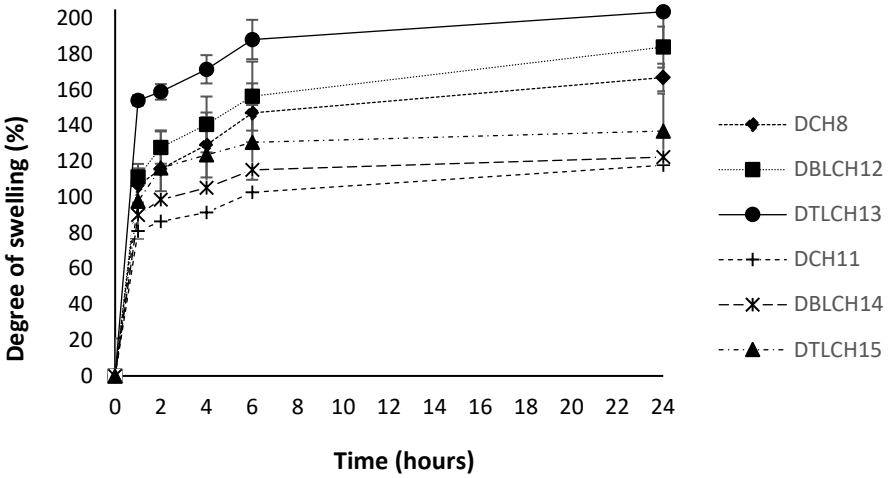


Figure 5.9: Swelling behaviour of crosslinked DEX loaded SL, BL, TL of LMW and MMW chitosan films at different time points ($n$ = 3, mean ± SD).

Figure 5.10 and 5.11 shows the weight loss of drug loaded multi-layer films of various formulations crosslinked with GA recorded at different time points. From the result, it was observed that TL films showed the highest weight loss ratio in comparison to BL and SL samples after 1 hours of soaking which is consistent with the swelling study in multi-layer films. The weight loss ratio of drug loaded TL formulations (CG, LMW CH and MMW CH films) were around 73 %, 67 % and 58 % respectively after 24 hours of soaking, whereas the weight loss ratio of drug loaded BL formulations (CG, LMW CH and MMW CH films) were around 64 %, 52 % and 47 % respectively after 24 hours of soaking. These results indicate that swelling and weight loss ratio is contributed by the layer-by-layer assembly of CG and CH films. Hence from the result, it is evident that when the layer increases an increasing swelling ratio was observed in the films, which can be due to the polymeric chains absorbing higher amount of PBS medium in each layer and thus samples with higher swelling ratio exhibited higher degradation rates. In the end, the swelling ratio and weight loss percentage of multi-layer films show similar trend.

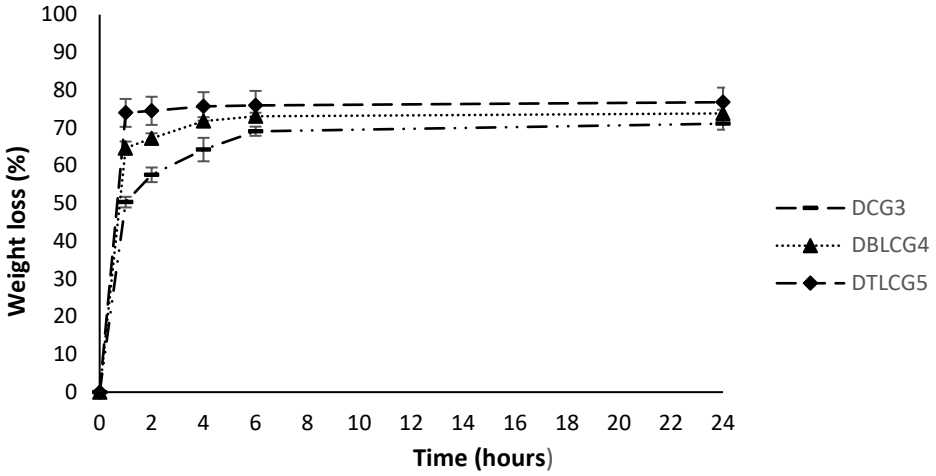


Figure 5.10: Weight loss of crosslinked DEX loaded SL, BL and TL CG films ($n$ = 3, mean ± SD).

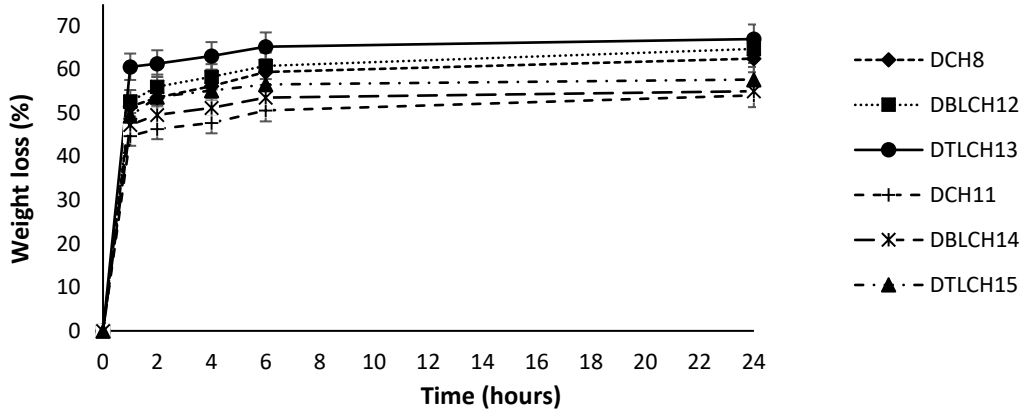


Figure 5.11: Weight loss of crosslinked DEX loaded SL, BL and TL CH films (LMW and MMW) ($n$ = 3, mean ± SD).

### 5.3.6. Anti-microbial activity of CG and CH

In this study, anti-bacterial activity of drug loaded crosslinked CG, CH (LMW and MMW) and DEX by itself was measured based on clear zone surrounding circular film solution by using a disc-agar diffusion test. If there was no clear zone surrounding, it was assumed that there is no inhibitory zone. From Figure 5.12 and 5.13, it can be observed that control, drug loaded and only drug samples, showed clear inhibitory zones against various bacterial strains with varying diameter as shown in Table 5.5. In this study, film forming solution of gelatine by itself (result not shown) did not show any antibacterial effect against bacterial strains but film with composite (chitosan and gelatine) components exhibited inhibitory activities against gram-positive bacteria (*Bacillus subtilis* ATCC 6633 and *Staphylococcus aureus* ATCC 25923)and gram-negative bacteria (*Escherichia coli* ATCC 25922 and *Pseudomonas aeruginosa* ATCC 27853). The film containing CH could subdue the bacterial growth, as the $NH^2$ group in chitosan becomes a quaternary amino group allowing chitosan to inhibit the growth of a variety of bacteria with higher inhibitory effect against gram (+) bacteria than for gram (−) bacteria. Previous study also showed that positively charged CH can interact with the negatively charged cell membranes, causing an increase in membrane permeability eventually rupturing leading to the leakage of intracellular components in microorganisms [293].

However, it can be observed from Figure 5.14, that DEX by itself did not show any noticeable inhibitory zone for the microorganism tested, indicating the absence of anti-microbial activity for the drug at the concentrations used in the preparation of the films.

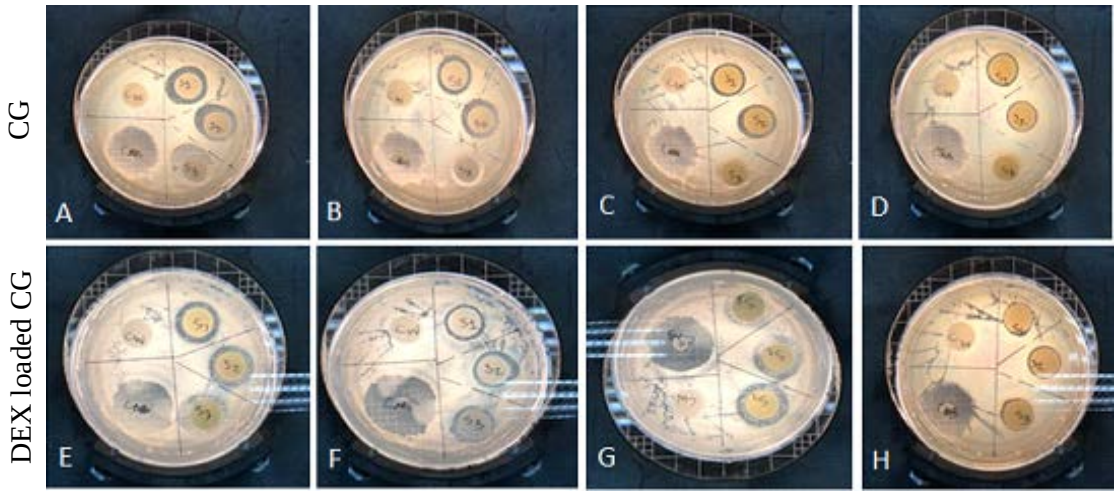


Figure 5.12: Inhibitory effect of CG and drug loaded crosslinked (0.6 % GA) CG solution on A and E) *Bacillus subtilis*; B and F) *Escherichia coli*; C and G) *Staphylococcus aureus* and D and H) *Pseudomonas aeruginosa.*

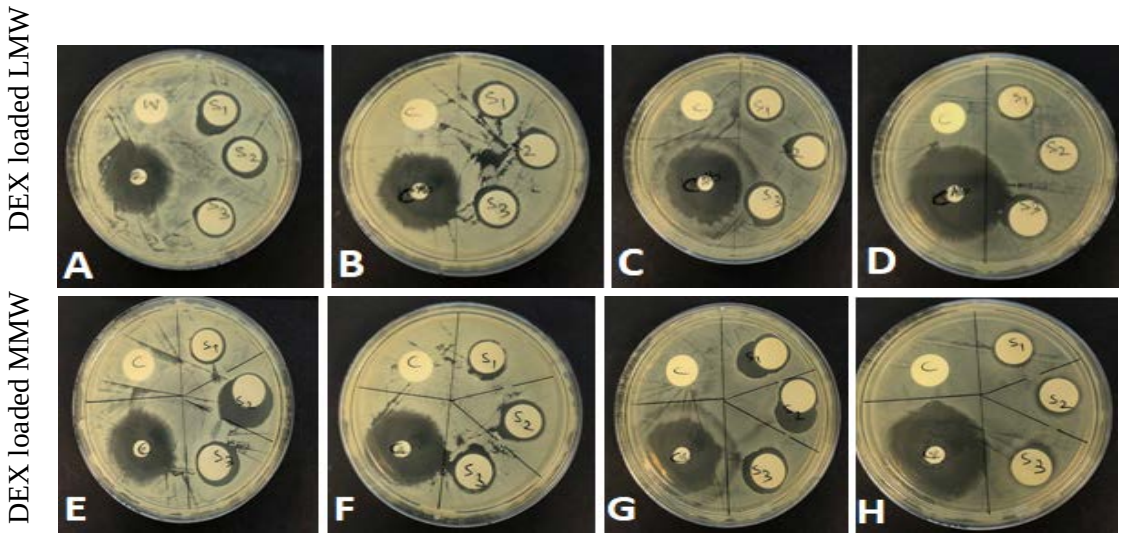


Figure 5.13: Inhibitory effect of drug loaded crosslinked (0.6 % GA) chitosan (LMW and MMW) on A&E) *Staphylococcus aureus* B&F) *Bacillus subtilis* C&G) *Escherichia coli* and D&H) *Pseudomonas aeruginosa*.

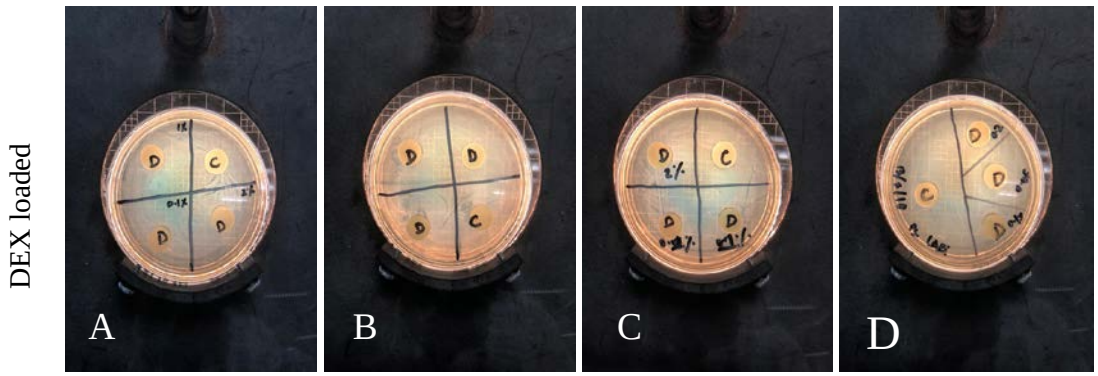


Figure 5.14:Inhibitory effect of DEX on A) *Staphylococcus aureus* B) *Bacillus subtilis* C) *Escherichia coli* and D) *Pseudomonas aeruginosa*.

Table 5.5: Anti-bacterial activity of CG, DEX loaded CG and CH (2 % LMW and 2 % MMW), ($n$ = 3, mean ± SD).

| Samples | Inhibition Zone (mm) | | | |
|---|---|---|---|---|
| | *B.subtilis* | *S.aureus* | *E.coli* | *P.aeruginosa* |
| CG | 3 ± 1 | 2.3 ± 0.5 | 2.4 ± 0.5 | 1 ± 0 |
| DEX loaded CG | 3 ± 1 | 2.7 ± 0.5 | 2.3 ± 0.5 | 1 ± 0 |
| LMW chitosan | 3.7 ± 1.5 | 5.4 ± 1.1 | 3.7 ± 1.1 | 2.3 ± 0.5 |
| DEX LMW chitosan | 3.7 ± 1.5 | 5.4 ± 1.1 | 3.7 ± 1.1 | 2.4 ± 0.5 |
| MMW chitosan | 3.8 ± 1 | 5.6 ± 0.5 | 3.7 ± 1.1 | 2.7 ± 0.5 |
| DEX MMW chitosan | 3.9 ± 1 | 5.6 ± 0.5 | 3.9 ± 1.1 | 2.7 ± 0.5 |

### 5.3.7. Drug loading

From Table 5.4, the measurement of DEX content in the films showed that the experimental drug content was very close to the theoretical one for each formulation, indicating that solvent-casting evaporation method is a suitable technique to produce drug loaded CG and CH films. From Table 5.3, the measurement of DEX content in the films showed that the experimental drug content was very close to the theoretical one for each formulation, indicating that solvent-casting evaporation method is a suitable technique to produce drug loaded films.

### 5.3.8. *In vitro* drug release from CG and CH films

*In vitro* release studies of DEX from CG and CH films were performed with respect to the concentrations of the crosslinker GA and multi-layer formulation. The release data presented in Figure 5.15 and 5.16, showed that multi-layer formulations showed sustained release over a period of 30 days, as expected. Results from swelling study and FTIR assessment showed that the pattern of drug release in this study were dependent on 1) concentration of the crosslinking amount and 2) number of layers. From the *in vitro* release study, it is evident that films with higher degree of crosslinking showed slower drug release rate. This finding confirms the possibility of controlling the drug release rate by varying crosslinking degree. Thus, as GA molecules increases, higher reaction with –OH groups of chitosan occur leaving a reduced number of unreacted hydroxyl groups to attract water molecules. Additionally, a higher crosslinking density translate to an added compact 3-dimensional macromolecular network with reduce space for free water to be absorbed in the hydrogel matrix so a decreased burst release for DEX was observed. This result is consistent with previous study which found the same effects of crosslinker concentration on the drug release rate [276]. Therefore, all SL formulations showed a burst release in the first 2 hours, but SL films with the highest crosslinker amount (0.6 % GA) such as DCG3, DCH8 and DCH11 films showed a slower DEX release rate. The burst release effect from all the SL formulations can be attributed to the free drug which is not bonded to the polymer matrix with GA, so the free drug was released at a faster rate, and in time swelling of the polymer matrix promoted solvent uptake along with drug dissolution [286].

In addition, it was also observed that the drug release rate was comparatively slower with TL films in comparison to SL and BL films. As the distance for diffusion for the drug has increased with increased layers, a continuous release profile was obtained. For multilayer films (Figure 5.15 and 5.16), it was observed that the release rate of DEX for DTLCG5

and DTLCH15 was about 10.6 % and 4.11 % respectively in the first 2 hours, with 88 % and 64 % respectively of the drug were released after 30 days (where $p < 0.05$ ($F(3, 56) = 5.150$, $p = 0.003$)). Furthermore, *in vitro* drug release assessment carried out in this study showed that TL CH film showed a slower DEX release rate in comparison to TL CG film, which can be attributed to the compact structure of higher molecular weight CH film in comparison to CG film, due to the reduced porous structure of CH forming an imperforate CH film, resulting in a slower and longer drug release profile. Thus, from the present release study it can be implied that sustained drug profile can be obtained by using this simple layer-by-layer technique.

From Figure 5.15, it can be observed that in DCG1 (0.2 % GA), DCG2 (0.4 % GA) and DCG3 (0.6 % GA) samples an initial burst release rate was observed in the first 2 hours (50.1 ± 0.4%, 46.3 ± 0.08% and 42.4 ± 0.4% respectively), with DCG3 sample showing a slower DEX release rate after 24 hours. The slow release rate for DCG3 sample in comparison to DCG1 and DCG2 samples can be accredited to its higher more compact structure with relatively minor pores due to the increased cross linker concentration. On the other hand, for multilayer CG films (Figure 5.15), it was observed that the release of DEX from trilayer film (DTLCG5) was slower in comparison to bilayer films (DBLCG4). The release rate for DEX observed in TL film was about 10.6 % in the first 2 hours with 88 % of the drug being released after 30 days whereas for BL film the release rate was 14.5 % in the first 2 hours which was progressively released up to and 92 % after 2 hours and 30 days respectively.

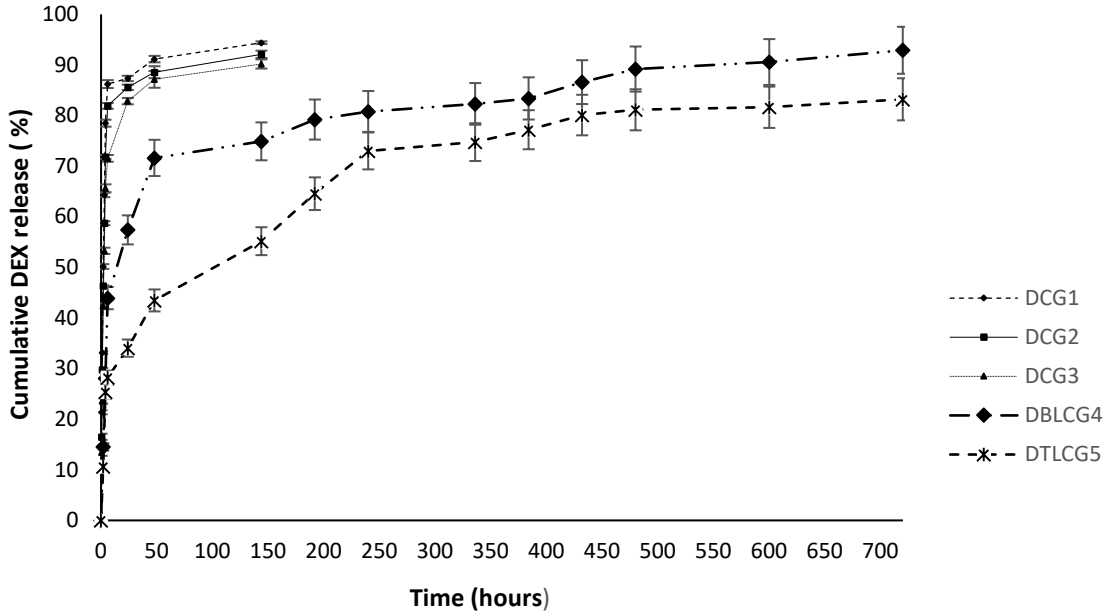


Figure 5.15: *In vitro* release profile of DEX loaded CG films, DEX-BL and DEX-TL CG films cross linked with GA ($n$ = 3, mean ± SD).

In Figure 5.16, it can be observed that a slower release rate was observed in the DCH8 and DCH11 formulations containing the highest cross linker concentration (0.6 % GA). The drug-release percentages for DCH8 and DCH11 formulations were 31.7 ± 0.5 % and 20.2 ±0.5 % in the first 2 hours respectively, with the release ratio slowing down after 24 hours and the final release percentages at 14 days were approximately 85 % and 74 % respectively. On the other hand, the drug release percentage for the lowest concentration of crosslinker samples (0.2 % GA) DCH6 and DCH9 were 77.1 ± 0.4 % and 53.9 ± 1.2 % at 2 hours respectively and the final release percentages after 14 days were approximately 99 % and 85 % respectively. Similarly, for CH multi-layer films (Figure 5.15), it was observed that the release of DEX from MMW TL film (DTLCH15) was slower in comparison to other multi-layer CH films. From the result, it can be observed that the maximum release rate was observed in LMW BL films showing 96.3 % released rate after 34 days in comparison to MMW TL films showing 64 % release rate after 34 days (where $p < 0.05$ ($F(3, 56) = 5.150$, $p = 0.003$)).

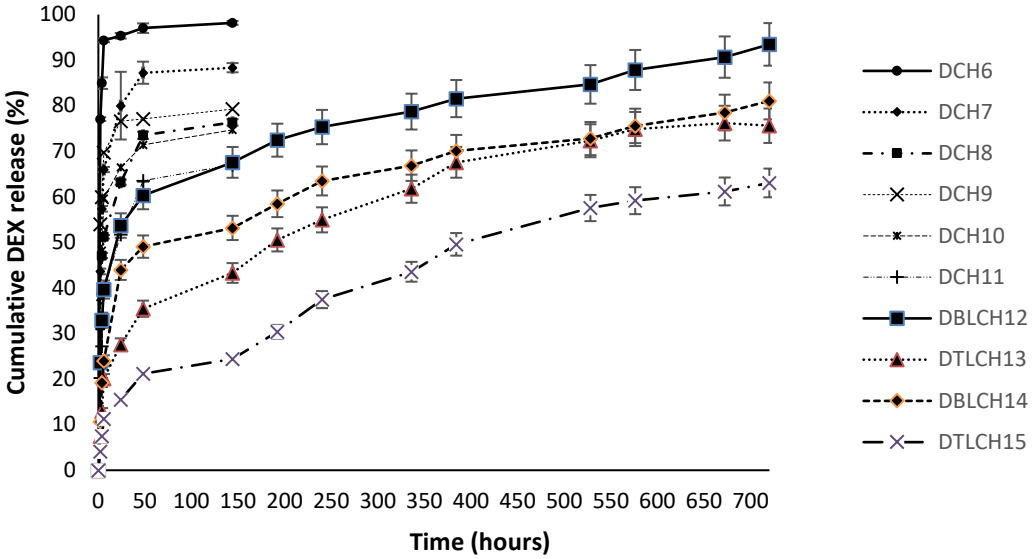


Figure 5.16: *In vitro* release profile of DEX loaded CH films, DEX-BL and DEX-TL chitosan films (LMW and MMW) cross linked with GA where ($n$ = 3, mean ± SD).

From this *in vitro* release study, it is evident that with higher degree of crosslinking films showed a slower drug release rate. This finding confirms the possibility of controlling the drug release rate by varying crosslinking degree where more GA bind with –OH groups of chitosan leaving a reduced number of unreacted hydroxyl groups to attract water molecules. Additionally, a higher crosslinking density translates to a more compact 3D macromolecular network with reduced space for free water to be absorbed in the hydrogel matrix so a decreased drug diffusion out from films. On the other hand, a faster *in vitro* DEX release behaviour can be attributed to the lower amount of cross linker used in these films, leading to lesser binding of the drug with the polymer matrix, so the free drug was released at a faster rate, promoting solvent uptake and drug dissolution. From the result it was observed that the drug release rate was comparatively slower with TL films in comparison to SL and BL films, as the distance for diffusion for the drug has increased with increased layers. In addition, it can also be observed that TL CH films showed a slower DEX release rate in comparison to TL CG film which can be attributed to the compact structure of higher molecular weight CH film in comparison to CG film, and the addition of a crosslinker relatively reduced the porosity of CH forming an imperforate CH film, which resulted in a slower and longer drug release profile. Thus, from the

present release study it can be implied that the drug release rate can be controlled by using this simple layer-by-layer technique [258, 294].

Furthermore, the drug release data obtained can be analysed by appropriate mathematical models to support the interpretation of mechanisms involved in the drug release process. In this study, different mathematical models were applied to *in vitro* drug dissolution release profiles and their respective coefficients are reported in Table 5.6 [295-297]. Drug release from films can occur in three main steps where, a) the drug-loaded film contains a minimum amount of water presenting minimum flexibility, pore size and drug mobility, b) the film undergoes relaxation becoming more flexible, pore size and drug mobility increase with increased hydration and in the last step c) the film is fully relaxed and hydrated with the pore size at its maximum, as is the rate of drug diffusion.

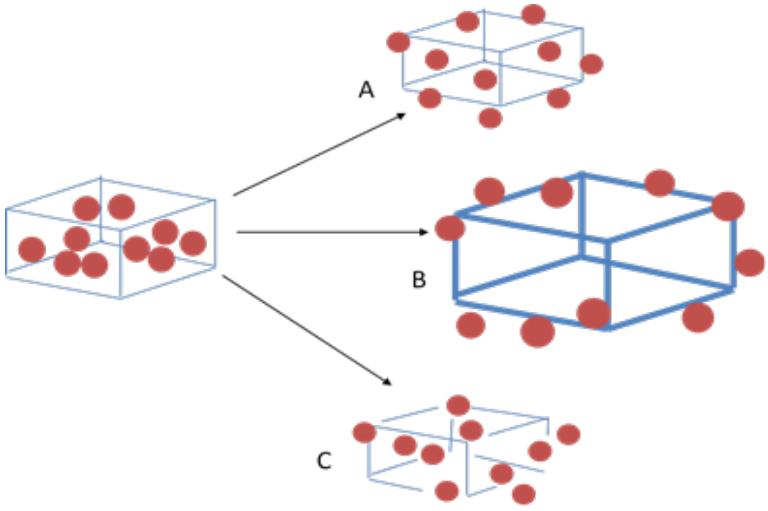


Figure 5.17: Schematic representation of the possible mechanisms of drug release from biodegradable films by A) diffusion, B) swelling and C) erosion of polymer matrix.

In this study, according to $R^2$ values in table 5.6, the different drug loaded multi-layer formulations (CG and CH films) fitted better with the Weibull model followed closely by the Korsmeyer-Peppas model, and the values of the kinetic rate constant (k), the correlation coefficient ($R^2$), and the release exponent (n) are all tabulated in Table 5.6. In this study, the Weibull function is used to describe the drug-release mechanism of the entire drug-release curve and the b coefficients values of the Weibull are correlated with

the release mechanism of drug throughout the polymer matrix. The b values <0.75 are related to Fickian diffusion, while b values between 0.75 and 1.0 suggest that release is governed by Fickian diffusion and case II transport [298, 299].

Table 5.6: Kinetics parameters of DEX release from multi-layer CG and CH films.

| **Formulations** | Zero order | | Korsmeyer-Peppas | | | Weibull | | | Hickson-Crowell | |
|---|---|---|---|---|---|---|---|---|---|---|
| | $K_0$ | $R^2$ | n | $K_{KP}$ | $R^2$ | a | b | $R^2$ | $K_{HC}$ | $R^2$ |
| **DBLCG4** | 0.147 | 0.594 | 0.183 | 28 | 0.974 | 4.24 | 0.366 | 0.987 | 0.002 | 0.339 |
| **DTLCG5** | 0.133 | 0.753 | 0.253 | 16 | 0.982 | 8.27 | 0.417 | 0.990 | 0.001 | 0.450 |
| **DBLCH12** | 0.155 | 0.7035 | 0.188 | 26 | 0.972 | 4.05 | 0.332 | 0.984 | 0.002 | 0.357 |
| **DTLCH13** | 0.125 | 0.8275 | 0.315 | 9.7 | 0.985 | 14 | 0.453 | 0.990 | 0.001 | 0.524 |
| **DBLCH14** | 0.133 | 0.7408 | 0.241 | 16 | 0.980 | 7.05 | 0.363 | 0.987 | 0.001 | 0.430 |
| **DTLCH15** | 0.098 | 0.9240 | 0.449 | 3.2 | 0.989 | 50.79 | 0.588 | 0.993 | 0.000 | 0.643 |

In this study, the single layer CG and CH samples showed b values ranging from 0.75 – 0.88 (data not shown here) signifying a combined diffusion and film relaxation mechanism. But for multi-layer samples (CG and CH films), the b coefficients values range from 0.36-0.58 respectively, indicating that the release mechanism of drug throughout the polymer matrix are related to a diffusion dominated drug release process (Fickian diffusion). Hence, a comparatively slower release rate was observed in multi-layer films in comparison to SL films as the distance for diffusion was increased with increased layers. Therefore, the initial quick release rate of DEX from multi-layer films can be attributed to the fact that drug located near the surface, had a short distance to

travel to the film surface, but as the distance of DEX increases from the film surface a slower and more sustained release of the drug was observed. In conclusion, film thickness or layer by layer assembly of films can be used to control the release rate and the percentage of the released amount of DEX from multi-layer films. In addition, according to the Korsmeyer–Peppas model the release exponent n which was obtained from the slope was below 0.5 (Table 5.6) further indicating that the DEX release from multi-layer films was a Fickian diffusion mechanism.

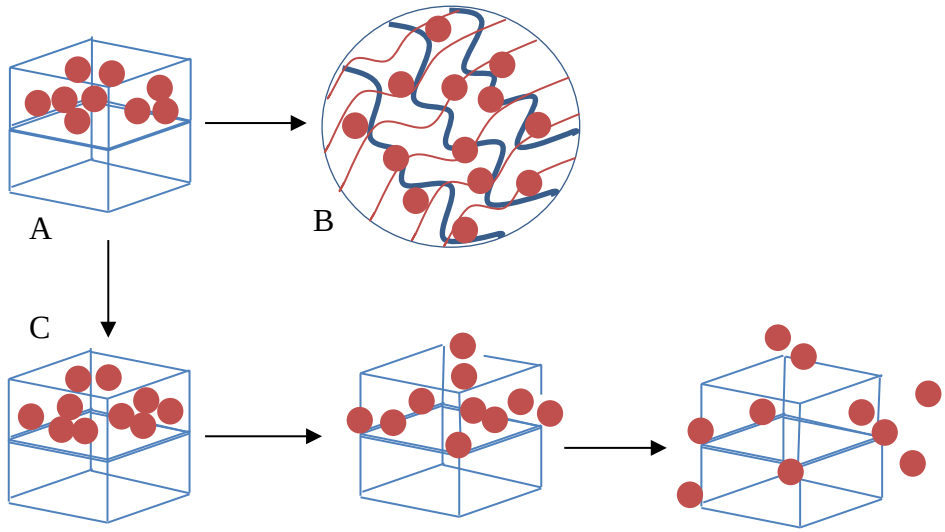


Figure 5.18: Schematic representation of A) bilayer cross linked drug loaded film B) proposed mechanism for the formation of GA cross linked C or CG with drug entrapped within the matrix and C) possible drug release mechanism by diffusion of polymer matrix over time.

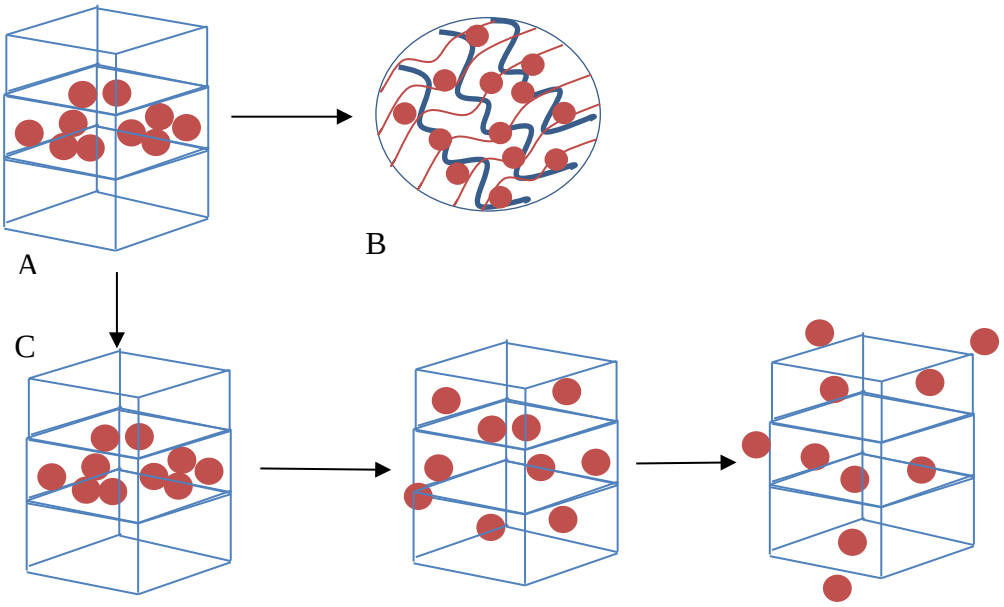

Figure 5.19: Schematic representation of A) trilayer cross linked drug loaded film B) proposed mechanism for the formation of GA cross linked C or CG with drug entrapped within the matrix and C) possible drug release mechanism by diffusion of polymer matrix over time.

## 5.4. Conclusion

In this work, the effect of layer-by-layer assembly on release profiles of CG and CH films was determined. It was observed that multi-layers cross linked films show higher water absorption, swelling and faster degradation which can be attributed to the films' thickness added by the layer by layer assembly. It was also observed, from this study, that the addition of layers to CG and CH film slowed the DEX release profile in comparison to single layer films, due to the presence of additional layers acting as a controlling membrane for drug diffusion. As such the addition of layers relatively deaccelerated the capability of water-filled channels to acts as conduits for solvent uptake, thereby reducing drug diffusion and as the distance between the drug and the films surface increased, a slower and longer drug release profile was obtained. In addition, it was also observed that multi-layer CH films with MMW has the slowest drug release profile in comparison to other multi-layer films with a similar crosslinking degree (0.6 % GA). This can be attributed to their compact polymeric chain structure which in turns leads to reduced porosity and solvent uptake. Furthermore, kinetic analysis of the drug release profile from crosslinked multi-layer films of various formulations was a Fickian diffusion from the polymeric chain leading to a control drug release kinetic behaviour with MMW TL CH showing the best adjusted $R^2$ values ($R^2$= 0.9930) for Weibull model. Therefore, from the *in vitro* anti-inflammatory drug release assessment carried out, a targeted sustained released of the drug for 30 days was achieved suggesting that these films can act as potential drug carriers. Moreover, the ability of these films to be able to provide antimicrobial activity at the administration site is advantageous making these multi-layer films an effective drug delivery vehicle for intranasal applications. In the end, this simple

layer by layer technique opens possibilities for developing drug loaded conformal thin films that can be used for various drug delivery applications.

## 5.5. Future directions

From this study, the layer-by-layer technique of producing multi-layer polymeric formulations provided a sustained drug release profile showing that this method can be used as an effective tool to control drug release. But, for future studies exploring the enhancement of the multilayer film's mechanical properties, long term storage and new type of stimuli (external/internal) responsive drug release mechanisms will be necessary. Hence, this simple layer-by-layer assembly technique may also enable the revival of old therapeutic approaches by modifying the delivery method for e.g., integration of these drug loaded conformal thin films into implants, stents, bandages or biomedical devices to trigger microscale drug release to localised regions within the body or through the skin. In the long run, being able to produce layer-by-layer films with new materials using a new rapid assembly method for sustained multi-drug release with complex three-dimensional geometries will also provide innovative opportunities for transforming biomaterials and drug delivery applications on a commercial scale. In this study, the sustained delivery of an anti-inflammatory agent independent of the stent structure was developed by using a multi-layer polymeric film as the drug carrier for local delivery.

# Chapter 6. Development of gelatine coating as an anti-fibrinolytic drug carrier

During functional endoscopic sinus surgery (FESS) bleeding usually occurs due to damage of the carotid arteries (external and internal) in this region which requires the use of haemostatic drugs. This **Chapter 6** investigates an anti-fibrinolytic loaded gelatine coating for the surface of the stent to provide haemostasis (Figure 6.1).

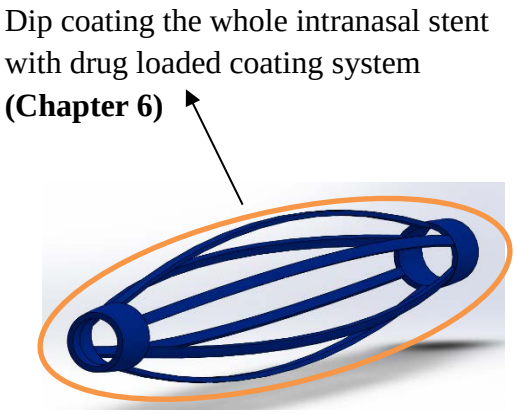


Figure 6.1: Diagrammatical representation of the dip-coated 3D printed intranasal stent.

## 6.1. Introduction

### 6.1.1. Gelatine as a coating agent for medical devices

Gelatine is an interesting biomaterial for drug delivery due to these following characteristics: i) it is relatively inexpensive, with an excellent film forming capacity ii) it has been generally recognized as a safe material by the FDA [300], iii) excellent biocompatibility and biodegradability, iv) not antigenic, v) nontoxic and v) can easily be applied as a thin coating [301]. In the medical and pharmaceutical fields, gelatine has been widely used as a coating agent for implants and devices [301-304]. However, since gelatine films are hydrophilic in nature they may swell, partially dissolving or disintegrating when immersed in aqueous solutions thus, crosslinkers are added to improve their structural properties. Chemicals crosslinkers such as glutaraldehyde (GA) and genipin (GP) have been used for their ability to interact with gelatine [305-307].

Hence, the degree of crosslinking in gelatine plays an important role in influencing its structural properties, swelling behaviour and other physiochemical properties that in turn can affect drug release profiles [308, 309]. But using chemical crosslinkers on gelatine to coat medical devices and implants may initiate calcification of these structures (due to the deposit of calcium salts especially calcium phosphate (hydroxyapatite), occurs in and on some materials used in the production of implantable devices, so there is a need for developing biocompatible crosslinkers derived from natural sources. Therefore, with regards to that other studies have shown that sugars (e.g. ribose, fructose) have the ability to interact with gelatine through a process called Maillard reaction, enabling these sugars to be used as crosslinkers for gelatine [310-312].

In this present study, a gelatine coating-based matrix crosslinked with lactose for the release of an anti-fibrinolytic agent was developed. The lactose-cross linked gelatine matrices will act as a reservoir for Tranexamic acid (TXA), allowing gradual elution of the drug. TXA is mostly used in surgical procedures for reducing blood loss and lowering transfusion rates [313, 314]. Apart from using lactose as the crosslinker, the number of gelatine coating cycle were varied to observe if different level of coating can provide a targeted release of the drug for 4 hours that can be used for coating the developed intranasal stent in the future. This study investigates the physio-chemical properties, *in vitro* release profile and drug release mechanism of the TXA loaded crosslinked multi-layer gelatine coatings.

## 6.2. Materials and methods

### 6.2.1. Materials

Gelatine (Porcine type A with 300 Bloom value), lactose, Tranexamic acid, phosphate buffered saline tablets, acetonitrile (LC-MS grade), water (LC-MS grade) and d,l-alanine-2,3,3,3-$d_4$ was purchased from Sigma-Aldrich, New Zealand. Snakeskin dialysis tubing

(7 kDa cut-off for protein recovery) was purchased from Thermo Fisher Scientific, New Zealand. PLA filament (UP fila, ø 1.75 mm) was purchased from 3D printing systems, New Zealand. The AccQ•Tag Ultra eluent concentrates and AccQ•Tag Ultra derivatisation kit were purchased from Waters Corporation, Milford, USA. Ultrapure water from Milli-Q water system was used to prepare the aqueous and buffer solutions.

### 6.2.2. Fabrication of the model object

A cylindrical scaffold was fabricated using a standard fused-deposition modelling 3D printer (UP Mini 3D printer, 3D printing Systems) [247] to resemble a drug eluting stent to be coated. The templates were designed with SolidWorks CAD software and exported as a stereolithography (.stl) file into the printer. The printer settings were as follows: Z resolution with the raft option deactivated and an extrusion temperature of 200 °C, speed while extruding (10 $cm^3$/h), nozzle outlet diameter (0.4 mm), resolution layer thickness (0.15 mm), number of shells (6) and fine quality with solid fill. The infill percentage was 100 %.

### 6.2.3. Preparation of gelatine coating

The crosslinked lactose gelatin coating was prepared as follows. Based on a previous study, 10 % w/v of gelatine solution with 20 wt. % lactose based on gelatine dry basis was prepared [307]. In this study, about 3g of type A gelatine with the required amount of lactose were dissolved in 20 ml of distilled water for 30 min at 50 °C under continuous stirring to obtain a homogeneous blend. For drug loaded gelatine coating, about 2 mg/mL of TXA was then added to the solution and it maintained at 50 °C for 5 mins under stirring. Then the printed PLA cylinders were dipped into the coating solutions (3 and 5 % w/w gelatine without and with TXA), and then immediately rotated to remove the excess solution and to form a uniform coating. The coated scaffolds were then dried at 40

°C for 24 hours. The dipping-drying steps were repeated three times to obtain thicker coating (Table 6.1).

Table 6.1: Different formulations of lactose crosslinked gelatine coatings.

| Formulation | Gelatine % (w/v) | Number of coating | Drug (W/V %) |
|---|---|---|---|
| GC1 | 3 | 1 | - |
| DGC1 | 3 | 1 | 2 |
| GC2 | 3 | 2 | - |
| DGC2 | 3 | 2 | 4 |
| GC3 | 3 | 3 | - |
| DGC3 | 3 | 3 | 6 |
| GC4 | 5 | 1 | - |
| DGC4 | 5 | 1 | 2 |
| GC5 | 5 | 2 | - |
| DGC5 | 5 | 2 | 4 |
| GC6 | 5 | 3 | - |
| DCG6 | 5 | 3 | 6 |

### 6.2.4. Weight change with recurrent coatings

Weight change of the cylinder during coating process was measured with the use of an electronic balance (AUW220D, Shimadzu, Japan) and the study was carried out in triplicate with their mean weight being calculated.

### 6.2.5. Scanning electron microscopy (SEM)

The morphology of the coated PLA cylinder obtained was assessed by scanning electron microscopy (SEM) (Hitachi SU-70, UK). The individual samples were fixed on aluminium stubs using carbon tapes and sputter-coated with platinum for 20 s (Hitachi E-

1045, UK). The surface morphology of individual samples was observed at an accelerating voltage of 5 kV.

### 6.2.6. Fourier transform infrared (FTIR) spectroscopy

FTIR was used to characterise the presence of specific chemical groups in the coatings. GC cross-linked with lactose were obtained and were analysed by FTIR spectra using a Spectrum Two PE instrument equipped with a horizontal attenuated total reflectance (ATR) crystal (ZnSe) (Nicolet iS10, Thermo Scientific, USA). The samples were placed directly onto the ATR crystal and spectra were collected in transmittance mode. FTIR spectra were collected with wavenumber ranging from 3800 to 600 $cm^{-1}$ during 64 scans, with 2 $cm^{-1}$ resolution. The FTIR spectra were normalised and major vibration bands were identified and associated with the main chemical groups.

### 6.2.7. Water uptake

The water uptake of gelatine coats was calculated under physiological conditions by submerging in a 20ml phosphate buffer solution (pH 7.4, 37 °C) and withdrawing at predetermined time intervals for 10, 20, 40, 120, 180, 140 and 1440 minutes. The coatings were carefully blotted with tissue paper to remove surface water and were weighed with an analytical balance. Triplicate measurements were obtained for each sample and expressed as means ± SD. The water uptake was determined using the following equations:

$$\text{Water uptake (\%)} = \frac{W_0 - W_1}{W_1} \mathbf{x}\ 100$$

Where, $W_0$ and $W_1$ are the weights of the film before and after infiltration, respectively.

### 6.2.8. Coating degradation

Printed cylinders with and without coating were prepared for testing. Each sample was immersed into a beaker containing 20 mL PBS (pH 7.4) at 37 °C for up to 24 hours. At

predetermined points of time for 10, 20, 40, 120, 180, 140 and 1440 minutes, samples were taken out and dried for 24 hours. The weight loss of the cylinder was measured.

### 6.2.9. *In vitro* drug release

The *in vitro* drug release profile of different formulations of films with TXA was carried out was carried out in physiological-simulated (PBS) media (40 mL, pH = 7.4) under sink condition. The coated cylinder with TXA was placed in snakeskin dialysis bag (7 kDa cut-off for protein recovery) before being placed in the above physiological solution shaken at 100 rpm ± 5 at 37 °C ± 0.5. Samples were withdrawn at predetermined time interval for 15, 30, 60, 120, 240, 360 and 1440 minutes. The volumes of withdrawn samples were replaced with physiological solution to maintain sink condition. The absorbance of the samples was measured with a LC-MS System (Agilent Technologies).

#### 6.2.9.1. AccQ•Tag derivatisation of TXA

In 50 µL of samples and standards, equal volume of internal standard $L^{-1}$d4-alanine was added before derivatisation for LC-MS analysis. TXA samples and standards derivatisation with AccQ•Tag reagents was conducted according to the manufacturer's protocol. For a short period of time, 10 µL of the withdrawn samples was mixed with 70 µL of AccQ•Tag Ultra borate buffer, and 10 µL of AccQ•Tag reagent previously dissolved in 1.0 mL of AccQ•Tag Ultra reagent diluent was added. The reaction could proceed for 10 min at 55 °C. Furthermore, AccQ•Tag derivatised samples and standards were added with a neutralising solution before LC-MS analysis as they must be free of particulates and alkalinity. In the end, the samples and standards were vortexed and stored at -20 °C for analysis.

#### 6.2.9.2. Calibration standards and drug loading determination

Stock solutions of TXA (10 mg/ml) in ultra-pure water and of the internal standard (IS, 0.5 mg/ml) in methanol–water (1:1, v/v) were prepared separately. TXA (0.3, 0.6, 1.25,

2.5, 5 and 10 µg/ml) and IS (125 µg/ml) calibration samples were prepared in triplicate by dilution of their stock solutions in ultra-pure water. For the determination of the drug loading of TXA, drug loaded GC were dissolved in a 10 ml PBS of pH 6.8 and stirred under magnetic stirrer for 24 hours at room temperature, followed by ultra-sonication for 10 min. The amount of TXA was determined with a LC-MS System (Agilent Technologies). The drug loading (DL) were calculated as typically reported.

$$\text{DL}\ (\%) = \frac{\text{Amount of drug}}{\text{Amount of polymer+drug}} \times 100$$

**6.2.9.3. Sensitivity**

The limit of quantification for TXA was determined based on the criteria that the analyte response at LOQ, defined as the lowest concentration could be measured with an accuracy of ± 20 % and the signal-to-noise (S/N) ratio ≥ 10. The limit of detection (LOD) was defined as the lowest concentration with (S/N) ratio of 3.

**6.2.9.4. LC-MS method of analysis**

The LC-MS-1260 Infinity system consist of a 6420A triple quadrupole LC-MS System with a hyperbolic quadrupole design, a high-pressure hexapole collision cell with linear acceleration and an off-axis high energy dynode detector (Agilent Technologies). A chromatographic reverse phase separation method was performed using an XSelect CSH C18 columns from Waters Corporation (3.5 µm, 4.6 mm X 100 mm). The mobile phase solvent A was 0.1 % formic acid in $H_2O$ and mobile phase solvent B was 100 % acetonitrile with 0.1 % acetic acid. The following gradient elution was used: 0−3 min A was 97 % and B was 3 % B; 3−4 min A was 70 % and B was 30 %; 4−5 min A was 20 % and B was 80 %; 5−6 min A was 97 % and B was 3 %. The flow rate was 0.4 mL/min, the injection volume was 2 µL, and the detection was at 250 nm [315]. From the value of absorbance, the percentage of drug release was calculated and graph of the percentage of

drug release against time was plotted. Release studies were performed in triplicate and expressed as mean ± SD.

### 6.2.10. Analysis of kinetic models

Drug dissolution data were fitted with different mathematical models (Table 6.2).

Table 6.2: kinetic release mathematical models.

| Model | Equation[a] |
|---|---|
| Weibull | $F = 1 - \exp(-at^b)$ |
| Korsmeyer-Peppas | $F = k_p t^n$ |
| Hixson and Crowell | $F = [1 - (1 - k_{HC} t)]^3$ |
| Zero order | $F = k_p t$ |

[a] $F$ = amount of drug release at time $t$; kHC and $k_p$ = release rate constants for different equations; $n$ and $b$ = release exponents.

### 6.2.11. Statistical analysis

Data were subjected to one-way analysis of variant [245] by means of a SPSS computer program (SPSS Statistic 20.0). Post-hoc multiple comparisons were determined by Tukey's test with a significance level set at $p < 0.05$. Error bars in the figures represent the standard deviation (SD).

## 6.3. Results and discussion

### 6.3.1. Change of coating weight with increased number of coating

As shown in Figure 6.2, the weight of the initial cylinder changed as the number of coats increased. There was a linear increase in the coating weight gain. Figure 6.3 shows that the coating weight gain of the cylinder with recurring coating cycle leads to a linear increase in coating implicating that the drug entrapment could be controlled with increased coating cycle. As such, drug release from recurring or cyclic coating can be

projected and controlled, as it can be directly proportional to the coating weight gain [316].

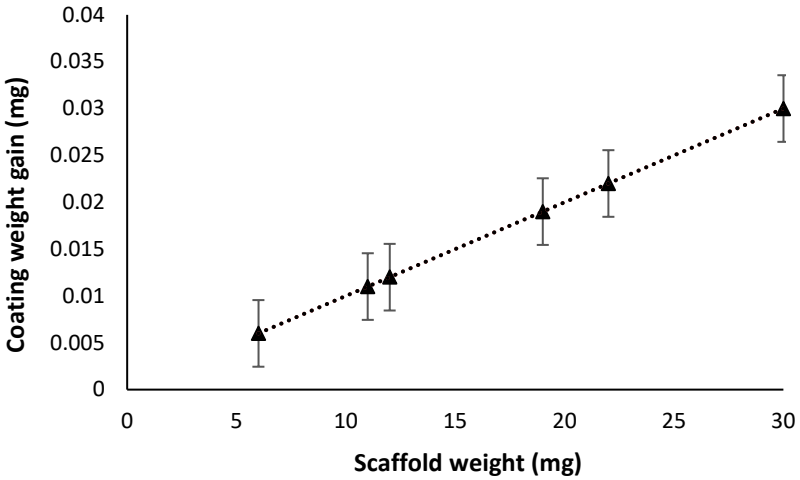


Figure 6.2: Weight gains of the GC cylinder scaffold, as represented with variation in the initial scaffold weight. Data showed a linear relationship with initial scaffold weight ($n$ = 3, mean ± SD).

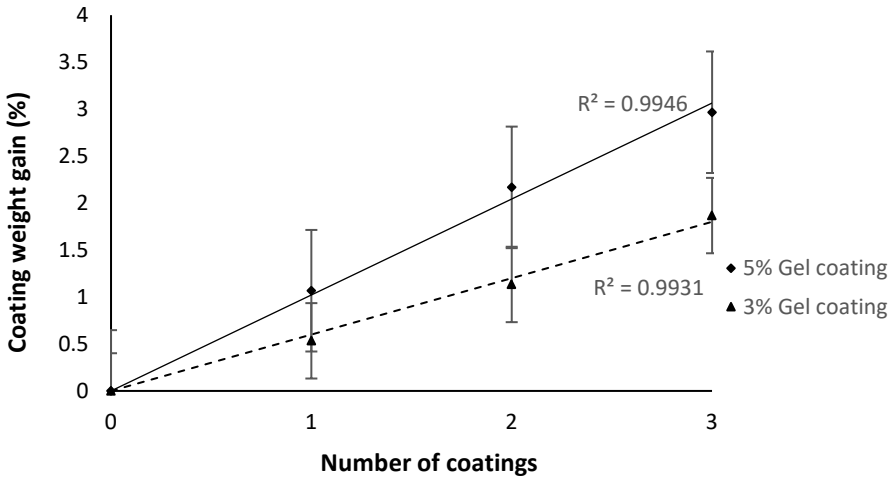


Figure 6.3: Weight gains of the GC cylinder scaffold, as represented with increasing number of coating. Data showed a linear relationship with increasing number of coating (n = 3, mean ± SD).

### 6.3.2. Morphological studies of GC on printed scaffold

The morphological properties of GC on printed scaffold were observed using SEM. The morphologies of the printed cylinder before and after coatings are shown in Figure 6.4 (A–H). Figure 6.4A, shows the uncoated cylinder has a rough surface but as the number of coating increases the surface of the cylinder revealed homogeneous and smoother surfaces covering the cylinder uniformly (Figure 6.4 C-H). Furthermore, from the below SEM images no drug particle was visible in GC matrix as TXA being a hydrophilic agent

would have dissolved as it was being mixed with the gelatine solution prior to coating the cylinder. The SEM images indicates that TXA is miscible and well dispersed in the gelatine polymer matrix [316, 317].

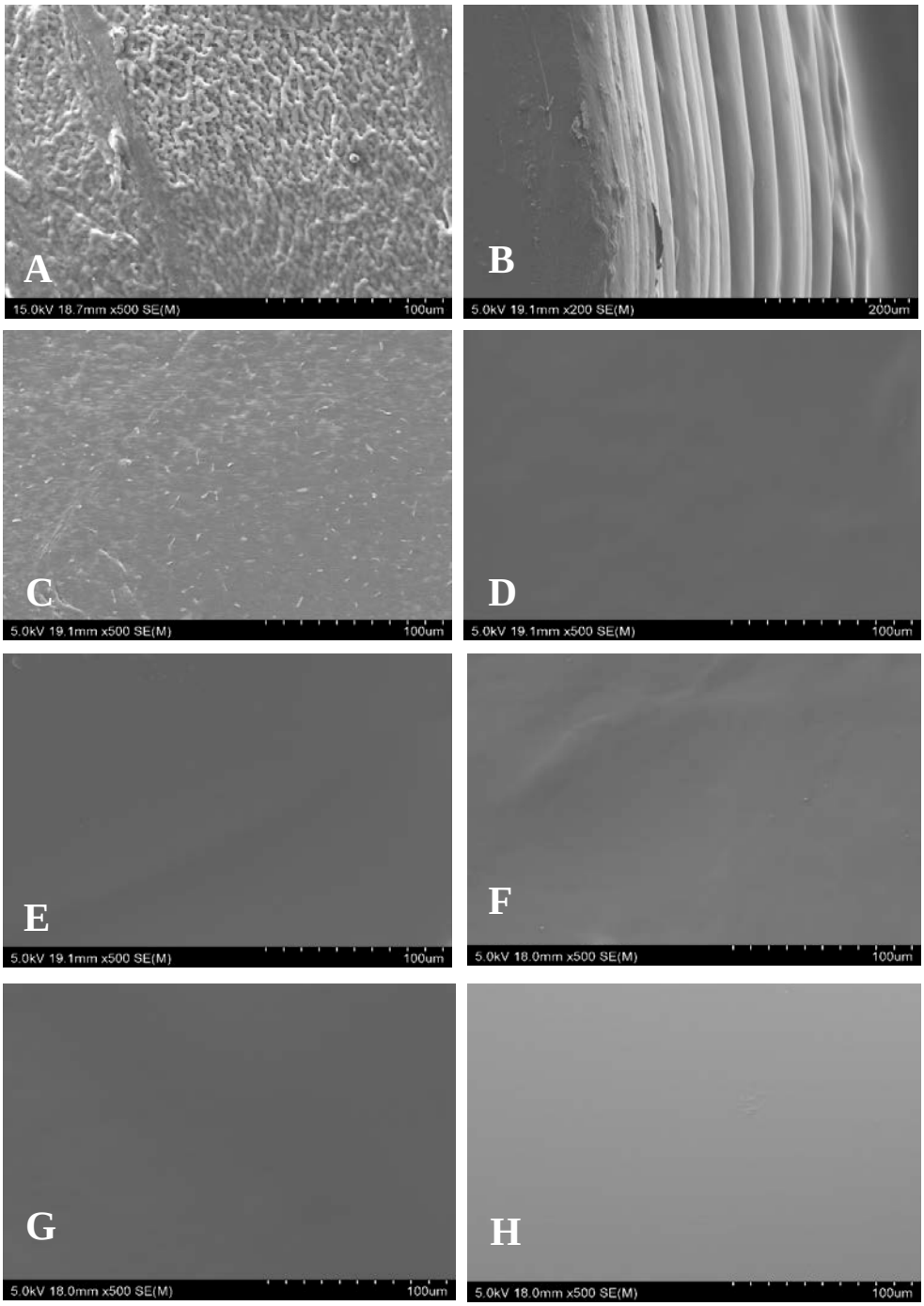


Figure 6.4: SEM morphologies of the (A) Printed cylinder surface without coating, (B) 3D Printed cylinder cross section without coating, and 3D printed cylinder surface with varying coating C-H (C) DGC1, (D) DGC2, (E) DGC3, (F) DGC4, (G) DGC5 and (H) DGC6.

### 6.3.3. Chemical interaction of crosslinker and drug with GC

FTIR analysis was carried out to compare the structural changes of gelatine, lactose, TXA and drug loaded GC as shown in Figure 6.5. The characteristic bands of gelatine observed at 3600–3200 $cm^{-1}$ (O–H stretching), 3070 $cm^{-1}$ and 2932 $cm^{-1}$ (N–H stretching) can be seen from the gelatine spectrum. Gelatine bands related to CO stretching at 1634 $cm^{-1}$ (amide I), NH bending at 1536 $cm^{-1}$ (amide II) and CN stretching at 1234 $cm^{-1}$ (amide III) were also observed (Table 6.3) [318]. The characteristic bands of lactose observed at 979 $cm^{-1}$ and 987 $cm^{-1}$ (C-C bonds) and 1034 $cm^{-1}$ (C-O vibration in $CH_2$-OH group) can be seen from the lactose spectrum [319]. In the spectrum of pure tranexamic acid, an absorption band at 1628 $cm^{-1}$ indicates the stretching vibration of C=O, bands at 1523 $cm^{-1}$ and 1540 $cm^{-1}$ can be ascribed to $NH_3^+$ deformational mode and bands at 1366 $cm^{-1}$ and 1008 $cm^{-1}$ are due to the asymmetrical and symmetrical stretching of the C–C–O system, respectively. Additionally, sharp absorption peaks of tranexamic acid at 900~690 $cm^{-1}$ are mainly caused by trans-isomerism vibration [320]. Subsequently, FTIR spectra of the heat treated GC was also performed to assess the effect of drug addition into gelatine formulations as well as protein-sugar-drug interactions since chemical changes were expected due to the Maillard reaction and protein-drug interactions [272].

Table 6.3: Position of amide I, amide II, and amide III bands of TXA loaded 3 % and 5 % GC cylinder scaffold.

| Coatings | Amide I ($cm^{-1}$) | Amide II ($cm^{-1}$) | Amide III ($cm^{-1}$) |
|---|---|---|---|
| DGC1 | 1634 | 1538 | 1234 |
| DGC2 | 1634 | 1538 | 1234 |
| DGC3 | 1634 | 1538 | 1234 |
| DGC4 | 1634 | 1538 | 1234 |
| DGC5 | 1634 | 1538 | 1234 |
| DGC6 | 1634 | 1538 | 1234 |

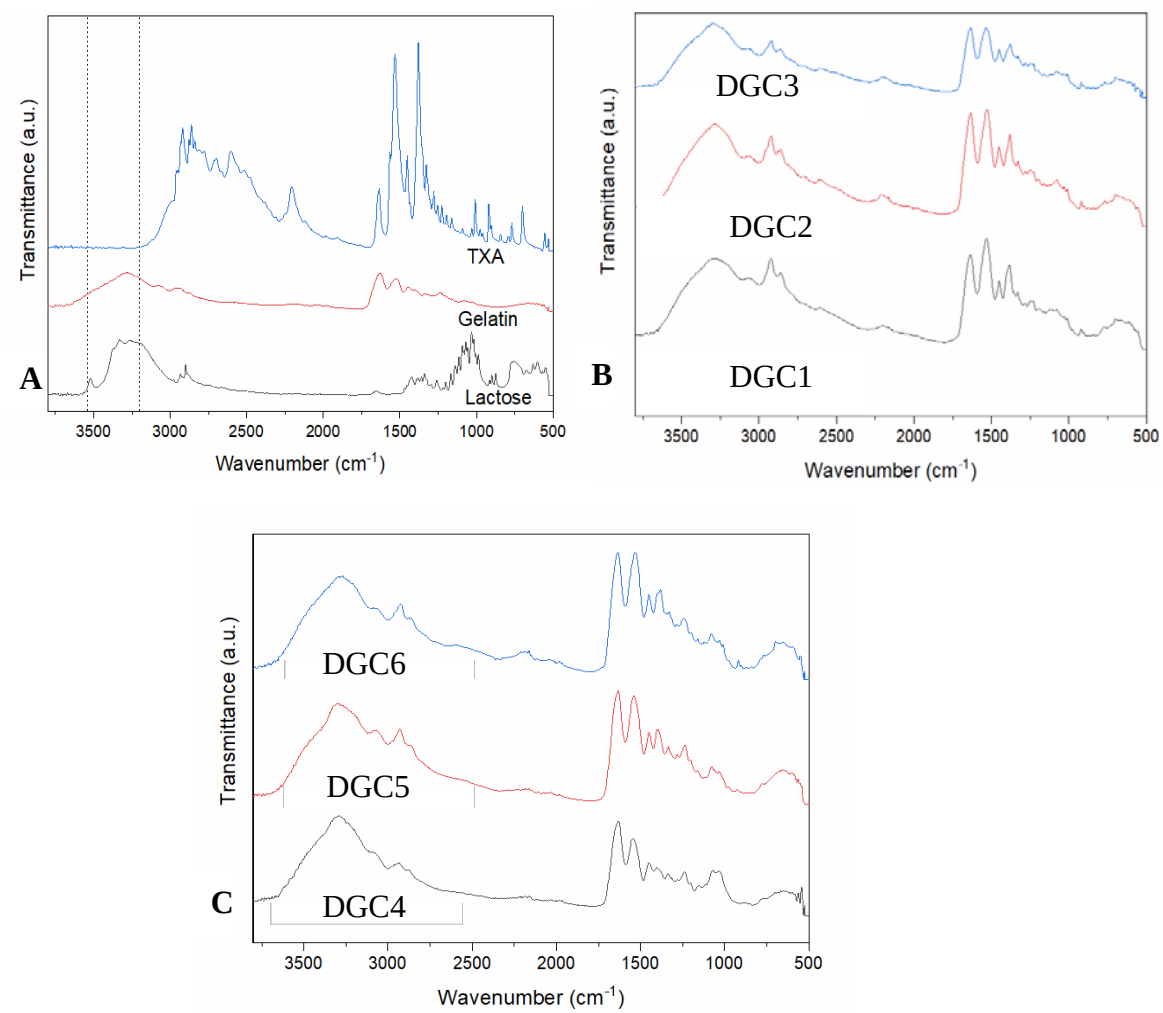


Figure 6.5: FTIR spectra of (A) TXA, gelatine and lactose, (B) 3 % gelatine-TXA with recurring coating (DGC1-single coating, DGC2-double coating and DGC3-triple coating) and (C) 5 % gelatine-TXA with recurring coating (DGC4-single coating, DGC5-double coating and DGC6-triple coating).

However, from FTIR spectra of heat treated TXA loaded GC, it can be observed that the position of amide II band shifted to higher wavenumber values, which can be attributed to both crosslinking reaction and $NH3^{+}$ deformational of TXA with amino acid residues in gelatine whereas the position of amide I and amide III bands remained the same [272]. Furthermore, it was also observed that the intensity of the O–H stretching band and carbonyl group in 3600–3200 $cm^{-1}$ and 1650-1540 $cm^{-1}$ respectively, increased when lactose and TXA was added suggesting the occurrence of protein-sugar-drug interaction. In addition, it can also be observed that an increased in an absorption band at

1450 $cm^{-1}$ in TXA loaded GC, can be attributed to the presence of the methylene group which is mainly contributed from TXA (Figure 6.5 B-C). As such the spectrum of crosslinked TXA-loaded GC was very similar to that of pure gelatine components suggesting that no significant chemical changes occurred in the polymer backbone.But, these observations suggest TXA existed in the GC polymer matrix with a possible interaction between the drug, cross linker and the polymer matrix.

### 6.3.4. Water uptake and degradation of GC

In this study, the water uptake capacity of the crosslinked GC along with the increasing number of GC was studied and it was observed, that the rate of water uptake increased with increasing coating level. From figure 6.6, GC3 and GC6 showed the highest percentage of water absorption capability with 2.0 % and 2.1 % absorption respectively after 40 mins of immersion. On the other hand, GC1 and GC4 presented the lowest water absorption capability (1.5 % and 1.7 % respectively after 40 min) in comparison to GC3 and GC6, demonstrating the effect of recurring coating on the water absorption behaviour.

Figure 6.7 shows the TXA loaded crosslinked GC water uptake capacity and it is worth noting that these samples presented a small increase in water absorption compared to the control samples but are not significantly different. It can be observed that DGC3 and DGC6 (triple coating drug loaded samples) showed the highest percentage of water absorption capability with 2.4 % and 2.6 % absorption respectively after 40 mins of immersion, which is quite similar to GC3 and GC6 samples (triple coating without drug samples). However, DGC1 and DGC4 (single coating drug loaded samples) showed the lowest water absorption capability (1.9 % and 2 % respectively after 40 mins).

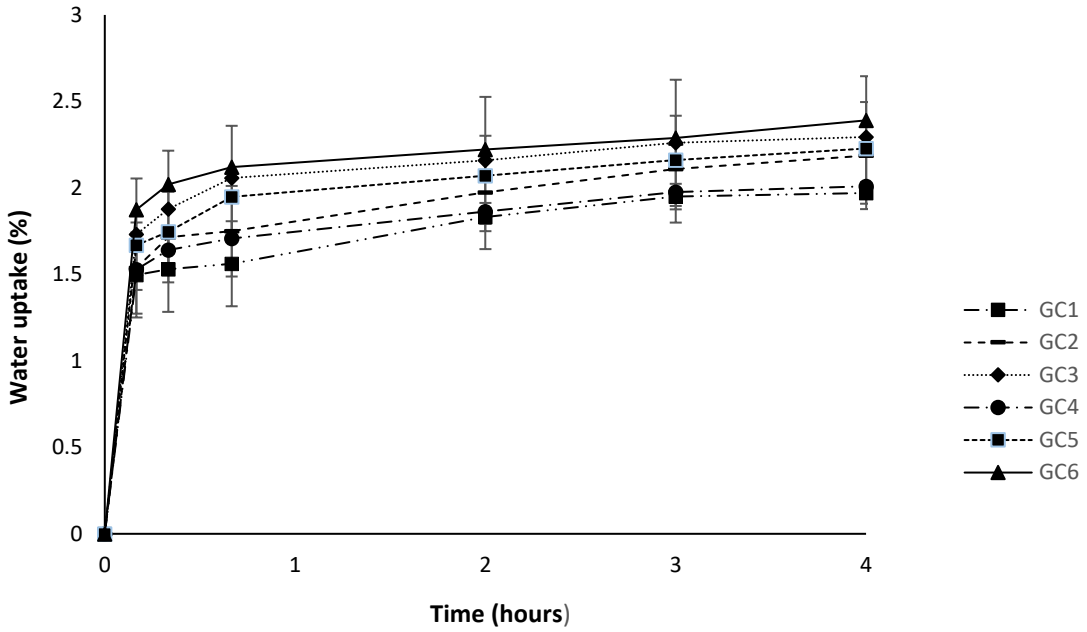


Figure 6.6: Water absorption behaviour of different formulations of GC ($n$ = 3, mean ± SD).

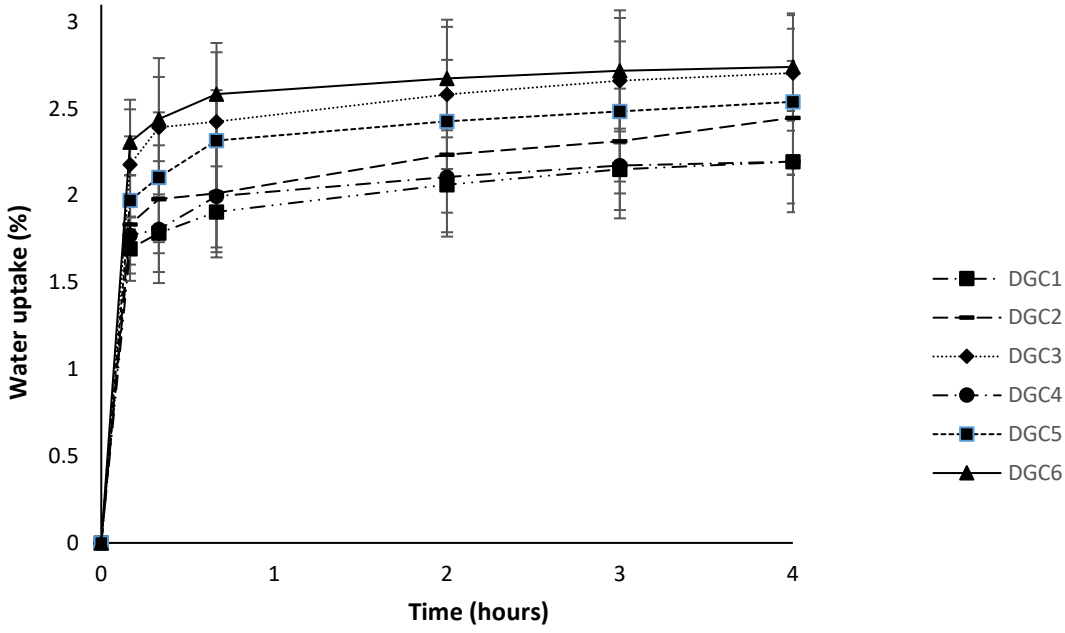


Figure 6.7: Water absorption behaviour of different formulations of TXA loaded GC ($n$ = 3, mean ± SD).

The small increase in water absorption of TXA loaded GC was related to a lower crosslinking degree between gelatin and lactose, as explained in FTIR results, which permitted a greater infiltration of water molecules into the core of the coating leading to the capability of the coating to hold higher capacity of water [305].

In addition, the degradation of the crosslinked GC cylinder scaffold (with and without drugs) with incubation in a phosphate-buffered saline (PBS) solution at 37°C for up to 24 hours was also investigated. Figure 6.8 and 6.9 represents the weight loss of the GC cylinder scaffold and it was observed that at different time points, the weight loss was higher when the number of coating increased. Furthermore, the weight loss of the coating layer was mainly due to the dissolution of the coating components, and since gelatine has a high water-uptake characteristic it can accelerate the degradation as the number of GC layers increases in comparison to the others [291].

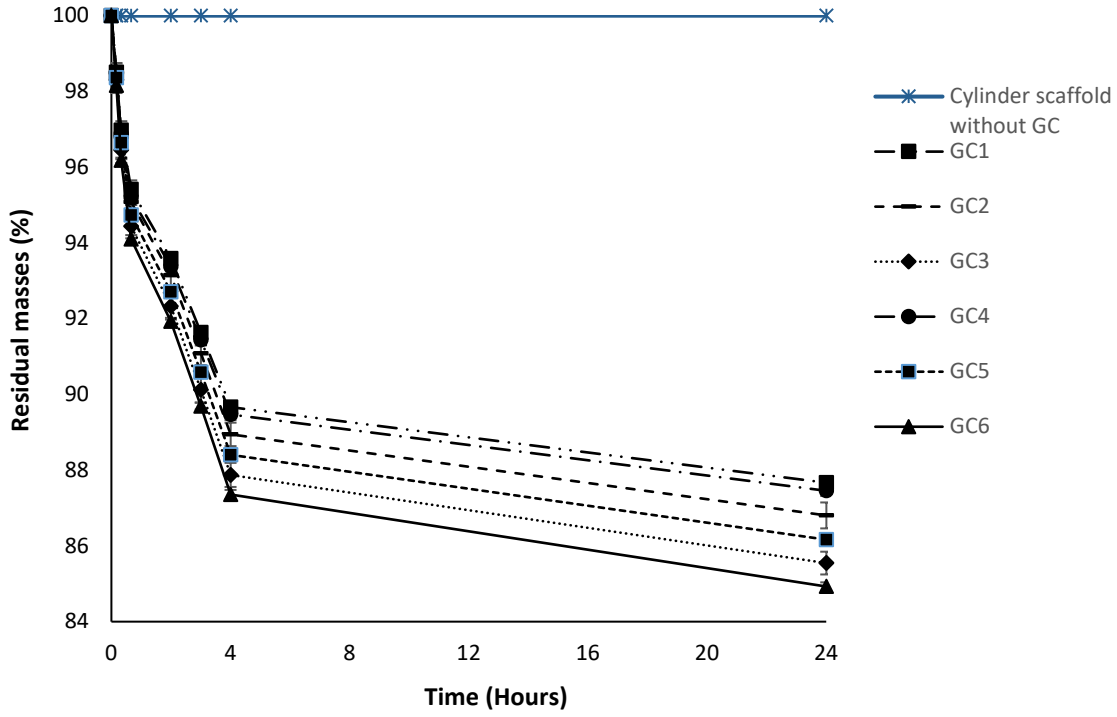


Figure 6.8: Degradation behaviours of different formulations of GC ($n$ = 3, mean ± SD).

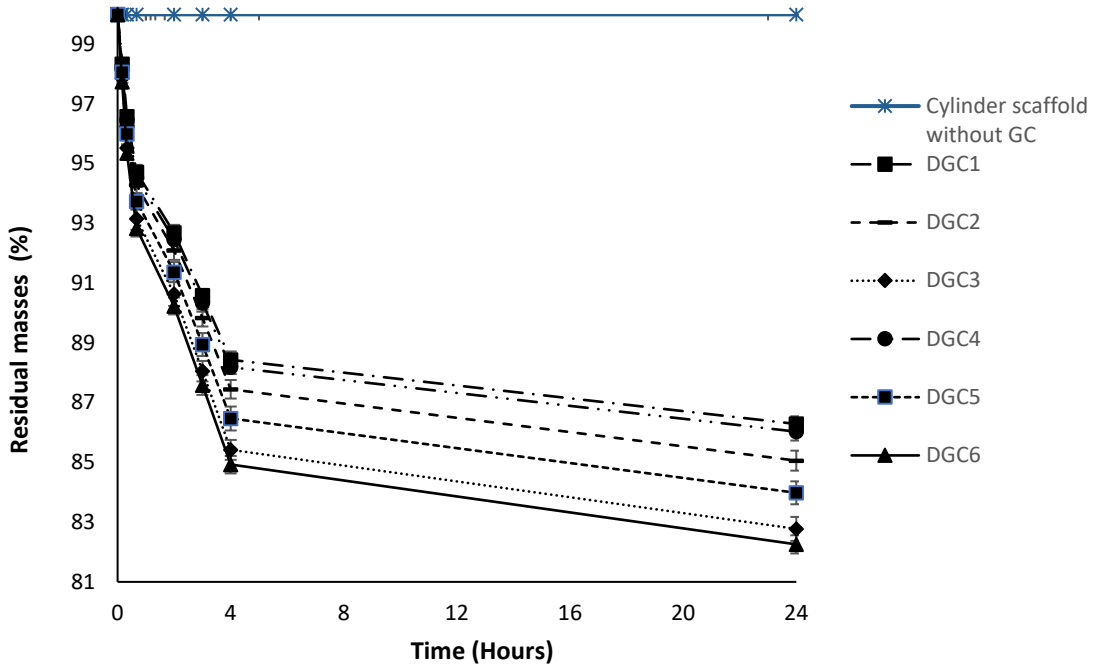


Figure 6.9: Degradation behaviours of different formulations of TXA loaded GC ($n$ = 3, mean ± SD).

Hence, from Figure 6.8 and 6.9 the highest degradation rate was also observed in GC3 and GC6 which is consistent with the water absorption study. As it is evident from the result, the DGC sample shows an increasing water absorption ratio in comparison to GC samples which can be attributed to gelatine polymeric chains becoming more accessible to infiltration of water molecules into the core of the coating due to a lower crosslinking degree between gelatin and lactose in the presence of TXA. Thus, the water absorption and degradation ratio of GC and DGC samples showed similar trend. It can also be observed that the degradation of the cylinder scaffold without the coating was insignificant when compared to various GC samples.

### 6.3.5. Calibration standard for TXA using LCMS

The calibration curves of TXA were linear [321] over the concentration ranges of 0.3 – 10 µg/ml, respectively which was constructed by plotting the peak area ratio of TXA/IS versus TXA concentration (Figure 6.10). The limit of detection [LOD] and limit of quantification [LOQ] in this study was 0.34 µg/ml and 1.1 µg/ml respectively for TXA

and the calibration equation was obtained by linear regression analysis (r2 = 0.9997) with the aid of Microsoft Excel (Microsoft Corporation):

y= ax +b, y=1x

Where, y is the peak area ratio, x the concentration, a the slope and b the intercept of the regression line.

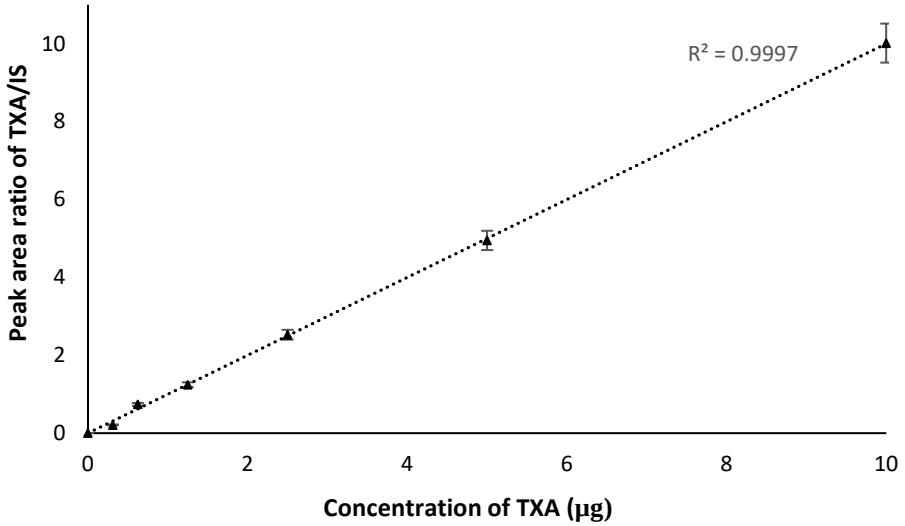


Figure 6.10: LC-MS calibration curve for TXA (*n* = 3, mean ± SD).

**6.3.6. Drug loading in GC by dip-coating**

The measurement of TXA content in GC samples was obtained for each formulation in Table 6.4.

Table 6.4: Drug loading of different formulations of GC coatings (*n* = 3, mean ± SD).

| Formulation | Theoretical drug loading (%) | Drug loaded (%) |
|---|---|---|
| DGC1 | 2 | 0.282 ± 1.15 |
| DGC2 | 4 | 0.528 ± 0.87 |
| DGC3 | 6 | 0.764 ± 0.93 |
| DGC4 | 2 | 0.289 ± 0.51 |
| DGC5 | 4 | 0.551 ± 0.49 |
| DCG6 | 6 | 0.773 ± 0.84 |

From table 6.4, it can be observed that the amount of drug loaded was lesser than theoretical loading but this indicates that the dip-coating method was efficient enough for this study, to produce a crosslinked drug loaded coating for the 3D printed scaffolds[316].

### 6.3.7. *In vitro* release study

Figure 6.11 shows the drug amount released from the coating layer for up to 6 hours which was measured with LCMS. The amount of drug entrapped was 6 % with respect to the total number of coating layer. From Figure 6.11, it was observed that the drug was released at a higher rate with increased coating, which can be attributed to the larger amount of drugs being entrapped along with higher degradation rate of gelatine coating (as shown in the coating degradation test in Figure 6.8 and 6.9) as the coating layers increased. But, for all the GC samples it was observed that the drug release rates (3 % and 5 % coating) behaved similarly, with an initial burst release within ~30 min leading to a gradual reduction in release rate thereafter. The increase in the initial burst release with increased coating in GC samples can be attributed to the higher drug loading amount with increased coating. Additionally, this initial burst effect can also be closely related with the rapid release of the drugs, which were on the coating surface as they were not entrapped efficiently (Table 6.5) [316, 322, 323].

Table 6.5: Amounts of drug released from different GC formulations ($n$ = 3, mean ± SD).

| Time | Drug release | Single coating | Double coating | Triple coating |
|---|---|---|---|---|
| 3% coating (30 min) | Apparent amount (mg/mL/g) | 0.064 | 0.132 | 0.224 |
| | Cumulative drug release (%) | 18.9 | 39.4 | 66.6 |
| 5% coating (30 min) | Apparent amount (mg/mL/g) | 0.064 | 0.170 | 0.205 |
| | Cumulative drug release (%) | 19.2 | 50.5 | 61.1 |
| 3% coating (6 h) | Apparent amount (mg/mL/g) | 0.086 | 0.169 | 0.254 |
| | Cumulative drug release (%) | 25.6 | 50.3 | 75.5 |

| | | | | |
|---|---|---|---|---|
| 5% coating (6 h) | Apparent amount (mg/mL/g) | 0.090 | 0.222 | 0.299 |
| | Cumulative drug release (%) | 26.7 | 66.1 | 89.1 |

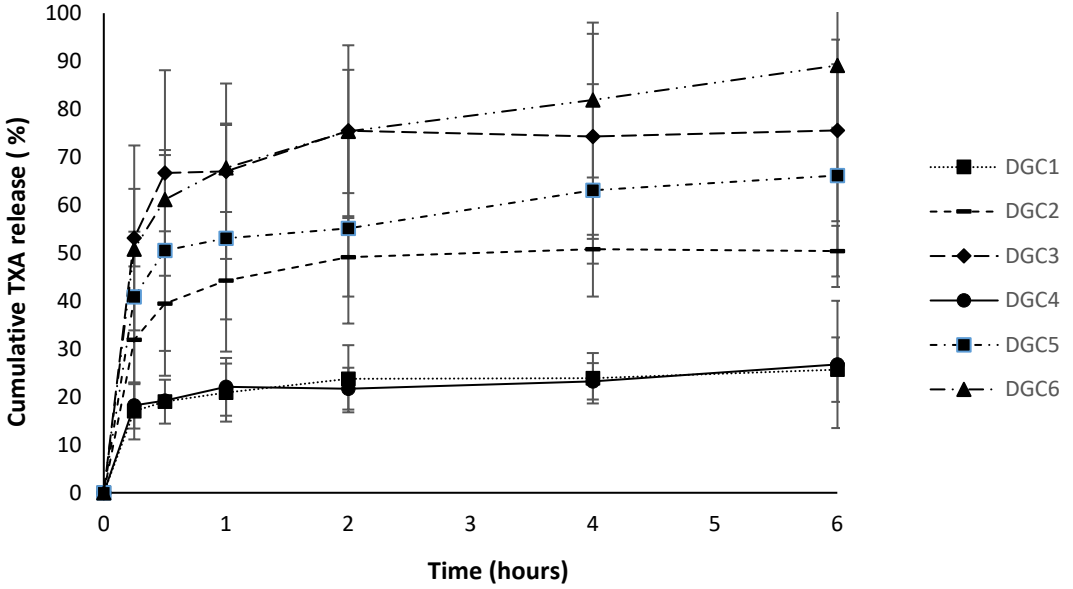


Figure 6.11: Cumulative drug release behaviours of 3 % and 5 % TXA loaded GC cylinder scaffold obtained at different coating cycles ($n$ = 3, mean ± SD).

From the above table, it was observed that the maximum release rate was observed in the system containing trilayer gelatine coating (DGC3 and DGC6) with 75 % and 89 % TXA being release within 6 h in comparison to other GC samples. However, for single layer gelatine coating (DGC1 and DGC4) the TAX release was lesser which can be due to lesser amount of drugs being entrapped within the coating along with the quick dissolution of the single layer gelatine coating. These results are also in accordance to the water absorption and degradation studies which shows that as the GC increases the absorption and degradation properties also increases affecting the drug release significantly. Hence, as observed in the result the drug release from the gelatine layer by layer coating can be altered by increasing the number of coating and drug loading amount to obtain the targeted release profile depending on the application.

For this study, the drug release data was analysed by various mathematical models to support the interpretation of the mechanisms involved in the control of the drug release

process. From the *in vitro* release data, TXA release behaviour from the various GC formulations fitted better with Weibull model closely followed by Kors–Peppas with the increasing number of coating. The respective coefficients of these two mathematical models applied to in vitro drug dissolution profiles were estimated (Table 6.6).

Table 6.6: Release coefficients for TXA fitted with different mathematical models.

| **Samples** | **Weibull model** | | **Korsmeyer-Peppas** | |
|---|---|---|---|---|
| | **($R^2$)** | **(b)** | **($R^2$)** | **(n)** |
| DGC1 | 0.9878 | 0.114 | 0.9875 | 0.123 |
| DGC2 | 0.9887 | 0.113 | 0.9877 | 0.128 |
| DGC3 | 0.9887 | 0.091 | 0.9868 | 0.091 |
| DGC4 | 0.9873 | 0.124 | 0.9870 | 0.109 |
| DGC5 | 0.9893 | 0.160 | 0.9877 | 0.134 |
| DGC6 | 0.9918 | 0.325 | 0.9884 | 0.162 |

The b coefficients values of the Weibull are correlated with the release mechanism of drug throughout the polymer matrix and values <0.75 are related to Fickian diffusion, while b values between 0.75 and 1.0 suggest that release is governed by Fickian diffusion and case II transport. In this study, according to $R^2$ values reported in table 6.6, the GC samples in this study presented b coefficient values lesser than 0.75 showing that the drug release is driven by Fickian mechanism. Based on Fickian diffusion, the drug release mechanism for TXA from GC samples can occurs at the surface and deep in the coating layer which is being diffused out through the diffusion path caused by water channels or pores. Hence, the drug release for TXA from recurring coating was highly affected by the diffusion process and since the drug itself is hydrophilic, it absorbs water easily, further facilitating the diffusion through the coating layer. In conclusion, increasing the coating cycle and drug loading amount increased the apparent drug release at both initial and

prolonged periods which can be used to control the release rate and the percentage of the released amount of TXA from GC. The Peppas model establish an exponential correlation between drug release and time [324] that characterise a fickian transport for cylindrical shaped samples as shown in Table 6.7. In addition, according to the Korsmeyer–Peppas model, the value of the release exponent *n* is correlated with the mechanism that drives the drug release and the *n* release exponent values of the recurring coated samples varied from 0.091 to 0.162 (Table 6.6) that shows the drugs were being released through a fickian diffusion, indicating that the drug is diffused through water filled pores which is in accordance with the result obtained from the Weibull model.

Table 6.7: Correlation between release exponent (*n*) values for the Korsmeyer–Peppas equation and drug release mechanisms depending on the geometry shape.

| **Thin film** | **Cylindrical** | **Sphere** | **Release mechanism** |
|---|---|---|---|
| 0.5 | 0.45 | 0.43 | Fickian diffusion |
| $0.5 < n < 0.89$ | $0.45 < n < 0.89$ | $0.43 < n < 0.85$ | Anomalous transport |
| 1.0 | 0.89 | 0.85 | Case II transport |

## 6.4. Conclusion

The aim of this work was to combine TAX, a clinically used antifibrinolytic agent, and gelatine a natural biopolymer, to produce a cross-linked coating which can be used to produce a drug delivery system coated on cylinder scaffold. In this study, the release behaviour of TXA molecule from gelatine coating in near physiological conditions was also carried out. The use of lactose as a crosslinking agent to improve the physicochemical properties of gelatine-based coating for controlled drug release applications was also demonstrated. The crosslinking reaction gave rise to a more water stable coating, and as the coating cycle increases a higher buffer absorption capacity and dissolution rate was observed. *In vitro* studies showed that TXA were released fast during the first hours and was governed by a process that involved diffusion of the drug from the coating. In the

end, this work shows that the results obtained are promising as the dip-coated recurring gelatine coating can deliver hemostatic activity while providing a soft contact wall between the synthetic polymer of an implant and the surrounding biological tissue. However, it was observed from this study that the presence of additional layers can act as a controlling membrane, as the addition of layers led to a higher drug loading capability by increasing the diffusion distance between the drug and the films surface. Thus, the present release study shows that TXA loaded GC can provide a targeted released of the drug for more than 4 hours which was possible by using the layer-by-layer formulation. Kinetic analysis of the TXA release profile showed that the drug release mechanism from cross-linked GC followed a Fickian diffusion mechanism with DGC6 showing the best adjusted $R^2$ value ($R^2$ = 0.9918). Hence, from this study it can be observed that sugar crosslinked drug loaded GC can be an effective TXA delivery vehicle for intranasal applications with hemostatic properties that can be optimised to allow higher incorporation of drugs for improving drug delivery confirming the feasibility of using lactose crosslinked drug loaded gelatine coated polymers as a drug release system.

## 6.5. Future directions

In this study, GC for cylinder scaffold were obtained by simple dip-coating method showing that this method can be used for drug delivery applications. However, beside dip-coating method there are various other coating techniques that are commonly used in biomedical study, such as thermal spraying, plasma spraying, sputter coating, dynamic mixing, sol–gel, electrophoretic deposition and biomimetic coating. But to coat temperature-sensitive drugs solvent few coating technologies performed without any heat such as compression coating, supercritical fluid spray coating, electrostatic coating, dry powder coating, and photo curable coating can also provide an alternative method. However out of these various techniques listed, plasma spraying is the only process, which is approved by the Food and Drug Administration (FDA), for biomedical coatings

due to its excellent coating properties as compared to other coating processes. So, for future studies using plasma-spraying process to develop drug loaded gelatine coating for implants or biomedical device can be an interesting avenue that can be used for local drug delivery. From this study, it can be observed that TXA loaded GC crosslinked with lactose provided a feasible drug release system, which can be used as a coating for the intranasal stent in future studies.

# Chapter 7. General discussion

## 7.1. General discussion

Chronic rhinosinusitis (CRS), a common chronic medical complaint, seems to be increasing in incidence and prevalence, with recent epidemiologic studies showing that CRS is predominant in about 10% of the adult population in industrialised countries (Bachert, Zhang, & Gevaert, 2015; Johnston & Sanderson, 2010). When normal conservative treatments are not effective, patients suffering from CRS often undergo functional endoscopic sinus surgery (FESS) (Ferguson et al., 2009). The success of surgery depends on various factors such as clearing diseased mucosa, removing infection, restoring normal drainage pathways, restoring ventilation (Al Badaai & Samaha, 2010) and the topical delivery of anti-inflammatory drugs (Ow, Groppo, Clutter, & Gawlicka, 2014b). Post-operative care plays an important role in post-surgical recovery, but current options could be improved (Kennedy et al., 2000). Plastic splints, biodegradable and non-biodegradable packings have potential drawbacks associated with obligatory mouth breathing, headache, dysphagia, risk of aspiration, airway obstruction, eustachian tube blockage, and bleeding and pain during removal (Günaydın et al., 2011).

This research was conducted to address the above shortcomings. The main aim of this thesis was to create a biodegradable 3D printed drug eluting stent.

As discussed in **Chapter 1,** the aim of this thesis was to:

1. Develop an expandable intranasal stent be designed to fit a patient's intranasal morphology.
2. Develop a composite polymer loaded with an anti-inflammatory agent within its matrix to provide sustained drug release profile (Technique 1).

3. Develop a cross-linked natural film loaded with an anti-inflammatory agent within its matrix to be able to provide a sustain release profile (Technique 2).
4. Develop a gelatine coating loaded with an anti-fibrinolytic agent be able to provide an immediate drug release profile within 4 hours for haemostatic effect.

*"Every once in a while, a new technology, an old problem, and a big idea turn into an innovation" Dean Kamen*

Figure 7.1: Post-operative care of patients by cauterising the wound with a heated iron rod after nasal surgery in the early 13th century (adapted from [325]).

This thesis consists of six chapters addressing the above objectives. In **Chapter 2**, a literature review was carried out, to present the current knowledge while identifying the research gaps. The main aim of this review was to elucidate the fact that there is a need to develop a novel intranasal drug delivery stent that can reduce postoperative bleeding, enhance post-surgical recovery, provide structural support to the nasal passageway to aid in patient breathability while preventing adhesions and aid in delivering drugs locally.

In **Chapter 3,** the main objective was to design and develop an expandable intranasal stent that can fit into patients' intranasal cavities. Using engineering and design methodology to research and evaluate viable options, the end goal was to develop and build an intranasal device for post-operative care in endoscopic sinus surgeries. After

evaluating various concepts to design a compressed and expanded form of the intranasal stent, the final design was a simple expansion mechanism that could be easily manufactured. Based on the key design selection criteria as described in **Section 3.3.3**, the stent design that was conceived featured a 3-part mechanism assembly featuring a cage like shape with six limbs evenly spaced attached to two tapered conical revolves that allow the nasal stent to be easily deployed into the nasal passage. This prototype intranasal stent developed with an inbuilt structural mechanism of expansion shapes itself to the individual's anatomy after being deployed.

Given the complex nasal anatomy and physiology, alongwith the presence of non-ciliated and ciliated regions located in the anterior and posterior part of the nasal cavity, respectively, the local delivery of therapeutic agents at the particular site is of importance for microciliary clearance and retaining the formulation in the nose [326]. Dosing accuracy is of critical importance in the delivery of therapeutic agents in order to minimise the potential side effects, while assuring effective relief after sinus surgery. However, the currently available post-operative care acceptance and compliance depends upon ease of use, sensory attributes, clinical efficacy, local deligvery of therapeutic agents and tolerability, but currently these attributes are lacking from the currently available post-operative care packings and splint [327]. However, the key advantage of using a 3D printer in this study, was its ability to create almost any complex shape or geometric feature. Hence, the design and development of a complete functional prototype showed that 3D printing could bring about the conception of a new era of complex geometry medical device for various biomedical applications. Additionally, the capability of 3D printing complex geometry stents incorporated with drug components within its matrices is an attractive prospect for local drug delivery applications in this study.

In **Chapter 4**, the anti-inflammatory drug, dexamethasone (DEX), was loaded into polymeric matrices by melt blending to study the efficacy of this method in obtaining a sustained release profile. For this study, poly vinyl alcohol (PVA) and polylactic acid (PLA) were chosen due to their biocompatibility, nontoxicity and biodegradability. From the *in vitro* anti-inflammatory drug release assessment carried out, a sustained release of DEX for more than 40 days was achieved. From the results, it can be observed that melt processing of composite polymers with DEX is a viable method of producing novel drug loaded composites for potential future drug delivery applications. Based on DSC results in **Section 4.3.3**, DEX loaded blended composite polymeric materials presented good thermal stability at 170 °C. It was also observed that the incorporation of PVA and drug reduced the melting point of PLA making it an advantage for material processing. In addition, the thermal stability of the composite blend was also improved due to intramolecular entanglements between PVA and PLA, by esterification of PVA hydroxylic groups and PLA carboxylic groups. Furthermore, evident from mechanical and morphological results in **Section 4.3.2** and **4.3.6**, PLA/PVA blends had partially compatible natures. In this context, the presence of higher amount of PVA in the composite blend; lowered the crystallinity of PLA while increasing the density of pores and hydrolytic degradation rate. This hydrolytic degradation of blends leads to improvement in the flexibility and softness of the composite blend. The result obtained from the *in vitro* drug release study and SEM analysis shows that the porous morphology facilitated solvent uptake and drug dissolution, leading to sustained drug release from all samples. The results obtained from this study indicate that drug loaded PLA/PVA blended samples can provide extended drug release by altering the ratio of the two polymers.

In various studies, the morphology, thermal and mechanical properties of PLA/PVA blends were investigated by various methods ranging from solvent casting to

electrospinning [328-330]. However, very few studies were carried out to investigate the morphology, thermal and mechanical properties of PLA/PVA blends prepared by the melt blending method using varying PLA/PVA ratios [176, 229]. In addition, no study has been carried out so far on the morphology, thermal and mechanical properties of dexamethasone loaded PLA/PVA blends prepared by the melt blending method using varying PLA/PVA ratios. The capability of producing drug loaded polymeric materials by using melt blending method will be beneficial for future innovations in formulation science and polymer chemistry, as further development of drug loaded polymers will enable printing or developing of bio-degradable drug eluting implants. However, the major drawbacks of using melt blending method are the high temperatures that are used during the process and the capability to process the drug loaded polymeric sample in the form of filaments that is suitable for FDM 3D printers. The drug used in this study was stable at the operating temperatures, but this could be a serious drawback for thermosenstive drugs.

For this reason, in **Chapter 5,** an alternative approach using multi-layer natural films was examined and optimised to provide a sustained DEX release profile. Previous studies carried out showed that bilayer dexamethasone-chitosan films were successfully obtained, and the release tests showed that these films are potential sustained-release carrier for dexamethasone for 4 weeks [258].

But for this study, biodegradable natural polymers, chitosan and gelatine, were chosen due to their unique gel and film forming properties, biocompatibility and biodegradability. Additionally, the respective advantageous properties of these natural polymers such as: gelatine capability to absorb excess water more than 5–10 times its weight, non-antigenic properties and its wound healing properties; chitosan capability to provide a broad range of antimicrobial activity against gram-positive/gram-negative

bacteria and, controlled drug release properties and its wound healing properties make them suitable carriers in this study. However, gelatine's rapid dispersion in aqueous environments reduces its practical applications for sustained drug delivery. But, gelatine's physio-chemical properties can be improved by blending with chitosan and adding a crosslinker. In this study, *in vitro* results from all single layer cross linked films showed a fast drug release profile, hence further optimisation of these films was carried out by using a simple layer-by-layer technique to slow down their release profile. After optimisation, the *in vitro* anti-inflammatory drug release assessment carried out showed that addition of multi-layers slowed the drug release profile to 30 days in comparison to single layer films which lasted for 3-6 days only. The result for optimised multi-layer films showed that the presence of additional layers relatively deaccelerated the capability of water-filled channels to acts as conduits for solvent uptake, thereby reducing drug diffusion and as the distance between the drug and the films surface increases, a slower and longer drug release profile was obtained. In addition, multi-layer dexamethasone loaded-chitosan films depending on their molecular weight had not been investigated before. This study showed that multi-layer dexamethasone loaded-chitosan films with higher molecular weight showed the slowest drug release profile in comparison to other multi-layer formulations even with similar crosslinking degree (0.6 % GA), which can be attributed to their compact polymeric chain structure as their molecular weight increases. Hence, a sustained release profile of DEX for 30 days was observed, suggesting that the molecular weight of chitosan can also be altered to alter the release profile of therapeutic agents as potential drug carriers. In addition, the key motivation in developing this multi-layer technique was to find a way to extend the sustained release of the therapeutic agent by using a simple solvent casting method that involves no heat for processing the samples while using minimal concentrations of crosslinking agent to improve samples' biocompatibility. Therefore, data from **Chapter 4 and 5**, showed that a sustained release

profile for the anti-inflammatory drug, DEX, developed by using two different methods; 1) melt blending and 2) layer-by-layer solvent casting. In the future, these two methods can be used to develop drug eluting stents that provide local anti-inflammatory drug delivery within the nasal cavity after FESS.

Nonetheless, after surgery bleeding usually occurs and effective haemostasis is desirable. Therefore, in **Chapter 6** the last objective of this thesis was to develop a coating that can provide fast release of an anti-fibrinolytic agent, tranexamic acid, within 4 hours post-operation. From the previous study, it was observed that gelatine by itself is quickly biodegradable making it a suitable candidate. Additionally, in the medical and pharmaceutical fields, gelatine has been widely used as a matrix that can be easily applied as thin coating for drug-eluting stents due to its superior swelling ratio and biocompatibility while being incorporated with drugs [331, 332]. As a coating component, when gelatine absorbs high amount of water it can change into a gel like structure, providing a soft contact area between the stent and the surrounding biological tissue [268].

Hence, the degree of crosslinking in gelatine plays an important role. In other studies, gelatin coating chemically crosslinked with glutaraldehyde or genipin had been carried out before. But using chemical crosslinkers on gelatine to coat medical devices and implants may initiate calcification of these structures, so there is a need for developing biocompatible crosslinkers derived from natural sources. Therefore, with regards to that other studies have shown that sugars (e.g. ribose, fructose) can interact with gelatine through a process called Maillard reaction, enabling these sugars to be used as crosslinkers for gelatine. Hence in this study, it was desirable for tranexamic acid to be released within 4 hours; as such lactose was used as a crosslinker rather than chemical crosslinkers, to link gelatine matrices that act as a reservoir for tranexamic acid to allow

gradual elution of the drug. Furthermore, varied coating cycles with dip-coating method were used to coat the printed cylindrical scaffold to observe the efficacy of this method in controlling the level of drug-release. From the *in vitro* assessment carried out, a targeted released of tranexamic acid for 6 hours was achieved. The drug release data from various coated layers show a fast drug release rate within the initial 1$^{st}$ hour, and the drug release rate increased with increased coating-cycle due to larger amount of drug being incorporated into the gelatine matrices with increased coating cycle. The drug kinetics data showed that the drug release mechanism is governed by a process that involves complete diffusion of the drug from the coating. This shows that the addition of layers relatively acted as a controlling membrane, as the addition of layers led to a higher drug loading capability by increasing the diffusion distance between the drug and the films surface making this method an effective drug delivery coating system. Hence, from this study it can be observed that sugar crosslinked drug loaded gelatine coating can be an effective way for intranasal delivery of tranexamic acid for haemostatic effect. In addition, gelatine has also been investigated in various studies for wound healing applications as it has the ability to accelerate the regeneration of damaged dermal and epidermal tissues, making it one of the desired components that can be coated onto the intranasal stent for post-operative care.

In summary, the data obtained from these independent experimental studies **(Chapter 3-6)** was useful in developing a proof of concept for the proposed drug-eluting intranasal stent. Together with the data presented in this thesis, future refinement and optimisation of the intranasal stent will be carried out for *in vivo* studies.

## 7.2. Study limitations

There were various limitations faced in this project which were overcomed by using alternative approaches. In **Chapter 3** designing the intranasal stent was not an easy task.

During the project, one of the limitations that was identified was the limited progression of the prototype design in certain directions. The key struggle while developing the intranasal stent prototype was adapting the patterns into a miniature size that would fit in the nasal cavity while being able to keep the foldability of the creases. The complexity of the nasal passageway demanded a small, functional intranasal design with an expansion mechanism. For designing the intranasal stent, various selection criteria were reviewed in regard to design features and research focus, which ultimately led to the development of diverse concepts. Each of these varying concepts had to be evaluated to perceive which would ideally provide the best functionality to create an expandable intranasal stent. Among those concepts, the Miura-Ori model was particularly interesting due to its ability to give a simple piece of paper an auxetic mechanical property but adapting this computational pattern into a workable design was not viable due to size, printing and budget limitations. In the end, a simple design adept with an expansion mechanism that would be easily manufacturable with the available resources at the university was developed.

Subsequently, early on during the research, FDM extrusion-based 3DP technique was chosen, as this technique was easily accessible, low-cost, and versatile and has a good potential for fabrication of different type, dose, and distribution of the active drug ingredient in the final printed product. Hence, using a single-screw hot melt extruder (HME) (Noztek Pro filament extruder, Noztek, UK), hot melt-extrusion of composite polymers comprising of different ratios of Poly lactic acid (PLA) and poly-vinyl alcohol (PVA) loaded with DEX was carried out to create drug-loaded filaments suitable for FDM 3D printing. The failure in producing these composite filaments was mainly attributed to the lack of required functionality in the desktop melt-extruder that was available at the university and the variability of these two polymers regarding their physio-technological characteristics and processing conditions affecting their blending capability. Polymer

blending is still a new topic that is being widely researched and the availability of libraries for processing conditions for drug loaded polymeric filaments was limited. Hence, relevant information that would help to bypass stability issues related to the operating temperatures involved by each material was missing. In the end, melt blending of PLA/PVA polymers loaded with dexamethasone, compressed to thin films was carried out. But melt processing of pure PVA polymer was impossible because the molecular weight and hydrolysis degree of the PVA polymer required for this study showed that its melting temperature is too close to its decomposition temperature. But when smaller ratios of PVA was added to PLA blend, the PVA's melting temperature reduced enabling the production of PLA/PVA blends with different ratios. This phenomenon showed that adding PLA into PVA enhanced polymer flexibility which in turn supported the compatibility of their blends, showing that polymeric blend is a new and interesting topic for research. Additionally, the data gathered from the drug loaded polymer study in **Chapter 4** will enable future developments of drug loaded filaments to be used for FDM 3D printing applications. Hence, it is significant to recap that each of these alternative approaches applied have their own applications and advantages in this study and possibly for future applications.

## 7.3. Future prespective

For future studies, further advancement of the prototype intranasal stent and development of drug loaded 3D printable composite polymer that are biocompatible and comply with 3D printing requirements are interesting endeavour for future research. Furthermore, future studies on composite polymers developed can be used to 3D print intranasal stents loaded with drugs in their matrices. These fabricated 3D printed drug loaded intranasal stents will also need to be evaluated to with regards to the effect of stent's geometry on the degradation profile in vitro and in animal studies. This study will be focused on the biocompatibility and bio absorption capability of the drug loaded 3D printed stent to

degrade within 4 weeks of exposure to the physiological environment. Additionally, a study with different molecular weight and hydrolysis degree of PVA material will also help to optimise targeted polymer degradation. Since, oxidative degradation caused by cellular components and cyclic mechanical load would affect the degradation speed of the stent as such for this reason an improved evaluation and optimisation with additional in vivo studies should be incorporated for the experimental setup of the 3D printed intranasal. In this proof-of-concept study, it was shown that computational-based 3D printed self-expandable intranasal stent can be successfully designed and also established that computational design has the capability to build models with realistic outcomes. In conclusion, the FDM 3D printing technique is a prospective manufacturing technique capable of interpreting computational models into physical prototypes that can enable future assessment of the mechanical performance of the intranasal stent based on various printable materials used.

What's more, 3D printing in drug delivery is an innovative technology that is constantly evolving, and its rapid development has created a new learning and research instrument for future development of drug delivery systems and bio-medical technologies. Currently, the selection of materials to be used is directly linked to the 3D printing process of various models and medical implants (Chapter 4). There are very few materials present that possess elastic properties that can mimic human tissue, which can be suitable for surgical training models and for printing medical implants. Even though, elastic materials such as silicone have already been successfully printed, further research into other materials is required as silicone is not suitable for printing complex geometrical structures. Hence, in the future the capability to generate printing materials capable of mimicking soft tissues by manipulating the currently available materials would be a novel area of research. Innovative materials formed from such studies will thereby improve the mechanical properties thus widening the possibilities of their application in 3D printing. Furthermore,

in drug delivery research, 3D printing also offers the possibility of improving drug therapies by personalisation of medicine. Since, 3D printing offers flexible fabrication capability, further development of this printing technology can benefit individual patients by providing tailor-made wound-healing treatments, medical devices and dosage forms (Figure 7.2).

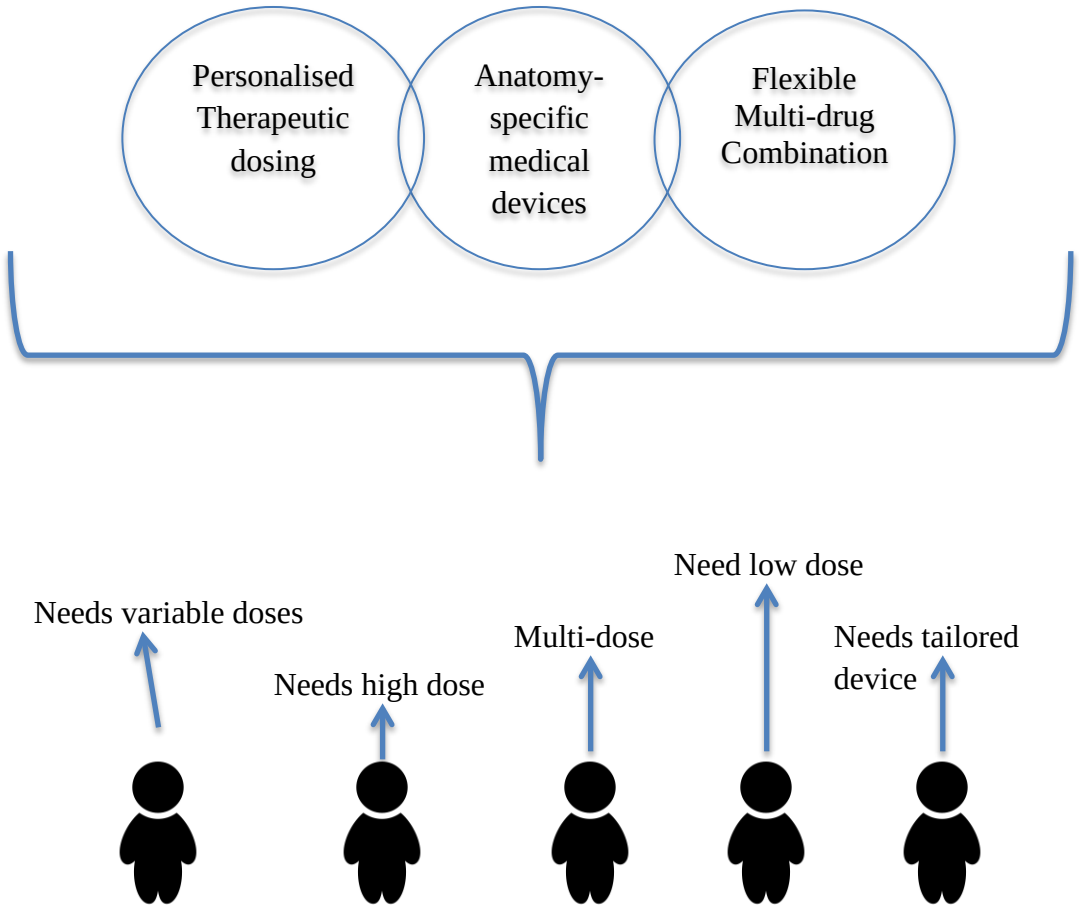


Figure 7.2:Example of printing technologies offering solutions to patients with the needs for personalised dosing, multidrug products and tailored medical devices.

## References


1. Lin, D.C., et al., *Association between severity of asthma and degree of chronic rhinosinusitis.* American journal of rhinology and allergy, 2011. **25**(4): p. 205.

2. Wee, J.H., et al., *Comparison between gelfoam packing and no packing after endoscopic sinus surgery in the same patients.* European archives of oto-rhino-laryngology, 2012. **269**(3): p. 897-903.

3. Thorne, R., et al., *Delivery of insulin-like growth factor-I to the rat brain and spinal cord along olfactory and trigeminal pathways following intranasal administration.* Neuroscience, 2004. **127**(2): p. 481-496.

4. Kennedy, D.W., E.D. Wright, and A.N. Goldberg, *Objective and subjective outcomes in surgery for chronic sinusitis.* The laryngoscope, 2000. **110**(S94): p. 29-31.

5. Baguley, C.J., et al., *Silastic splints reduce middle meatal adhesions after endoscopic sinus surgery.* American journal of rhinology and allergy, 2012. **26**(5): p. 414-417.

6. Lin, D.C., et al., *Association between severity of asthma and degree of chronic rhinosinusitis.* American journal of rhinology and allergy, 2011. **25**(4): p. 205.

7. Hsu, K., M. Ericksen, and P. Catalano, *Effect of a chitosan-based biodegradable middle meatal dressing after endoscopic sinus surgery: a prospective randomized comparative study.* Sinusitis, 2016. **1**(1): p. 3-12.

8. Durisin, M., et al., *A novel biodegradable frontal sinus stent (MgNd2): a long-term animal study.* European archives of oto-rhino-laryngology, 2016. **273**(6): p. 1455-1467.

9. Durand, M., et al., *Sonic aerosol therapy to target maxillary sinuses.* European annals of otorhinolaryngology, head and neck diseases, 2012. **129**(5): p. 244-250.

10. Parikh, A., et al., *Drug-eluting nasal implants: formulation, characterization, clinical applications and challenges.* Pharmaceutics, 2014. **6**(2): p. 249-267.

11. Günaydın, R.Ö., et al., *Nasal packing and transseptal suturing techniques: surgical and anaesthetic perspectives.* European archives of oto-rhino-laryngology, 2011. **268**(8): p. 1151-1156.

12. Jacob, A., B.T. Faddis, and R.A. Chole, *MeroGel hyaluronic acid sinonasal implants: osteogenic implications.* The laryngoscope, 2002. **112**(1): p. 37-42.

13. Vaiman, M., E. Eviatar, and S. Segal, *The use of fibrin glue as hemostatic in endonasal operations: a prospective, randomized study.* Rhinology, 2002. **40**(4): p. 185-188.

14. Tom, L.W., et al., *The effects of gelatin film stents in the middle meatus.* American journal of rhinology, 1997. **11**(3): p. 229-232.

15. Antisdel, J.L., et al., *Microporous polysaccharide hemospheres do not increase synechiae after sinus surgery: randomized controlled study.* American journal of rhinology & allergy, 2011. **25**(4): p. 268-271.

16. Shaw, C.-k.L., et al., *Effect of packing on nasal mucosa of sheep.* The journal of laryngology & otology, 2000. **114**(7): p. 506-509.

17. Li, P.F., D. Downie, and P.H. Hwang, *Controlled steroid delivery via bioabsorbable stent: safety and performance in a rabbit model.* American journal of rhinology & allergy, 2009. **23**(6): p. 591-596.

18. Malki, D., S. Quine, and A. Pfleiderer, *Nasal splints, revisited.* The journal of laryngology & otology, 1999. **113**(8): p. 725-727.

19. Hajiioannou, J.K., et al., *Optimal time for nasal packing removal after septoplasty. A comparative study.* Rhinology, 2007. **45**(1): p. 68.

20. Eaton, D.J., et al., *Device and methods for treating paranasal sinus conditions*. 2011, Google patents.

21. Kennedy, D.W., *The propel™ steroid-releasing bioabsorbable implant to improve outcomes of sinus surgery.* Expert review of respiratory medicine, 2012. **6**(5): p. 493-498.

22. Aetna. *Devices for post-operative use following endoscopic sinus surgery*. 2013 [cited 2016 26/08]; Available from: http://www.aetna.com/cpb/medical/data/800_899/0840.html.

23. McMahon, S., et al., *Bio-resorbable polymer stents: a review of material progress and prospects.* Progress in polymer science, 2018. **83**: p. 79-96.

24. Food and Drug Administration. *Technical considerations for additive manufactured devices; draft guidance for industry and food and drug administration staff; Availbility*. 2016 [cited 2016 10/05]; Available from: https://www.federalregister.gov/articles/2016/05/10/2016-10924/technical-considerations-for-additive-manufactured-devices-draft-guidance-for-industry-and-food-and.

25. Orlandi, R.R., et al. *International consensus statement on allergy and rhinology: rhinosinusitis*. *International forum of allergy & rhinology*. 2016. Wiley Online Library.

26. Alobid, I. and J. Mullol, *Role of medical therapy in the management of nasal polyps.* Current allergy and asthma reports, 2012. **12**(2): p. 144-153.

27. DeCastro, A., L. Mims, and W.J. Hueston, *Rhinosinusitis.* Primary care: clinics in office practice, 2014. **41**(1): p. 47-61.

28. Rosenfeld, R.M., et al., *Clinical practice guideline (update): adult sinusitis.* Otolaryngology–head and neck surgery, 2015. **152**(2_suppl): p. S1-S39.

29. Guastella, A.J., et al., *Recommendations for the standardisation of oxytocin nasal administration and guidelines for its reporting in human research.* Psychoneuroendocrinology, 2013. **38**(5): p. 612-625.

30. Marple, B.F., et al., *Advance II: a prospective, randomized study assessing safety and efficacy of bioabsorbable steroid-releasing sinus implants.* Otolaryngology--head and neck surgery, 2012. **146**(6): p. 1004-1011.

31. Lavigne, F., et al. *Steroid‐eluting sinus implant for in‐office treatment of recurrent nasal polyposis: a prospective, multicenter study*. *International forum of allergy & rhinology*. 2014. Wiley Online Library.

32. Han, J.K., et al. *Effect of steroid‐releasing sinus implants on postoperative medical and surgical interventions: an efficacy meta‐analysis*. *International forum of allergy & rhinology*. 2012. Wiley Online Library.

33. Gufford, B., et al., *Comparison of a new intranasal naloxone formulation to intramuscular naloxone: Results from hypothesis‐generating small clinical studies.* Clinical and translational science, 2017.

34. Rubin, B.K., *Secretion properties, clearance, and therapy in airway disease.* Translational respiratory medicine, 2014. **2**(1): p. 6.

35. Jones, N., *The nose and paranasal sinuses physiology and anatomy.* Advanced drug delivery reviews, 2001. **51**(1-3): p. 5-19.

36. Illum, L., *Nasal drug delivery--possibilities, problems and solutions.* J Control Release, 2003. **87**(1-3): p. 187-98.

37. Marttin, E., et al., *Nasal mucociliary clearance as a factor in nasal drug delivery.* Advanced drug delivery reviews, 1998. **29**(1): p. 13-38.

38. Pires, A., et al., *Intranasal drug delivery: how, why and what for?* 2009.

39. Sahin-Yilmaz, A. and R.M. Naclerio, *Anatomy and physiology of the upper airway.* Proceedings of the american thoracic society, 2011. **8**(1): p. 31-39.

40. Dondeti, P., H. Zia, and T.E. Needham, *Bioadhesive and formulation parameters affecting nasal absorption.* International journal of pharmaceutics, 1996. **127**(2): p. 115-133.

41. Zia, H., P. Dondeti, and T. Needham, *Intranasal drug delivery.* Clinical research and regulatory affairs, 2008.

42. Costantino, H.R., et al., *Intranasal delivery: physicochemical and therapeutic aspects.* International journal of pharmaceutics, 2007. **337**(1): p. 1-24.

43. Charlton, S., et al., *Distribution and clearance of bioadhesive formulations from the olfactory region in man: Effect of polymer type and nasal delivery device.* European journal of pharmaceutical sciences, 2007. **30**(3): p. 295-302.

44. Ugwoke, M.I., et al., *Nasal mucoadhesive drug delivery: background, applications, trends and future perspectives.* Advanced drug delivery reviews, 2005. **57**(11): p. 1640-1665.

45. Fortuna, A., et al., *Intranasal delivery of systemic-acting drugs: small-molecules and biomacromolecules.* European journal of pharmaceutics and biopharmaceutics, 2014. **88**(1): p. 8-27.

46. Meltzer, E.O., et al., *Rhinosinusitis: establishing definitions for clinical research and patient care.* Journal of allergy and clinical immunology, 2004. **114**(6): p. 155-212.

47. Rosenfeld, R.M., et al., *Clinical practice guideline: adult sinusitis.* Otolaryngology-head and neck surgery, 2007. **137**(3): p. S1-S31.

48. Lanza, D.C. and D.W. Kennedy, *Adult rhinosinusitis defined.* Otolaryngology–head and neck surgery, 1997. **117**(3_suppl): p. S1-S7.

49. Slavin, R.G., et al., *The diagnosis and management of sinusitis: a practice parameter update.* Journal of allergy and clinical immunology, 2005. **116**(6): p. S13-S47.

50. Fokkens, W., et al., *EAACI position paper on rhinosinusitis and nasal polyps executive summary.* Allergy, 2005. **60**(5): p. 583-601.

51. Fokkens, W., V. Lund, and J. Mullol, *European position paper on rhinosinusitis and nasal polyps 2007.* Rhinology supplement, 2006(20): p. 1-136.

52. Fokkens, W.J., et al., *European position paper on rhinosinusitis and nasal polyps 2012.* Rhinology supplement, 2012(23): p. 3 p preceding table of contents, 1-298.

53. Scadding, G., et al., *BSACI guidelines for the management of rhinosinusitis and nasal polyposis.* Clinical and experimental allergy, 2008. **38**(2): p. 260-275.

54. Thwala, L.N., V. Préat, and N.S. Csaba, *Emerging delivery platforms for mucosal administration of biopharmaceuticals: a critical update on nasal, pulmonary and oral routes.* Expert opinion on drug delivery, 2017. **14**(1): p. 23-36.

55. Ghori, M.U., et al., *Nasal drug delivery systems: An overview.* American journal of pharmacological sciences, 2015. **3**(5): p. 110-119.

56. Banov, C.H. and P. Lieberman, *Efficacy of azelastine nasal spray in the treatment of vasomotor (perennial nonallergic) rhinitis.* Annals of allergy, asthma & immunology, 2001. **86**(1): p. 28-35.

57. Waddell, A., et al., *Intranasal steroid sprays in the treatment of rhinitis: is one better than another?* The Journal of laryngology & otology, 2003. **117**(11): p. 843-845.

58. Nayak, A.S., et al., *Effective dose range of mometasone furoate nasal spray in the treatment of acute rhinosinusitis.* Annals of allergy, asthma & immunology, 2002. **89**(3): p. 271-278.

59. Perl, T.M., et al., *Intranasal mupirocin to prevent postoperative Staphylococcus aureus infections.* New england journal of medicine, 2002. **346**(24): p. 1871-1877.

60. Gompel, A., et al., *Endometrial safety and tolerability of AERODIOL®(intranasal estradiol) for 1 year.* Maturitas, 2000. **36**(3): p. 209-215.

61. Hurlemann, R., et al., *Oxytocin enhances amygdala-dependent, socially reinforced learning and emotional empathy in humans.* Journal of neuroscience, 2010. **30**(14): p. 4999-5007.

62. Majithiya, R.J., et al., *Thermoreversible-mucoadhesive gel for nasal delivery of sumatriptan.* AAPS pharmscitech, 2006. **7**(3): p. E80-E86.

63. Jain, R., et al., *Micellar nanocarriers: potential nose-to-brain delivery of zolmitriptan as novel migraine therapy.* Pharmaceutical research, 2010. **27**(4): p. 655-664.

64. Gizurarson, S., *The effect of cilia and the mucociliary clearance on successful drug delivery.* Biological and pharmaceutical bulletin, 2015. **38**(4): p. 497-506.

65. Schipper, N.G., J.C. Verhoef, and F.W. Merkus, *The nasal mucociliary clearance: relevance to nasal drug delivery.* Pharmaceutical research, 1991. **8**(7): p. 807-814.

66. White, D.E., J. Bartley, and R.J. Nates, *Model demonstrates functional purpose of the nasal cycle.* Biomedical engineering online, 2015. **14**(1): p. 38.

67. Aboca and Fitonasal 2Act. *The nasal mucosa*. 2016 [cited 2016 19/08]; Available from: http://www.fitonasal2act.com/.

68. Huang, C.H., et al., *Mechanism of nasal absorption of drugs I: Physicochemical parameters influencing the rate of in situ nasal absorption of drugs in rats.* Journal of pharmaceutical sciences, 1985. **74**(6): p. 608-611.

69. Dhuria, S.V., L.R. Hanson, and W.H. Frey, *Novel vasoconstrictor formulation to enhance intranasal targeting of neuropeptide therapeutics to the central nervous system.* Journal of pharmacology and experimental therapeutics, 2009. **328**(1): p. 312-320.

70. Karageorgiou, V. and D. Kaplan, *Porosity of 3D biomaterial scaffolds and osteogenesis.* Biomaterials, 2005. **26**(27): p. 5474-5491.

71. Pezron, I., et al., *Prodrug strategies in nasal drug delivery.* Expert opinion on therapeutic patents, 2002. **12**(3): p. 331-340.

72. Bitter, C., K. Suter-Zimmermann, and C. Surber, *Nasal drug delivery in humans.* Curr probl dermatol, 2011. **40**: p. 20-35.

73. Dimova, S., et al., *The use of human nasal in vitro cell systems during drug discovery and development.* Toxicology in vitro, 2005. **19**(1): p. 107-122.

74. Illum, L., *Nasal drug delivery: new developments and strategies.* Drug discov today, 2002. **7**(23): p. 1184-9.

75. McMartin, C., et al., *Analysis of structural requirements for the absorption of drugs and macromolecules from the nasal cavity.* Journal of pharmaceutical sciences, 1987. **76**(7): p. 535-540.

76. Corbo, D.C., J.C. Liu, and Y.W. Chienx, *Characterization of the barrier properties of mucosal membranes.* Journal of pharmaceutical sciences, 1990. **79**(3): p. 202-206.

77. Washington, N., et al., *Determination of baseline human nasal pH and the effect of intranasally administered buffers.* International journal of pharmaceutics, 2000. **198**(2): p. 139-146.

78. Lipworth, B.J. and C.M. Jackson, *Safety of inhaled and intranasal corticosteroids.* Drug safety, 2000. **23**(1): p. 11-33.

79. Krishnamoorthy, R. and A.K. Mitra, *Prodrugs for nasal drug delivery.* Advanced drug delivery reviews, 1998. **29**(1): p. 135-146.

80. Arora, P., S. Sharma, and S. Garg, *Permeability issues in nasal drug delivery.* Drug discovery today, 2002. **7**(18): p. 967-975.

81. Kao, H.D., et al., *Enhancement of the systemic and CNS specific delivery of L-dopa by the nasal administration of its water soluble prodrugs.* Pharmaceutical research, 2000. **17**(8): p. 978-984.

82. Wang, H., A.A. Hussain, and P.J. Wedlund, *Nipecotic acid: systemic availability and brain delivery after nasal administration of nipecotic acid and n-butyl nipecotate to rats.* Pharmaceutical research, 2005. **22**(4): p. 556-562.

83. Yang, C., H. Gao, and A.K. Mitra, *Chemical stability, enzymatic hydrolysis, and nasal uptake of amino acid ester prodrugs of acyclovir.* Journal of pharmaceutical sciences, 2001. **90**(5): p. 617-624.

84. Bernkop-Schnürch, A., *The use of inhibitory agents to overcome the enzymatic barrier to perorally administered therapeutic peptides and proteins.* Journal of controlled release, 1998. **52**(1): p. 1-16.

85. Machida, M., et al., *Effects of surfactants and protease inhibitors on nasal absorption of recombinant human granulocyte colony-stimulating factor (rhG-CSF) in rats.* Biol pharm bull, 1994. **17**(10): p. 1375-8.

86. Hoang, V.D., et al., *Characterization of human nasal primary culture systems to investigate peptide metabolism.* International journal of pharmaceutics, 2002. **238**(1): p. 247-256.

87. O'Hagan, D.T., et al., *Nasal absorption enhancers for biosynthetic human growth hormone in rats.* Pharmaceutical research, 1990. **7**(7): p. 772-776.

88. Wang, J., Y. Tabata, and K. Morimoto, *Aminated gelatin microspheres as a nasal delivery system for peptide drugs: evaluation of in vitro release and in vivo*

*insulin absorption in rats.* Journal of controlled release, 2006. **113**(1): p. 31-37.

89. Bogdanffy, M.S., *Biotransformation enzymes in the rodent nasal mucosa: the value of a histochemical approach.* Environmental health perspectives, 1990. **85**: p. 177.

90. Hersey, S. and R. Jackson, *Effect of bile salts on nasal permeability in vitro.* Journal of pharmaceutical sciences, 1987. **76**(12): p. 876-879.

91. Baglioni, C. and R.J. Phipps, *Nasal absorption of interferon: enhancement by surfactant agents.* Journal of interferon research, 1990. **10**(5): p. 497-504.

92. Illum, L., N.F. Farraj, and S.S. Davis, *Chitosan as a novel nasal delivery system for peptide drugs.* Pharmaceutical research, 1994. **11**(8): p. 1186-1189.

93. Ekelund, K., et al., *Correlation between epithelial toxicity and surfactant structure as derived from the effects of polyethyleneoxide surfactants on caco‐2 cell monolayers and pig nasal mucosa.* Journal of pharmaceutical sciences, 2005. **94**(4): p. 730-744.

94. Sinswat, P. and P. Tengamnuay, *Enhancing effect of chitosan on nasal absorption of salmon calcitonin in rats: comparison with hydroxypropyl-and dimethyl-β-cyclodextrins.* International journal of pharmaceutics, 2003. **257**(1): p. 15-22.

95. Zaki, N., et al., *Rapid-onset intranasal delivery of metoclopramide hydrochloride: Part II: Safety of various absorption enhancers and pharmacokinetic evaluation.* International journal of pharmaceutics, 2006. **327**(1): p. 97-103.

96. Kaur, H., C. Singh, and G. Gupta, *Nasal drug delivery-review.* Indo american journal of pharmaceutical research, 2015. **5**(8): p. 2522-2530.

97. Illum, L., *Nanoparticulate systems for nasal delivery of drugs: a real improvement over simple systems?* Journal of pharmaceutical sciences, 2007. **96**(3): p. 473-483.

98. Giunchedi, P., et al., *Formulation and in vivo evaluation of chlorhexidine buccal tablets prepared using drug-loaded chitosan microspheres.* European journal of pharmaceutics and biopharmaceutics, 2002. **53**(2): p. 233-239.

99. Maestrelli, F., et al., *Influence of chitosan and its glutamate and hydrochloride salts on naproxen dissolution rate and permeation across Caco-2 cells.* International journal of pharmaceutics, 2004. **271**(1): p. 257-267.

100. Kumar, M.R., et al., *Chitosan chemistry and pharmaceutical perspectives.* Chemical reviews, 2004. **104**(12): p. 6017-6084.

101. Pujara, C.P., et al., *Effects of formulation variables on nasal epithelial cell integrity: Biochemical evaluations.* International journal of pharmaceutics, 1995. **114**(2): p. 197-203.

102. Asai, K., et al., *The effects of water-soluble cyclodextrins on the histological integrity of the rat nasal mucosa.* International journal of pharmaceutics, 2002. **246**(1): p. 25-35.

103. Babu, R.J., P. Dayal, and M. Singh, *Effect of cyclodextrins on the complexation and nasal permeation of melatonin.* Drug delivery, 2008. **15**(6): p. 381-388.

104. Jug, M. and M. Bećirević-Laćan, *Development of a cyclodextrin-based nasal delivery system for lorazepam.* Drug development and industrial pharmacy, 2008. **34**(8): p. 817-826.

105. Merkus, F., et al., *Cyclodextrins in nasal drug delivery.* Advanced drug delivery reviews, 1999. **36**(1): p. 41-57.

106. Alsarra, I.A., et al., *Mucoadhesive polymeric hydrogels for nasal delivery of acyclovir.* Drug development and industrial pharmacy, 2009. **35**(3): p. 352-362.

107. Jogani, V.V., et al., *Intranasal mucoadhesive microemulsion of tacrine to improve brain targeting.* Alzheimer disease & associated disorders, 2008. **22**(2): p. 116-124.

108. Gavini, E., et al., *Mucoadhesive microspheres for nasal administration of an antiemetic drug, metoclopramide: in ‐ vitro/ex ‐ vivo studies.* Journal of pharmacy and pharmacology, 2005. **57**(3): p. 287-294.

109. Gavini, E., et al., *Mucoadhesive microspheres for nasal administration of cyclodextrins.* Journal of drug targeting, 2009. **17**(2): p. 168-179.

110. Patil, S.B. and K.K. Sawant, *Development, optimization and in vitro evaluation of alginate mucoadhesive microspheres of carvedilol for nasal delivery.* Journal of microencapsulation, 2009. **26**(5): p. 432-443.

111. Alsarra, I.A., A.Y. Hamed, and F.K. Alanazi, *Acyclovir liposomes for intranasal systemic delivery: development and pharmacokinetics evaluation.* Drug delivery, 2008. **15**(5): p. 313-321.

112. Jain, A.K., et al., *Muco-adhesive multivesicular liposomes as an effective carrier for transmucosal insulin delivery.* Journal of drug targeting, 2007. **15**(6): p. 417-427.

113. Law, S., et al., *Enhancement of nasal absorption of calcitonin loaded in liposomes.* Journal of liposome research, 2001. **11**(2-3): p. 165-174.

114. Muramatsu, K., et al., *The relationship between the rigidity of the liposomal membrane and the absorption of insulin after nasal administration of liposomes modified with an enhancer containing insulin in rabbits.* Drug development and industrial pharmacy, 1999. **25**(10): p. 1099-1105.

115. Lee, V.H., A. Yamamoto, and U.B. Kompella, *Mucosal penetration enhancers for facilitation of peptide and protein drug absorption.* Critical reviews in therapeutic drug carrier systems, 1991. **8**(2): p. 91-192.

116. Vyas, S., S. Goswami, and R. Singh, *Liposomes based nasal delivery system of nifedipine: Development and characterization.* International journal of pharmaceutics, 1995. **118**(1): p. 23-30.

117. Zhao, X., et al. *A systematic review of nonabsorbable, absorbable, and steroid‐impregnated spacers following endoscopic sinus surgery*. in *International forum of allergy and rhinology*. 2013. Wiley online library.

118. Ferguson, B.J., B.A. Otto, and H. Pant, *When surgery, antibiotics, and steroids fail to resolve chronic rhinosinusitis.* Immunology and allergy clinics of North America, 2009. **29**(4): p. 719-732.

119. Albu, S., *Novel drug-delivery systems for patients with chronic rhinosinusitis.* Drug design, development and therapy, 2012. **6**: p. 125.

120. Beule, A.G., et al., *Effects of a dexamethasone-releasing stent on osteoneogenesis in a rabbit model.* American journal of rhinology and allergy, 2009. **23**(4): p. 433-436.

121. Beule, A.G., et al., *Effects of topically applied dexamethasone on mucosal wound healing using a drug‐releasing stent.* The laryngoscope, 2008. **118**(11): p. 2073-2077.

122. Poetker, D.M. and D.D. Reh, *A comprehensive review of the adverse effects of systemic corticosteroids.* Otolaryngologic clinics of North America, 2010. **43**(4): p. 753-768.

123. Cope, D. and R. Bova, *Steroids in otolaryngology.* The laryngoscope, 2008. **118**(9): p. 1556-1560.

124. Rizan, C. and H.A. Elhassan, *Post‐sinus surgery insertion of steroid‐eluting bioabsorbable intranasal devices: a systematic review.* The laryngoscope, 2016. **126**(1): p. 86-92.

125. Aggarwal, R., A. Cardozo, and J. Homer, *The assessment of topical nasal drug distribution.* Clinical otolaryngology & allied sciences, 2004. **29**(3): p. 201-205.

126. Merkus, P., et al., *The 'best method'of topical nasal drug delivery: comparison of seven techniques.* Rhinology, 2006. **44**(2): p. 102-7.

127. Kublik, H. and M. Vidgren, *Nasal delivery systems and their effect on deposition and absorption.* Advanced drug delivery reviews, 1998. **29**(1): p. 157-177.

128. Harris, A., et al., *Effect of viscosity on particle size, deposition, and clearance of nasal delivery systems containing desmopressin.* Journal of pharmaceutical sciences, 1988. **77**(5): p. 405-408.

129. Aptar. *Pharma, Nasal drug delivery routes*. 2016 [cited 2016 26/08]; Available from: https://pharma.aptar.com/?_ga=1.58222186.1967589663.1472010534.

130. Djupesland, P.G., *Nasal drug delivery devices: characteristics and performance in a clinical perspective—a review.* Drug delivery and translational research, 2013. **3**(1): p. 42-62.

131. Berger, W.E., J.W. Godfrey, and A.L. Slater, *Intranasal corticosteroids: the development of a drug delivery device for fluticasone furoate as a potential step toward improved compliance.* Expert opinion on drug delivery, 2007. **4**(6): p. 689-701.

132. Dyer, A., et al., *Nasal delivery of insulin using novel chitosan based formulations: a comparative study in two animal models between simple chitosan formulations and chitosan nanoparticles.* Pharmaceutical research, 2002. **19**(7): p. 998-1008.

133. Soane, R., et al., *Evaluation of the clearance characteristics of bioadhesive systems in humans.* International journal of pharmaceutics, 1999. **178**(1): p. 55-65.

134. White, A. and J. Murray, *Intranasal adhesion formation following surgery for chronic nasal obstruction.* Clinical otolaryngology, 1988. **13**(2): p. 139-143.

135. Zhao, X., et al. *A systematic review of nonabsorbable, absorbable, and steroid‐impregnated spacers following endoscopic sinus surgery*. *International forum of allergy & rhinology*. 2013. Wiley online library.

136. Lin, D.C., et al., *Association between severity of asthma and degree of chronic rhinosinusitis.* American journal of rhinology & allergy, 2011. **25**(4): p. 205.

137. Deniz, M., et al., *The impact of different nasal packings on postoperative complications.* American journal of otolaryngology, 2014. **35**(5): p. 554-557.

138. Weber, R., et al., *Packing in endonasal surgery.* American journal of otolaryngology, 2001. **22**(5): p. 306-320.

139. Smith and nephew. *Sinu-knit*. 2016 [cited 2016 20/10/2016]; Available from: http://www.smith-nephew.com/key-products/key-ent/sinus/sinu-knit/.

140. Medtronic. *Merogel nasal packing*. 2016 [cited 2016 20/10/2016]; Available from: http://www.medtronic.com/us-en/healthcare-professionals/products/ear-nose-throat/bio-packing/bio-nasal-packing/merogel.html.

141. Wang, J., C. Cai, and S. Wang, *Merocel versus nasopore for nasal packing: a meta-analysis of randomized controlled trials.* Plos one, 2014. **9**(4).

142. Stryker. *Nasopore*. 2016 [cited 2016 20/10/2016]; Available from: http://www.stryker.com/en-us/products/NeurosurgicalSpineENT/ENTProducts/Bioresorbables/Nasopore/index.htm.

143. Medtronic. *Merocel*. 2016 [cited 2016 23/09]; Available from: http://www.merocel.com/products/index.htm.

144. Weber, R., F. Hochapfel, and W. Draf, *Packing and stents in endonasal surgery.* Rhinology, 2000. **38**(2): p. 49-62.

145. Asaka, D., et al., *Nasal splinting using silicone plates without gauze packing following septoplasty combined with inferior turbinate surgery.* Auris nasus larynx, 2012. **39**(1): p. 53-58.

146. Summit medical. *Nasal splints*. 2016 [cited 2016 23/09]; Available from: http://www.summitmedicalusa.com/products/ent/rhinology/splint-stent.php.

147. U.S. Food and drug administration. *Medical devices*. 2016 [cited 2016 24/08]; Available from: http://www.fda.gov/MedicalDevices/DeviceRegulationandGuidance/HowtoMarketYourDevice/.

148. Maisel, W.H., *Unanswered questions—drug-eluting stents and the risk of late thrombosis.* New england journal of medicine, 2007. **356**(10): p. 981-984.

149. Weitzel, E.K. and P.-J. Wormald, *A scientific review of middle meatal packing/stents.* American journal of rhinology, 2008. **22**(3): p. 302-307.

150. Bednarski, K.A. and F.A. Kuhn, *Stents and drug-eluting stents.* Otolaryngologic clinics of North America, 2009. **42**(5): p. 857-866.

151. Ow, R., et al. *Steroid‐eluting sinus implant for in‐office treatment of recurrent polyposis: a pharmacokinetic study*. *International forum of allergy and rhinology*. 2014. Wiley Online Library.

152. Lavigne, F., et al. *Steroid‐eluting sinus implant for in‐office treatment of recurrent nasal polyposis: a prospective, multicenter study*. *International forum of allergy and rhinology*. 2014. Wiley Online Library.

153. Riese, P., et al., *Intranasal formulations: promising strategy to deliver vaccines.* Expert opinion on drug delivery, 2014. **11**(10): p. 1619-1634.

154. Taulu, R., et al., *Image-guided, navigation-assisted relieva stratus microflow spacer insertion into the ethmoid sinus.* European archives of oto-rhino-laryngology, 2015. **272**(9): p. 2335-2340.

155. Catalano, P.J., et al., *The microflow spacer: a drug-eluting stent for the ethmoid sinus.* Indian journal of otolaryngology and head and neck surgery, 2011. **63**(3): p. 279-284.

156. Antisdel, J.L., et al., *Microporous polysaccharide hemospheres do not increase synechiae after sinus surgery: randomized controlled study.* American journal of rhinology and allergy, 2011. **25**(4): p. 268-271.

157. Shaw, C.-k.L., et al., *Effect of packing on nasal mucosa of sheep.* Journal of laryngology and otology, 2000. **114**(07): p. 506-509.

158. Li, P.F., D. Downie, and P.H. Hwang, *Controlled steroid delivery via bioabsorbable stent: safety and performance in a rabbit model.* American journal of rhinology and allergy, 2009. **23**(6): p. 591-596.

159. Malki, D., S. Quine, and A. Pfleiderer, *Nasal splints, revisited.* The journal of laryngology and otology, 1999. **113**(08): p. 725-727.

160. Intersect ENT Inc. *PROPEL sinus implant meta-analysis: Safety and effectiveness following ethmoid sinus surgery*. 2016 [cited 2016 26/08]; Available from: http://www.intersectent.com/.

161. Chadwell, J.S., L.M. Gustafson, and T.A. Tami, *Toxic shock syndrome associated with frontal sinus stents.* Otolaryngology-head and neck surgery, 2001. **124**(5): p. 573-574.

162. Brunton, L.L., B.A. Chabner, and B.C. Knollmann, *Goodman & Gilman's The pharmacological basis of therapeutics, 12e.* Pharmacotherapy of the epilepsies, valproic acid, 2011.

163. Venekamp, R.P., et al., *Systemic corticosteroids for acute sinusitis.* Cochrane database of systematic reviews, 2014(3).

164. Dunn, C.J. and K.L. Goa, *Tranexamic acid.* Drugs, 1999. **57**(6): p. 1005-1032.

165. Dalmau, A., et al., *Tranexamic acid reduces red cell transfusion better than ε-aminocaproic acid or placebo in liver transplantation.* Anesthesia & analgesia, 2000. **91**(1): p. 29-34.

166. Zhang, Y.J., B. Gao, and X.W. Liu, *Topical and effective hemostatic medicines in the battlefield.* International journal of clinical and experimental medicine, 2015. **8**(1): p. 10.

167. Kheirabadi, B.S., et al., *Development of hemostatic dressings for use in military operations*. 2004, DTIC Document.

168. Mohandas, A., et al., *Exploration of alginate hydrogel/nano zinc oxide composite bandages for infected wounds.* International journal of nanomedicine, 2015. **10**(Suppl 1): p. 53.

169. Sadigh-Eteghad, S., et al., *Effects of Levodopa loaded chitosan nanoparticles on cell viability and caspase-3 expression in PC12 neural like cells.* Neurosciences, 2013. **18**(3): p. 281-3.

170. Djagny, K.B., Z. Wang, and S. Xu, *Gelatin: a valuable protein for food and pharmaceutical industries: review.* Critical reviews in food science and nutrition, 2001. **41**(6): p. 481-492.

171. Freiberg, S. and X. Zhu, *Polymer microspheres for controlled drug release.* International journal of pharmaceutics, 2004. **282**(1): p. 1-18.

172. Cappabianca, P., et al., *Use of a thrombin–gelatin haemostatic matrix in endoscopic endonasal extended approaches: technical note.* Acta neurochirurgica, 2009. **151**(1): p. 69-77.

173. Sheikh, Z., et al., *Biodegradable materials for bone repair and tissue engineering applications.* Materials, 2015. **8**(9): p. 5744-5794.

174. Nair, L.S. and C.T. Laurencin, *Biodegradable polymers as biomaterials.* Progress in polymer science, 2007. **32**(8-9): p. 762-798.

175. Food and Drug Administration, F. *Technical Considerations for additive manufactured devices; draft guidance for industry and food and drug administration staff; availability*. 2016 [cited 2016 10/05]; Available from: https://www.federalregister.gov/articles/2016/05/10/2016-10924/technical-considerations-for-additive-manufactured-devices-draft-guidance-for-industry-and-food-and.

176. Restrepo, I., et al., *The effect of molecular weight and hydrolysis degree of poly (vinyl alcohol)(PVA) on the thermal and mechanical properties of poly (lactic acid)/PVA blends.* Polímeros, 2018. **28**(2): p. 169-177.

177. Itävaara, M., S. Karjomaa, and J.-F. Selin, *Biodegradation of polylactide in aerobic and anaerobic thermophilic conditions.* Chemosphere, 2002. **46**(6): p. 879-885.

178. Byrne, R.A., M. Joner, and A. Kastrati, *Stent thrombosis and restenosis: what have we learned and where are we going? The Andreas grüntzig lecture ESC 2014.* European heart journal, 2015. **36**(47): p. 3320-3331.

179. Orlandi, R.R., et al. *International consensus statement on allergy and rhinology: rhinosinusitis*. *International forum of allergy & rhinology*. 2016. Wiley Online Library.

180. Goole, J. and K. Amighi, *3D printing in pharmaceutics: a new tool for designing customized drug delivery systems.* International journal of pharmaceutics, 2016. **499**(1-2): p. 376-394.

181. Gross, B.C., et al., *Evaluation of 3D printing and its potential impact on biotechnology and the chemical sciences*. 2014, ACS publications.

182. Spencer, O.O., O.T. Yusuf, and T.C. Tofade, *Additive manufacturing technology development: A trajectory towards industrial revolution.* American journal of mechanical and industrial engineering, 2018. **3**(5): p. 80-90.

183. Aguado, B.A., et al., *Engineering precision biomaterials for personalized medicine.* Science translational medicine, 2018. **10**(424): p. eaam8645.

184. Legrand, D., et al., *The STIB score: a simple clinical test to predict clopidogrel resistance.* Acta cardiologica, 2015. **70**(5): p. 516-521.

185. Alligri, A., et al., *The mandibular permanent second molars and their risk of impaction: a retrospective study.* Eur J paediatr dent, 2015. **16**(3): p. 246-250.

186. Farahani, R.D., M. Dubé, and D. Therriault, *Three‐dimensional printing of multifunctional nanocomposites: manufacturing techniques and applications.* Advanced materials, 2016. **28**(28): p. 5794-5821.

187. Henson, B. and M.A. Edens, *Anatomy, head and neck, nose Sinuses*, in *Statpearls [Internet]*. 2018, Statpearls publishing.

188. Anatomy. *The Nasal Cavity*. 2019 [cited 2019 23/07]; Available from: https://teachmeanatomy.info/head/organs/the-nose/nasal-cavity/.

189. Sorguç, A.G., I. Hagiwara, and S. Selcuk, *Origamics in architecture: a medium of inquiry for design in architecture.* Metu Jfa, 2009. **2**: p. 235-247.

190. Johnson, M., et al., *Fabricating biomedical origami: a state-of-the-art review.* International journal of computer assisted radiology and surgery, 2017. **12**(11): p. 2023-2032.

191. Calleja, A. and G.J. Pace, *A domain-specific embedded language approach for the scripting of game artificial intelligence.*

192. Debnath, S. and L. Fei, *Origami theory and its applications: a literature review.* World academy of science, engineering and technology, 2013: p. 1131-1135.

193. Lang, R.J., *Treemaker 4.0: A program for origami design*. 1998.

194. Erickson, S.J., R.W. Prost, and M. Timins, *The" magic angle" effect: background physics and clinical relevance.* Radiology, 1993. **188**(1): p. 23-25.

195. Tachi, T., *Simulation of rigid origami.* Origami, 2009. **4**: p. 175-187.

196. Peraza-Hernandez, E.A., et al., *Origami-inspired active structures: a synthesis and review.* Smart materials and structures, 2014. **23**(9): p. 094001.

197. Oates, C., *Twofold: space-saving folding furniture.* San diego state university, 2015.

198. Felton, S., et al., *A method for building self-folding machines.* Science, 2014. **345**(6197): p. 644-646.

199. Xu, L., T.C. Shyu, and N.A. Kotov, *Origami and kirigami nanocomposites.* Acs nano, 2017. **11**(8): p. 7587-7599.

200. Liu, S., et al., *Deformation of the Miura-ori patterned sheet.* International journal of mechanical sciences, 2015. **99**: p. 130-142.

201. Nakase, Y., et al., *A novel procedure for introducing large sheet-type surgical material with a self-expanding origami structure using a slim trocar (chevron pleats procedure).* Surgical endoscopy, 2017. **31**(9): p. 3749-3754.

202. Zhao, Y., et al., *Approximating 3D surfaces using generalized waterbomb tessellations.* Journal of computational design and engineering, 2018. **5**(4): p. 442-448.

203. Liu, Y., et al., *Nature-inspired structural materials for flexible electronic devices.* Chemical reviews, 2017. **117**(20): p. 12893-12941.

204. Pydah, A. and R. Batra, *Crush dynamics and transient deformations of elastic-plastic miura-ori core sandwich plates.* Thin-walled structures, 2017. **115**: p. 311-322.

205. Becker, P.J. and B.E. Brownell, *The Feasibility and sustainability of Architectural biomaterials.* 2016.

206. Technologies, T.l. *Orimetic*. 2019 [cited 2019 1/06]; Available from: http://trexlab.com/.

207. Prawoto, Y., *Seeing auxetic materials from the mechanics point of view: a structural review on the negative Poisson's ratio.* Computational materials science, 2012. **58**: p. 140-153.

208. Alizadeh, M., et al., *Towards polymers with molecular auxeticity.* CHIMIA international journal for chemistry, 2019. **73**(1): p. 25-28.

209. Mir, M., et al., *Review of mechanics and applications of auxetic structures.* Advances in materials science and engineering, 2014. **2014**.

210. Evans, K.E. and A. Alderson, *Auxetic materials: functional materials and structures from lateral thinking!* Advanced materials, 2000. **12**(9): p. 617-628.

211. Formlabs. *How to 3D print anatomical models for preoperative planning and enhanced patient consent*. 2017 [cited 2019 5/02/2019]; Available from: https://formlabs.com/media/upload/Formlabs-White-Paper_How-to-3D-Print-Anatomical-Models.pdf.

212. Ning, F., et al., *Additive manufacturing of carbon fiber reinforced thermoplastic composites using fused deposition modeling.* Composites part B: engineering, 2015. **80**: p. 369-378.

213. Gebeshuber, I.-C. and R. Crawford, *Micromechanics in biogenic hydrated silica: hinges and interlocking devices in diatoms.* Proceedings of the institution of mechanical engineers, Part J: journal of engineering tribology, 2006. **220**(8): p. 787-796.

214. Redwood, B. *How to design living hinges for 3D printing*. 2018 [cited 2019 01/06]; Available from: https://www.3dhubs.com/knowledge-base/how-design-living-hinges-3d-printing.

215. Momeni, F., X. Liu, and J. Ni, *A review of 4D printing.* Materials & design, 2017. **122**: p. 42-79.

216. Castro, N.J., et al., *Current developments in multifunctional smart materials for 3D/4D bioprinting.* Current opinion in biomedical engineering, 2017. **2**: p. 67-75.

217. Lyons, J.G., et al., *The incorporation of an organically modified layered silicate in monolithic polymeric matrices produced using hot melt extrusion.* Materials chemistry and physics, 2007. **103**(2-3): p. 419-426.

218. Ge, H., et al., *Thermal, mechanical, and rheological properties of plasticized poly (L‐lactic acid).* Journal of applied polymer science, 2013. **127**(4): p. 2832-2839.

219. Yu, L., K. Dean, and L. Li, *Polymer blends and composites from renewable resources.* Progress in polymer science, 2006. **31**(6): p. 576-602.

220. Dawson, L. and R. Boopathy, *Use of post-harvest sugarcane residue for ethanol production.* Bioresource technology, 2007. **98**(9): p. 1695-1699.

221. Tsuji, H. and H. Muramatsu, *Blends of aliphatic polyesters: V non-enzymatic and enzymatic hydrolysis of blends from hydrophobic poly (l-lactide) and hydrophilic poly (vinyl alcohol).* Polymer degradation and stability, 2001. **71**(3): p. 403-413.

222. Shuai, X., et al., *Miscibility and phase structure of binary blends of poly (l‐lactide) and poly (vinyl alcohol).* Journal of applied polymer science, 2001. **81**(3): p. 762-772.

223. Tsuji, H. and H. Muramatsu, *Blends of aliphatic polyesters. IV. Morphology, swelling behavior, and surface and bulk properties of blends from hydrophobic poly (L‐lactide) and hydrophilic poly (vinyl alcohol).* Journal of applied polymer science, 2001. **81**(9): p. 2151-2160.

224. Vila, A., et al., *PLA‐PEG nanospheres: New carriers for transmucosal delivery of proteins and plasmid DNA.* Polymers for advanced technologies, 2002. **13**(10‐12): p. 851-858.

225. Huda, M.S., et al., *Chopped glass and recycled newspaper as reinforcement fibers in injection molded poly (lactic acid)(PLA) composites: a comparative study.* Composites science and technology, 2006. **66**(11-12): p. 1813-1824.

226. Jawalkar, S.S. and T.M. Aminabhavi, *Molecular modeling simulations and thermodynamic approaches to investigate compatibility/incompatibility of poly (l-lactide) and poly (vinyl alcohol) blends.* Polymer, 2006. **47**(23): p. 8061-8071.

227. Zhang, J.H., et al., *Novel polylactide/vermiculite nanocomposites by in situ intercalative polymerization. I. Preparation, characterization, and properties.* Polymer composites, 2007. **28**(4): p. 545-550.

228. Lucke, A., et al., *Biodegradable poly (D, L-lactic acid)-poly (ethylene glycol)-monomethyl ether diblock copolymers: structures and surface properties relevant to their use as biomaterials.* Biomaterials, 2000. **21**(23): p. 2361-2370.

229. Yeh, J.-T., et al., *Study on the crystallization kinetic and characterization of poly (lactic acid) and poly (vinyl alcohol) blends.* Polymer-plastics technology and engineering, 2008. **47**(12): p. 1289-1296.

230. Ren, G., et al., *Electrospun poly (vinyl alcohol)/glucose oxidase biocomposite membranes for biosensor applications.* Reactive and functional polymers, 2006. **66**(12): p. 1559-1564.

231. Mc Gann, M.J., et al., *The synthesis of novel pH-sensitive poly (vinyl alcohol) composite hydrogels using a freeze/thaw process for biomedical applications.* International journal of pharmaceutics, 2009. **372**(1-2): p. 154-161.

232. Islam, A. and T. Yasin, *Controlled delivery of drug from pH sensitive chitosan/poly (vinyl alcohol) blend.* Carbohydrate polymers, 2012. **88**(3): p. 1055-1060.

233. Bocqué, M., et al., *Petro‐based and bio‐based plasticizers: Chemical structures to plasticizing properties.* Journal of polymer science part A: polymer chemistry, 2016. **54**(1): p. 11-33.

234. Holländer, J., et al., *Three-dimensional printed PCL-based implantable prototypes of medical devices for controlled drug delivery.* Journal of pharmaceutical sciences, 2016. **105**(9): p. 2665-2676.

235. Forster, A., et al., *Selection of excipients for melt extrusion with two poorly water-soluble drugs by solubility parameter calculation and thermal analysis.* International journal of pharmaceutics, 2001. **226**(1-2): p. 147-161.

236. Kolbina, M., et al., *Evaluation of hydrogenated soybean phosphatidylcholine matrices prepared by hot melt extrusion for oral controlled delivery of water-soluble drugs.* AAPS Pharmscitech, 2019. **20**(4): p. 159.

237. Guo, G., et al., *Preparation of curcumin loaded poly (ε-caprolactone)-poly (ethylene glycol)-poly (ε-caprolactone) nanofibers and their in vitro antitumor activity against Glioma 9L cells.* Nanoscale, 2011. **3**(9): p. 3825-3832.

238. Morizane, K., et al., *Implantable composite devices of unsintered hydroxyapatite and poly-l-lactide with dispersive marbling morphology to enhance in vivo bioactivity and bioresorbability.* Materials science and engineering: C, 2019. **97**: p. 698-706.

239. Chen, L. and M. Wang, *Production and evaluation of biodegradable composites based on PHB–PHV copolymer.* Biomaterials, 2002. **23**(13): p. 2631-2639.

240. Barbieri, D., et al., *Controlling dynamic mechanical properties and degradation of composites for bone regeneration by means of filler content.* Journal of the mechanical behavior of biomedical materials, 2013. **20**: p. 162-172.

241. Zhang, R., W. Xu, and F. Jiang, *Fabrication and characterization of dense chitosan/polyvinyl-alcohol/poly-lactic-acid blend membranes.* Fibers and polymers, 2012. **13**(5): p. 571-575.

242. Bourges, J., et al., *Intraocular implants for extended drug delivery: therapeutic applications.* Advanced drug delivery reviews, 2006. **58**(11): p. 1182-1202.

243. Belter, M., A. Sajnóg, and D. Barałkiewicz, *Over a century of detection and quantification capabilities in analytical chemistry–historical overview and trends.* Talanta, 2014. **129**: p. 606-616.

244. Bechthold, L., et al., *3D printing: A qualitative assessment of applications, recent trends and the technology's future potential*. 2015, Studien zum deutschen innovationssystem.

245. Braver, S.L., D.P. MacKinnon, and M. Page, *Levine's guide to SPSS for analysis of variance*. 2003: Psychology press.

246. Goyanes, A., et al., *3D printing of medicines: engineering novel oral devices with unique design and drug release characteristics.* Molecular pharmaceutics, 2015. **12**(11): p. 4077-4084.

247. Skowyra, J., K. Pietrzak, and M.A. Alhnan, *Fabrication of extended-release patient-tailored prednisolone tablets via fused deposition modelling (FDM) 3D printing.* European journal of pharmaceutical sciences, 2015. **68**: p. 11-17.

248. Goyanes, A., et al., *3D printing of modified-release aminosalicylate (4-ASA and 5-ASA) tablets.* European journal of pharmaceutics and biopharmaceutics, 2015. **89**: p. 157-162.

249. Niranjana Prabhu, T. and K. Prashantha, *A review on present status and future challenges of starch based polymer films and their composites in food packaging applications.* Polymer composites, 2018. **39**(7): p. 2499-2522.

250. Mains, J., C.G. Wilson, and A. Urquhart, *ToF-SIMS analysis of dexamethasone distribution in the isolated perfused eye.* Investigative ophthalmology & visual science, 2011. **52**(11): p. 8413-8419.

251. Fukushima, K., D. Tabuani, and G. Camino, *Nanocomposites of PLA and PCL based on montmorillonite and sepiolite.* Materials science and engineering: C, 2009. **29**(4): p. 1433-1441.

252. Ranganathan, V., et al., *Formulation and characterization of mouth dissolving tablets of dexamethasone using synthetic superdisintegrants.* Research journal of pharmacy and technology, 2018. **11**(4): p. 1429-1435.

253. Ray, S. and R.P. Cooney, *Thermal degradation of polymer and polymer composites*, in *Handbook of environmental degradation of materials*. 2018, Elsevier. p. 185-206.

254. Tsuji, H., *Poly (lactide) stereocomplexes: formation, structure, properties, degradation, and applications.* Macromolecular bioscience, 2005. **5**(7): p. 569-597.

255. Nalbandi, A., *Kinetics of thermal degradation of polylactic acid under N-2 atmosphere.* 2001.

256. Ding, J., et al., *Synthesis and properties of thermoplastic poly (vinyl alcohol)-graft-lactic acid copolymers.* Industrial & engineering chemistry research, 2008. **48**(2): p. 788-793.

257. Holland, B. and J. Hay, *The thermal degradation of poly (vinyl alcohol).* Polymer, 2001. **42**(16): p. 6775-6783.

258. Rodrigues, L.B., et al., *In vitro release and characterization of chitosan films as dexamethasone carrier.* International journal of pharmaceutics, 2009. **368**(1-2): p. 1-6.

259. Li, X., et al., *In vitro degradation kinetics of pure PLA and Mg/PLA composite: Effects of immersion temperature and compression stress.* Acta biomaterialia, 2017. **48**: p. 468-478.

260. Rebia, R.A., et al., *Biodegradable PHBH/PVA blend nanofibers: fabrication, characterization, in vitro degradation, and in vitro biocompatibility.* Polymer degradation and stability, 2018. **154**: p. 124-136.

261. Liu, Y., et al., *Simultaneous enhancement of strength and toughness of PLA induced by miscibility variation with PVA.* Polymers, 2018. **10**(10): p. 1178.

262. Li, D., et al., *PLA/F68/dexamethasone implants prepared by hot-melt extrusion for controlled release of anti-inflammatory drug to implantable medical devices: I. Preparation, characterization and hydrolytic degradation study.* International journal of pharmaceutics, 2013. **441**(1-2): p. 365-372.

263. Moydeen, A.M., et al., *Single-nozzle core-shell electrospun nanofibers of PVP/Dextran as drug delivery system.* Fibers and polymers, 2019. **20**(10): p. 2078-2089.

264. Aguirre, A., R. Borneo, and A.E. León, *Properties of triticale protein films and their relation to plasticizing–antiplasticizing effects of glycerol and sorbitol.* Industrial crops and products, 2013. **50**: p. 297-303.

265. Patel, V.F., F. Liu, and M.B. Brown, *Advances in oral transmucosal drug delivery.* Journal of controlled release, 2011. **153**(2): p. 106-116.

266. Sharma, D., et al., *Fast dissolving oral films technology: a recent trend for an innovative oral drug delivery system.* International journal of drug delivery, 2015. **7**(2): p. 60-75.

267. Dixit, R. and S. Puthli, *Oral strip technology: overview and future potential.* Journal of controlled release, 2009. **139**(2): p. 94-107.

268. García, M.C., et al., *Bioadhesive and biocompatible films as wound dressing materials based on a novel dendronized chitosan loaded with ciprofloxacin.* Carbohydrate polymers, 2017. **175**: p. 75-86.

269. Su, J.-F., et al., *Moisture sorption and water vapor permeability of soy protein isolate/poly (vinyl alcohol)/glycerol blend films.* Industrial crops and products, 2010. **31**(2): p. 266-276.

270. Bhattarai, N., J. Gunn, and M. Zhang, *Chitosan-based hydrogels for controlled, localized drug delivery.* Advanced drug delivery reviews, 2010. **62**(1): p. 83-99.

271. Ansari, N.N., et al., *A randomized clinical trial comparing pulsed ultrasound and erythromycin phonophoresis in the treatment of patients with chronic rhinosinusitis.* Physiotherapy theory and practice, 2015. **31**(3): p. 166-172.

272. Etxabide, A., et al., *Ultra thin hydro-films based on lactose-crosslinked fish gelatin for wound healing applications.* International journal of pharmaceutics, 2017. **530**(1-2): p. 455-467.

273. Leonida, M., P. Ispas-Szabo, and M.A. Mateescu, *Self-stabilized chitosan and its complexes with carboxymethyl starch as excipients in drug delivery.* Bioactive materials, 2018. **3**(3): p. 334-340.

274. Yadollahi, M., S. Farhoudian, and H. Namazi, *One-pot synthesis of antibacterial chitosan/silver bio-nanocomposite hydrogel beads as drug delivery systems.* International journal of biological macromolecules, 2015. **79**: p. 37-43.

275. Cui, L., et al., *Preparation and characterization of IPN hydrogels composed of chitosan and gelatin cross-linked by genipin.* Carbohydrate polymers, 2014. **99**: p. 31-38.

276. Rohindra, D.R., A.V. Nand, and J.R. Khurma, *Swelling properties of chitosan hydrogels.* The south pacific journal of natural and applied sciences, 2004. **22**(1): p. 32-35.

277. Mirzaei B, E., et al., *Studies on glutaraldehyde crosslinked chitosan hydrogel properties for drug delivery systems.* International journal of polymeric materials and polymeric biomaterials, 2013. **62**(11): p. 605-611.

278. Yoo, H.J. and H.D. Kim, *Synthesis and properties of waterborne polyurethane hydrogels for wound healing dressings.* Journal of biomedical materials research part b: applied biomaterials, 2008. **85**(2): p. 326-333.

279. Fu, J., et al., *Construction of anti-adhesive and antibacterial multilayer films via layer-by-layer assembly of heparin and chitosan.* Biomaterials, 2005. **26**(33): p. 6684-6692.

280. Martucci, J.F., A. Accareddu, and R.A. Ruseckaite, *Preparation and characterization of plasticized gelatin films cross-linked with low concentrations of Glutaraldehyde.* Journal of materials science, 2012. **47**(7): p. 3282-3292.

281. Rivero, S., M. García, and A. Pinotti, *Composite and bi-layer films based on gelatin and chitosan.* Journal of food engineering, 2009. **90**(4): p. 531-539.

282. Liu, Y., et al., *Preparation and characterization of chitosan-gelatin/glutaraldehyde scaffolds.* Journal of macromolecular science, part b, 2014. **53**(2): p. 309-325.

283. Pereda, M., et al., *Chitosan-gelatin composites and bi-layer films with potential antimicrobial activity.* Food hydrocolloids, 2011. **25**(5): p. 1372-1381.

284. Abruzzo, A., et al., *Mucoadhesive chitosan/gelatin films for buccal delivery of propranolol hydrochloride.* Carbohydrate polymers, 2012. **87**(1): p. 581-588.

285. Qiao, C., et al., *Molecular interactions in gelatin/chitosan composite films.* Food chemistry, 2017. **235**: p. 45-50.

286. Patel, S., et al., *Preparation and optimization of chitosan-gelatin films for sustained delivery of lupeol for wound healing.* International journal of biological macromolecules, 2018. **107**: p. 1888-1897.

287. Costa-Júnior, E.S., et al., *Preparation and characterization of chitosan/poly (vinyl alcohol) chemically crosslinked blends for biomedical applications.* Carbohydrate polymers, 2009. **76**(3): p. 472-481.

288. Ramachandran, S., S. Nandhakumar, and M.D. Dhanaraju, *Formulation and characterization of glutaraldehyde cross-linked chitosan biodegradable microspheres loaded with famotidine.* Tropical journal of pharmaceutical research, 2011. **10**(3).

289. Chiang, Z.-C., et al., *Preparation and characterization of dexamethasone-immobilized chitosan scaffold.* Journal of bioscience and bioengineering, 2012. **113**(5): p. 654-660.

290. Zhu, J. and R.E. Marchant, *Design properties of hydrogel tissue-engineering scaffolds.* Expert review of medical devices, 2011. **8**(5): p. 607-626.

291. Kim, S., et al., *Chitosan/gelatin–based films crosslinked by proanthocyanidin.* Journal of biomedical materials research part b: applied biomaterials: an official journal of the society for biomaterials, the japanese society for biomaterials, and the australian society for biomaterials and the korean society for biomaterials, 2005. **75**(2): p. 442-450.

292. Xin-Yuan, S. and T. Tian-Wei, *New contact lens based on chitosan/gelatin composites.* Journal of bioactive and compatible polymers, 2004. **19**(6): p. 467-479.

293. Wiarachai, O., et al., *Surface-quaternized chitosan particles as an alternative and effective organic antibacterial material.* Colloids and surfaces b: biointerfaces, 2012. **92**: p. 121-129.

294. Li, J., et al., *Surface characterization and biocompatibility of micro-and nano-hydroxyapatite/chitosan-gelatin network films.* Materials science and engineering: C, 2009. **29**(4): p. 1207-1215.

295. Dash, S., et al., *Kinetic modeling on drug release from controlled drug delivery systems.* Acta Pol pharm, 2010. **67**(3): p. 217-23.

296. Singhvi, G. and M. Singh, *In-vitro drug release characterization models.* Int j pharm stud res, 2011. **2**(1): p. 77-84.

297. Shaikh, H.K., R. Kshirsagar, and S. Patil, *Mathematical models for drug release characterization: a review.* World j. pharm. pharm. sci, 2015. **4**(4): p. 324-338.

298. Costa, P. and J.M.S. Lobo, *Modeling and comparison of dissolution profiles.* European journal of pharmaceutical sciences, 2001. **13**(2): p. 123-133.

299. Samaha, D., R. Shehayeb, and S. Kyriacos, *Modeling and comparison of dissolution profiles of diltiazem modified-release formulations.* Diss technol, 2009. **16**(2): p. 41-6.

300. Santoro, M., A.M. Tatara, and A.G. Mikos, *Gelatin carriers for drug and cell delivery in tissue engineering.* Journal of controlled release, 2014. **190**: p. 210-218.

301. Chiou, B.-S., et al., *Cold water fish gelatin films: Effects of cross-linking on thermal, mechanical, barrier, and biodegradation properties.* European polymer journal, 2008. **44**(11): p. 3748-3753.

302. Bigi, A., S. Panzavolta, and K. Rubini, *Relationship between triple-helix content and mechanical properties of gelatin films.* Biomaterials, 2004. **25**(25): p. 5675-5680.

303. Dreßler, M., et al., *Influence of gelatin coatings on compressive strength of porous hydroxyapatite ceramics.* Journal of the european ceramic society, 2011. **31**(4): p. 523-529.

304. Yakimets, I., et al., *Mechanical properties with respect to water content of gelatin films in glassy state.* Polymer, 2005. **46**(26): p. 12577-12585.

305. Reddy, N., R. Reddy, and Q. Jiang, *Crosslinking biopolymers for biomedical applications.* Trends in biotechnology, 2015. **33**(6): p. 362-369.

306. De Clercq, K., et al., *Genipin-crosslinked gelatin microspheres as a strategy to prevent postsurgical peritoneal adhesions: In vitro and in vivo characterization.* Biomaterials, 2016. **96**: p. 33-46.

307. Etxabide, A., et al., *Effects of cross-linking in nanostructure and physicochemical properties of fish gelatins for bio-applications.* Reactive and functional polymers, 2015. **94**: p. 55-62.

308. Gómez-Guillén, M., et al., *Functional and bioactive properties of collagen and gelatin from alternative sources: a review.* Food hydrocolloids, 2011. **25**(8): p. 1813-1827.

309. Olsen, D., et al., *Recombinant collagen and gelatin for drug delivery.* Advanced drug delivery reviews, 2003. **55**(12): p. 1547-1567.

310. Etxabide, A., et al., *Lactose-crosslinked fish gelatin-based porous scaffolds embedded with tetrahydrocurcumin for cartilage regeneration.* International journal of biological macromolecules, 2018. **117**: p. 199-208.

311. Etxabide, A., et al., *Improvement of barrier properties of fish gelatin films promoted by gelatin glycation with lactose at high temperatures.* LWT-food science and technology, 2015. **63**(1): p. 315-321.

312. Etxabide, A., et al., *Control of cross-linking reaction to tailor the properties of thin films based on gelatin.* Materials letters, 2016. **185**: p. 366-369.

313. De Bonis, M., et al., *Topical use of tranexamic acid in coronary artery bypass operations: a double-blind, prospective, randomized, placebo-controlled study.* The journal of thoracic and cardiovascular surgery, 2000. **119**(3): p. 575-580.

314. Napolitano, L.M., et al., *Tranexamic acid in trauma: how should we use it?* Journal of trauma and acute care surgery, 2013. **74**(6): p. 1575-1586.

315. Fabresse, N., et al., *LC–MS/MS determination of tranexamic acid in human plasma after phospholipid clean-up.* Journal of pharmaceutical and biomedical analysis, 2017. **141**: p. 149-156.

316. Kim, H.W., J.C. Knowles, and H.E. Kim, *Development of hydroxyapatite bone scaffold for controlled drug release via poly (ϵ ‐ caprolactone) and hydroxyapatite hybrid coatings.* Journal of biomedical materials research part b: applied biomaterials: an official journal of the society for biomaterials, the japanese society for biomaterials, and the australian society for biomaterials and the korean society for biomaterials, 2004. **70**(2): p. 240-249.

317. Long, J., et al., *Development of customised 3D printed biodegradable projectile for administrating extended-release contraceptive to wildlife.* International journal of pharmaceutics, 2018. **548**(1): p. 349-356.

318. Hossana, M.J., et al., *Preparation and characterization of gelatin-hydroxyapatite composite for bone tissue engineering.* International journal of engineering & technology IJET-IJENS, 2014. **14**(1): p. 24-32.

319. Ottenhof, M.-A., W. MacNaughtan, and I.A. Farhat, *FTIR study of state and phase transitions of low moisture sucrose and lactose.* Carbohydrate research, 2003. **338**(21): p. 2195-2202.

320. Arayne, M.S., et al., *Spectrophotometric techniques to determine tranexamic acid: Kinetic studies using ninhydrin and direct measuring using ferric chloride.* Journal of molecular structure, 2008. **891**(1-3): p. 475-480.

321. Delyle, S.G., et al., *A validated assay for the quantitative analysis of tranexamic acid in human serum by liquid chromatography coupled with electrospray ionization mass spectrometry.* Clinica chimica acta, 2010. **411**(5-6): p. 438-443.

322. Wang, J., B.M. Wang, and S.P. Schwendeman, *Characterization of the initial burst release of a model peptide from poly (D, L-lactide-co-glycolide) microspheres.* Journal of controlled release, 2002. **82**(2-3): p. 289-307.

323. Pitt, C., *The controlled parenteral delivery of polypeptides and proteins.* International journal of pharmaceutics, 1990. **59**(3): p. 173-196.

324. Serra, L., J. Doménech, and N.A. Peppas, *Drug transport mechanisms and release kinetics from molecularly designed poly (acrylic acid-g-ethylene glycol) hydrogels.* Biomaterials, 2006. **27**(31): p. 5440-5451.

325. Trinity college library, C. *Treasures from the collection*. 2019 [cited 2019 4/06]; Available from: https://trinitycollegelibrarycambridge.wordpress.com/2015/07/29/surgery/.

326. Kublik, H. and M. Vidgren, *Nasal delivery systems and their effect on deposition and absorption.* Advanced drug delivery reviews, 1998. **29**(1-2): p. 157-177.

327. Khanna, P. and A. Shah, *Assessment of sensory perceptions and patient preference for intranasal corticosteroid sprays in allergic rhinitis.* American journal of rhinology, 2005. **19**(3): p. 316-321.

328. Hu, Y., Q. Wang, and M. Tang, *Preparation and properties of Starch-g-PLA/poly (vinyl alcohol) composite film.* Carbohydrate polymers, 2013. **96**(2): p. 384-388.

329. Gonçalves, R.P., et al., *Morphology and thermal properties of core-shell PVA/PLA ultrafine fibers produced by coaxial electrospinning.* Materials sciences and applications, 2015. **6**(02): p. 189.

330. Wang, H., et al., *Study on hydrophilicity and degradability of polyvinyl alcohol/polylactic acid blend film.* Journal of biomedical engineering, 2008. **25**(1): p. 139-142.

331. Puranik, A.S., E.R. Dawson, and N.A. Peppas, *Recent advances in drug eluting stents.* International journal of pharmaceutics, 2013. **441**(1-2): p. 665-679.

332. Lamberti, F.V., R.C. Klann, and R.S. Hill, *Immobilized bioactive hydrogel matrices as surface coatings*. 2017, Google patents.